

Spin-Dynamics in Strongly Excited Ferromagnetic Systems

Dissertation

Zur Erlangung des Doktorgrades der Naturwissenschaften
(Dr. rer. nat.)

der

Naturwissenschaftlichen Fakultät II
Chemie, Physik und Mathematik

der Martin-Luther-Universität
Halle-Wittenberg

vorgelegt von

Herr Kevin Krieger
geb. am 07.01.1979 in Zeulenroda

Datum der Verteidigung:
08. November 2016

Gutachter:

Prof. Dr. E. Gross, Prof. Dr. M. Marques, Prof. Dr. A. Rubio

Contents

1. Introduction	1
2. Many-electron systems in intense laser fields	3
2.1. The many-body problem	3
2.2. Density-functional theory	4
2.2.1. The Hohenberg-Kohn theorem	4
2.2.2. The Kohn-Sham equations	5
2.2.3. Extensions of DFT	7
2.2.4. A modified SDFT scheme with spin-orbit coupling	11
2.2.5. Approximate functionals	16
2.3. Time-dependent DFT	18
2.3.1. Fundamental theorems and the time-dependent KS scheme	18
2.3.2. Extensions of TDDFT	21
2.3.3. Approximate functionals	23
2.4. Interaction with laser pulses	24
2.4.1. Ultrashort laser pulses	24
2.4.2. The dipole approximation	25
3. Real-time spin-dynamics - simulation framework	29
3.1. Theoretical aspects of the simulation	29
3.1.1. Spin-coupling terms	29
3.1.2. A time-dependent SDFT scheme with spin-orbit coupling .	32
3.1.3. Time-dependent SDFT in extended systems	33
3.1.4. The dynamical equation of the density, the magnetization, and the moment	37
3.1.5. The zero-torque theorem	41
3.2. Real-time propagation algorithm and implementation	44
3.3. Time-dependent density of states	49
4. Ultrafast change of the moment in extended systems	55
4.1. A first investigation in bulk nickel	55
4.2. Response of the moment for different fields in bulk nickel	58
4.3. The demagnetization process	61
4.3.1. Initial change of the local moment and charge	62
4.3.2. Approximation of the spin-orbit coupling term	66
4.3.3. A closer look at the demagnetization process	69
4.3.4. Spin-orbit angular momentum torques and the ground state	72
4.3.5. The Spin-flip process	77
4.3.6. Summary	84

4.4.	Response of the moment in bulk iron	87
4.5.	Response of the moment in a five-atom nickel slab	89
4.5.1.	Simulation, results and discussion	89
4.5.2.	Relation to experiments	91
5.	Conclusions	95
A.	Appendix	97
A.1.	The general concept of densities and current densities	97
A.1.1.	Observable densities	97
A.1.2.	Observable current densities	98
A.1.3.	Gauge invariance - paramagnetic and diamagnetic current densities	100
A.1.4.	Operator representation of the current densities	101
A.1.5.	Coupling to local fields	102
A.2.	Magnetization, current and spin-currents for many-electron systems	102
A.3.	The gauge transformation	103
A.4.	The Helmholtz decomposition	106
A.5.	Time-dependent Bloch states and the \mathbf{k} -point method	106
A.6.	Auxiliary calculations	108
A.6.1.	Rules	108
A.6.2.	Spin-orbit coupling	108
A.6.3.	Time-dependent density, magnetization, and moment	109
A.6.4.	Spin-orbit angular momentum torque terms	116
A.6.5.	Spin-current representation for the radial SOC and for the spin-orbit angular momentum torque	121
A.7.	Many-electron systems and change of the moment	122
	Bibliography	131

Notation

Symbol	Description
x	a scalar (lowercase, normal font)
\mathbf{x}	a vector in 3-dimensional space (lowercase, bold font)
$\mathbf{x} _l$	the l th component of vector \mathbf{x} , i.e. x_l
∂_x	derivative with respect to x ($\hat{=} \frac{\partial}{\partial x}$)
$[\cdot, \cdot]$	commutator
$\{\cdot, \cdot\}$	anti-commutator
$\underline{\varphi}(\mathbf{r})$	a spinor, i.e. a vector in 2-dimensional space: $\begin{pmatrix} \varphi^\uparrow(\mathbf{r}) \\ \varphi^\downarrow(\mathbf{r}) \end{pmatrix}$
$\underline{\underline{O}}$	a matrix in spinor space
$\underline{\underline{\underline{O}}}$	a matrix in spinor space, an operator in position space

General remarks

- All equations, quantities and plots in this work are presented in Hartree atomic units, i.e. $\hbar = |e| = m_e = 1$.
 → One exception is the intensity of electromagnetic fields, which will always be presented in W/cm^2 (this is a commonly used unit in experiments, the relation to *a.u.* is: $I[W/cm^2] \hat{=} 3.51 \cdot 10^{16} E^2[a.u.]$).
- “*a.u.*” stands for the particular unit, e.g. time or length, in atomic units.
 → time: $1 fs \hat{=} 41.34 a.u.$, length: $1 nm \hat{=} 18.9 a.u.$
- All electro-dynamical equations and quantities are represented in the CGS-formulation, while atomic units are used.
- All quantum mechanical operators are in first quantization.
- The components of 3-dimensional vectors have the indices $\{1, 2, 3\}$, the index notation $\{x, y, z\}$ is not used. The 3 Cartesian unit vectors are $\mathbf{e}_1, \mathbf{e}_2, \mathbf{e}_3$.
- We will primarily use two state notations:
 → The Dirac notation, where the (many-particle) states are represented in the usual bra-ket notation, e.g. $|\Psi\rangle$. In this notation, we will represent all operators in terms of the position operator $\hat{\mathbf{r}}$, the momentum operator $\hat{\mathbf{p}}$, and the Pauli spin operators $\hat{\sigma}_1, \hat{\sigma}_2$, and $\hat{\sigma}_3$. If many-particle problems are discussed, each operator gets a particle index (usually i), i.e. $\hat{\mathbf{r}}_i$ or $\hat{\sigma}_{3,i}$, meaning that the operator acts only on the individual single-particle space. In this notation, single-particle states will have a particle index as well, e.g. $|\varphi\rangle_i$.
 → The two-component spinor notation, where the single-particle states are represented by two-component wave functions in the position space, e.g. $\underline{\varphi}(\mathbf{r})$. In this representation, the position operator is given by \mathbf{r} (i.e. by an ordinary vector; note that no “ $\hat{}$ ” is used), the momentum operator is given by $\hat{\mathbf{p}} = -i\nabla$, and the spin operators are given by the 2×2 Pauli matrices $\underline{\underline{\sigma}}_1, \underline{\underline{\sigma}}_2$, and $\underline{\underline{\sigma}}_3$.

Acronyms

ALDA	adiabatic LDA
ALSDA	adiabatic LSDA
APW	augmented plane wave
CDFT	current DFT
DA	dipole approximation
DFT	density-functional theory
DOS	density of states
FWHM	full width at half maximum
HK	Hohenberg-Kohn
IR	interstitial region
KS	Kohn-Sham
LDA	local density approximation
LO	local orbital
LSDA	local spin-density approximation
MT	muffin-tin
RDFT	relativistic DFT
RG	Runge-Gross
SCDFT	spin-current DFT
SDFT	spin DFT
SOC	spin-orbit coupling
TDDFT	time-dependent DFT
TDDOS	time-dependent DOS
TDSDFD	time-dependent spin-DFT
xc	exchange-correlation

1. Introduction

Spintronics is an important emerging field of research and a very promising technology for the future development of nano devices. The idea behind spintronics is that, in addition to the electron charge, it makes use of the intrinsic electron spin. This, in principle, allows it to scale down the size of logic elements and permits the development of tiny non-volatile storage devices, leading to higher storage densities and more efficient logic devices. For example, tiny spin-magnetic domains (possibly on the atomic scale) could act as binary data bits within such a technology. In order to achieve fast writing times, the ultrafast manipulation of such domains would be of particular importance.

Currently, the fastest way to modify spin-magnetic domains is optical manipulation by ultrashort laser pulses. During the last two decades, various experiments have shown that an ultrashort laser pulse can induce a very fast partial demagnetization in ferromagnetic materials. While first experiments concluded that a demagnetization in transition metals can happen within approximately one picosecond [1, 2], later experiments showed that the initial drop in the magnetization occurs at even shorter time scales of less than 100 femtoseconds [3, 4, 5]. However, despite numerous experimental in-depth investigations and several theoretical attempts to describe the observed behavior, the demagnetization process is not yet understood in detail and still highly controversial.

A common way to describe the demagnetization process is to employ a phenomenological three-temperature model, where a temperature is assigned to the electron system, to the spin system, and to the lattice system [6]. Within this model, the heating by a short laser pulse leads, in *3d*-transition metals, to a fast increase in the electronic temperature during the first 100...200 femtoseconds. During the same time, a considerable amount of energy is transferred from the electronic system to the spin system, leading to an increase in the spin temperature, and consequently to a strong drop in the spin-magnetic moment. For times later than ≈ 200 femtoseconds, the energy transfer between the lattice system and the electron and spin system becomes more and more important, and spin-lattice relaxation processes take place, leading to a slow increase in the moment until the thermal equilibrium is reached after 1...2 picoseconds. However, we point out that, even if the three-temperature model describes the observed demagnetization quite well, the underlying microscopic processes are still unclear and a subject of ongoing debate.

In this work, we will focus on the processes that occur during the initial time, i.e. the excitation of the electronic system and the accompanied fast drop in the spin-magnetic moment. As stated before, the increase in the lattice temperature during the initial time is marginal. Hence, even if phonon mediated spin-flip processes might be more important than initially assumed [7], it is reasonable to neglect the

nuclear motion when studying the microscopic processes that occur during the first ≈ 100 femtoseconds. If the nuclei are assumed to be fixed, there are principally only two relevant processes that can considerably change the local moment of an excited system (we use the expression “local moment” because only a certain region of a larger system is usually probed in experiments). First, a fraction of the local moment can be transferred from the heated region into adjacent regions as a result of the time evolution of the locally excited system. This diffusive process was recently modeled via a dynamical scattering approach, known as superdiffuse spin transport, which is based on a difference in the scattering probability between the spin-majority and spin-minority. It was shown that this mechanism can lead to a fast loss in the local moment if an inhomogeneous energy deposition of the laser pulse is assumed, and if a different adjacent material than the probed one is present [8]. A second mechanism that can lead to a significant loss in the moment is a spin-orbit coupling mediated spin-flip process that occurs for excited Coulomb interacting many-electron systems [9, 10]. Note that the latter mechanism takes place even if periodic systems are assumed, in contrast to the first mechanism.

In this work, we will for the first time perform a fully ab-initio investigation into the second mechanism for $3d$ -transition metals. We will assume translational invariant and periodic systems, and we will employ time-dependent density-functional theory [11] to investigate the real-time evolution of excited systems. Note that effects beyond the linear response regime are covered within this framework.

This work is organized in the following way: In chapter 2, we will introduce density-functional theory and its time-dependent extension, which forms the basis for all calculations presented in this work. Furthermore, we will discuss some particularities concerning spin-orbit coupling and the interaction with laser pulses. In chapter 3, we will discuss some theoretical aspects that are specifically related to the dynamics of excited extended spin-magnetic systems, and we present the algorithm that was applied in the calculations. We also introduce a time-dependent density of states as a useful tool for the investigation of excited systems. In chapter 4, the spin-magnetic response of excited bulk iron and bulk nickel, and the response of an excited nickel slab will be studied. Additionally, we will investigate the behavior of the spin-magnetic moment analytically, as well as numerically in detail. Finally, a comparison to experiments will be given.

2. Many-electron systems in intense laser fields

The theoretical description of short-time phenomena of interacting electrons subjected to intense laser fields is a challenging task, since it involves the treatment of several non-trivial problems. In this chapter, these problems will be discussed, and the framework in which they are treated will be introduced. First, the many-body problem will be discussed, and the method to tackle this problem, density-functional theory, will be introduced. Second, the time-dependent generalization of density-functional theory, which allows the study of short-time phenomena of interacting systems, will be introduced. Finally, the theoretical treatment of high-intensity, short laser pulses that interact with electronic systems will be discussed.

2.1. The many-body problem

The fundamental equation that describes the properties of non-relativistic quantum mechanical systems is the many-body Schrödinger equation. This equation treats, in the general case, the coupled motion of electrons and nuclei. In condensed matter physics, one is typically interested in optical or magnetic properties. If the short-time behavior of these properties is of interest, the relevant problem to solve is typically given by the electronic many-body Schrödinger equation, because the mass of the nuclei is much larger than the mass of the electrons, meaning that the nuclear motion can be neglected:

$$i\partial_t|\Psi(t)\rangle = \hat{H}(t)|\Psi(t)\rangle, \quad \text{with} \quad \hat{H}(t) = \hat{T} + \hat{W} + \hat{V}_{\text{ext}}(t). \quad (2.1)$$

$|\Psi(t)\rangle$ is the electronic many-body state and \hat{H} is the Hamiltonian, which is constructed from the kinetic, the electron-electron interaction, and the external potential term:

$$\hat{T} = \sum_{i=1}^N \frac{\hat{p}_i^2}{2}, \quad \hat{W} = \frac{1}{2} \sum_{i \neq j}^N \frac{1}{|\hat{\mathbf{r}}_i - \hat{\mathbf{r}}_j|}, \quad \hat{V}_{\text{ext}}(t) = \sum_{i=1}^N v_{\text{ext}}(\hat{\mathbf{r}}_i, t). \quad (2.2)$$

N is the number of electrons and $v_{\text{ext}}(\mathbf{r}, t)$ is the external single-particle potential, which describes the interaction of the electrons with the nuclear potential, and possibly with an additional time-dependent external potential such as an electric field.

If the external field is time-independent, and if the system is initially in an eigenstate, the solution of equation (2.1) can be reduced to an eigenvalue problem:

$$|\Psi(t)\rangle = e^{-iEt}|\Psi\rangle, \quad \text{with} \quad \hat{H}|\Psi\rangle = E|\Psi\rangle. \quad (2.3)$$

The equation on the right hand side is referred as the time-independent Schrödinger equation. For the solution of this equation, one typically would have to calculate the wave function:

$$\Psi(\mathbf{r}_1, \dots, \mathbf{r}_N) = [\langle \mathbf{r}_1 |_1 \dots \langle \mathbf{r}_N |_N | \Psi \rangle]. \quad (2.4)$$

This wave function is a function of $3N$ variables, which makes it very hard or even impossible to solve equation (2.3), even for a moderate number of electrons.

2.2. Density-functional theory

The difficulty in solving equation (2.3) arises from the electron-electron interaction term \hat{W} . Within the framework of density-functional theory (DFT) it is possible to recast the ground state problem of interacting electrons into a ground state problem of non-interacting electrons, which is much easier to solve.

In the previous discussion we did not consider the electronic spin degrees of freedom explicitly, which is justified for a variety of systems. In the following two sections we will continue to do so. However, whenever one is interested in magnetic properties, the treatment of spin is essential. Thus, in section 2.2.3 the framework of DFT will be generalized to spin-polarized systems.

2.2.1. The Hohenberg-Kohn theorem

The Schrödinger equation (2.3) defines the many-electron ground state for any external potential $v_{\text{ext}}(\mathbf{r})$. The corresponding ground state density $n_0(\mathbf{r})$ follows simply from

$$n_0(\mathbf{r}) = \langle \Psi_0 | \hat{n}(\mathbf{r}) | \Psi_0 \rangle, \quad \text{with} \quad \hat{n}(\mathbf{r}) = \sum_{i=1}^N \delta(\mathbf{r} - \hat{\mathbf{r}}_i). \quad (2.5)$$

Thus, the external potential determines the interacting ground state density:

$$v_{\text{ext}}(\mathbf{r}) \xrightarrow{(2.3)} |\Psi_0\rangle \xrightarrow{(2.5)} n_0(\mathbf{r}). \quad (2.6)$$

The beginning of DFT dates back to 1964 with a publication by Hohenberg and Kohn [12] in which they proved that the map (2.6) is invertible for non-degenerate ground states:

$$v_{\text{ext}}(\mathbf{r}) \xleftarrow{\text{HK}} n_0(\mathbf{r}). \quad (2.7)$$

This unique one-to-one mapping is known today as the Hohenberg-Kohn (HK) theorem. Later it was shown that the inverse of (2.6) can also be established for degenerate ground states [13].

One consequence of this mapping is that each external potential can be understood as a functional of the corresponding ground state density: $v_{\text{ext}}[n_0](\mathbf{r})$. Together with the Schrödinger equation (2.3) it follows that the ground state is

given as a density functional as well: $|\Psi_0[n_0]\rangle$. As a result, each observable quantity of the interacting system can, in principle, be calculated from the ground state density:

$$\langle \hat{O} \rangle = \langle \Psi_0 | \hat{O} | \Psi_0 \rangle = \langle \Psi_0[n_0] | \hat{O} | \Psi_0[n_0] \rangle = O[n_0]. \quad (2.8)$$

From (2.8) it follows immediately that also the ground state energy is a functional of $n_0(\mathbf{r})$:

$$E_0[n_0] = \langle \Psi_0 | \hat{T} + \hat{W} + \hat{V}_{\text{ext}} | \Psi_0 \rangle = T[n_0] + W[n_0] + \int d\mathbf{r} v_{\text{ext}}(\mathbf{r}) n_0(\mathbf{r}), \quad (2.9)$$

where we have defined the interacting kinetic energy functional and the electron-electron interaction functional. In their original work, Hohenberg and Kohn showed, with the help of the Rayleigh-Ritz principle, another important fact:

$$E_0[n_0] < E_0[n], \quad \forall \quad n(\mathbf{r}) \neq n_0(\mathbf{r}). \quad (2.10)$$

This variational property means that the ground state density $n_0(\mathbf{r})$ is the density that minimizes the energy functional $E_0[n]$ for a fixed $v_{\text{ext}}(\mathbf{r})$ ¹. In an actual calculation, the ground state density is typically obtained by using a set of single-particle Schrödinger equations, the so-called Kohn-Sham equations.

2.2.2. The Kohn-Sham equations

In 1965, Kohn and Sham proposed a scheme that allows to calculate an interacting ground state density by using a fictitious system of non-interacting electrons [14]:

$$\left[-\frac{\nabla^2}{2} + v_s(\mathbf{r}) \right] \varphi_i(\mathbf{r}) = \epsilon_i \varphi_i(\mathbf{r}), \quad \text{with} \quad n_s(\mathbf{r}) = \sum_{i=1}^N |\varphi_i(\mathbf{r})|^2. \quad (2.11)$$

The system (2.11), which contains an effective single-particle potential $v_s(\mathbf{r})$ that will be specified later, is called Kohn-Sham (KS) system. The main hypothesis of Kohn and Sham is that one can find a potential $v_s(\mathbf{r})$ such that the density of the KS system and the interacting system is equal: $n_s(\mathbf{r}) = n_0(\mathbf{r})$.

Since the HK theorem (2.7) holds for any particle interaction, the results discussed in the previous section can also be applied to the non-interacting KS system. Thus, the corresponding energy functional is given by

$$E_s[n] = T_s[n] + \int d\mathbf{r} v_s(\mathbf{r}) n(\mathbf{r}), \quad (2.12)$$

where we have defined the non-interacting kinetic energy functional²

$$T_s[n] = -\frac{1}{2} \sum_{i=1}^N \int d\mathbf{r} \varphi_i^*(\mathbf{r}) \nabla^2 \varphi_i(\mathbf{r}). \quad (2.13)$$

¹The actual search for an energy minimum would have to be performed over v -representable densities, i.e. densities that can be obtained via (2.6) for some $v_{\text{ext}}(\mathbf{r})$.

²Note that $T_s[n]$ is calculated from the set of KS orbitals that give the density $n(\mathbf{r})$, according to (2.11).

The ground state density of this system can, according to (2.10), be obtained by solving an Euler-Lagrange equation:

$$\frac{\delta}{\delta n(\mathbf{r})} E_s[n] = \frac{\delta T_s[n]}{\delta n(\mathbf{r})} + v_s(\mathbf{r}) = 0. \quad (2.14)$$

Since the HK theorem, in its original form, is valid for a fixed (integer) particle number, we must make sure that the density variation conserves the number of electrons N .

Now we go back to the interacting system and we define the Hartree energy functional

$$E_H[n] = \frac{1}{2} \int d\mathbf{r} \int d\mathbf{r}' \frac{n(\mathbf{r}) n(\mathbf{r}')}{|\mathbf{r} - \mathbf{r}'|}, \quad (2.15)$$

and the exchange-correlation (xc) energy functional

$$E_{xc}[n] = (T[n] - T_s[n]) + (W[n] - E_H[n]). \quad (2.16)$$

With these definitions we can write the interacting energy functional (2.9) as

$$E_0[n] = T_s[n] + E_H[n] + E_{xc}[n] + \int d\mathbf{r} v_{\text{ext}}(\mathbf{r}) n(\mathbf{r}). \quad (2.17)$$

The ground state density of the interacting system can again be obtained by variation via an Euler-Lagrange equation, which gives

$$\frac{\delta T_s[n]}{\delta n(\mathbf{r})} + \frac{\delta E_H[n]}{\delta n(\mathbf{r})} + \frac{\delta E_{xc}[n]}{\delta n(\mathbf{r})} + v_{\text{ext}}(\mathbf{r}) = 0. \quad (2.18)$$

When we compare now equation (2.18) with the Euler-Lagrange equation of the KS system (2.14), and when we assume that both equations give the same density, we can identify the effective single-particle potential to be

$$v_s(\mathbf{r}) = v_s[n](\mathbf{r}) = v_{\text{ext}}(\mathbf{r}) + v_H[n](\mathbf{r}) + v_{xc}[n](\mathbf{r}). \quad (2.19)$$

Here we have defined the Hartree and the xc potential by

$$v_H[n](\mathbf{r}) = \frac{\delta E_H[n]}{\delta n(\mathbf{r})} = \int d\mathbf{r}' \frac{n(\mathbf{r}')}{|\mathbf{r} - \mathbf{r}'|}, \quad v_{xc}[n](\mathbf{r}) = \frac{\delta E_{xc}[n]}{\delta n(\mathbf{r})}. \quad (2.20)$$

We conclude that the solution of the KS system (2.11) with the effective single-particle potential (2.19) will give the same ground state density as the interacting system.

In practice, the KS equations have to be solved iteratively since the density calculated from this system enters the effective potential $v_s[n](\mathbf{r})$. We reemphasize that the KS system is not a physical system, it is rather a fictitious system that allows to indirectly solve the Euler-Lagrange equation (2.18), which leads to the exact interacting ground state density. Once the KS system is solved, the exact interacting ground state energy can be obtained via (2.17).

In all derivations above we have assumed that we have the exact $E_{xc}[n]$ and hence $v_{xc}[n](\mathbf{r})$. Unfortunately, the exact form of these functionals is not known, and in practice they have to be approximated (see section 2.2.5).

2.2.3. Extensions of DFT

In section 2.2.1 the formal basis of DFT was discussed, and in section 2.2.2 the KS system, which allows to calculate the ground state density in practice, was introduced. If one is interested in spin-dependent phenomena, especially in the spin magnetization $\mathbf{m}(\mathbf{r})$, one can in principle calculate the latter as a functional of the density, $\mathbf{m}(\mathbf{r}) = \mathbf{m}[n](\mathbf{r})$, as guaranteed by the HK theorem (2.8). Since functionals like $\mathbf{m}[n](\mathbf{r})$ are largely unknown, the treatment of spins via a corresponding extension of the KS scheme is essential. Over the years, many extensions to the previously shown DFT framework appeared. We will, however, in the following discuss only those extensions that are related to magnetism.

In 1972, von Barth and Hedin [15] proved an unique relationship between the ground state and the density and magnetization, assumed that an external potential and magnetic field is present:

$$v_{\text{ext}}(\mathbf{r}), \mathbf{B}_{\text{ext}}(\mathbf{r}) : |\Psi_0\rangle \longleftrightarrow n(\mathbf{r}), \mathbf{m}(\mathbf{r}). \quad (2.21)$$

This unique mapping allows it to establish a HK-like variational principle (see (2.10)), and, in the same way as shown in the section before, a KS system that gives the exact ground state density and magnetization can be derived. Note that such a spin density-functional theory (SDFT) treats only the coupling of the spins to the external \mathbf{B} -field. In practice it turned out that the application of SDFT is very useful when dealing with spin-polarized ground states (even in cases where the external \mathbf{B} -field is zero).

SDFT is only justified if the coupling of the magnetic field to the spins is much stronger than the coupling to the orbital currents. If the opposite is the case, a current density-functional theory (CDFT) has to be applied. The theoretical foundation of such a CDFT was provided in 1987 by Vignale and Rasolt [16]. Note that the current density couples to the vector potential in CDFT.

If one wants to treat both, the coupling of the magnetic field to the spins and to the orbital currents, a current- and spin-density-functional theory or even a spin-current density-functional theory (SCDFT) would be needed [17, 18, 19]. In the following we will derive the KS equations for a system where both couplings are present. We will investigate this KS scheme in more detail because the previously discussed CDFT and SDFT can be seen as a special case of SCDFT. Furthermore, the form of the coupling of the different densities and current densities to the external fields will become more clear.

Definitions

Before we start to derive the KS equation for SCDFT, we will define some important quantities which will be used in the following and throughout the whole

work. First, we define the magnetization operator ³

$$\hat{\mathbf{m}}(\mathbf{r}) = \sum_{i=1}^N \hat{\boldsymbol{\sigma}}_i \delta(\mathbf{r} - \hat{\mathbf{r}}_i) \quad \text{with} \quad \hat{\boldsymbol{\sigma}}_i = \begin{pmatrix} \hat{\sigma}_{1,i} \\ \hat{\sigma}_{2,i} \\ \hat{\sigma}_{3,i} \end{pmatrix}, \quad (2.22)$$

which has a similar form as the density operator (2.5), with the difference that the vector of Pauli-spin operators appears. The index i runs over all electrons. One usually works in the two-dimensional spinor space, in which the Pauli-spin operators are represented by the Pauli-matrices:

$$\underline{\underline{\sigma}}_1 = \begin{pmatrix} 0 & 1 \\ 1 & 0 \end{pmatrix}, \quad \underline{\underline{\sigma}}_2 = \begin{pmatrix} 0 & -i \\ i & 0 \end{pmatrix}, \quad \underline{\underline{\sigma}}_3 = \begin{pmatrix} 1 & 0 \\ 0 & -1 \end{pmatrix}, \quad (2.23)$$

and in which the single-particle states are represented by two-component wave functions:

$$\underline{\varphi}(\mathbf{r}) = \begin{pmatrix} \varphi^\uparrow(\mathbf{r}) \\ \varphi^\downarrow(\mathbf{r}) \end{pmatrix}. \quad (2.24)$$

Next, we define the paramagnetic (subscript ‘‘p’’) and diamagnetic (subscript ‘‘d’’) current density operator:

$$\hat{\mathbf{j}}_p(\mathbf{r}) = \sum_{i=1}^N \frac{1}{2} \{\delta(\mathbf{r} - \hat{\mathbf{r}}_i), \hat{\mathbf{p}}_i\}, \quad \hat{\mathbf{j}}_d(\mathbf{r}) = \frac{1}{c} \mathbf{A}_{\text{ext}}(\mathbf{r}) \hat{n}(\mathbf{r}). \quad (2.25)$$

In the same way as the density, the current density can be extended by the spin degree of freedom, which defines the paramagnetic ⁴ and diamagnetic spin-current density operator:

$$\hat{\mathbf{j}}_p^u(\mathbf{r}) = \sum_{i=1}^N \frac{1}{2} \hat{\sigma}_{u,i} \{\delta(\mathbf{r} - \hat{\mathbf{r}}_i), \hat{\mathbf{p}}_i\}, \quad \hat{\mathbf{j}}_d^u(\mathbf{r}) = \frac{1}{c} \mathbf{A}_{\text{ext}}(\mathbf{r}) \hat{m}_u(\mathbf{r}), \quad u = \{1, 2, 3\}. \quad (2.26)$$

Instead of this notation, one commonly finds the spin-current tensor notation in the literature. The spin-current tensor operators are 3×3 matrices that are constructed by the vectors from (2.26) via

$$\hat{J}_{p,uv}(\mathbf{r}) = \hat{\mathbf{j}}_p^u(\mathbf{r}) \Big|_v, \quad \hat{J}_{d,uv}(\mathbf{r}) = \hat{\mathbf{j}}_d^u(\mathbf{r}) \Big|_v, \quad (2.27)$$

(note that $\mathbf{j}|_v$ stands for the v th component of vector \mathbf{j}). Most of the time we will use the spin-current density notation, since it allows a more intuitive interpretation: each spin-current density vector describes the flow of the probability of finding the system in the spin-up and spin-down channels of the corresponding spin-projection. However, from time to time we will use the spin-current tensor notation because this allows, in some cases, a more compact notation.

³Note that a common definition uses the prefactor $g_e \mu_B / 2$ which is $\approx -1/2$ in *a.u.* (with the gyromagnetic ratio $g_e \approx -2$, and with the Bohr magneton $\mu_B = 1/2$).

⁴A common definition uses the prefactor $g_e \mu_B / 2$.

Up to now we have defined only operators. The actual observables follow, as usual, from the expectation values, i.e. the magnetization follows from $\mathbf{m}(\mathbf{r}) = \langle \hat{\mathbf{m}}(\mathbf{r}) \rangle$, the paramagnetic current density follows from $\mathbf{j}_p(\mathbf{r}) = \langle \hat{\mathbf{j}}_p(\mathbf{r}) \rangle$, and so on. We emphasize that the physical current densities, i.e. the gauge invariant current densities, follow from the sum of the paramagnetic and diamagnetic terms, e.g.: $\mathbf{j}(\mathbf{r}) = \mathbf{j}_p(\mathbf{r}) + \mathbf{j}_d(\mathbf{r})$.

Spin-polarized systems are generally distinguished by two types: systems in which the direction of the magnetization is always parallel in space, and systems for which the direction of the magnetization changes in space. The former are called collinear systems and the latter are called non-collinear systems:

$$\mathbf{m}(\mathbf{r}) \parallel \mathbf{m}(\mathbf{r}') \iff \text{collinear}, \quad \mathbf{m}(\mathbf{r}) \not\parallel \mathbf{m}(\mathbf{r}') \iff \text{non-collinear}. \quad (2.28)$$

A general discussion and a detailed derivation of the densities and current densities is given in appendix A.1.

A KS scheme for SCDFT

In the following we will derive a KS scheme for SCDFT. We will present this framework in detail, because we will discover later in this work that the application of a time-dependent extension of such a framework would most probably be needed for a proper description of spin-dynamics in solids. Additionally, the SCDFT that will be derived in the following will include spin-orbit coupling (SOC). A proper treatment of SOC is of particular importance for the study of spin-dynamics, as will be found out later in this work as well. Moreover, the derivation that is provided in the following illustrates how the different external fields couple to the different local DFT variables.

For the derivation of the SCDFT scheme, we will follow the route that is provided in [20]. The starting point is the many-electron Hamiltonian

$$\begin{aligned} \hat{H} = \sum_{i=1}^N & \left[\frac{1}{2} \left(\hat{\mathbf{p}}_i + \frac{1}{c} \mathbf{A}_{\text{ext}}(\hat{\mathbf{r}}_i) \right)^2 + v_{\text{ext}}(\hat{\mathbf{r}}_i) + \frac{1}{2c} \hat{\boldsymbol{\sigma}}_i \cdot \mathbf{B}_{\text{ext}}(\hat{\mathbf{r}}_i) \right. \\ & \left. + \frac{1}{4c^2} \hat{\boldsymbol{\sigma}}_i \cdot \left(\nabla v_{\text{ext}}(\hat{\mathbf{r}}_i) \times \hat{\mathbf{p}}_i \right) \right] + \frac{1}{2} \sum_{i \neq j}^N \frac{1}{|\hat{\mathbf{r}}_i - \hat{\mathbf{r}}_j|}, \end{aligned} \quad (2.29)$$

which includes a current coupling to an external vector-potential. This coupling is accomplished by replacing the canonical momentum in the kinetic term with the gauge invariant momentum:

$$\hat{\mathbf{p}} \longrightarrow \hat{\mathbf{p}} + \frac{1}{c} \mathbf{A}(\hat{\mathbf{r}}). \quad (2.30)$$

This replacement is usually called minimal coupling. In addition, a coupling of the spins to an external \mathbf{B} -field is present, which is called Zeeman coupling⁵. Note that both fields have to be related via $\mathbf{B}_{\text{ext}} = \nabla \times \mathbf{A}_{\text{ext}}$. Furthermore, the

⁵Both, the minimal coupling and the Zeeman term are components of the Pauli-Hamiltonian, which follows from the non-relativistic limit of the Dirac equation [21].

Hamiltonian contains a one-particle SOC term⁶ which couples the spin-currents to ∇v_{ext} . (Note that the replacement (2.30) is neglected in the SOC term, because the SOC energy contribution coming from \mathbf{A}_{ext} is assumed to be very small.) Whether this form of SOC is actually a justified choice will be discussed in the next section. For now we can think of this term as an approximation in the inclusion of relativistic effects.

With the density and current operator definitions (2.22) to (2.27) the Hamiltonian (2.29) can be rewritten as

$$\begin{aligned} \hat{H} = & \hat{T} + \hat{W} + \int d\mathbf{r} v_{\text{ext}}(\mathbf{r}) \hat{n}(\mathbf{r}) + \int d\mathbf{r} \frac{1}{c} \mathbf{A}_{\text{ext}}(\mathbf{r}) \cdot \hat{\mathbf{j}}_{\text{p}}(\mathbf{r}) + \int d\mathbf{r} \frac{1}{2c^2} A_{\text{ext}}^2(\mathbf{r}) \hat{n}(\mathbf{r}) \\ & + \int d\mathbf{r} \frac{1}{2c} \mathbf{B}_{\text{ext}}(\mathbf{r}) \cdot \hat{\mathbf{m}}(\mathbf{r}) + \int d\mathbf{r} \sum_{u,v=1}^3 \overset{\leftrightarrow}{V}_{\text{SO},uv}(\mathbf{r}) \overset{\leftrightarrow}{J}_{\text{p},uv}(\mathbf{r}), \end{aligned} \quad (2.31)$$

where we have defined the SOC matrix

$$\overset{\leftrightarrow}{V}_{\text{SO}}(\mathbf{r}) = \frac{1}{4c^2} \begin{pmatrix} 0 & -\partial_{r_3} v_{\text{ext}}(\mathbf{r}) & \partial_{r_2} v_{\text{ext}}(\mathbf{r}) \\ \partial_{r_3} v_{\text{ext}}(\mathbf{r}) & 0 & -\partial_{r_1} v_{\text{ext}}(\mathbf{r}) \\ -\partial_{r_2} v_{\text{ext}}(\mathbf{r}) & \partial_{r_1} v_{\text{ext}}(\mathbf{r}) & 0 \end{pmatrix}. \quad (2.32)$$

For a Hamiltonian of this type, a HK-like variational principle can also be established [20]. As a consequence, the KS approach to solve the ground state problem can be applied as well. The derivation of the KS equations would follow the same route as shown previously. The only difference to sections (2.2.1) and (2.2.2), where the central problem was described by only one variable (the density $n(\mathbf{r})$), is that we have to deal now with 16 variables: the density $n(\mathbf{r})$, the 3 components of $\mathbf{m}(\mathbf{r})$, the 3 components of $\mathbf{j}_{\text{p}}(\mathbf{r})$ and the 9 components of $\overset{\leftrightarrow}{J}_{\text{p}}(\mathbf{r})$.

With the definitions (2.13), (2.15) and (2.16), the interacting ground state energy functional is given by

$$\begin{aligned} E_0[n, \mathbf{m}, \mathbf{j}_{\text{p}}, \overset{\leftrightarrow}{J}_{\text{p}}] = & T_{\text{s}}[n, \mathbf{m}, \mathbf{j}_{\text{p}}, \overset{\leftrightarrow}{J}_{\text{p}}] + E_{\text{H}}[n] + E_{\text{xc}}[n, \mathbf{m}, \mathbf{j}_{\text{p}}, \overset{\leftrightarrow}{J}_{\text{p}}] \\ & + \int d\mathbf{r} \left(v_{\text{ext}}(\mathbf{r}) + \frac{1}{2c^2} A_{\text{ext}}^2(\mathbf{r}) \right) n(\mathbf{r}) + \int d\mathbf{r} \frac{1}{c} \mathbf{A}_{\text{ext}}(\mathbf{r}) \cdot \mathbf{j}_{\text{p}}(\mathbf{r}) \\ & + \int d\mathbf{r} \frac{1}{2c} \mathbf{B}_{\text{ext}}(\mathbf{r}) \cdot \mathbf{m}(\mathbf{r}) + \int d\mathbf{r} \sum_{u,v=1}^3 \overset{\leftrightarrow}{V}_{\text{SO},uv}(\mathbf{r}) \overset{\leftrightarrow}{J}_{\text{p},uv}(\mathbf{r}), \end{aligned} \quad (2.33)$$

which is a functional of all 16 variables. Instead of directly minimizing this functional, we can again solve a KS system:

$$\left(\frac{1}{2} \left[\hat{\mathbf{p}} + \frac{1}{c} \mathbf{A}_{\text{s}}(\mathbf{r}) \right]^2 + v_{\text{s}}(\mathbf{r}) + \frac{1}{2c} \underline{\underline{\boldsymbol{\sigma}}} \cdot \mathbf{B}_{\text{s}}(\mathbf{r}) + \sum_{u,v=1}^3 \overset{\leftrightarrow}{V}_{\text{s},uv}(\mathbf{r}) \underline{\underline{\sigma}}_u \hat{p}_v \right) \varphi_i(\mathbf{r}) = \epsilon_i \varphi_i(\mathbf{r}), \quad (2.34)$$

⁶This form of SOC arises from the Dirac equation after a Foldy-Wouthuysen transformation and the non-relativistic limit [21].

which is defined in such a way that it gives the exact 16 ground state variables of the interacting system. The associated effective single-particle fields follow from the functional derivatives of (2.33) with respect to all 16 variables:

$$\begin{aligned} v_s(\mathbf{r}) &= v_{\text{ext}}(\mathbf{r}) + v_H(\mathbf{r}) + v_{\text{xc}}(\mathbf{r}) + \frac{1}{2c^2} (A_{\text{ext}}^2(\mathbf{r}) - A_s^2(\mathbf{r})), \\ \mathbf{A}_s(\mathbf{r}) &= \mathbf{A}_{\text{ext}}(\mathbf{r}) + \mathbf{A}_{\text{xc}}(\mathbf{r}), \\ \mathbf{B}_s(\mathbf{r}) &= \mathbf{B}_{\text{ext}}(\mathbf{r}) + \mathbf{B}_{\text{xc}}(\mathbf{r}), \\ \overleftrightarrow{V}_s(\mathbf{r}) &= \overleftrightarrow{V}_{\text{SO}}(\mathbf{r}) + \overleftrightarrow{V}_{\text{xc}}(\mathbf{r}). \end{aligned} \quad (2.35)$$

The xc fields have been defined by:

$$\mathbf{A}_{\text{xc}}(\mathbf{r}) = c \frac{\delta E_{\text{xc}}}{\delta \mathbf{j}_p(\mathbf{r})}, \quad \mathbf{B}_{\text{xc}}(\mathbf{r}) = 2c \frac{\delta E_{\text{xc}}}{\delta \mathbf{m}(\mathbf{r})}, \quad \overleftrightarrow{V}_{\text{xc}, uv}(\mathbf{r}) = \frac{\delta E_{\text{xc}}}{\delta \overleftrightarrow{J}_p, uv(\mathbf{r})}. \quad (2.36)$$

The $v_H(\mathbf{r})$ and $v_{\text{xc}}(\mathbf{r})$ follow from (2.20). Note that all xc fields, and consequently all effective single-particle fields, are functionals of all 16 variables, since $E_{\text{xc}} = E_{\text{xc}}[n, \mathbf{m}, \mathbf{j}_p, \overleftrightarrow{J}_p]$.

In conclusion, equations (2.34) to (2.36) define the KS system for SCDFT that gives the exact interacting ground state variables $n(\mathbf{r})$, $\mathbf{m}(\mathbf{r})$, $\mathbf{j}_p(\mathbf{r})$, and $\overleftrightarrow{J}_p(\mathbf{r})$. Note that the KS system, or more precisely the definitions (2.36), use the paramagnetic currents as variables. Therefore, the effective single-particle fields are not gauge invariant. However, once a gauge is chosen this no longer constitutes a problem [19].

2.2.4. A modified SDFT scheme with spin-orbit coupling

The main concern of this work is the investigation of spin-dynamics. We will see later in this work that a proper treatment of SOC is of particular importance for this subject. One way how SOC could be included into a SDFT scheme was shown in the previous section, where we have derived a SCDFT framework. In this section, we will focus on the case where the coupling of the magnetic field to the orbital currents can be neglected (note that the same assumption is made in standard SDFT), but where SOC has non-negligible contributions. From the discussion in the previous section one might think that one would need 13 variables to describe the corresponding SDFT framework, namely the density $n(\mathbf{r})$, the magnetization $\mathbf{m}(\mathbf{r})$, and the spin-current tensor $\overleftrightarrow{J}_p(\mathbf{r})$. Contrary to this, we will propose in this section a modified SDFT scheme that incorporates SOC, and that is based on only 4 variables. The consideration of this modified SDFT scheme has several motivations, as we will discuss in the following paragraphs.

First, we point out that the previously discussed SCDFT scheme has no Hartree contribution in the SOC term of the KS equations (see (2.35) and (2.36)). In practice, however, one commonly finds that a Hartree potential is present in the SOC term of the KS equations, and one might wonder if this is actually justified. (The appearance of the Hartree term results from the fact that the applied KS equations follow from the non-relativistic limit of relativistic DFT. At this point, we

wish to mention that the non-relativistic limit approach is, for a proper description of the spin, not straightforward. We will come back to this issue at the end of this section.) For the SDFT scheme that will be derived in this section, we will see that the Hartree term in SOC arises naturally, and we will see that this term should, in fact, be present (since it represents a many-electron SOC interaction that gives, in the time-dependent case, a non-negligible contribution to the spin-dynamics, as we will see later in this work).

As a second point, we want to emphasize that the SDFT scheme that will be derived is based on a non-relativistic many-electron Hamiltonian (as usual for most of the DFT schemes). This has the advantage that exact properties of the xc fields can easily be derived and discussed (this subject will become more clear in section 3.1.5, where we will discuss the properties of the xc \mathbf{B} -field for a time-dependent SDFT that includes SOC). Moreover, the KS equations that will be derived will have a similar form to the equations that have been applied in the calculations of this work. Hence, the equations applied in the calculations could be seen, in a sense, as an approximation to the SDFT framework that is discussed here. However, we point out that no functionals exist for the proposed SDFT scheme, and that the functionals that have been applied in the calculations follow, in principle, from standard SDFT (thus, care should be taken concerning the interpretation as an approximation).

Finally, we wish to mention that we will refer to the proposed SDFT framework (and its time-dependent extension, respectively) in several places later in this work. We will do this mainly due to the fact that the proposed framework can serve as formally exact SDFT that includes SOC. This allows it to draw some general conclusions that should apply to any SDFT scheme that includes SOC contributions.

The starting point of our considerations is the following many-electron Hamiltonian:

$$\hat{H} = \hat{T} + \hat{W} + \sum_{i=1}^N \left[v_{\text{ext}}(\hat{\mathbf{r}}_i) + \frac{1}{4c^2} \hat{\boldsymbol{\sigma}}_i \cdot \left(\nabla v_{\text{ext}}(\hat{\mathbf{r}}_i) \times \hat{\mathbf{p}}_i \right) + \frac{1}{2c} \hat{\boldsymbol{\sigma}}_i \cdot \mathbf{B}_{\text{ext}}(\hat{\mathbf{r}}_i) \right]. \quad (2.37)$$

We see that we have a Zeeman term and SOC, but we neglect the coupling of the magnetic field to the orbital currents. Additionally, we have an electron-electron interaction \hat{W} , whose exact form will be specified later. For now, we only demand that \hat{W} does not depend on any external field. All following steps are related to the derivation of a proper KS scheme that gives the same magnetization as a system with the Hamiltonian (2.37).

In order to proceed with the next steps, we will ask the following preliminary questions: The Hamiltonian (2.37) contains the same external potential in the ordinary density coupling term, and in the SOC term. Is it possible to write these two terms as only one term that contains a coupling to one density? And if yes, is it possible to derive a reasonable DFT framework with this density as variable? In the following we will show that both questions can be answered with yes.

First of all, we note that the SOC operator can be rewritten to a form where

we have a local coupling to the external potential:

$$\sum_{i=1}^N \frac{1}{4c^2} \hat{\boldsymbol{\sigma}}_i \cdot \left(\nabla v_{\text{ext}}(\hat{\mathbf{r}}_i) \times \hat{\mathbf{p}}_i \right) = -\frac{1}{4c^2} \int d\mathbf{r} v_{\text{ext}}(\mathbf{r}) \sum_{i=1}^3 (\nabla_{\mathbf{r}} \times \hat{\mathbf{j}}_p^i(\mathbf{r})) \cdot \mathbf{e}_i, \quad (2.38)$$

where we have used the definition (2.26). A detailed derivation of relation (2.38) is given in appendix A.6.2. As a consequence of (2.38) it makes sense to define the following operator:

$$\hat{\gamma}(\mathbf{r}) = \hat{n}(\mathbf{r}) - \frac{1}{4c^2} \sum_{i=1}^3 (\nabla_{\mathbf{r}} \times \hat{\mathbf{j}}_p^i(\mathbf{r})) \cdot \mathbf{e}_i, \quad (2.39)$$

which is constructed from the ordinary density operator, and from a contraction of the curl of the spin-current density operators. With the new defined operator $\hat{\gamma}(\mathbf{r})$, and with relation (2.38), we can now write the Hamiltonian (2.37) as

$$\hat{H} = \hat{T} + \hat{W} + \int d\mathbf{r} v_{\text{ext}}(\mathbf{r}) \hat{\gamma}(\mathbf{r}) + \int d\mathbf{r} \frac{1}{2c} \mathbf{B}_{\text{ext}}(\mathbf{r}) \cdot \hat{\mathbf{m}}(\mathbf{r}). \quad (2.40)$$

The important result of (2.40) is that we have represented our many-electron Hamiltonian in a form where only the operator $\hat{\gamma}(\mathbf{r})$ couples locally to the external potential. Moreover, the Hamiltonian (2.40) has, in principle, the same form as the many-electron Hamiltonian that is used in the derivation of the standard SDFT framework (see e.g. [22]). Hence, $\gamma(\mathbf{r}) = \langle \hat{\gamma}(\mathbf{r}) \rangle$, which can be seen as an effective density⁷, plays here the same role as $n(\mathbf{r})$ in standard SDFT. In fact, it is straightforward to establish a HK-like variational principle for a system with the Hamiltonian (2.40) and with $\gamma(\mathbf{r})$ and $\mathbf{m}(\mathbf{r})$ as basic variables. One simply has to follow the steps from the SDFT derivation and one has to replace $n(\mathbf{r})$ by $\gamma(\mathbf{r})$.

So far we have not said anything specific about the interaction term \hat{W} . In fact, it should be possible to establish a HK-like variational principle for any interaction term, as long as it represents a pure electron-electron interaction. As a next step, we will show the interaction term that will be considered in the following, and furthermore, we will argue why we choose this term:

$$\hat{W} = \frac{1}{2} \sum_{i \neq j}^N \frac{1}{|\hat{\mathbf{r}}_i - \hat{\mathbf{r}}_j|} + \frac{1}{4c^2} \sum_{i \neq j}^N \hat{\boldsymbol{\sigma}}_i \cdot \left(\nabla_{\hat{\mathbf{r}}_i} \frac{1}{|\hat{\mathbf{r}}_i - \hat{\mathbf{r}}_j|} \times \hat{\mathbf{p}}_i \right). \quad (2.41)$$

The first term on the right hand side is the usual Coulomb term which is, from the energy point of view, the most important electron-electron interaction term. The second term is an electron-electron SOC term. This term follows, in addition to other terms, from quantum electrodynamics by taking the non-relativistic limit up to the order $1/c^2$ [23].

At this point we wish to reemphasize that we are interested in the spin properties. Hence, the electron-electron SOC term, which is a direct spin-coupling term that could give non-negligible spin contributions, might have to be taken into

⁷Note that the integral over the curl part vanishes, which gives: $\int d\mathbf{r} \gamma(\mathbf{r}) = N$.

account, even if its energy contribution is much smaller than the energy contribution from the Coulomb term. Moreover, we point out that the SOC term from (2.41) is in principle similar to the one particle SOC term from (2.37), with the difference that the electron spin i sees the electric field produced by all other electrons $\sum_j \nabla_{\mathbf{r}_i} 1/|\mathbf{r}_i - \mathbf{r}_j|$, rather than the external electric field $\nabla v_{\text{ext}}(\mathbf{r}_i)$. Thus, if the one-particle SOC term becomes important, also the many-electron SOC term should be taken into account. In the next paragraphs, we will discuss one more point that is related to the many-electron SOC term and that concerns the Hartree term. The effective many-electron Hamiltonian that is derived in [23] contains two more spin-coupling terms of the order $1/c^2$, namely a spin-orbital-current-coupling term, and a spin-spin-coupling term, which will be neglected here.

As usual for most of the DFT schemes, the interaction will be absorbed into the xc functional. Typically, the xc functional is not known and it has to be approximated. Hence, the xc functional is usually formulated such that its numerical value is as small as possible. In standard DFT, this is achieved by subtracting the Hartree energy from the interaction energy (see (2.16)). At this point, we wish to mention that the Hartree energy can be understood as the classical analog of the electron-electron Coulomb interaction energy. In the following we will follow the same route: First, we will calculate a Hartree-like energy, and it will turn out that this energy can also be understood as the classical analog of the interaction energy. Next, we will use this energy to define a reasonable xc energy.

Calculating the Hartree energy in the usual way, but now with our new variable $\gamma(\mathbf{r})$, gives

$$\begin{aligned} E_{\text{H}}[\gamma] &= \frac{1}{2} \int d\mathbf{r} \int d\mathbf{r}' \frac{\gamma(\mathbf{r})\gamma(\mathbf{r}')}{|\mathbf{r} - \mathbf{r}'|} \\ &= E_{\text{H}}[n] - \frac{1}{4c^2} \int d\mathbf{r} \int d\mathbf{r}' \sum_{i=1}^3 (\nabla_{\mathbf{r}} \times \mathbf{j}_{\text{p}}^i(\mathbf{r})) \cdot \mathbf{e}_i \frac{n(\mathbf{r}')}{|\mathbf{r} - \mathbf{r}'|} \\ &+ \frac{1}{32c^4} \int d\mathbf{r} \int d\mathbf{r}' \sum_{i,j=1}^3 \frac{(\nabla_{\mathbf{r}} \times \mathbf{j}_{\text{p}}^i(\mathbf{r})) \cdot \mathbf{e}_i (\nabla_{\mathbf{r}'} \times \mathbf{j}_{\text{p}}^j(\mathbf{r}')) \cdot \mathbf{e}_j}{|\mathbf{r} - \mathbf{r}'|}. \end{aligned} \quad (2.42)$$

The first term on the right hand side is the usual Hartree term. As already stated, this term can be understood as the classical analog of the Coulomb interaction term, i.e. as the analog of the first term from (2.41). In a similar manner, the second term from (2.42) can be identified as the classical analog of the many-electron SOC term from (2.41). This becomes more obvious when we rewrite these two terms. Rewriting the second term of (2.42) gives

$$\frac{1}{4c^2} \int d\mathbf{r} \int d\mathbf{r}' \sum_{i=1}^3 \left(\nabla_{\mathbf{r}} \frac{n(\mathbf{r}')}{|\mathbf{r} - \mathbf{r}'|} \times \mathbf{j}_{\text{p}}^i(\mathbf{r}') \right) \cdot \mathbf{e}_i, \quad (2.43)$$

while rewriting the second term from (2.41) leads to

$$\frac{1}{4c^2} \sum_{j \neq k}^N \int d\mathbf{r} \int d\mathbf{r}' \sum_{i=1}^3 \left(\nabla_{\mathbf{r}} \frac{\delta(\mathbf{r}' - \hat{\mathbf{r}}_k)}{|\mathbf{r} - \mathbf{r}'|} \times \hat{\sigma}_{i,j} \frac{1}{2} \{ \delta(\mathbf{r} - \hat{\mathbf{r}}_j), \hat{\mathbf{p}}_j \} \right) \cdot \mathbf{e}_i. \quad (2.44)$$

The last term in (2.42) has no corresponding interaction term (this term probably corresponds to a higher order interaction term). However, since this term is of the order $1/c^4$, its contribution should be negligible.

With the Hartree energy (2.42) we can now define the xc energy:

$$\tilde{E}_{\text{xc}}[\gamma, \mathbf{m}] = (T[\gamma, \mathbf{m}] - T_{\text{s}}[\gamma, \mathbf{m}]) + (\tilde{W}[\gamma, \mathbf{m}] - E_{\text{H}}[\gamma]), \quad (2.45)$$

and write down the energy functional as

$$E_0[\gamma, \mathbf{m}] = T_{\text{s}}[\gamma, \mathbf{m}] + E_{\text{H}}[\gamma] + \tilde{E}_{\text{xc}}[\gamma, \mathbf{m}] + \int d\mathbf{r} v_{\text{ext}}(\mathbf{r})\gamma(\mathbf{r}) + \int d\mathbf{r} \frac{1}{2c} \mathbf{B}_{\text{ext}}(\mathbf{r}) \cdot \mathbf{m}(\mathbf{r}), \quad (2.46)$$

where $T_{\text{s}}[\gamma, \mathbf{m}]$ is, as usual, the non-interacting kinetic energy functional. In the same way as discussed in the previous sections, the $\gamma(\mathbf{r})$ and $\mathbf{m}(\mathbf{r})$ that minimize (2.46) can also be obtained by solving a non-interacting KS system:

$$\left(\frac{\hat{p}^2}{2} + v_{\text{s}}(\mathbf{r}) + \frac{1}{4c^2} \underline{\underline{\boldsymbol{\sigma}}} \cdot [\nabla v_{\text{s}}(\mathbf{r}) \times \hat{\mathbf{p}}] + \frac{1}{2c} \underline{\underline{\boldsymbol{\sigma}}} \cdot \mathbf{B}_{\text{s}}(\mathbf{r}) \right) \underline{\varphi}_i(\mathbf{r}) = \epsilon_i \underline{\varphi}_i(\mathbf{r}), \quad (2.47)$$

with $i = 1, \dots, N$. Here we have used the spinor representation (2.23) and (2.24), and we have decomposed the γ -coupling term into the density coupling and the SOC term. The effective potentials follow from the functional derivatives of (2.46):

$$\begin{aligned} v_{\text{s}}[\gamma, \mathbf{m}](\mathbf{r}) &= v_{\text{ext}}(\mathbf{r}) + v_{\text{H}}[\gamma](\mathbf{r}) + v_{\text{xc}}[\gamma, \mathbf{m}](\mathbf{r}), \\ \mathbf{B}_{\text{s}}[\gamma, \mathbf{m}](\mathbf{r}) &= \mathbf{B}_{\text{ext}}(\mathbf{r}) + \mathbf{B}_{\text{xc}}[\gamma, \mathbf{m}](\mathbf{r}), \end{aligned} \quad (2.48)$$

with the Hartree potential

$$v_{\text{H}}[\gamma](\mathbf{r}) = \int d\mathbf{r}' \frac{\gamma(\mathbf{r}')}{|\mathbf{r} - \mathbf{r}'|} = v_{\text{H}}[n](\mathbf{r}) - \frac{1}{4c^2} \int d\mathbf{r}' \sum_{i=1}^3 \frac{(\nabla_{\mathbf{r}'} \times \mathbf{j}_{\text{p}}^i(\mathbf{r}')) \cdot \mathbf{e}_i}{|\mathbf{r} - \mathbf{r}'|}, \quad (2.49)$$

and the xc fields

$$v_{\text{xc}}[\gamma, \mathbf{m}](\mathbf{r}) = \frac{\delta \tilde{E}_{\text{xc}}[\gamma, \mathbf{m}]}{\delta \gamma(\mathbf{r})}, \quad \mathbf{B}_{\text{xc}}[\gamma, \mathbf{m}](\mathbf{r}) = 2c \frac{\delta \tilde{E}_{\text{xc}}[\gamma, \mathbf{m}]}{\delta \mathbf{m}(\mathbf{r})}. \quad (2.50)$$

To summarize, the equations (2.47) to (2.50) define a KS scheme for SDFT that includes SOC, and that leads to the same ground state magnetization $\mathbf{m}(\mathbf{r})$ as an interacting system with the Hamiltonian (2.37). Note that the system would, however, not give the interacting ground state density $n(\mathbf{r})$, it would rather give the interacting effective density $\gamma(\mathbf{r})$, defined by (2.39).

The KS equations (2.47) contain the same effective potential in the density coupling term and the SOC term (this results from the fact that we have derived the KS scheme with $\gamma(\mathbf{r})$ as basic variable). We emphasize in particular that the SOC term in the KS equations contains the Hartree potential (2.49) (note that this Hartree potential has in principle two contributions: the usual density Hartree term, and a spin-current Hartree term which should be much smaller due to the factor $1/c^2$). This Hartree SOC term, or more precisely its density Hartree part, corresponds to a many-electron SOC contribution. This can for example be

seen by calculating the corresponding KS expectation value, which leads to the expression (2.43).

The KS equations applied in the calculations of this work are very similar to the equations (2.47). However, the functionals that have been applied are based on standard SDFT, and they are different to the functionals (2.50). Furthermore, the usual density Hartree potential was used, and some additional relativistic corrections, such as the mass-velocity and the Darwin term, were applied in the calculations (the framework that has been applied followed the route provided in [24]). We will explain the applied KS equations in more detail in section 3.1.3 and 3.2. The approximate functionals that have been applied will be introduced in the following section.

As a last point, we wish to mention that there also exists a relativistic generalization of DFT (RDFT) [25, 26]. A set of KS equations similar to (2.47) can, within this framework, also be derived by taking the non-relativistic limit of a set of relativistic KS Dirac equations [27]. However, we want to emphasize one important point: the standard RDFT framework is constructed in such a way that it uses the four-current (i.e. the density and current density) as basic variable, and not the magnetization. Thus, the corresponding non-relativistic limit would not necessarily lead directly to the exact magnetization (directly meaning simply from the KS expectation value), and the corresponding KS equations would probably not be applicable for our concerns in a straightforward way. There exists, in fact, a spin extension of RDFT [28], which could be the starting point for a non-relativistic limit approach. We will, however, not discuss any further details here, since it is beyond the scope of this work.

In conclusion, we derived a SDFT KS framework that incorporates SOC effects. In contrary to the usual approach, where the non-relativistic limit of the RDFT framework is taken, we started from a non-relativistic many-electron Hamiltonian containing single- and many-electron SOC contributions. The resulting KS equations are very similar to the equations that follow from the non-relativistic limit of RDFT, however, the functionals are different. At the moment, it is not clear whether this difference has any significant consequences at all. Hence, this issue should be further investigated in future work. Furthermore, we showed that the Hartree SOC term (which is commonly present in KS schemes that contain SOC) corresponds to a many-electron SOC interaction. In order to discuss exact properties of KS schemes that include SOC contributions, we will refer later to this proposed framework.

2.2.5. Approximate functionals

One important ingredient in all of the different KS schemes discussed before is the xc energy functional. As already mentioned, the form of these functionals is in general not known and they have to be approximated. The oldest and most popular approximation for standard DFT is the local density approximation (LDA):

$$E_{\text{xc}}^{\text{LDA}}[n] = \int d\mathbf{r} e_{\text{xc}}^{\text{hom}}(n(\mathbf{r})), \quad (2.51)$$

where $e_{\text{xc}}^{\text{hom}}(n)$ is the xc energy density of the homogeneous electron gas with density n . The $e_{\text{xc}}^{\text{hom}}(n)$ can be separated into an exchange part, which is analytically known, and into a correlation part, which has been calculated by Monte-Carlo methods [29] and parameterized in convenient ways [30].

Over the years, a vast number of approximations for the xc energy functionals and potentials appeared [31]. In the following we will, however, only discuss the spin-polarized generalization of the LDA, the so-called local spin-density approximation (LSDA), because the xc functionals applied in this work are based on this approximation.

The LSDA is, within the SDFE framework, commonly used for the calculation of spin-polarized systems. In SDFE, one typically works with the spin-density matrix, which is defined by the density and magnetization via

$$\underline{\underline{\rho}}(\mathbf{r}) = \frac{1}{2} \begin{pmatrix} n(\mathbf{r}) + m_3(\mathbf{r}) & m_1(\mathbf{r}) - im_2(\mathbf{r}) \\ m_1(\mathbf{r}) + im_2(\mathbf{r}) & n(\mathbf{r}) - m_3(\mathbf{r}) \end{pmatrix}. \quad (2.52)$$

Note that working with $\underline{\underline{\rho}}(\mathbf{r})$ is equivalent to working with the set $(n(\mathbf{r}), \mathbf{m}(\mathbf{r}))$, because both are uniquely related.

At first we consider a collinear system and we assume that $\mathbf{B}_{\text{ext}}(\mathbf{r})$ is parallel to \mathbf{e}_3 (this choice is always possible for collinear systems). As a consequence, only $n(\mathbf{r})$ and $m_3(\mathbf{r})$ are needed as basic variables, meaning that the corresponding SDFE has only $v_{\text{xc}}(\mathbf{r})$ and $B_{\text{xc},3}(\mathbf{r})$ as xc fields. Since the $B_{\text{xc},3}(\mathbf{r})$ couples only to $\underline{\underline{\sigma}}_3$, the corresponding two-component spinor KS equations decouple in two regular equations for the spin-up and spin-down components, respectively. As a result, the $v_{\text{xc}}(\mathbf{r})$ and $B_{\text{xc},3}(\mathbf{r})$ act together as one local potential for each spin-component:

$$v_{\text{xc},\uparrow}(\mathbf{r}) = v_{\text{xc}}(\mathbf{r}) + \frac{1}{2c} B_{\text{xc},3}(\mathbf{r}), \quad v_{\text{xc},\downarrow}(\mathbf{r}) = v_{\text{xc}}(\mathbf{r}) - \frac{1}{2c} B_{\text{xc},3}(\mathbf{r}). \quad (2.53)$$

Moreover, the spin-density matrix has, for collinear systems, only diagonal elements, which are usually represented in the following notation:

$$n^\uparrow(\mathbf{r}) = \frac{1}{2}(n(\mathbf{r}) + m_3(\mathbf{r})), \quad n^\downarrow(\mathbf{r}) = \frac{1}{2}(n(\mathbf{r}) - m_3(\mathbf{r})). \quad (2.54)$$

The LSDA xc energy functional for collinear systems is given by

$$E_{\text{xc}}^{\text{LSDA}}[n^\uparrow, n^\downarrow] = \int d\mathbf{r} e_{\text{xc}}^{\text{hom}}(n^\uparrow(\mathbf{r}), n^\downarrow(\mathbf{r})), \quad (2.55)$$

where $e_{\text{xc}}^{\text{hom}}(n^\uparrow, n^\downarrow)$ is the xc energy density of the spin-polarized homogeneous electron gas with the spin-densities n^\uparrow and n^\downarrow . As for LDA, the exchange part of $e_{\text{xc}}^{\text{hom}}(n^\uparrow, n^\downarrow)$ is known analytically, while the correlation part has been calculated by Monte-Carlo techniques [32] and parameterized in several ways [33]. The corresponding xc potentials follow from the functional derivative:

$$v_{\text{xc},\alpha}^{\text{LSDA}}[n^\uparrow, n^\downarrow](\mathbf{r}) = \frac{\delta E_{\text{xc}}^{\text{LSDA}}}{\delta n^\alpha(\mathbf{r})} = \left. \frac{\partial e_{\text{xc}}^{\text{hom}}(\bar{n}^\uparrow, \bar{n}^\downarrow)}{\partial \bar{n}^\alpha} \right|_{\bar{n}^\alpha = n^\alpha(\mathbf{r})}, \quad \alpha = \{\uparrow, \downarrow\}. \quad (2.56)$$

The previously discussed LSDA can only be applied in collinear systems. The usual way to generalize the LSDA to non-collinear systems is to treat each point

in space as a collinear system [34]. This means in practice that for each point in space the spinor system is rotated by a unitary transformation such that the spin-density matrix is diagonal:

$$\underline{\underline{\rho}}(\mathbf{r}) \longrightarrow \underline{\underline{\tilde{\rho}}}(\mathbf{r}) = \underline{\underline{U}}(\mathbf{r})\underline{\underline{\rho}}(\mathbf{r})\underline{\underline{U}}^\dagger(\mathbf{r}) = \begin{pmatrix} \tilde{n}^\uparrow(\mathbf{r}) & 0 \\ 0 & \tilde{n}^\downarrow(\mathbf{r}) \end{pmatrix}. \quad (2.57)$$

As a next step, the xc potential (2.56) is applied, which gives a local xc matrix that is diagonal:

$$\underline{\underline{\tilde{v}}}_{\text{xc}}[\tilde{n}^\uparrow, \tilde{n}^\downarrow](\mathbf{r}) = \begin{pmatrix} v_{\text{xc},\uparrow}^{\text{LSDA}}[\tilde{n}^\uparrow, \tilde{n}^\downarrow](\mathbf{r}) & 0 \\ 0 & v_{\text{xc},\downarrow}^{\text{LSDA}}[\tilde{n}^\uparrow, \tilde{n}^\downarrow](\mathbf{r}) \end{pmatrix}. \quad (2.58)$$

Finally, the unitary matrix from (2.57) is used to rotate the xc matrix back, which gives a non-diagonal xc matrix:

$$\underline{\underline{\tilde{v}}}_{\text{xc}}[\tilde{n}^\uparrow, \tilde{n}^\downarrow](\mathbf{r}) \longrightarrow \underline{\underline{v}}_{\text{xc}}[n, \mathbf{m}](\mathbf{r}) = \underline{\underline{U}}^\dagger(\mathbf{r})\underline{\underline{\tilde{v}}}_{\text{xc}}(\mathbf{r})\underline{\underline{U}}(\mathbf{r}). \quad (2.59)$$

In the usual formulation of non-collinear SDFT, a $v_{\text{xc}}(\mathbf{r})$ and a $\mathbf{B}_{\text{xc}}(\mathbf{r})$ is used instead of a xc matrix. By evaluating the matrix $\underline{\underline{U}}(\mathbf{r})$, one finds that $\underline{\underline{v}}_{\text{xc}}(\mathbf{r})$ can be separated and brought into the usual form, which finally gives

$$\begin{aligned} v_{\text{xc}}^{\text{LSDA}}[n, \mathbf{m}](\mathbf{r}) &= \frac{1}{2} \left(v_{\text{xc},\uparrow}^{\text{LSDA}}[\tilde{n}^\uparrow, \tilde{n}^\downarrow](\mathbf{r}) + v_{\text{xc},\downarrow}^{\text{LSDA}}[\tilde{n}^\uparrow, \tilde{n}^\downarrow](\mathbf{r}) \right), \\ \mathbf{B}_{\text{xc}}^{\text{LSDA}}[n, \mathbf{m}](\mathbf{r}) &= c \left(v_{\text{xc},\uparrow}^{\text{LSDA}}[\tilde{n}^\uparrow, \tilde{n}^\downarrow](\mathbf{r}) - v_{\text{xc},\downarrow}^{\text{LSDA}}[\tilde{n}^\uparrow, \tilde{n}^\downarrow](\mathbf{r}) \right) \frac{\mathbf{m}(\mathbf{r})}{|\mathbf{m}(\mathbf{r})|}. \end{aligned} \quad (2.60)$$

All calculations that are presented in this work used the previously discussed LSDA for the xc functionals:

$$v_{\text{xc}}(\mathbf{r}) = v_{\text{xc}}^{\text{LSDA}}[n, \mathbf{m}](\mathbf{r}), \quad \mathbf{B}_{\text{xc}}(\mathbf{r}) = \mathbf{B}_{\text{xc}}^{\text{LSDA}}[n, \mathbf{m}](\mathbf{r}). \quad (2.61)$$

2.3. Time-dependent DFT

2.3.1. Fundamental theorems and the time-dependent KS scheme

The Runge-Gross theorem

At the heart of DFT lies the HK theorem, which establishes an one-to-one mapping between the external potential and the ground state density of an interacting many-electron system. In 1984, Runge and Gross extended this theorem to time-dependent situations [11], i.e. they proved an one-to-one correspondence between time-dependent external potentials, $v_{\text{ext}}(\mathbf{r}, t)$, and the corresponding time-dependent interacting many-electron densities $n(\mathbf{r}, t) = \langle \Psi(t) | \hat{n}(\mathbf{r}) | \Psi(t) \rangle$. This mapping is known today as the Runge-Gross (RG) theorem, and it forms the fundamental basis for time-dependent DFT (TDDFT).

In their proof, Runge and Gross showed that two densities, $n(\mathbf{r}, t)$ and $n'(\mathbf{r}, t)$, which evolve from a many-electron state $|\Psi_0\rangle$ under the potentials $v_{\text{ext}}(\mathbf{r}, t)$ and

$v'_{\text{ext}}(\mathbf{r}, t)$, are always different, assuming that the potentials differ by more than a purely time-dependent function:

$$v_{\text{ext}}(\mathbf{r}, t) \neq v'_{\text{ext}}(\mathbf{r}, t) + c(t) \xrightarrow{\text{RG}} n(\mathbf{r}, t) \neq n'(\mathbf{r}, t). \quad (2.62)$$

Hence, the time-dependent density uniquely determines the external potential up to a purely function of time. From the time-dependent Schrödinger equation (2.1) follows in turn that also the time-dependent many-electron state is uniquely determined by the density (and the initial state) up to a time-dependent phase factor, which can be neglected since it has no physical meaning: $|\Psi(t)\rangle = |\Psi[n, \Psi_0](t)\rangle$. As a consequence, all observable many-electron quantities can, in principle, also be calculated from the corresponding time-dependent density:

$$\langle \hat{O} \rangle(t) = \langle \Psi(t) | \hat{O} | \Psi(t) \rangle = \langle \Psi[n, \Psi_0](t) | \hat{O} | \Psi[n, \Psi_0](t) \rangle = O[n, \Psi_0](t). \quad (2.63)$$

When the system is in the ground state for $t = 0$, the functional dependence on $|\Psi_0\rangle$ vanishes by means of the HK theorem: $|\Psi_0\rangle = |\Psi_0[n_0]\rangle$, meaning that all observables can, in principle, be calculated from the time-dependent density alone.

The van Leeuwen theorem

The time-dependent density of the interacting many-electron system is the central variable in TDDFT, and the RG theorem establishes the one-to-one mapping between $v_{\text{ext}}(\mathbf{r}, t)$ and $n(\mathbf{r}, t)$. The RG theorem does, however, not tell us how to actually obtain the density. As a practical scheme, one could apply a time-dependent version of the KS scheme, i.e. one could use a fictitious non-interacting system to obtain $n(\mathbf{r}, t)$. However, if such a system (or more precisely a non-interacting potential) actually exists is not clear a priori. This so-called v-representability problem was solved in 1999 by van Leeuwen [35].

In his proof, van Leeuwen showed that each time-dependent density $n(\mathbf{r}, t)$, produced from a system with interaction \hat{W} that evolves according to (2.1) from an initial state $|\Psi_0\rangle$ under a potential $v(\mathbf{r}, t)$, can always be obtained by a system with a different interaction \hat{W}' that evolves under $v'(\mathbf{r}, t)$ from the initial state $|\Psi'_0\rangle$. It was shown that the potential $v'(\mathbf{r}, t)$ is uniquely determined (up to a purely time-dependent function) by the initial states, the interactions, $n(\mathbf{r}, t)$, and $v(\mathbf{r}, t)$, while the two initial states are restricted to have the same density and its time derivative:

$$\begin{aligned} \left(|\Psi_0\rangle, \hat{W}, v(\mathbf{r}, t) \right) &\xrightarrow{(2.1)} n(\mathbf{r}, t) \xrightarrow{\text{v.L.}} \left(|\Psi'_0\rangle, \hat{W}' \right) : v'(\mathbf{r}, t), \\ \left(|\Psi_0\rangle, |\Psi'_0\rangle \right) &\longrightarrow \left(n(\mathbf{r}, 0), \partial_t n(\mathbf{r}, 0) \right). \end{aligned} \quad (2.64)$$

We will refer to this unique relation as the van Leeuwen theorem.

We will now consider two special cases: First, we assume that $\hat{W} = \hat{W}'$ and that $|\Psi_0\rangle = |\Psi'_0\rangle$. The van Leeuwen theorem then states that there exists an unique $v'(\mathbf{r}, t)$ that yields $n(\mathbf{r}, t)$, which is exactly the statement of the RG theorem. Thus, the RG theorem emerges as a special case from the van Leeuwen theorem.

Second, we consider that $\hat{W}' = 0$, i.e. we choose the primed system to be non-interacting, and we assume that a corresponding non-interacting state $|\Phi_0\rangle$ exists that has the same density and its time derivative as $|\Psi_0\rangle$. The van Leeuwen theorem then tells us that there exists a unique single-particle potential $v_s(r, t)$ (up to a purely time-dependent constant which has no physical meaning) that gives the same density as the interacting system. This solves the v-representability problem and builds the basis for the application of the time-dependent KS scheme.

The time-dependent KS scheme

As discussed previously, the van Leeuwen theorem guarantees that the time-dependent density of an interacting system can be obtained by a non-interacting system, which is called time-dependent KS system. The system evolves in an effective single-particle potential $v_s(\mathbf{r}, t)$. From the van Leeuwen theorem it follows that this potential depends (for a given external potential) on the initial interacting state $|\Psi_0\rangle$, the initial non-interacting state $|\Phi_0\rangle$, and the density:

$$v_s(\mathbf{r}, t) = v_s[\Psi_0, \Phi_0, n](\mathbf{r}, t). \quad (2.65)$$

If the system starts to evolve from the ground state, which is the case for all calculations in this work, the HK theorem applies at $t = 0$. As a consequence, $|\Psi_0\rangle$ and $|\Phi_0\rangle$ are determined by $n(\mathbf{r}, 0)$, and the time-dependent effective potential is in turn given as a functional of the density alone: $v_s[n](\mathbf{r}, t)$.

The time-dependent KS system is given by

$$\partial_t \varphi_i(\mathbf{r}, t) = \left[-\frac{\nabla^2}{2} + v_s(\mathbf{r}) \right] \varphi_i(\mathbf{r}, t), \quad \text{with} \quad n(\mathbf{r}, t) = \sum_{i=1}^N |\varphi_i(\mathbf{r}, t)|^2, \quad (2.66)$$

and $i = \{1, \dots, N\}$. N is the number of electrons, and the $\varphi_i(\mathbf{r}, t)$ are called time-dependent KS orbitals. The single-particle potential is defined in the same way as for the ground state case:

$$v_s[n](\mathbf{r}, t) = v_{\text{ext}}(\mathbf{r}, t) + \int d\mathbf{r}' \frac{n(\mathbf{r}', t)}{|\mathbf{r} - \mathbf{r}'|} + v_{\text{xc}}[n](\mathbf{r}, t). \quad (2.67)$$

The term in the middle on the right hand side is the usual Hartree potential, which is calculated at each time from the instantaneous density. The term on the right hand side is the time-dependent xc potential, which is a functional that depends in general on the whole history of $n(\mathbf{r}, t)$.

The equations (2.66) and (2.67), together with the van Leeuwen theorem, can be seen as the definition of $v_{\text{xc}}[n](\mathbf{r}, t)$. A variational principle similar to that used in the ground state to obtain the xc potential can not be used in the time-dependent case, since the energy is in general not conserved. There exists, however, an analogous principle, namely the stationary principle of the quantum mechanical action, that can be used to define $v_{\text{xc}}[n](\mathbf{r}, t)$ [36]. Similarly to the ground state, the time-dependent xc potential is not known and it has to be approximated. In section 2.3.3 we will briefly discuss the approximations that are typically used.

We conclude that the KS system (2.66) will lead to the exact interacting density, assumed that the exact $v_{xc}[n](\mathbf{r}, t)$ is applied. Nevertheless, all time-dependent observables of the interacting systems that are not trivially related to the density, are in general not easily accessible via the KS system. Rather, they would have to be calculated by density functionals, as argued in (2.63).

2.3.2. Extensions of TDDFT

Analogous to ground state DFT, several extensions for TDDFT have appeared over the years. For example, TDDFT has been extended to spin-polarized systems [37]. In this time-dependent spin-DFT (TDSDF) the system couples to $v_{\text{ext}}(\mathbf{r}, t)$ and $\mathbf{B}_{\text{ext}}(\mathbf{r}, t)$, and the corresponding KS system will give the interacting $n(\mathbf{r}, t)$ and $\mathbf{m}(\mathbf{r}, t)$. TDDFT has also been extended to time-dependent current-DFT (TDCDFT) [38], where the system couples to a vector potential $\mathbf{A}_{\text{ext}}(\mathbf{r}, t)$, and where the current density $\mathbf{j}(\mathbf{r}, t)$ is the basic variable. We will discuss the TDCDFT later in more detail, because the calculations presented in this work also applied a coupling to a time-dependent external \mathbf{A} -field (in fact, we applied a certain approximation from the TDCDFT framework as will be discussed later).

TDDFT has also been extended to the full relativistic case of coupled electron and electromagnetic field dynamics. It was shown that, under reasonable conditions, the full quantum electrodynamics problem can be described by a coupled system of KS Dirac equations and a Maxwell equation [39, 40]. The basic variables of this theory are the four-current and the four-potential, meaning that this theory would give the exact time-dependent density and current density, since $j^\mu(\mathbf{r}, t) = (n(\mathbf{r}, t), \mathbf{j}(\mathbf{r}, t))$.

Furthermore, we wish to mention that it is not an uncommon practice to use a certain extension of TDDFT in numerical simulations, although the rigorous existence proof, for example of the van Leeuwen theorem type, does not exist. This has for example been done for time-dependent spin-current DFT [41], for which, nevertheless, approximate functionals already exist [42]. The calculations presented in this work also follow this route, since they correspond, in a sense, to a time-dependent generalization of SDF that includes SOC contributions (i.e. we could, for example, think of a generalization of the SDF framework from section 2.2.4). We will discuss the applied framework and the approximate xc potentials in more detail in section 3.1.2.

TDCDFT

Below, we will discuss the formal framework of TDCDFT. We will investigate the corresponding equations in some detail to allow us to understand what terms were neglected and approximated in the calculations of this work. We will discuss this subject in detail in section 3.1.3.

We consider a many-electron system with interaction \hat{W} in a time-dependent external electromagnetic field, described by the Hamiltonian

$$\hat{H}(t) = \sum_{i=1}^N \frac{1}{2} \left[\hat{\mathbf{p}}_i + \frac{1}{c} \mathbf{A}(\hat{\mathbf{r}}_i, t) \right]^2 + \hat{W}. \quad (2.68)$$

Note that there is no local potential $v(\mathbf{r}, t)$ present in (2.68). This form of $\hat{H}(t)$ can always be obtained with a gauge transformation (see appendix A.3) by choosing the gauge field $\Lambda(\mathbf{r}, t)$ such that $\partial_t \Lambda(\mathbf{r}, t) = -v(\mathbf{r}, t)$.

In 2004, Vignale showed a van Leeuwen theorem type proof for systems which are described by the Hamiltonian of type (2.68), which laid the basis for a KS approach to TDCDFE [43]. In his proof, he showed that each time-dependent current $\mathbf{j}(\mathbf{r}, t)$, produced from a system with interaction \hat{W} that evolves from an initial state $|\Psi_0\rangle$ under a vector potential $\mathbf{A}(\mathbf{r}, t)$, can always be obtained by a system with a different interaction \hat{W}' that evolves under $\mathbf{A}'(\mathbf{r}, t)$ from the initial state $|\Psi'_0\rangle$. It was shown that the vector potential $\mathbf{A}'(\mathbf{r}, t)$ is uniquely determined by the initial states, the interactions, $\mathbf{j}(\mathbf{r}, t)$, and $\mathbf{A}(\mathbf{r}, t)$, while the two initial states are restricted to have the same density and current density:

$$\begin{aligned} \left(|\Psi_0\rangle, \hat{W}, \mathbf{A}(\mathbf{r}, t) \right) &\longrightarrow \mathbf{j}(\mathbf{r}, t) \longrightarrow \left(|\Psi'_0\rangle, \hat{W}' \right) : \mathbf{A}'(\mathbf{r}, t), \\ \left(|\Psi_0\rangle, |\Psi'_0\rangle \right) &\longrightarrow \left(n(\mathbf{r}, 0), \mathbf{j}(\mathbf{r}, 0) \right). \end{aligned} \quad (2.69)$$

From this proof we can in principle obtain similar conclusions as discussed for the van Leeuwen theorem. Of particular importance is the conclusion for $\hat{W}' = 0$, which states that the exact interacting current density can be obtained by a non-interacting system, i.e. a KS system of the form:

$$\partial_t \varphi_i(\mathbf{r}, t) = \frac{1}{2} \left[\hat{\mathbf{p}} + \frac{1}{c} \mathbf{A}_s(\mathbf{r}, t) \right]^2 \varphi_i(\mathbf{r}, t). \quad (2.70)$$

From the continuity equation it is clear that we also have the exact time-dependent density if we have the exact $\mathbf{j}(\mathbf{r}, t)$ and $n(\mathbf{r}, 0)$:

$$\partial_t n(\mathbf{r}, t) = -\nabla \cdot \mathbf{j}(\mathbf{r}, t) \longrightarrow n(\mathbf{r}, t) = n(\mathbf{r}, 0) - \int_0^t dt' \nabla \cdot \mathbf{j}(\mathbf{r}, t'). \quad (2.71)$$

We will now assume that the system starts to evolve from the ground state. Hence, the system is, according to CDFE, for $t = 0$ completely described by $n(\mathbf{r}, 0) = n_0(\mathbf{r})$ and $\mathbf{j}(\mathbf{r}, 0)$. Thus, the vector potential of the KS equation is a functional of the ground state density and the time-dependent current density: $\mathbf{A}_s(\mathbf{r}, t) = \mathbf{A}_s[n_0, \mathbf{j}](\mathbf{r}, t)$.

We will now bring the KS equations (2.70) to a somewhat different form, that is sometimes found in literature. First, we decompose the effective vector potential into the external potential and the residual term (which corresponds to the interactions), which will be further decomposed into its transversal and longitudinal component (see appendix A.4):

$$\mathbf{A}_s(\mathbf{r}, t) = \mathbf{A}_{\text{ext}}(\mathbf{r}, t) + \mathbf{A}(\mathbf{r}, t) = \mathbf{A}_{\text{ext}}(\mathbf{r}, t) + \mathbf{A}_T(\mathbf{r}, t) + \mathbf{A}_L(\mathbf{r}, t). \quad (2.72)$$

Next, we gauge away the longitudinal component of \mathbf{A} (which can always be done, see appendix A.3). This leads to a local potential, which is then decomposed into the usual Hartree term and a residual local potential, which will be defined as the xc potential:

$$\text{gauge: } \nabla \Lambda(\mathbf{r}, t) = -\frac{1}{c} \mathbf{A}_L(\mathbf{r}, t) \longrightarrow \partial_t \Lambda(\mathbf{r}, t) = v_H(\mathbf{r}, t) + v_{\text{xc}}(\mathbf{r}, t). \quad (2.73)$$

With these gauge relations, and by labeling \mathbf{A}_T as $\mathbf{A}_{xc,T}$, we get the following KS equation:

$$\begin{aligned} \partial_t \varphi_i(\mathbf{r}, t) = & \left(\frac{1}{2} \left[\hat{\mathbf{p}} + \frac{1}{c} \mathbf{A}_{\text{ext}}(\mathbf{r}, t) + \frac{1}{c} \mathbf{A}_{xc,T}[n_0, \mathbf{j}](\mathbf{r}, t) \right]^2 \right. \\ & \left. + v_H[n](\mathbf{r}, t) + v_{xc}[n_0, \mathbf{j}](\mathbf{r}, t) \right) \varphi_i(\mathbf{r}, t). \end{aligned} \quad (2.74)$$

Here we have explicitly shown the functional dependencies. Note that this equation is equivalent to equation (2.70), i.e. with an equation of the form (2.74), an exact interacting current density can always be obtained. Finally, we wish to mention that, in the same way as shown before, parts of the $\mathbf{A}_{\text{ext}}(\mathbf{r}, t)$ could also be gauged away. This could, for example, be done for the part of $\mathbf{A}_{\text{ext}}(\mathbf{r}, t)$ that contains a static nuclear potential, which would give an additional $v_{\text{ext}}(\mathbf{r})$.

2.3.3. Approximate functionals

The time-dependent KS system (2.66) is defined such that it gives the exact time-dependent interacting density. Similar to ground state DFT, the crucial ingredient is the xc potential, defined in (2.67), which is not known and which has to be approximated. If the system starts to evolve from the ground state, the xc potential is given solely as a functional of the time-dependent density: $v_{xc}[n](\mathbf{r}, t)$. The functional dependence on the density is in general such that v_{xc} depends on the whole history, i.e. it depends on $n(\mathbf{r}, t')$ for all $t' \leq t$.

The approximation usually applied in TDDFT is the so-called adiabatic approximation. In this approximation, the dependence on the history is ignored, and the exact ground state xc potential $v_{xc}^0[n](\mathbf{r})$ is applied with the instantaneous density:

$$v_{xc}^A[n](\mathbf{r}, t) = v_{xc}^0[n_0](\mathbf{r}) \Big|_{n_0(\mathbf{r})=n(\mathbf{r},t)}. \quad (2.75)$$

If the system would evolve infinitesimally slow in time, it would, according to the adiabatic theorem, always remain in the ground state. In this case, the adiabatic approximation would, according to ground state DFT, become exact. However, the exact ground state xc potential is also not known and it has, on top of the adiabatic approximation, also to be approximated. The most famous approximation uses the LDA (2.51), and it is called adiabatic LDA (ALDA):

$$v_{xc}^{\text{ALDA}}[n](\mathbf{r}, t) = \frac{d e_{xc}^{\text{hom}}(\bar{n})}{d \bar{n}} \Big|_{\bar{n}=n(\mathbf{r},t)}. \quad (2.76)$$

The ALDA seems to be a very crude approximation, because it reduces the general functional to a functional that is local in space and time. However, it has been shown that the ALDA performs very well in the calculation of excitation energies for finite systems. Unfortunately, this is not generally the case in solids, where the ALDA has known problems to describe the correct excitation energies [44].

The adiabatic approximation can, in the same manner as shown before, also be applied to the extensions of TDDFT. The xc functionals used in this work are

based on the adiabatic LSDA (ALSDA) for collinear systems, as defined in (2.60):

$$\begin{aligned} v_{\text{xc}}^{\text{ALSDA}}[n, \mathbf{m}](\mathbf{r}, t) &= v_{\text{xc}}^{\text{LSDA}}[\bar{n}, \bar{\mathbf{m}}](\mathbf{r}) \Big|_{\substack{\bar{n}(\mathbf{r})=n(\mathbf{r},t) \\ \bar{\mathbf{m}}(\mathbf{r})=\mathbf{m}(\mathbf{r},t)}}, \\ \mathbf{B}_{\text{xc}}^{\text{ALSDA}}[n, \mathbf{m}](\mathbf{r}, t) &= \mathbf{B}_{\text{xc}}^{\text{LSDA}}[\bar{n}, \bar{\mathbf{m}}](\mathbf{r}) \Big|_{\substack{\bar{n}(\mathbf{r})=n(\mathbf{r},t) \\ \bar{\mathbf{m}}(\mathbf{r})=\mathbf{m}(\mathbf{r},t)}}. \end{aligned} \quad (2.77)$$

2.4. Interaction with laser pulses

In the previous section we introduced TDDFT as a framework to study the dynamics of many-electron system subjected to time-dependent potentials. For a full description of the interaction of electrons with laser pulses, i.e. with photon fields, the framework of quantum electrodynamics would have to be invoked. However, if the number of photons is large enough, or more specific, if the photon density ρ_{ph} fulfills $\rho_{\text{ph}} \gg 1/\lambda^3$, with the wavelength λ , the photon field can be described by classical fields [45]. In this work, we will deal with optical laser pulses with peak intensities of $I_0 \geq 10^{12} \text{W/cm}^2$, for which $\rho_{\text{ph}} \gg 1/\lambda^3$ holds. Therefore, it is justified to describe the photon field by a classical field together with the corresponding TDDFT to study the interaction of the laser pulses with many-electron systems.

2.4.1. Ultrashort laser pulses

One of the most important tools for the microscopic investigation and manipulation of matter is certainly the laser. Over the years, laser technology has experienced tremendous progress. Today, it is possible to create laser pulses of very high intensities, which are very short in time ($T < 1 \text{fs}$), and whose electric field can almost be shaped arbitrarily [46].

Laser radiation can be described classically by the source-free Maxwell equations. Instead of solving the Maxwell equations in the \mathbf{E} - and \mathbf{B} -field representation, one typically uses the equivalent description via the vector potential $\mathbf{A}(\mathbf{r}, t)$, and the scalar potential $\phi(\mathbf{r}, t)$. A solution of the source-free Maxwell equations in vacuum is given by plane waves for the vector potential, together with $\phi(\mathbf{r}, t) = 0$ [47]. Thus, a short laser pulse can be represented as a superposition of vector field plane waves:

$$\mathbf{A}(\mathbf{r}, t) = \epsilon \int dk \tilde{A}(k) e^{ik(\mathbf{n}\cdot\mathbf{r}-ct)} \quad \text{with} \quad \epsilon \perp \mathbf{n}, \quad \phi(\mathbf{r}, t) = 0. \quad (2.78)$$

ϵ is the polarization vector, which has to be perpendicular to the vector of the propagation direction \mathbf{n} , c is the speed of light, and k is the absolute value of the

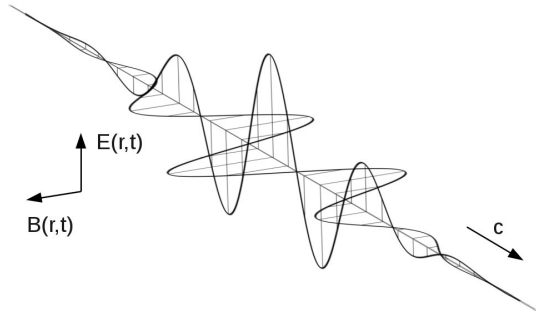


Fig. 2.1.: \mathbf{E} - and \mathbf{B} -field of a free propagating plane wave pulse corresponding to (2.78).

wave vector that is related to the wavelength via $k = 2\pi/\lambda$. For the solution (2.78) the constant dispersion relation $\omega = ck$ was used, meaning that a propagation in vacuum was assumed. In practice, however, laser pulses usually propagate through air, in which the dispersion relation is not constant, and where the pulses would in fact disperse. Since the dimensions of the quantum mechanical systems under study are assumed to be small compared to the optical wave lengths of the laser pulse, the radiation field in the region of our system can be assumed to be dispersion free and thus properly described by the solution (2.78).

The pulse (2.78) is a so-called linear polarized pulse, meaning that the corresponding electric field oscillates in only one direction. The \mathbf{E} - and \mathbf{B} -field follow from the usual relations:

$$\mathbf{E}(\mathbf{r}, t) = -\nabla\phi(\mathbf{r}, t) - \frac{1}{c}\partial_t\mathbf{A}(\mathbf{r}, t), \quad \text{and} \quad \mathbf{B}(\mathbf{r}, t) = \nabla \times \mathbf{A}(\mathbf{r}, t), \quad (2.79)$$

which gives for (2.78) an \mathbf{E} -field that is parallel to the \mathbf{A} -field, and a \mathbf{B} -field that has the same shape and phase as the \mathbf{E} -field, but which is perpendicular to \mathbf{A} and \mathbf{n} (see figure 2.1). Since the \mathbf{E} - and \mathbf{B} -field are perpendicular to the propagation direction \mathbf{n} , such pulses are called transverse wave pulses.

The solution (2.78) is a plane wave solution, i.e. we have wave fronts that have an infinite dimension perpendicular to the propagation direction \mathbf{n} . A more physical description of a short pulse would be given by a Gaussian beam, which is also a solution of the free Maxwell equations. The Gaussian beam has an intensity profile perpendicular to the propagation direction that behaves like a Gaussian function [48]. This intensity profile allows to define a radius of a laser beam⁸. However, since the dimension of the systems under study is typically much smaller than the radius of a laser beam, the description of the radiation field by (2.78) is justified.

A laser pulse is typically characterized by its \mathbf{E} -field. An important quantity is the intensity of the electric field, which is given by $I = E^2c/8\pi$, and which gives, for commonly used units, the following relation: $I[W/cm^2] = 3.51 \cdot 10^{16} E^2[a.u.]$. Finally, we wish to mention an important constraint for the electric field of a free pulse [48]: $\int dt \mathbf{E}(\mathbf{r}, t) = 0$. This constraint means that the DC component of the electric field (which is $\tilde{\mathbf{E}}(\mathbf{r}, \omega \rightarrow 0) = \lim_{\omega \rightarrow 0} \int dt e^{i\omega t} \mathbf{E}(\mathbf{r}, t)$) must vanish in order to describe an electric field with finite energy.

2.4.2. The dipole approximation

The dipole approximation (DA) is a commonly used approximation whenever one studies small systems in radiation fields. In literature one often finds the following statement as the definition of the DA: the dimension of the system is small compared to the wave length of the radiation, therefore the \mathbf{A} -field can be assumed to be purely time-dependent: $\mathbf{A}(t)$. As a consequence, occasionally one argues that the corresponding \mathbf{B} -field is, with respect to relation (2.79), zero, and therefore no Zeeman term should be present. In the following we will show that the

⁸The radius of a Gaussian laser beam is defined as the transverse distance in which the peak intensity I_0 falls to I_0/e^2 .

DA (which is, de facto, generally defined via a mathematical expression) in fact keeps the Zeeman term. We will see that the argument of the small dimension of the system is not the starting point of this approximation, it is rather one condition that has to be fulfilled in order to justify the application of the the DA.

In the following we will assume a radiation field of the form (2.78) with $\boldsymbol{\epsilon} = \mathbf{e}_1$ and $\mathbf{n} = \mathbf{e}_3$. We will further define the purely time-dependent \mathbf{A} -, \mathbf{E} - and \mathbf{B} -field by the field that would be seen by an observer sitting at $\mathbf{r} = 0$:

$$\mathbf{A}(t) = \mathbf{e}_1 a(t), \quad \text{with} \quad a(t) = \int dk \tilde{A}(k) e^{-ikct}, \quad \text{and}$$

$$\mathbf{E}(t) = \mathbf{e}_1 b(t), \quad \mathbf{B}(t) = \mathbf{e}_2 b(t), \quad \text{with} \quad b(t) = \int dk ik \tilde{A}(k) e^{-ikct}. \quad (2.80)$$

Moreover, we will choose the coordinate system such that $\langle \hat{\mathbf{r}} \rangle(t=0) = 0$. The following discussion investigates the Zeeman term and the minimal coupling kinetic term for a single-particle system. The generalization to a many-particle systems is straightforward.

The general definition of the DA states that the plane wave expression $e^{i\mathbf{k}\mathbf{n}\cdot\mathbf{r}}$ is, for any external electromagnetic field, set to 1. Thus, by referring to the Taylor series of the plane wave $e^{i\mathbf{k}\mathbf{n}\cdot\mathbf{r}} = e^{ik\mathbf{e}_3\cdot\mathbf{r}} = e^{ikr_3}$:

$$e^{ikr_3} = 1 + \underbrace{ikr_3 - \frac{1}{2}(kr_3)^2 + \dots}_{(\square)}, \quad (2.81)$$

all terms of (\square) are set to zero in the DA. Furthermore, we wish to recall that an approximation in quantum mechanics typically assumes that certain matrix elements or expectations values are set to zero. Hence, the proper application of the DA is described by the following procedure: take all terms in the Hamiltonian that contain a coupling to the external \mathbf{A} -field (and possibly ϕ -field), use the plain wave expression of the field (in our case expression (2.78)), and set all matrix elements that contain the terms (\square) of (2.81) to zero. The matrix elements that are set to zero then determine what has to be fulfilled to justify this approximation in the first place.

First, we will investigate the Zeeman term, and we will use the expression $\langle \dots \rangle$, which stands in the following for both, the calculation of matrix elements or expectation values. Calculating the elements of the Zeeman term for our vector field gives

$$\frac{1}{2c} \langle \hat{\boldsymbol{\sigma}} \cdot (\nabla_{\hat{\mathbf{r}}} \times \mathbf{A}(\hat{\mathbf{r}}, t)) \rangle = \frac{1}{2c} \int dk ik \tilde{A}(k) e^{-ikct} \langle \hat{\sigma}_2 (1 + ik\hat{r}_3 + \dots) \rangle, \quad (2.82)$$

where we have written the exponential expression as a series. Applying the DA, i.e. setting (\square) from (2.81) to zero, gives

$$\frac{1}{2c} \langle \hat{\boldsymbol{\sigma}} \cdot (\nabla_{\hat{\mathbf{r}}} \times \mathbf{A}(\hat{\mathbf{r}}, t)) \rangle \xrightarrow{\text{DA}} \frac{1}{2c} b(t) \langle \hat{\sigma}_2 \rangle = \frac{1}{2c} \langle \hat{\boldsymbol{\sigma}} \cdot \mathbf{B}(t) \rangle, \quad (2.83)$$

where we have used the expressions from (2.80). We see that the DA leads to a Zeeman term that couples to a purely time-dependent \mathbf{B} -field. We will now discuss

under what conditions this approximation can be applied. Setting the first term of (\square) to zero is justified if $|\langle ik\hat{\sigma}_2\hat{r}_3\rangle| \ll |\langle\hat{\sigma}_2\rangle|$ which is true if $|\langle\hat{\sigma}_2\hat{r}_3\rangle| \ll \lambda|\langle\hat{\sigma}_2\rangle|$, where we have used the relation $k = 2\pi/\lambda$. This condition is usually fulfilled if the dimension of the system is much smaller than the wavelengths λ from which the pulse is composed. This is typically true for small quantum mechanical systems and wavelengths in the optical range. The investigation of the higher terms leads to similar conclusions, i.e. these terms can usually be neglected if the dimension of the system is small compared to λ .

Next, we will investigate the kinetic term with minimal coupling, which can be decomposed into 3 terms:

$$\frac{1}{2}\left[\hat{\mathbf{p}} + \frac{1}{c}\mathbf{A}(\hat{\mathbf{r}}, t)\right]^2 = \frac{\hat{p}^2}{2} + \frac{1}{c}\mathbf{A}(\hat{\mathbf{r}}, t) \cdot \hat{\mathbf{p}} + \frac{1}{2c^2}\mathbf{A}(\hat{\mathbf{r}}, t) \cdot \mathbf{A}(\hat{\mathbf{r}}, t). \quad (2.84)$$

We have used $\nabla \cdot \mathbf{A}(\mathbf{r}, t) = 0$, which follows for all free propagating pulses of the form (2.78). Calculating the elements of the second term on the right hand side gives

$$\frac{1}{c}\langle\mathbf{A}(\hat{\mathbf{r}}, t) \cdot \hat{\mathbf{p}}\rangle = \frac{1}{c}\int dk \tilde{A}(k) e^{-ikct} \langle(1 + ik\hat{r}_3 + \dots)\hat{p}_1\rangle, \quad (2.85)$$

which leads after the application of the DA to

$$\frac{1}{c}\langle\mathbf{A}(\hat{\mathbf{r}}, t) \cdot \hat{\mathbf{p}}\rangle \xrightarrow{\text{DA}} \frac{1}{c}a(t) \langle\hat{p}_1\rangle = \frac{1}{c}\langle\mathbf{A}(t) \cdot \hat{\mathbf{p}}\rangle, \quad (2.86)$$

where we have used the relations from (2.80). Obviously, the DA is only justified if $|\langle ik\hat{r}_3\hat{p}_1\rangle| \ll |\langle\hat{p}_1\rangle|$. When we assume that $|\langle\hat{r}_3\hat{p}_1\rangle| \approx |\langle\hat{r}_3\rangle||\langle\hat{p}_1\rangle|$, we end up with the condition $|\langle\hat{r}_3\rangle| \ll \lambda$, which is certainly fulfilled if the system is small compared to the wavelengths, as already demanded before. However, this condition reveals another requirement on the system concerning its dynamics (note that the previous conditions have to be fulfilled at each point in time). To see this, we consider the time evolution for $t = t' \dots t' + T$, where T is the time of one wave length cycle: $T = \lambda/c$. Furthermore, we assume that $\langle\hat{r}_3\rangle(t') \approx 0$, and that the dynamics of the system is approximately constant, i.e. $\partial_t\langle\hat{r}_3\rangle(t) \approx p_3$ with $\langle\hat{p}_3\rangle(t) \approx p_3$. Integrating the previous condition leads, with these assumptions, to $\int_{t'}^{t'+T} dt |\langle\hat{r}_3\rangle(t)| \approx |p_3|T^2/2 \ll \lambda T$, giving the condition $|p_3| \ll c$. This condition states that the DA is only justified if the electrons move non-relativistically. Similar arguments also hold for the higher terms of the series from (2.85).

In the same way as shown before, the DA can be applied to the term on the right hand side of (2.84), which gives

$$\frac{1}{2c^2}\langle\mathbf{A}(\hat{\mathbf{r}}, t) \cdot \mathbf{A}(\hat{\mathbf{r}}, t)\rangle \xrightarrow{\text{DA}} \frac{1}{2c^2}\langle A^2(t)\rangle. \quad (2.87)$$

Again, the condition of a small system has to be fulfilled to justify this approximation. With the relations (2.80), (2.86), and (2.87) we can summarize the DA of the kinetic term with minimal coupling as

$$\frac{1}{2}\left[\hat{\mathbf{p}} + \frac{1}{c}\mathbf{A}(\hat{\mathbf{r}}, t)\right]^2 \xrightarrow{\text{DA}} \frac{1}{2}\left[\hat{\mathbf{p}} + \frac{1}{c}\mathbf{A}(t)\right]^2. \quad (2.88)$$

Velocity gauge and length gauge

The previous discussion shows that the DA, applied on the minimal coupling kinetic term (2.88), changes the character of the \mathbf{A} -field. To be more specific: the $\mathbf{A}(\mathbf{r}, t)$, corresponding to (2.78), is a purely transversal vector field, while the $\mathbf{A}(t)$ -field, obtained via the DA, acts like a longitudinal vector field (see appendix A.4). This longitudinal vector field can be gauged away by choosing the gauge field $\Lambda(\mathbf{r}, t) = -\mathbf{r} \cdot \mathbf{A}(t)/c$ (see appendix A.3), which leads to

$$\frac{1}{2} \left[\hat{\mathbf{p}} + \frac{1}{c} \mathbf{A}(t) \right]^2 \xrightarrow{\text{gauge trans.}} \frac{\hat{p}^2}{2} + \mathbf{r} \cdot \mathbf{E}(t), \quad (2.89)$$

where we have used $\mathbf{E}(t) = -\partial_t \mathbf{A}(t)/c$, corresponding to (2.79). The gauge on the left hand side is called velocity gauge, while the gauge on the right hand side is called length gauge.

Gauge invariance and relation to the B-field

We have shown before that the DA can be applied to both, the Zeeman term (2.83), and the minimal coupling kinetic term (2.88). Thus, a corresponding Hamiltonian in the DA would then contain these two terms. It is clear that the \mathbf{B} - and \mathbf{A} -field present in this approximate Hamiltonian do not satisfy the relation $\mathbf{B} = \nabla \times \mathbf{A}$ anymore, and one might wonder if this violation is crucial. Furthermore, it is, at first sight, not clear if it is justified to perform a transformation of the kind (2.89) with the kinetic term, and at the same time leave the Zeeman term in the DA unchanged. These concerns, however, disappear when we recall what the DA is: it is an approximation that leads, under certain conditions (as stated before), to similar results as those that would have been obtained by solving the problem with the full field. Moreover, it has to be clear that the Hamiltonian is, before applying the DA, in fact gauge invariant, meaning that the previously mentioned issues constitute no problem. (Note that the gauge transformation with the field $\Lambda(\mathbf{r}, t) = -\mathbf{r} \cdot \mathbf{A}(t)/c$, which leaves \mathbf{B} unchanged, could also be performed on the Hamiltonian with the full field, which would after the DA in fact lead to the DA Hamiltonian in the length gauge.)

3. Real-time spin-dynamics - simulation framework

The purpose of this work is the investigation of the short time behavior of excited spin-magnetic systems, which requires a proper treatment of the electron spin. Since the electron spin has its natural origin in relativistic quantum mechanics, we will in the first section of this chapter investigate all spin-coupling terms that arise from a non-relativistic limit. Moreover, we will incorporate all important spin-coupling terms into a proper KS-TDDFT scheme, thus including many-electron effects, and allowing a real-time treatment. At the end of the first section, the dynamical equations of the magnetization and the moment that arise from the TDDFT scheme will be discussed. Furthermore, the properties of the corresponding xc \mathbf{B} -field will be discussed as well. In the second section, the algorithm that is used to solve the KS equations in real-time will be introduced, and some details concerning the implementation will be discussed. In the last section of this chapter, a time-dependent density of states will be introduced, which allows it to investigate and characterize the excited spin-system.

3.1. Theoretical aspects of the simulation

The main concern of this work is the description of real-time spin-dynamics of many-electron systems irradiated by short laser pulses. The representation of the laser field is straightforward, since it can be described classically, as discussed previously. However, the proper description of spin-dynamics is rather involved due to the following two reasons: First, the exact description of the electron spin would, in principle, require a full relativistic treatment, which is in general hard to accomplish. Therefore, an appropriate non-relativistic treatment has to be adopted. Second, a proper electron-electron interaction has to be incorporated, since this is essential for the description of certain spin-magnetic effects, such as ferromagnetism.

To overcome these issues, we will in the following section investigate the different single-particle terms that arise from the non-relativistic limit of the Dirac equation, and that couple to external fields. Then in the next section, we will take the single-particle terms that turned out to be important, and we will incorporate them into an appropriate TDDFT scheme to include many-electron effects.

3.1.1. Spin-coupling terms

A relativistic particle that moves in an electromagnetic field is described by the Dirac equation. We will in the following investigate all terms that arise from a non-relativistic limit of this equation, and we will further study how these terms

change by applying the DA. Moreover, we will, in view of a correct description of spin-dynamics, discuss the relative importance of each of these terms.

The usual way to obtain the non-relativistic limit of the Dirac equation is to first apply a Foldy-Wouthuysen transformation, which block diagonalizes the Dirac-Hamiltonian for arbitrary electromagnetic fields. Following this, one takes the non-relativistic limit and one ends up with a two-component spinor equation for the electrons [21]:

$$i\partial_t \underline{\varphi}(\mathbf{r}, t) = \underline{\hat{h}}(t) \underline{\varphi}(\mathbf{r}, t), \quad \text{with} \quad (3.1)$$

$$\begin{aligned} \underline{\hat{h}}(t) = & \left(\frac{1}{2} \left[\hat{\mathbf{p}} + \frac{1}{c} \mathbf{A}(\mathbf{r}, t) \right]^2 - \frac{1}{8c^2} \hat{p}^4 + \frac{1}{8c^2} \nabla \cdot \mathbf{E}(\mathbf{r}, t) + v(\mathbf{r}, t) + c^2 \right) \\ & + \underline{\boldsymbol{\sigma}} \cdot \left(\underbrace{\frac{i}{8c^2} \nabla \times \mathbf{E}(\mathbf{r}, t)}_{\text{SOC I}} + \underbrace{\frac{1}{4c^2} \mathbf{E}(\mathbf{r}, t) \times \left[\hat{\mathbf{p}} + \frac{1}{c} \mathbf{A}(\mathbf{r}, t) \right]}_{\text{SOC II}} + \underbrace{\frac{1}{2c} \mathbf{B}(\mathbf{r}, t)}_{\text{Zeeman}} \right). \end{aligned}$$

First of all, we see that the Hamiltonian (3.1) contains two parts. The first part is diagonal in the spinor space, while the second part, which consists of two SOC terms and a Zeeman term, couples to the vector of Pauli-matrices. Hence, we have a Hamiltonian of the form $\hat{h} = \hat{a} + \hat{\boldsymbol{\sigma}} \cdot \hat{\mathbf{b}}$. By considering the corresponding dynamical equation of $\langle \hat{\boldsymbol{\sigma}} \rangle$ (according to Ehrenfest's theorem):

$$\partial_t \langle \hat{\boldsymbol{\sigma}} \rangle = -i \langle [\hat{\boldsymbol{\sigma}}, \hat{h}] \rangle = -i \langle [\hat{\boldsymbol{\sigma}}, \hat{a} + \hat{\boldsymbol{\sigma}} \cdot \hat{\mathbf{b}}] \rangle = -i \langle [\hat{\boldsymbol{\sigma}}, \hat{\boldsymbol{\sigma}} \cdot \hat{\mathbf{b}}] \rangle = 2 \langle \hat{\mathbf{b}} \times \hat{\boldsymbol{\sigma}} \rangle, \quad (3.2)$$

it follows that the spin-dynamical contributions from the second part are essential for our concerns, since only these contributions lead directly to a change of $\langle \hat{\boldsymbol{\sigma}} \rangle$. Therefore, the relativistic corrections present in the first part of the Hamiltonian (3.1) will be omitted in the following discussion, and we will rather focus on the contributions from the second part (we wish to mention that a radial version of the second and the third term of the first part of (3.1), which are known as mass-velocity and Darwin term, were used in the calculations). The Hamiltonian (3.1) is, except for the \hat{p}^4 term, gauge invariant (see appendix A.3). This follows immediately from the usual formulation with the gauge invariant \mathbf{E} - and \mathbf{B} -field:

$$\mathbf{E}(\mathbf{r}, t) = \nabla v(\mathbf{r}, t) - \frac{1}{c} \partial_t \mathbf{A}(\mathbf{r}, t) \quad \text{and} \quad \mathbf{B}(\mathbf{r}, t) = \nabla \times \mathbf{A}(\mathbf{r}, t). \quad (3.3)$$

We will in the following assume that the system is irradiated by a linear polarized laser pulse, i.e. we assume that $\mathbf{A}(\mathbf{r}, t)$ is of the form (2.78). Furthermore, we will assume that a $v(\mathbf{r}, t)$ is present, which stems for example from the nuclei.

The application of the DA on the SOC II term and on the Zeeman term is straightforward, and leads in fact to similar results as discussed in section 2.4.2. The application on the SOC I term, on the other hand, is a bit more involved and needs a closer inspection. First of all, we see from (3.3) that the SOC I term seems to have two contributions. However, the contribution from the scalar potential always vanishes, since $\nabla \times \nabla v(\mathbf{r}, t) = 0$. Nevertheless, the $\partial_t \mathbf{A}$ -field term would, by applying the DA rigorously, as shown in section 2.4.2, not vanish. Next, we note that the SOC I term is associated to the $\mathbf{E}(\mathbf{r}, t) \times \hat{\mathbf{p}}$ -term from SOC II. To be

more precise: only these two terms together are hermitian. Hence, we will in the following consider both terms. Calculating the expectation value of the $\partial_t \mathbf{A}$ -field part for both SOC terms with the full field (i.e. before the DA) gives

$$\begin{aligned} & -\frac{1}{8c^3} \left(\langle i\hat{\boldsymbol{\sigma}} \cdot (\nabla \times \partial_t \mathbf{A}(\hat{\mathbf{r}}, t)) \rangle + 2\langle \hat{\boldsymbol{\sigma}} \cdot (\partial_t \mathbf{A}(\hat{\mathbf{r}}, t) \times \hat{\mathbf{p}}) \rangle \right) \\ &= -\frac{1}{8c^3} \left(\underbrace{\text{Re} \langle i\hat{\boldsymbol{\sigma}} \cdot (\nabla \times \partial_t \mathbf{A}(\hat{\mathbf{r}}, t)) \rangle}_{=0} + 2\text{Re} \langle \hat{\boldsymbol{\sigma}} \cdot (\partial_t \mathbf{A}(\hat{\mathbf{r}}, t) \times \hat{\mathbf{p}}) \rangle \right) \\ &= -\frac{1}{4c^3} \text{Re} \langle \hat{\boldsymbol{\sigma}} \cdot (\partial_t \mathbf{A}(\hat{\mathbf{r}}, t) \times \hat{\mathbf{p}}) \rangle. \end{aligned} \quad (3.4)$$

Applying the DA on the result of (3.4) gives

$$-\frac{1}{4c^3} \text{Re} \langle \hat{\boldsymbol{\sigma}} \cdot (\partial_t \mathbf{A}(\hat{\mathbf{r}}, t) \times \hat{\mathbf{p}}) \rangle \xrightarrow{\text{DA}} \frac{1}{4c^2} \langle \hat{\boldsymbol{\sigma}} \cdot (\mathbf{E}(t) \times \hat{\mathbf{p}}) \rangle, \quad (3.5)$$

where we have used the notation from (2.80). As a result, we see that the rigorous application of the DA, i.e. the application on hermitian terms only, leads to the disappearance of the $\partial_t \mathbf{A}$ -field term from SOC I, i.e. the whole SOC I term vanishes.

In summary, we can write down all spin-coupling terms from (3.1) that are obtained by applying the DA:

$$\underline{\boldsymbol{\sigma}} \cdot \left(\underbrace{\frac{1}{4c^2} \nabla v(\mathbf{r}, t) \times \left[\hat{\mathbf{p}} + \frac{1}{c} \mathbf{A}(t) \right]}_{(i)} + \underbrace{\frac{1}{4c^2} \mathbf{E}(t) \times \left[\hat{\mathbf{p}} + \frac{1}{c} \mathbf{A}(t) \right]}_{(ii)} + \underbrace{\frac{1}{2c} \mathbf{B}(t)}_{(iii)} \right), \quad (3.6)$$

where we have used the notation from (2.80). We will now investigate the individual terms of (3.6). The Zeeman term *(iii)* couples directly to the \mathbf{B} -field component of the laser pulse, which can, for high-intensity laser pulses, become quite large. Therefore, this term should not be neglected in the following discussions. Next, we will discuss the importance of term *(ii)* by investigating the corresponding contribution to the dynamics of $\langle \hat{\sigma}_3 \rangle$. We assume we have an external pulse of the form (2.80) (i.e. a propagation along \mathbf{e}_3 and polarization along \mathbf{e}_1), which leads according to (3.2) to

$$\partial_t \langle \hat{\sigma}_3 \rangle_{\mathbf{E}} = \frac{1}{2c^2} \langle (\mathbf{E}(t) \times \hat{\mathbf{p}}) \times \hat{\boldsymbol{\sigma}} \rangle_3 = \frac{1}{2c^2} b(t) \langle (\mathbf{e}_1 \times \hat{\mathbf{p}}) \times \hat{\boldsymbol{\sigma}} \rangle_3 = \frac{1}{2c^2} b(t) \langle \hat{\sigma}_1 \hat{p}_3 \rangle. \quad (3.7)$$

For a clear view, we used a shorthand notation for the gauge invariant momentum: $\hat{\mathbf{p}} = (\hat{\mathbf{p}} + \mathbf{A}(t)/c)$. The same analysis can be done with the Zeeman term *(iii)*, which gives

$$\partial_t \langle \hat{\sigma}_3 \rangle_{\mathbf{B}} = \frac{1}{c} \langle \mathbf{B}(t) \times \hat{\boldsymbol{\sigma}} \rangle_3 = \frac{1}{c} b(t) \langle \mathbf{e}_2 \times \hat{\boldsymbol{\sigma}} \rangle_3 = -\frac{1}{c} b(t) \langle \hat{\sigma}_1 \rangle. \quad (3.8)$$

When we now assume that we have a non-relativistically system, we get by comparing (3.7) with (3.8):

$$\frac{|\partial_t \langle \hat{\sigma}_3 \rangle_{\mathbf{B}}|}{|\partial_t \langle \hat{\sigma}_3 \rangle_{\mathbf{E}}|} = 2c \frac{\langle \hat{\sigma}_1 \rangle}{\langle \hat{\sigma}_1 \hat{p}_3 \rangle} \gg 1 \quad \longrightarrow \quad |\partial_t \langle \hat{\sigma}_3 \rangle_{\mathbf{B}}| \gg |\partial_t \langle \hat{\sigma}_3 \rangle_{\mathbf{E}}|. \quad (3.9)$$

We can conclude that the laser-induced contribution to the dynamics of $\langle \hat{\sigma} \rangle$ from the Zeeman term is much larger than the contribution from the SOC term (*ii*). Therefore, the term (*ii*) from (3.6) should be negligible. Finally, we point out that the term (*i*) should, of course, not be neglected, since it contains the $\nabla v(\mathbf{r}, t)$ -term, which can become very large close to a nucleus.

We can now write down all single-particle spin-terms that couple to external fields and that should be present in a spin-dynamical simulation:

$$\frac{1}{4c^2} \underline{\underline{\boldsymbol{\sigma}}} \cdot \left(\nabla v_n(\mathbf{r}) \times \left[\hat{\mathbf{p}} + \frac{1}{c} \mathbf{A}_{\text{ext}}(t) \right] \right) + \frac{1}{2c} \underline{\underline{\boldsymbol{\sigma}}} \cdot \mathbf{B}_{\text{ext}}(t). \quad (3.10)$$

$v_n(\mathbf{r})$ is the static nuclear potential, and $\mathbf{A}_{\text{ext}}(t)$ and $\mathbf{B}_{\text{ext}}(t)$ are the fields from the laser pulse (which are purely time-dependent in the DA, and which have been labeled as external fields). We emphasize that a Hamiltonian that would contain the spin-terms (3.10) would have to be formulated in terms of the momentum $(\hat{\mathbf{p}} + \mathbf{A}_{\text{ext}}(t)/c)$ (this is particularly important for the kinetic term). This condition is necessary to assure consistency with our initial Hamiltonian (3.1) and the approximations that have been assumed.

Finally, we wish to mention one more important point: in (3.10), a time-independent nuclear potential $v_n(\mathbf{r})$ is assumed. Since we are interested in the spin-dynamics on a time scale of a few femtoseconds, the assumption of static nuclei should be justified. However, if investigations on longer time scales are pursued, the time-dependence of the nuclear potential has to be taken into account. When we define the relative change of the nuclear potential as $\delta v_n(\mathbf{r}, t) = v_n(\mathbf{r}, t) - v_n(\mathbf{r})$, with $v_n(\mathbf{r})$ as the potential at $t = 0$, we would get for non-static nuclei the following additional spin-coupling term:

$$\frac{1}{4c^2} \underline{\underline{\boldsymbol{\sigma}}} \cdot \left(\nabla \delta v_n(\mathbf{r}, t) \times \left[\hat{\mathbf{p}} + \frac{1}{c} \mathbf{A}_{\text{ext}}(t) \right] \right). \quad (3.11)$$

This term couples the spin-currents to the dynamics of the nuclei (i.e. to the dynamics of the lattice) and very likely contributes to spin-lattice relaxation and similar processes. Note that such a spin-lattice relaxation is, to some extent, described within the Elliott-Yafet mechanism (see e.g. [49]).

3.1.2. A time-dependent SDFT scheme with spin-orbit coupling

In this section we will incorporate all single-particle spin-coupling terms, that arose from the discussion in the previous section, into a TDDFT scheme. We will see that the derived TDDFT scheme can be understood as a time-dependent extension of the SDFT scheme that includes SOC from section 2.2.4. In section 3.1.5, we will utilize this scheme to discuss some general properties concerning the xc \mathbf{B} -field that arise when SOC is present.

The starting point is a Hamiltonian of a finite many-electron system subjected to an external electromagnetic field. The external field is treated in the DA, and all the spin-terms from (3.6) will be considered:

$$\hat{H}(t) = \hat{T} + \hat{W} + \sum_{i=1}^N \hat{h}_i(t), \quad \text{with} \quad (3.12)$$

$$\hat{h}_i(t) = v_n(\hat{\mathbf{r}}_i) + \frac{1}{4c^2} \hat{\boldsymbol{\sigma}}_i \cdot \left(\left[\nabla v_n(\hat{\mathbf{r}}_i) + \mathbf{E}_{\text{ext}}(t) \right] \times \left[\hat{\mathbf{p}}_i + \frac{1}{c} \mathbf{A}_{\text{ext}}(t) \right] \right) + \frac{1}{2c} \hat{\boldsymbol{\sigma}}_i \cdot \mathbf{B}_{\text{ext}}(t).$$

$v_n(\mathbf{r})$ is the static nuclear potential, and \hat{W} is the electron-electron interaction (it is convenient to assume that the interaction is of the form (2.41), i.e. it contains a many-electron SOC contribution, due to the reasons that have been discussed in section 2.2.4). Note that the kinetic operator (and if necessary also the interaction term) has to be formulated with the gauge invariant momentum. Applying a gauge transformation with the gauge field $\Lambda(\mathbf{r}, t) = -\mathbf{r} \cdot \mathbf{A}_{\text{ext}}(t)/c$ gives

$$\hat{H}(t) = \hat{T} + \hat{W} + \sum_{i=1}^N \left(v_{\text{ext}}(\hat{\mathbf{r}}_i, t) + \frac{1}{4c^2} \hat{\boldsymbol{\sigma}}_i \cdot \left[\nabla v_{\text{ext}}(\hat{\mathbf{r}}_i, t) \times \hat{\mathbf{p}}_i \right] + \frac{1}{2c} \hat{\boldsymbol{\sigma}}_i \cdot \mathbf{B}_{\text{ext}}(t) \right),$$

with $v_{\text{ext}}(\mathbf{r}, t) = v_n(\mathbf{r}) + \mathbf{r} \cdot \mathbf{E}_{\text{ext}}(t)$, (3.13)

where we have used $\mathbf{E}_{\text{ext}}(t) = -\partial_t \mathbf{A}_{\text{ext}}(t)/c$. We see now that the Hamiltonian (3.13) has exactly the same form as the Hamiltonian (2.37), which was the starting point in the derivation of the ground state SDFT with SOC from section 2.2.4. We will now assume that a corresponding time-dependent extension exists. Thus, the exact time-dependent magnetization of the system (3.13) could, by referring to (2.47), also be obtained by solving the following time-dependent KS system:

$$i\partial_t \varphi'_i(\mathbf{r}, t) = \left(\frac{\hat{p}^2}{2} + v'_s(\mathbf{r}, t) + \frac{1}{4c^2} \underline{\boldsymbol{\sigma}} \cdot \left[\nabla v'_s(\mathbf{r}, t) \times \hat{\mathbf{p}} \right] + \frac{1}{2c} \underline{\boldsymbol{\sigma}} \cdot \mathbf{B}_s(\mathbf{r}, t) \right) \varphi'_i(\mathbf{r}, t), \quad (3.14)$$

with $v'_s(\mathbf{r}, t) = v_n(\mathbf{r}) + \mathbf{r} \cdot \mathbf{E}_{\text{ext}}(t) + v_H(\mathbf{r}, t) + v_{\text{xc}}(\mathbf{r}, t)$.

With the gauge field $\Lambda(\mathbf{r}, t) = \mathbf{r} \cdot \mathbf{A}_{\text{ext}}(t)/c$, the system (3.14) can be gauged back, which gives

$$i\partial_t \varphi_i(\mathbf{r}, t) = \left(\frac{1}{2} \left[\hat{\mathbf{p}} + \frac{1}{c} \mathbf{A}_{\text{ext}}(t) \right]^2 + v_s(\mathbf{r}, t) + \frac{1}{2c} \underline{\boldsymbol{\sigma}} \cdot \mathbf{B}_s(\mathbf{r}, t) \right. \\ \left. + \frac{1}{4c^2} \underline{\boldsymbol{\sigma}} \cdot \left(\left[\nabla v_s(\mathbf{r}, t) + \mathbf{E}_{\text{ext}}(t) \right] \times \left[\hat{\mathbf{p}} + \frac{1}{c} \mathbf{A}_{\text{ext}}(t) \right] \right) \right) \varphi_i(\mathbf{r}, t), \quad (3.15)$$

with $v_s(\mathbf{r}, t) = v_n(\mathbf{r}) + v_H(\mathbf{r}, t) + v_{\text{xc}}(\mathbf{r}, t)$, $\mathbf{B}_s(\mathbf{r}, t) = \mathbf{B}_{\text{ext}}(t) + \mathbf{B}_{\text{xc}}(\mathbf{r}, t)$.

We can summarize that the KS system (3.15) gives the same time-dependent magnetization as the finite interacting many-electron system (3.12), assuming that a corresponding time-dependent extension of the ground state SDFT with SOC exists.

3.1.3. Time-dependent SDFT in extended systems

The systems that will be studied in this work are bulk materials and few atom layers. Such systems are usually described by Hamiltonians that are lattice periodic in two or three dimensions, according to the particular crystal structure. Additionally, we consider time-dependent external electromagnetic fields which are always purely time-dependent in our simulations (as result of the DA). Thus,

the many-electron Hamiltonians of the systems under study would always be invariant under a lattice translation for all times, meaning that all local quantities, such as the density, are also lattice periodic. Therefore, a KS system that is used to reproduce an exact time-dependent interacting local quantity (in our case the density and magnetization) has to be based on a lattice periodic Hamiltonian as well.

The usual way to calculate properties of lattice periodic systems is to apply the \mathbf{k} -point method, which uses the Bloch state representation. All calculations in this work are based on this method, and the time-dependent Bloch states will be represented as two-component spinors (see (2.24)): $\langle \alpha, \mathbf{r} | \varphi_i^{\mathbf{k}}(t) \rangle = \varphi_i^{\mathbf{k}, \alpha}(\mathbf{r}, t)$, with \mathbf{k} as the particular \mathbf{k} -point and $\alpha = \{\uparrow, \downarrow\}$. A short overview of time-dependent Bloch states and the \mathbf{k} -point method is given in appendix A.5, while more detailed information can be found in [50].

In the following, the Hamiltonian that was applied in all calculations will be shown and discussed. At this point we already wish to mention that the applied Hamiltonian contained also some relativistic corrections that are not shown in the following, because these terms are not relevant for the later discussions, and the contributions of these terms to the spin-dynamics is most probably negligible. We will come back to this subject at the end of the next subsection. Following this, we will discuss some particularities, and the associated problems, that occur when extended periodic systems are considered.

Real-time spin-dynamics - the applied KS scheme

The KS scheme that was solved in this work was similar to (3.15), with the difference that the $(\mathbf{E}_{\text{ext}} \times [\hat{\mathbf{p}} + \mathbf{A}_{\text{ext}}/c])$ -term from the SOC was neglected, i.e. only the external spin-coupling terms that are shown in (3.10) have been considered (note that only these terms are relevant, as discussed in section 3.1.1). Moreover, the \mathbf{k} -point method was applied, meaning that KS Bloch states were used, and the xc functionals have been approximated by the ALSDA (2.77). In summary, the KS system that was solved in the calculations of this work has the form

$$i\partial_t \varphi_i^{\mathbf{k}}(\mathbf{r}, t) = \left(\frac{1}{2} \left[\hat{\mathbf{p}} + \frac{1}{c} \mathbf{A}_{\text{ext}}(t) \right]^2 + v_s(\mathbf{r}, t) + \frac{1}{2c} \underline{\underline{\boldsymbol{\sigma}}} \cdot \mathbf{B}_s(\mathbf{r}, t) + \frac{1}{4c^2} \underline{\underline{\boldsymbol{\sigma}}} \cdot \left(\nabla v_s(\mathbf{r}, t) \times \left[\hat{\mathbf{p}} + \frac{1}{c} \mathbf{A}_{\text{ext}}(t) \right] \right) \right) \varphi_i^{\mathbf{k}}(\mathbf{r}, t),$$

$$\text{with} \quad v_s(\mathbf{r}, t) = v_n(\mathbf{r}) + v_H[n](\mathbf{r}, t) + v_{\text{xc}}^{\text{ALSDA}}[n, \mathbf{m}](\mathbf{r}, t),$$

$$\mathbf{B}_s(\mathbf{r}, t) = \mathbf{B}_{\text{ext}}(t) + \mathbf{B}_{\text{xc}}^{\text{ALSDA}}[n, \mathbf{m}](\mathbf{r}, t),$$

$$\text{and} \quad n(\mathbf{r}, t) = \frac{1}{N^{\mathbf{k}}} \sum_{i, \mathbf{k}} f_i^{\mathbf{k}} |\varphi_i^{\mathbf{k}}(\mathbf{r}, t)|^2,$$

$$\mathbf{m}(\mathbf{r}, t) = \frac{1}{N^{\mathbf{k}}} \sum_{i, \mathbf{k}} f_i^{\mathbf{k}} \varphi_i^{\mathbf{k}\dagger}(\mathbf{r}, t) \underline{\underline{\boldsymbol{\sigma}}} \varphi_i^{\mathbf{k}}(\mathbf{r}, t), \quad (3.16)$$

where $f_i^{\mathbf{k}}$ is the occupation number and $N^{\mathbf{k}}$ is the number of \mathbf{k} -points. The system (3.16) was solved in the following way: First, the ground state of the system was calculated, which has to be done by a self-consistency cycle, since $n(\mathbf{r})$ and $\mathbf{m}(\mathbf{r})$ enter the functionals. Note that the ground state run also determines the state and \mathbf{k} -point dependent occupation numbers $f_i^{\mathbf{k}}$, by occupying all lowest states. Next, all occupied states were propagated forward in real-time. We point out that the KS Hamiltonian keeps for all times its translational symmetry, meaning that all KS states remain orthogonal Bloch states. The propagation scheme and further details about the calculation will be discussed in section 3.2.

As stated before, the KS Hamiltonian that was applied in the calculations involved also some relativistic corrections, such as the Darwin term and the mass-velocity term (recall that these two terms have been briefly discussed in section 3.1.1). Since these relativistic corrections do not have any significant relevance for our concerns, we neglected these terms in the previously shown Hamiltonian, and we will ignore these terms in all following discussions as well (i.e. we will always refer to the system (3.16)). Details about the applied framework and the relativistic corrections can be found in [24].

Next, we wish to mention that the contribution of $\underline{\underline{\sigma}} \cdot [\nabla v_s(\mathbf{r}) \times \mathbf{A}_{\text{ext}}]/4c^3$ (i.e. the diamagnetic part of SOC) to the spin-dynamics has been investigated. It turned out that this term is negligible, at least for such situations that are discussed in this work (in fact, this term was neglected in all calculations presented in this work). However, in view of a gauge invariant formulation, we will take this term into account in the following discussions. Moreover, we point out that an approximated radial SOC term has been applied in the calculations, which, however, did not lead to any differences compared to the calculations with the full SOC term from (3.16). We will come back to this subject in section 4.3.2. To keep the following theoretical discussions as general as possible, we will, for the moment, keep the full SOC term.

The calculation of KS expectation values involves the sum over all occupied states and \mathbf{k} -points. In all following sections, we will use a shorthand notation for these calculations:

$$\frac{1}{N^{\mathbf{k}}} \sum_{i,\mathbf{k}} f_i^{\mathbf{k}} \int_{\Omega} d\mathbf{r} \underline{\underline{\varphi}}_i^{\mathbf{k}\dagger}(\mathbf{r}, t) \hat{O} \underline{\underline{\varphi}}_i^{\mathbf{k}}(\mathbf{r}, t) \quad \longrightarrow \quad \sum_i \langle \hat{O}_i \rangle(t). \quad (3.17)$$

Note that the state and \mathbf{k} -point index pair will be represented as only one index: $(i, \mathbf{k}) \rightarrow i$. Furthermore, we point out that the expectation values are always calculated per unit cell volume Ω .

Extended systems - particularities

All calculations in this work considered extended, periodic systems. We will in the following discuss some issues that, in principle, arise solely from the assumption of such extended systems. The discussed issues might be problematic under certain circumstances and they should be kept in mind.

First of all, we point out that the framework (3.16) (which was applied in the calculations) might be derived for a finite system, as demonstrated in section

3.1.2. The first step in the derivation was that the external $\mathbf{A}(t)$ -field was gauged away, which led to a local potential of the form $\mathbf{r} \cdot \mathbf{E}(t)$. It is clear that such a local potential is not lattice periodic and it becomes infinitely large for $|\mathbf{r}| \rightarrow \infty$. Thus, it is questionable if this first step would actually be justified in our derivation, considering extended systems. To clarify the problems that arise from the actual TDDFT treatment, we will for the moment ignore the Zeeman and the SOC term. In fact, for such systems (i.e. extended systems that only have a $\mathbf{r} \cdot \mathbf{E}(t)$ -term as external coupling) the RG proof does not apply [51]. As a matter of fact, TDCDFT would be the correct framework to describe extended systems that have minimal coupling to external $\mathbf{A}(t)$ -fields. Thus, we could argue that our framework considers the longitudinal part of the \mathbf{A}_{xc} -field, which has been gauged away and approximated by the lattice periodic v_{xc} , and neglects the transversal component of the \mathbf{A}_{xc} -field (the longitudinal and transversal \mathbf{A}_{xc} -field within TDCDFT has been discussed in section 2.3.2). However, this is not the whole story and the problem is more involved in our case since we have, beside the minimal coupling kinetic term, also a Zeeman term and a SOC term. Therefore, a time-dependent extension of SCDFE, similar to that discussed in section 2.2.3, would most probably be needed for a correct treatment. Nevertheless, in our simulations the framework (3.16) was used, and already in this scheme the xc fields have to be approximated. In the end, we have to admit that it is very hard or even impossible to make clear statements about the magnitude of the individual errors that have been introduced at the different stages of the approximations. Therefore, in future work the consequences of the different approximations applied should be investigated in more detail.

Next, we recall that the simulation framework used is based on the DA. In section 2.4.2, it was shown that the DA is only justified if the central wavelength of the external laser pulse is much larger than the size of the considered system. This condition is, however, for extended systems generally not satisfied. Therefore, we have to be a bit more precise under what exact situations the DA is justified, and, if the DA is not justified, it has to be discussed what this means in the individual case. First, we will consider a few atom layer. Such a scenario is usually described via a system that is periodic in the layer plane, i.e. it is periodic in two dimensions. When we now assume that the polarization of the laser pulse lies in the plane, i.e. that the pulse propagation is perpendicular to the plane, it follows that the DA is, in fact, justified. The simulations of few atom layers presented in this work assume such a configuration, meaning that the DA does not constitute a problem in this case.

However, when we consider bulk materials, i.e. systems that are periodic in three dimensions, the DA is not justified, and one might ask what situation would actually be simulated by using the DA in such systems. An answer could be that we simulate regions inside bulk materials that are large enough to be treated as extended systems, but still small enough such that the DA makes sense. The external $\mathbf{A}(t)$ -field could then be understood as an effective field that is present in this specific region, and that results from the propagation of a laser pulse through the material. This is in fact the situation that we should have in mind when we discuss the simulations of periodic bulk materials in this work. With the

previously discussed points in mind, one could argue that it should, in principle, be possible to describe the propagation of a laser pulse through a large but finite material, by simulating a coupled array of individual regions. In fact, a simulation based on such an approach was recently demonstrated for spin-less systems [52].

The last point of discussion concerns the external \mathbf{A} -field. As already noted in the previous paragraph, the field of propagating laser pulses typically changes once they propagate inside a material. The reason is that the external field from a free propagating pulse, \mathbf{A}_{ext} , induces currents inside the material, which, on their part, produce according to Maxwell's equations an induced field, \mathbf{A}_{ind} . Therefore, the field used in the simulation of the quantum mechanical system should be the effective field $\mathbf{A} = \mathbf{A}_{\text{ext}} + \mathbf{A}_{\text{ind}}$, rather than the field \mathbf{A}_{ext} alone. The induced currents in small systems (e.g. atoms or molecules) are typically very small, and in such systems it is justified to neglect \mathbf{A}_{ind} . In extended systems, on the other hand, the induced currents can become large, and therefore the induced field might become important, as demonstrated in [53]. The calculations presented in this work, however, neglected any induced fields, because the focus of this work lies on the investigation of the behavior of excited spin-systems, rather than on the detailed description of pulse propagations or similar effects. Therefore, the applied external field should be seen as an effective driving field that excites the system. Finally, we wish to mention that the investigation of the influence of the induced field is, in fact, a subject of ongoing work.

3.1.4. The dynamical equation of the density, the magnetization, and the moment

For the calculations in this work, the KS scheme (3.16) was solved in real-time by a forward propagation. One advantage of this approach is that processes beyond the linear response regime are included. Another advantage is that one has easy access to all time-dependent KS expectation values, since they can be calculated directly during the forward propagation. Of particular interest for our concerns is the time-dependent magnetization and moment. In order to reveal some insights about the spin-dynamics of excited systems, we will in the following discuss the dynamical equation of these two observables. Moreover, we will discuss the dynamical equation of the density, because this quantity enters, along with the magnetization, the xc functionals.

Time-dependent density

The dynamical equation of any observable follows from Ehrenfest's theorem, i.e. it follows from the commutator with the time-dependent Hamiltonian of the system (see e.g. (3.2)). Calculating the dynamical equation of the density from the Hamiltonian (3.16) gives

$$\partial_t n(\mathbf{r}, t) = -\nabla \cdot \mathbf{j}(\mathbf{r}, t) - \nabla \cdot \frac{1}{4c^2} \left[\mathbf{m}(\mathbf{r}, t) \times \nabla v_s(\mathbf{r}, t) \right]. \quad (3.18)$$

A detailed derivation is given in appendix A.6.3. The first term on the right hand side is the usual current density term, which is known from the ordinary conti-

nunity equation. The second term, however, is only present if we have SOC. We see that this term couples the dynamics of the magnetization to the dynamics of the density. The integral of the right hand side of (3.18) over the whole system vanishes, which follows from Gauss's theorem together with the assumption of finite or periodic systems. This, in fact, has to be fulfilled since equation (3.18) is a continuity equation, and the vanishing of the integral simply means that the number of electrons is conserved.

Time-dependent magnetization

Next, the dynamical equation of the magnetization is calculated from the Hamiltonian of (3.16), which gives

$$\begin{aligned} \partial_t \mathbf{m}(\mathbf{r}, t) = & - \nabla \cdot \overset{\leftrightarrow}{J}(\mathbf{r}, t) + \frac{1}{c} [\mathbf{B}_s(\mathbf{r}, t) \times \mathbf{m}(\mathbf{r}, t)] + \frac{1}{4c^2} [\nabla n(\mathbf{r}, t) \times \nabla v_s(\mathbf{r}, t)] \\ & + \frac{1}{2c^2} [\overset{\leftrightarrow}{J}^T(\mathbf{r}, t) - \text{Tr}\{\overset{\leftrightarrow}{J}(\mathbf{r}, t)\}] \cdot \nabla v_s(\mathbf{r}, t). \end{aligned} \quad (3.19)$$

A detailed derivation is shown in appendix A.6.3. The equation contains beside the density and the magnetization the gauge invariant spin-current tensor, which is given by the sum of the paramagnetic and the diamagnetic part, as defined in (2.26) and (2.27).

The first term on the right hand side of (3.19) is the kinetic contribution. The representation of this term has to be understood as follows: Each row vector of the 3×3 spin-current tensor is contracted by taking the divergence, which gives a 3-component vector. This kinetic term has the following meaning: Each component of the magnetization has its own current density, which can transport the local spin and, in consequence, it can locally change the corresponding component of the magnetization. Since this term is a transport term, it can not change the integral of the magnetization, i.e. the moment, which will be discussed in the next subsection.

The second term is a local Larmor precession term, which has the same form as the torque term in the dynamical equation of a magnetic dipole that moves in a magnetic field. Thus, the magnetization can be imagined as the quantum mechanical analog of a local magnetic dipole. The torque vector stemming from the Larmor term is always perpendicular to the local \mathbf{B} -field and the magnetization. Hence, the magnetization would perform a precession movement around the local \mathbf{B} -field if this field would be constant in time, and if the Larmor term would be the only torque term that contributes to the dynamics. In our calculations, the \mathbf{B} -field has two contributions: \mathbf{B}_{ext} and \mathbf{B}_{xc} . The \mathbf{B}_{xc} applied in our calculations is approximated by the ALSDA, meaning that

$$\mathbf{B}_{\text{xc}}^{\text{ALSDA}}[n, \mathbf{m}](\mathbf{r}, t) \times \mathbf{m}(\mathbf{r}, t) = 0, \quad (3.20)$$

where we have used (2.60). Thus, the direct \mathbf{B} -field contribution to the dynamics of the magnetization comes solely from the external \mathbf{B} -field in our calculations.

The third and the fourth term of (3.19) are SOC contributions. We see that the third term couples the dynamics of the density to the dynamics of the magnetization. Next, we explain how the representation of the fourth term has to

be understood: The trace of the spin-current tensor is subtracted from the diagonal elements of the transpose of the spin-current tensor. The resulting tensor is then multiplied with ∇v_s , giving the corresponding torque vector. Note that the fourth term couples the spin-current densities to ∇v_s , while ∇v_s acts as an effective electric field. In the following subsection, we will discuss this subject in more detail.

Time-dependent moment

The moment (or more precisely: spin-magnetic moment) is the observable that describes the macroscopic spin-magnetic character of quantum mechanical systems. It is defined as the expectation value of the vector of Pauli operators¹ (remember that the sum over i involves also the sum over \mathbf{k} -points, see (3.17)):

$$\mathbf{M}(t) = \sum_i \langle \hat{\boldsymbol{\sigma}}_i \rangle(t). \quad (3.21)$$

The investigation of the dynamics of the moment for systems where SOC is present will be the main subject of this work. Hence, a central equation in this work is the dynamical equation of the moment which is given by

$$\partial_t \mathbf{M}(t) = \underbrace{\sum_i \frac{1}{c} \langle \mathbf{B}_s(\hat{\mathbf{r}}_i, t) \times \hat{\boldsymbol{\sigma}}_i \rangle(t)}_{=\partial_t \mathbf{M}_B(t)} + \underbrace{\sum_i \frac{1}{2c^2} \langle (\nabla v_s(\hat{\mathbf{r}}_i, t) \times [\hat{\mathbf{p}}_i + \frac{1}{c} \mathbf{A}(t)]) \times \hat{\boldsymbol{\sigma}}_i \rangle(t)}_{=\partial_t \mathbf{M}_{\text{SOC}}(t)}, \quad (3.22)$$

by considering the Hamiltonian from (3.16). We see that the dynamics has two contributions: one contribution comes from the \mathbf{B} -field interaction and the other comes from SOC. The derivation of equation (3.22), as well as the derivation of the following relations, can be found in appendix A.6.3.

The moment follows from the integral of the magnetization. Hence, also the time derivative should follow from the corresponding integral:

$$\partial_t \mathbf{M}(t) = \partial_t \int d\mathbf{r} \sum_i \langle \delta(\mathbf{r} - \hat{\mathbf{r}}_i) \hat{\boldsymbol{\sigma}}_i \rangle(t) = \int d\mathbf{r} \partial_t \mathbf{m}(\mathbf{r}, t). \quad (3.23)$$

From equation (3.23) it follows that the local integral representation of (3.22) should lead to an expression that should contain the terms from (3.19). Calculating the local integral representation of (3.22) gives

$$\begin{aligned} \partial_t \mathbf{M}(t) &= \underbrace{\frac{1}{c} \int d\mathbf{r} \left[\mathbf{B}_s(\mathbf{r}, t) \times \mathbf{m}(\mathbf{r}, t) \right]}_{=\partial_t \mathbf{M}_B(t)} \\ &+ \underbrace{\frac{1}{2c^2} \int d\mathbf{r} \left[\overset{\leftrightarrow}{J}^T(\mathbf{r}, t) - \text{Tr}\{\overset{\leftrightarrow}{J}(\mathbf{r}, t)\} \right] \cdot \nabla v_s(\mathbf{r}, t)}_{=\partial_t \mathbf{M}_{\text{SOC}}(t)}. \end{aligned} \quad (3.24)$$

¹A common definition uses the prefactor $g_e \mu_B / 2$ which is $\approx -1/2$ in *a.u.*, i.e. the moment (3.21) can be interpreted as defined in units of $-\mu_B$ since $\mu_B = 1/2$ in *a.u.*

We see that the first and the third term of (3.19) give no contribution to the dynamics of the moment. The first term of (3.19), which is the kinetic contribution, can easily be shown to vanish by Gauss's theorem. As already mentioned, the kinetic contribution is a spin transport contribution, that can locally change the magnetization by spin-currents that flow into or out of a region. The corresponding integral over the whole system can, however, not change as we have seen, meaning that the kinetic term conserves the moment. The integral of the third term of (3.19), which is part of the SOC contribution, can be shown to vanish via integration by parts.

The $\partial_t \mathbf{M}_{\mathbf{B}}$ -term from (3.24) is simply the integral over the local Larmor precession term, which has been discussed in the previous subsection. As already mentioned, this term has in principle two contributions: one from \mathbf{B}_{ext} and one from \mathbf{B}_{xc} . Remember, however, that the \mathbf{B}_{xc} contribution vanishes in our case (since the ALSDA is applied; see (3.20)). Hence, only the \mathbf{B}_{ext} will contribute to the dynamics of the moment in our calculations. In TDSDFt the vanishing of the \mathbf{B}_{xc} contribution is, in fact, an important condition that has to be fulfilled. However, this condition, which is called zero-torque theorem for TDSDFt, does not necessarily have to be fulfilled for a TDSDFt that involves SOC, as will be discussed in the following section.

We now come to the $\partial_t \mathbf{M}_{\text{SOC}}$ -term from (3.24), which will turn out to be a very important term regarding the dynamics of the moment. With the gauge invariant spin-current densities (2.26), this term can be represented in a different way:

$$\partial_t \mathbf{M}_{\text{SOC}}(t) = \frac{1}{2c^2} \int d\mathbf{r} \begin{pmatrix} \mathbf{e}_1 \\ \mathbf{e}_2 \\ \mathbf{e}_3 \end{pmatrix} \times \begin{pmatrix} [\nabla v_s(\mathbf{r}, t) \times \mathbf{j}^1(\mathbf{r}, t)] \\ [\nabla v_s(\mathbf{r}, t) \times \mathbf{j}^2(\mathbf{r}, t)] \\ [\nabla v_s(\mathbf{r}, t) \times \mathbf{j}^3(\mathbf{r}, t)] \end{pmatrix}, \quad (3.25)$$

where $\{\mathbf{e}_l\}$ are the unit vectors. Here, we have defined a cross product of vectors that are constructed from vectors, which is calculated in the usual sense, while the regular multiplication corresponds here to the dot product. As an example, we show the dynamical equation of the \mathbf{e}_3 -component:

$$\partial_t M_{\text{SOC},3}(t) = \frac{1}{2c^2} \int d\mathbf{r} \mathbf{e}_1 \cdot [\nabla v_s(\mathbf{r}, t) \times \mathbf{j}^2(\mathbf{r}, t)] - \mathbf{e}_2 \cdot [\nabla v_s(\mathbf{r}, t) \times \mathbf{j}^1(\mathbf{r}, t)]. \quad (3.26)$$

We see that only the spin-current densities \mathbf{j}^1 and \mathbf{j}^2 contribute to the dynamics of M_3 .

To get an idea how the equation (3.26) could be interpreted, we will help ourselves with some classical considerations. First, we assume that the spin-current densities can be described with the fluid dynamical picture:

$$\mathbf{j}^i(\mathbf{r}, t) = \mathbf{u}^i(\mathbf{r}, t) m_i(\mathbf{r}, t), \quad i = \{1, 2, 3\}. \quad (3.27)$$

Here, we have defined the velocity field \mathbf{u}^i via the i th component of the magnetization. Equation (3.27) means the following: the spin-current density of spin-component i at point \mathbf{r} can be understood as a local magnetic dipole at point \mathbf{r} that moves according to the velocity vector $\mathbf{u}^i(\mathbf{r})$, while the local magnetic dipole corresponds to the i th component of the magnetization. Next, we recall that

$\nabla v_s(\mathbf{r})$ corresponds to an electric field, and that a particle that moves with the velocity \mathbf{u} in an electric field \mathbf{E} sees a magnetic field $\mathbf{B} = \mathbf{E} \times \mathbf{u}/c$. With these considerations we can, according to (3.26), define the following effective \mathbf{B} -field components that are seen by our moving local magnetic dipoles:

$$\mathbf{e}_1 \cdot [\nabla v_s(\mathbf{r}, t) \times \mathbf{u}^2(\mathbf{r}, t)]/c = \tilde{B}_1(\mathbf{r}, t), \quad \mathbf{e}_2 \cdot [\nabla v_s(\mathbf{r}, t) \times \mathbf{u}^1(\mathbf{r}, t)]/c = \tilde{B}_2(\mathbf{r}, t). \quad (3.28)$$

With these effective fields we get, together with (3.27), for (3.26):

$$\begin{aligned} \partial_t M_{\text{SOC},3}(t) &= \frac{1}{2c} \int d\mathbf{r} \tilde{B}_1(\mathbf{r}, t) m_2(\mathbf{r}, t) - \tilde{B}_2(\mathbf{r}, t) m_1(\mathbf{r}, t) \\ &\hat{=} \frac{1}{2c} \int d\mathbf{r} \tilde{\mathbf{B}}(\mathbf{r}, t) \times \mathbf{m}(\mathbf{r}, t) \Big|_3. \end{aligned} \quad (3.29)$$

We see that the previous assumptions led to a term that has a similar form as the $\partial_t \mathbf{M}_{\mathbf{B}}(t)$ -term from (3.24), which describes the dynamics of a local dipole in a magnetic field. Therefore, we can conclude that the work mechanism of $\partial_t \mathbf{M}_{\text{SOC}}(t)$ can be imagined as follows: Each component of the local magnetization acts as a local magnetic dipole that moves according to the local spin-current density into the electric field produced from the local potential. The movement in this electric field produces a magnetic field that leads to a torque on the local dipole, and hence to a change of the magnetization. We point out that the expression in (3.29) has a factor 1/2 that is not present in the $\partial_t \mathbf{M}_{\mathbf{B}}(t)$ -term. This factor is the well known Thomas precession factor that incorporates relativistic corrections into the previously drawn picture.

As a final remark we wish to emphasize that a spin-current density can exist even if its corresponding magnetization component is zero (in contrast to the probability density and its current), which is, in fact, the case in our calculations (see appendix A.2). Hence, one should be careful with the interpretation of the demagnetization process via the previously given explanation, because a change in the moment can also occur if the associated magnetization component (according to (3.27)) is zero.

3.1.5. The zero-torque theorem

The concept behind any KS-TDDFT scheme is that one or more variables of an interacting system (e.g. the density or magnetization) are produced by the non-interacting KS system. Of particular importance are the xc fields which incorporate many-body contributions to the KS system. By comparing the dynamical equations of the variables of the many-body system to the corresponding equations of the KS system, exact conditions for the xc fields can be derived. We will in the following demonstrate this concept for standard TDSDF without SOC, and we will discuss what changes occur if SOC is present.

We assume to have the following many-electron Hamiltonian:

$$\hat{H}(t) = \sum_{i=1}^N \left[\frac{\hat{p}_i^2}{2} + v_{\text{ext}}(\hat{\mathbf{r}}_i, t) + \frac{1}{2c} \hat{\boldsymbol{\sigma}}_i \cdot \mathbf{B}_{\text{ext}}(\hat{\mathbf{r}}_i, t) \right] + \frac{1}{2} \sum_{i \neq j}^N \frac{1}{|\hat{\mathbf{r}}_i - \hat{\mathbf{r}}_j|}. \quad (3.30)$$

The corresponding KS Hamiltonian within the TDSDFD framework is given by

$$\hat{h}(t) = \frac{\hat{p}^2}{2} + v_s(\hat{\mathbf{r}}, t) + \frac{1}{2c} \hat{\boldsymbol{\sigma}} \cdot \mathbf{B}_s(\hat{\mathbf{r}}, t), \quad \text{with} \quad \mathbf{B}_s(\hat{\mathbf{r}}, t) = \mathbf{B}_{\text{ext}}(\hat{\mathbf{r}}, t) + \mathbf{B}_{\text{xc}}(\hat{\mathbf{r}}, t). \quad (3.31)$$

Calculating the dynamical equation of the magnetization for (3.30) gives

$$\partial_t \mathbf{m}(\mathbf{r}, t) = -\nabla \cdot \overleftrightarrow{J}(\mathbf{r}, t) + \frac{1}{c} \left[\mathbf{B}_{\text{ext}}(\mathbf{r}, t) \times \mathbf{m}(\mathbf{r}, t) \right], \quad (3.32)$$

while calculating the corresponding equation for (3.31) gives

$$\partial_t \mathbf{m}(\mathbf{r}, t) = -\nabla \cdot \overleftrightarrow{J}_{\text{KS}}(\mathbf{r}, t) + \frac{1}{c} \left[(\mathbf{B}_{\text{ext}}(\mathbf{r}, t) + \mathbf{B}_{\text{xc}}(\mathbf{r}, t)) \times \mathbf{m}(\mathbf{r}, t) \right], \quad (3.33)$$

where we have explicitly labeled the KS spin-current tensor. By construction, the time-dependent magnetization is equal in both systems. The spin-current tensor (or more precisely: the divergence of it), on the other hand, is usually different. Thus, the \mathbf{B}_{xc} can be understood as a field that compensates this difference, in order to achieve the correct magnetization in the KS system. This can be seen immediately by subtracting (3.32) from (3.33), which gives

$$\nabla \cdot \left[\overleftrightarrow{J}_{\text{KS}}(\mathbf{r}, t) - \overleftrightarrow{J}(\mathbf{r}, t) \right] = \frac{1}{c} \left[\mathbf{B}_{\text{xc}}(\mathbf{r}, t) \times \mathbf{m}(\mathbf{r}, t) \right]. \quad (3.34)$$

Integrating this expression leads to

$$\int d\mathbf{r} \mathbf{B}_{\text{xc}}(\mathbf{r}, t) \times \mathbf{m}(\mathbf{r}, t) = 0, \quad (3.35)$$

where we have used Gauss's theorem. The expression (3.35) is known as zero-torque theorem² for TDSDFD [37]. This theorem has a clear physical meaning: it states that the \mathbf{B}_{xc} cannot exert a net spin-torque on the whole system, which is clear, because the \mathbf{B}_{xc} incorporates only bare Coulomb interaction effects between the electrons, that should not lead to a net spin-torque. Thus, the zero-torque theorem should always be satisfied when performing a TDSDFD calculation, because otherwise non-physical spin-torques on the whole systems would occur.

The calculations in this work employed a time-dependent spin-DFT that includes SOC contributions. As previously discussed, the zero-torque theorem should be satisfied for standard TDSDFD. However, one might wonder if this theorem should also be satisfied if SOC contributions are considered. To investigate this issue, we will follow the same route as before, with the difference that we will refer to the time-dependent SDFD scheme from section 3.1.2 (this scheme will in the following serve as a formally exact SDFD scheme that includes SOC contributions, which allows us to draw some general conclusions that should apply for any spin-DFT framework that considers SOC contributions).

²There exists also a zero-torque theorem for CDFT, which is connected to the torque on the orbital angular momentum.

The dynamical equation of the magnetization of the many-electron Hamiltonian (3.12) is given by

$$\begin{aligned} \partial_t \mathbf{m}(\mathbf{r}, t) = & -\nabla \cdot \overset{\leftrightarrow}{J}(\mathbf{r}, t) + \frac{1}{c} [\mathbf{B}_{\text{ext}}(t) \times \mathbf{m}(\mathbf{r}, t)] + \frac{1}{4c^2} [\nabla n(\mathbf{r}, t) \times \nabla v_n(\mathbf{r})] \\ & + \frac{1}{2c^2} \left[\overset{\leftrightarrow}{J}^T(\mathbf{r}, t) - \text{Tr}\{\overset{\leftrightarrow}{J}(\mathbf{r}, t)\} \right] \cdot \nabla v_n(\mathbf{r}) + \frac{1}{i} \langle [\hat{\mathbf{m}}(\mathbf{r}), \hat{W}] \rangle(t), \end{aligned} \quad (3.36)$$

where we have neglected the $(\mathbf{E}_{\text{ext}} \times \hat{\mathbf{p}})$ -term from the SOC. (We will neglect this term, because it was shown in section 3.1.1 that its contribution to the spin-dynamics is negligible. However, it is clear that this term would actually also be present in what follows.) Note that the many-electron SOC term \tilde{W} (see (2.41)) appears in the dynamical equation, because this term allows a transfer between orbital angular momentum and spin-angular momentum.

The corresponding dynamical equation for the KS system has already been discussed in section 3.1.4. Subtracting the dynamical equation of the magnetization of the KS system (3.19) from the corresponding equation of the interacting system (3.36), and integrating it, gives

$$\begin{aligned} & \int d\mathbf{r} \frac{1}{c} \mathbf{B}_{\text{xc}}(\mathbf{r}, t) \times \mathbf{m}(\mathbf{r}, t) \quad (3.37) \\ = & \int d\mathbf{r} \frac{1}{2c^2} \left[\left(\overset{\leftrightarrow}{J}^T(\mathbf{r}, t) - \text{Tr}\{\overset{\leftrightarrow}{J}(\mathbf{r}, t)\} \right) - \left(\overset{\leftrightarrow}{J}_{\text{KS}}^T(\mathbf{r}, t) - \text{Tr}\{\overset{\leftrightarrow}{J}_{\text{KS}}(\mathbf{r}, t)\} \right) \right] \cdot \nabla v_n(\mathbf{r}) \\ + & \int d\mathbf{r} \frac{1}{i} \langle [\hat{\mathbf{m}}(\mathbf{r}), \hat{W}] \rangle(t) - \frac{1}{2c^2} \left[\overset{\leftrightarrow}{J}_{\text{KS}}^T(\mathbf{r}, t) - \text{Tr}\{\overset{\leftrightarrow}{J}_{\text{KS}}(\mathbf{r}, t)\} \right] \cdot \nabla v_{\text{H,xc}}(\mathbf{r}, t). \end{aligned}$$

We have again specifically labeled the KS spin-current tensor, and we have summed the Hartree and the xc potential. From (3.37) it follows immediately that the usual zero-torque theorem does not apply for our spin-DFT scheme with SOC. The integral condition that led in the standard TDSDFE to the zero-torque theorem is given here by a rather complicated expression, that does not necessarily reduce to (3.35). In fact, the expression (3.37) has a clear meaning, as will be discussed now.

First of all, we point out that (3.37) describes all possible spin-torque differences that might exist between the KS system and the interacting system: The second line of (3.37) corresponds to a spin-torque difference that arises from the fact that the spin-currents in the interacting system and in the KS system are not necessarily equal. This difference between the spin-currents can then, via the nuclear potential, lead to a spin-torque difference (remember that the corresponding potential mediated spin-torque process has been discussed at the end of the previous section). The right part of the third line of (3.37) corresponds to a spin-torque in the KS system that is caused by the spin-currents and the Hartree and xc potential, while the left part corresponds to a spin-torque in the interacting system that is caused by the many-electron SOC interaction. These two spin-torques (which both correspond to an electron-electron interaction mediated transfer between spin and orbital angular momentum) are in general not equal, meaning that the third line corresponds to a spin-torque difference as well. The spin-torque differences coming from the second and third line would, in an exact

framework, have to be compensated by the xc \mathbf{B} -field via the integral expression from the first line (in order to prevent non-physical spin-torques on the KS system). Note that the expression (3.37) corresponds, in a way, also to a zero-torque theorem. This theorem is, however, in contrast to standard TDSDFE much more involved, and it reveals an exact relation between the xc potential and the xc \mathbf{B} -field.

We wish to mention that the previously discussed aspects should, at least in some sense, also apply for other spin-DFT schemes that include SOC (and that describe similar physical situation as the scheme from section 3.1.2). Furthermore, we point out that the second line of (3.37) would vanish if a time-dependent SCDFE would be applied (since the spin-currents in the KS and the interacting system would be equal). However, the third line of (3.37) would not necessarily vanish, meaning that the zero-torque condition (3.35) would most probably also not apply for a SCDFE scheme that includes SOC.

We conclude that the zero-torque theorem (3.35) is not a necessary condition when a time-dependent spin-DFT with SOC is applied. In fact, the zero-torque condition that has to be fulfilled when SOC is present is much more complicated, as we showed. All calculations that are presented in this work used the ALSDA, i.e. the applied \mathbf{B}_{xc} always satisfied the condition (3.35) (this follows immediately from relation (3.20)). Hence, any unphysical spin-torque contributions that might exist due to the right term of (3.37) are not canceled by the applied \mathbf{B}_{xc} . Thus, in future work it has to be investigated if this leads, at least for such situations that are considered in this work, to any significant influences in the spin-dynamics.

3.2. Real-time propagation algorithm and implementation

In the sections 3.1.2 and 3.1.3, the theoretical framework that was applied to describe the real-time spin-dynamics has been introduced. In the following, we will describe in detail how the corresponding KS equations were solved. The algorithm that was used to solve the KS equations has been implemented in the ELK code [54], and all calculation presented in this work have been performed with this code.

The calculations in this work are based on a real-time propagation of the KS system (3.16). In all calculations, the system started to evolve from the ground state. Thus, the first step in each calculation was a ground state run. As already discussed in section 3.1.3, the ground state run has to be performed by a self-consistency cycle, since the density and the magnetization enter the functionals. We will now be a bit more precise about how the ground state is calculated in the ELK code. An important feature of the ELK code is that it is an all-electron code, i.e. all electrons will be incorporated in the calculation and no pseudo-potentials, or similar, are used. This means, in practice, that two types of KS states are used: core states and valence states. The core states have much lower energy eigenvalues as the valence states, and they are localized in a tiny region around the nucleus, while the valence states are generally much more delocalized.

In each step of the self-consistency cycle, the core states are treated relativistically by solving a radial KS-Dirac equation (see [24]), which gives a core state density contribution. The valence states are calculated with the framework (3.16) (together with some additional relativistic corrections, as discussed in section 3.1.3), which gives a valence state density contribution and the magnetization. The core and valence state densities are then summed together to obtain the total density, which is then used, together with the magnetization, to calculate the xc fields for the next cycle. These steps are repeated until convergence is reached.

We want to emphasize one point concerning the real-time propagation: The propagation scheme that will be introduced in the following was only applied to the valence states, while the core states were frozen during the propagation. Thus, the core density contribution, that enters the Hartree and the xc potential during the propagation of the valence KS system (3.16), was always constant and equal to the converged ground state contribution. If the external field is weak enough, this approach should be justified, since the influence of the this field on the strongly bound core states should be negligible. If, however, the external field is very strong, the time evolution of the core states would most probably have to be taken into consideration. In fact, at the moment it is not entirely clear if the time evolution of the core states would give any non-negligible contributions for the external fields that have been used in the calculations of this work. Hence, this issue should be investigated in future work.

In this section, the real-time propagation algorithm that was applied to propagate the valence states will be presented. Following this, the basis that was used to represent the time-dependent KS states, will be discussed.

Real-time propagation scheme

Next, the real-time propagation algorithm that was used to propagate the system (3.16) will be presented. For a clear view, we will represent the KS spinors in the general state representation: $\varphi_i^{\mathbf{k}}(\mathbf{r}, t) \rightarrow |\varphi_i(t)\rangle$. Moreover, we will omit the \mathbf{k} -point label, as the propagation scheme is identical for all \mathbf{k} -points. In practice, the propagation of the \mathbf{k} -points is performed independently, and the only step where all \mathbf{k} -point dependent states are needed is when the density and the magnetization is calculated (as can be seen in the scheme (3.16)). Furthermore, N_{occ} will stand for the number of occupied KS states, and N_{max} will stand for the number of basis states that are used to expand the KS states.

The solution of the time-dependent KS equations can be represented by means of the time evolution operator:

$$i\partial_t|\varphi_i(t)\rangle = \hat{h}_s(t)|\varphi_i(t)\rangle \quad \longrightarrow \quad |\varphi_i(T)\rangle = \hat{U}(T, 0)|\varphi_i(0)\rangle, \quad (3.38)$$

where $\hat{h}_s(t)$ is the KS Hamiltonian from (3.16), and $\hat{U}(T, 0)$ is the time evolution operator that propagates all KS states from time $t = 0$ to the final time $t = T$. The time evolution operator satisfies the following property:

$$\hat{U}(T, 0) = \hat{U}(T, T - \Delta t) \dots \hat{U}(2\Delta t, \Delta t) \hat{U}(\Delta t, 0), \quad (3.39)$$

which states that the propagation of one large time step T can be split into several small propagation steps of time Δt . The presented propagation scheme is based on

this property, because all KS states will be propagated stepwise forward in time, i.e. for the time t , the time evolution operator $\hat{U}(t + \Delta t, t)$ has to be calculated. The corresponding time evolution operator is given by

$$\hat{U}(t + \Delta t, t) = \sum_{n=0}^{\infty} \frac{(-i)^n}{n!} \int_t^{t+\Delta t} dt_1 \dots \int_t^{t+\Delta t} dt_n \tilde{\text{T}}[\hat{h}_s(t_1) \dots \hat{h}_s(t_n)], \quad (3.40)$$

where $\tilde{\text{T}}$ is the time ordering operator, which orders all time-dependent elements such that the elements with later times are always to the left of elements with earlier times. If the time step size Δt is small enough, such that the change of $\hat{h}_s(t)$ between t and $t + \Delta t$ becomes negligible, the time evolution operator can be approximated by an exponential expression:

$$\Delta t \rightarrow 0: \quad \tilde{\text{T}}[\hat{h}_s(t_1) \dots \hat{h}_s(t_n)] \approx \hat{h}_s^n(t) \quad \longrightarrow \quad \hat{U}(t + \Delta t, t) \approx e^{-i\hat{h}_s(t)\Delta t}. \quad (3.41)$$

This exponential expression can be used to stepwise propagate all KS states forward in time:

$$|\varphi_i(t + \Delta t)\rangle = e^{-i\hat{h}_s(t)\Delta t} |\varphi_i(t)\rangle, \quad i = \{1, \dots, N_{\text{occ}}\}. \quad (3.42)$$

This time evolution step involves an exponential expression of an operator, which is in general not easy to calculate. To permit an accurate calculation of (3.42), the KS Hamiltonian can be diagonalized at each time step, and the time-dependent KS states can be expanded in the corresponding instantaneous eigenstates:

$$\hat{h}_s(t) |u_t\rangle = \epsilon_{t,u} |u_t\rangle \quad \longrightarrow \quad |\varphi_i(t)\rangle = \sum_{u=1}^{N_{\text{max}}} c_{ui}(t) |u_t\rangle, \quad (3.43)$$

which replaces the exponential of the operator by an ordinary scalar exponential. We point out that the instantaneous eigenstates $|u_t\rangle$ and the corresponding eigenvalues $\epsilon_{t,u}$ do not have any direct physical meaning, and they should be seen as an auxiliary tool.

The propagation algorithm used in the calculations follows solely from the relations (3.42) and (3.43). The applied propagation scheme can be summarized by the following three steps, which allow it to successively propagate all KS states forward in time:

$$\begin{aligned} (1) \quad & |\varphi_i(t + \Delta t)\rangle = \sum_{u=1}^{N_{\text{max}}} c_{ui}(t) e^{-i\epsilon_{t,u}\Delta t} |u_t\rangle \\ (2) \quad & \langle \hat{n}(\mathbf{r}) \rangle(t + \Delta t), \langle \hat{\mathbf{m}}(\mathbf{r}) \rangle(t + \Delta t) \xrightarrow{\text{ALSDA}} \hat{h}_s[n, \mathbf{m}](t + \Delta t) \xrightarrow{(3.43)} \{|u_{t+\Delta t}\rangle\} \\ (3) \quad & c_{ui}(t + \Delta t) = \langle u_{t+\Delta t} | \varphi_i(t + \Delta t) \rangle, \end{aligned} \quad (3.44)$$

where the three steps correspond to a propagation from t to $t + \Delta t$. Step (1) is the actual forward propagation of all states. This step follows directly from (3.42) with the expansion (3.43). In step (2), the density and the magnetization are calculated according to (3.16), which are then used to construct the KS Hamiltonian at

time $t + \Delta t$ by applying the ALSDA. The KS Hamiltonian is then diagonalized which gives the eigenstates and eigenvalues at time $t + \Delta t$. Finally, in step (3) the expansion coefficients of the KS states in the instantaneous eigenstates are calculated, which completes all steps that are needed to perform one propagation cycle. Since the propagation starts always from the ground state in our case, the initial eigenstates are given by the ground state KS states, leading to the following initial condition:

$$|\varphi_u(t=0)\rangle = |u_{t=0}\rangle \quad \longrightarrow \quad c_{ui}(t=0) = \delta_{ui}. \quad (3.45)$$

The accuracy of the propagation algorithm (3.44) depends primarily on two variables. First, it depends on the time step size Δt that determines how well the time evolution operator is approximated. A smaller time step size means in general a better approximation, but also a longer computation time, since more time steps are necessary to propagate to the final time T . In practice, the parameters of an algorithm have to be adapted until convergence is reached. In our calculation, the converged time step sizes lie, depending on the individual system, between $\Delta t = 0.025 \dots 0.1 \text{ a.u.}$ ($= 0.6 \dots 2.4 \cdot 10^{-3} \text{ fs}$). The second variable that determines the accuracy is N_{\max} , i.e. the number of instantaneous eigenstates that are used to expand the time-dependent KS states. From the algorithm (3.44) it is clear that a larger N_{\max} means a more expensive computation. For calculations with primitive unit cells, a number of ≈ 120 empty states ($= N_{\max} - N_{\text{occ}}$) led to a sufficient convergence, while for super cells or atomic layers more empty states were needed (typically 300 \dots 600 for 4-atom cells). We finally recall that also the number of \mathbf{k} -points has to be converged, since the density and the magnetization, and thus the KS Hamiltonian, depends on this number. We will say a few words about the \mathbf{k} -point convergence at the end of section 4.2.

The basis

In the previous subsection the applied propagation algorithm has been explained. One major concept of this algorithm is that the time-dependent KS states are expanded in the instantaneous eigenstates $|u_t\rangle$, according to relation (3.43). All calculations in this work have been performed with the ELK code, which uses a APW+LO (augmented plane wave and local orbital) basis. Hence, the APW+LO basis is the underlying basis that was used to represent the instantaneous eigenstates. These eigenstates, and thus also the corresponding expansion coefficients in reference to the APW+LO basis, are in general \mathbf{k} -point dependent. Since the \mathbf{k} -points are calculated independently, and to be consistent with the previous subsection, we will in the following omit the \mathbf{k} -point label. Keep in mind that the \mathbf{k} -point dependence can

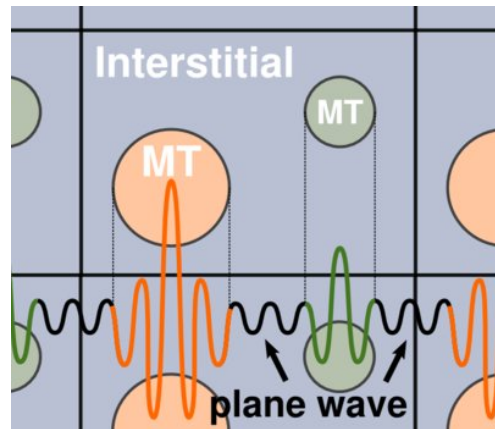


Fig. 3.1.: Schematic of the APW+LO basis.

be treated by applying a \mathbf{k} -point dependent Hamiltonian, where each \mathbf{k} -point dependent state is described by a lattice periodic function (see appendix A.5, relation (A.57)). Hence, all states have to be understood as lattice periodic functions in the following discussion.

Each instantaneous eigenstate is represented in the following way:

$$|u_t\rangle = \sum_{\mathbf{G}}^{N_{\max}^{\mathbf{G}}} a_{\mathbf{G}u}(t) |\psi_{\mathbf{G}}^{\text{APW}}\rangle + \sum_{l=0}^{l_{\max}} \sum_{m=-l}^l \sum_{n=1}^{N_{\max}^l} b_{lmn,u}(t) |\psi_{lmn}^{\text{LO}}\rangle. \quad (3.46)$$

The APW sum on the left hand side runs over the reciprocal lattice vectors \mathbf{G} , where $N_{\max}^{\mathbf{G}}$ is the number of reciprocal lattice vectors, which is determined from an appropriate cutoff length. The LO sum on the right hand side runs over the azimuthal number l up to the cutoff l_{\max} , over the magnetic number m , and over n up to N_{\max}^l , which determines how many LOs are used for a certain azimuthal number l . l_{\max} and N_{\max}^l have to be chosen large enough such that convergence is reached.

The main concept of the APW+LO basis is that the unit cell is divided in two regions: in a so-called muffin-tin (MT) region, and in an interstitial region (IR). The MTs correspond to spheres around each nucleus, while each nucleus sits at the center of the sphere. The IR is the region outside the spheres. A schematic of these regions is given in figure 3.1. Each LO is a wave function that is zero outside a MT, and that is represented by spherical harmonics inside a MT:

$$\langle \alpha, r, \theta, \phi | \psi_{lmn}^{\text{LO}} \rangle = f_{lmn}^{\alpha}(r) Y_{lm}(\theta, \phi), \quad \alpha = \{\uparrow, \downarrow\}. \quad (3.47)$$

The $Y_{lm}(\theta, \phi)$ are the spherical harmonics and we have used the spherical coordinate representation (r, θ, ϕ) . The radial functions $f_{lmn}^{\alpha}(r)$ are typically constructed in convenient ways. We will, however, at this point only state that the radial functions are constructed such that they are zero at the MT surface. The term on the right hand side of (3.46) runs in general also over the several MTs in the unit cell, i.e. each MT has its own set of LOs. For simplicity, we omitted this additional sum.

Each \mathbf{G} -vector dependent APW is represented by a corresponding plane wave in the IR: $\langle \alpha, \mathbf{r} | \psi_{\mathbf{G}}^{\text{APW}} \rangle \sim e^{i\mathbf{G}\cdot\mathbf{r}}$. Inside the MTs, each APW is represented by a sum of radial functions. These radial functions are similar to the LOs, with the difference that the sum of these functions is constructed such that the wave function value matches the corresponding plain wave value at the MT surface³. A schematic of a APW is given in figure 3.1. Finally, we wish to mention that the APW+LO basis is a non-orthogonal basis. General details about the construction and the properties of APWs and LOs can be found in [55], while ELK specific details are provided in the ELK manual [54].

³ELK supports also LAPWs (Linearized APWs), which are similar to APWs, with the difference that also derivatives of the wave functions are matched at each MT surface.

3.3. Time-dependent density of states

In this section, we will discuss how a time-dependent density of states (TDDOS) can be defined. Moreover, we will derive an approximated expression for this TD-DOS, which can be calculated very efficiently during the real-time propagation. The central quantity that will be used for the definition of the TDDOS is the spectral function, which provides information about the nature of electronic states, and which is, for time-dependent problems, defined from the non-equilibrium Green functions. The non-equilibrium Green functions are the central objects in the perturbative calculation of time-dependent quantities, such as one-particle expectation values or response functions. An overview of non-equilibrium Green functions and the related perturbation theory can be found in [44].

The TDDOS that will be derived in the following will be calculated from the KS Green functions and not from the true Green functions. These two types of quantities are in general different, however, they produce in principle the same time-dependent magnetization. Thus, a corresponding spin-resolved KS-TDDOS could, for example, be used to reveal some insights about spin-dynamical processes. The Green functions and all related quantities are in general functions of two time and two space variables. In the following, these objects will be treated as time-dependent operators in the single-particle space, i.e. for spin-less systems:

$$G(\mathbf{r}_1 t_1, \mathbf{r}_2 t_2) = \langle \mathbf{r}_1 | \hat{G}(t_1, t_2) | \mathbf{r}_2 \rangle. \quad (3.48)$$

Furthermore, we will, for simplicity, again omit the \mathbf{k} -point label. Each sum over the occupied KS states has to be understood as a sum over all \mathbf{k} -points and the corresponding occupied states, as shown in (3.16).

The spectral function $\hat{A}(t_1, t_2)$ is defined from the greater Green function $\hat{G}^>(t_1, t_2)$ and from the lesser Green function $\hat{G}^<(t_1, t_2)$, and it is, for the KS system, directly given by the time-dependent KS states [44]:

$$\hat{A}(t_1, t_2) = i[\hat{G}^>(t_1, t_2) - \hat{G}^<(t_1, t_2)] = \sum_i |\varphi_i(t_1)\rangle \langle \varphi_i(t_2)|. \quad (3.49)$$

$\hat{A}(t_1, t_2)$ contains information from all available states, while $\hat{G}^<(t_1, t_2)$ gives the contribution from all occupied states, and $\hat{G}^>(t_1, t_2)$ gives the contribution from all unoccupied states. Thus, a spectral function that contains only the information from the occupied states can be defined by taking only $\hat{G}^<(t_1, t_2)$ into account:

$$\hat{A}_{\text{occ}}(t_1, t_2) = -i\hat{G}^<(t_1, t_2) = \sum_i f_i |\varphi_i(t_1)\rangle \langle \varphi_i(t_2)|, \quad (3.50)$$

where f_i is the occupation number at $t = 0$, i.e. in our case the ground state occupation number. We see that the full spectral function from (3.49) is in principle given by the same expression as the occupied spectral function, with the difference that f_i is always 1 for the full spectral function. Hence, we will in the following always use f_i , since all derived quantities can then easily be calculated for the full contribution of all states, or for the contribution of the occupied states only:

$$\text{full: } f_i = 1 \quad \forall i, \quad \text{occupied: } f_i = \begin{cases} 1, & \text{if state } i \text{ is occupied} \\ 0, & \text{else} \end{cases}. \quad (3.51)$$

As a first step, we transform the spectral function to a time-frequency form by applying a Wigner transformation:

$$\hat{A}(\omega, t) = \int d\tau e^{i\omega\tau} \hat{A}(t + \frac{\tau}{2}, t - \frac{\tau}{2}). \quad (3.52)$$

Transformations of this type are commonly used to describe or analyze the time-dependent spectral properties of quickly changing and finite signals (e.g. ultra-short laser pulse analysis [48]). With this time and frequency dependent spectral function, a corresponding TDDOS can, according to the equilibrium definition, be defined [56]:

$$\rho(\omega, t) = \frac{1}{2\pi} \text{Tr}\{\hat{A}(\omega, t)\} = \frac{1}{2\pi} \sum_i f_i \int d\tau e^{i\omega\tau} \text{Tr}\{|\varphi_i(t + \frac{\tau}{2})\rangle\langle\varphi_i(t - \frac{\tau}{2})|\}. \quad (3.53)$$

The integral expression on the right hand side of (3.53) is a so-called Wigner distribution function, which typically serves as a joint probability density for conjugate variables (in our case ω and t).

The TDDOS as defined in (3.53) is, for a KS system (where the Hamiltonian depends on the corresponding time-dependent variables, e.g. the density), very hard to calculate. In the following we design a numerically less heavy approximation to the TDDOS. In order to do this, we will approximate the time evolution operator by

$$\hat{U}(t \pm \frac{\tau}{2}, t) \approx e^{-i\hat{h}_s(t)(\pm\frac{\tau}{2})}, \quad (3.54)$$

which gives for (3.53)

$$\rho(\omega, t) = \frac{1}{2\pi} \sum_i f_i \int d\tau e^{i\omega\tau} \text{Tr}\{e^{-i\hat{h}_s(t)\frac{\tau}{2}} |\varphi_i(t)\rangle\langle\varphi_i(t)| e^{-i\hat{h}_s(t)\frac{\tau}{2}}\}. \quad (3.55)$$

This approximation has to be understood as a quasi static approximation, i.e. it is assumed that the time evolution of the instantaneous state was for all past times, and is for all future times, governed by the instantaneous Hamiltonian. Hence, this approximation should be justified if the Hamiltonian changes slowly. This is usually the case if there is no time-dependent external field, or if the change of the external field is slow enough. Nevertheless, we have to keep in mind that the KS Hamiltonian is, in principle, always time-dependent if the system is not in the groundstate. However, it turned out in our calculations that the change of the KS Hamiltonian, that is caused solely by the oscillating density and magnetization of an excited state, is very small, largely because the fraction of excited electrons only produces a small contribution to the total density.

In order to calculate the expression (3.55), we expand the time-dependent KS states in the instantaneous eigenstates and we use the instantaneous eigenvalues,

which gives according to (3.43):

$$\begin{aligned}
\rho(\omega, t) &= \frac{1}{2\pi} \sum_i f_i \int d\tau e^{i\omega\tau} \sum_{u,v} c_{ui}(t) c_{vi}^*(t) \text{Tr}\{e^{-i\epsilon_{t,u}\frac{\tau}{2}} |u_t\rangle \langle v_t| e^{-i\epsilon_{t,v}\frac{\tau}{2}}\}. \\
&= \sum_{u,v} \text{Tr}\{|u_t\rangle \langle v_t|\} \frac{1}{2\pi} \int d\tau e^{i(\omega - \frac{1}{2}[\epsilon_{t,u} + \epsilon_{t,v}])\tau} \sum_i f_i c_{ui}(t) c_{vi}^*(t) \\
&= \sum_{u,v} \text{Tr}\{|u_t\rangle \langle v_t|\} \delta(\omega - \frac{1}{2}[\epsilon_{t,u} + \epsilon_{t,v}]) \sum_i f_i c_{ui}(t) c_{vi}^*(t). \quad (3.56)
\end{aligned}$$

The instantaneous eigenstates are orthonormal, which gives $\text{Tr}\{|u_t\rangle \langle v_t|\} = \delta_{uv}$, and we finally get

$$\rho(\omega, t) = \sum_u \delta(\omega - \epsilon_{t,u}) \underbrace{\sum_i f_i |c_{ui}(t)|^2}_{\cong \tilde{f}_u(t)}. \quad (3.57)$$

The TDDOS (3.57) looks similar to the ground state density of states, with the difference that we have now time-dependent occupation numbers $\tilde{f}_u(t)$, and we have contributions from the time-dependent eigenvalues $\epsilon_{t,u}$. Note that the time-dependent eigenvalues correspond, in principle, to a time-dependent band structure $\epsilon_{t,u}(\mathbf{k})$, which is occupied according to $\tilde{f}_u(\mathbf{k}, t)$. With (3.51) we can now calculate from (3.57) the full TDDOS, $\rho_{\text{full}}(\omega, t)$, and the occupied TDDOS, $\rho_{\text{occ}}(\omega, t)$.

The trace over the one-particle space can be calculated by

$$\text{Tr}\{\dots\} = \sum_{\alpha=\uparrow,\downarrow} \int d\mathbf{r} \langle \alpha, \mathbf{r} | \dots | \alpha, \mathbf{r} \rangle, \quad (3.58)$$

which allows it to split the TDDOS in a spin-up and a spin-down part. Hence, we can, according to (3.56), define a spin-resolved TDDOS:

$$\rho^\alpha(\omega, t) = \sum_{u,v} \left(\int d\mathbf{r} \langle \alpha, \mathbf{r} | u_t \rangle \langle v_t | \alpha, \mathbf{r} \rangle \right) \delta(\omega - \frac{1}{2}[\epsilon_{t,u} + \epsilon_{t,v}]) \sum_i f_i c_{ui}(t) c_{vi}^*(t), \quad (3.59)$$

with $\alpha = \{\uparrow, \downarrow\}$. According to (3.51), the full and the occupied spin-resolved TDDOS can be calculated. The occupied spin-resolved TDDOS gives information about the time-dependent occupation of the spin-up and spin-down states, while the full spin-resolved TDDOS reveals information about the corresponding available states. The \mathbf{e}_3 -component of the moment can be calculated via

$$M_3(t) = \int d\omega \rho_{\text{occ}}^\uparrow(\omega, t) - \rho_{\text{occ}}^\downarrow(\omega, t), \quad (3.60)$$

which follows directly from (3.59).

In the same manner as before, a region-resolved TDDOS can also be defined by splitting the integral from (3.58) into a sum of integrals over different volumes. Since the APW+LO basis is used in the calculations, it is a natural choice to split the integral volume into the MT and IR:

$$\int d\mathbf{r} \dots = \int_{\text{MT}} d\mathbf{r} \dots + \int_{\text{IR}} d\mathbf{r} \dots, \quad (3.61)$$

which defines, according to (3.59), the spin-resolved MT-TDDOS, $\rho^{\alpha,\text{MT}}(\omega, t)$, and the IR-TDDOS, $\rho^{\alpha,\text{IR}}(\omega, t)$. With these definitions, the number of electrons in the spin-up and spin-down channels in the different regions can be calculated:

$$N^{\alpha,\text{MT}}(t) = \int d\omega \rho_{\text{occ}}^{\alpha,\text{MT}}(\omega, t), \quad N^{\alpha,\text{IR}}(t) = \int d\omega \rho_{\text{occ}}^{\alpha,\text{IR}}(\omega, t). \quad (3.62)$$

It is then straightforward to calculate the \mathbf{e}_3 -component of the moment in the different regions. For the MT, for example, follows:

$$M_3^{\text{MT}}(t) = N^{\uparrow,\text{MT}}(t) - N^{\downarrow,\text{MT}}(t). \quad (3.63)$$

We will now come back to the total TDDOS (3.57). The full total TDDOS contains information about all available states at a certain time t . Hence, a corresponding time-dependent Fermi energy, $\epsilon_{\text{F}}(t)$, can be defined by

$$N = \int_{-\infty}^{\epsilon_{\text{F}}(t)} d\omega \rho_{\text{full}}(\omega, t), \quad (3.64)$$

where N is the number of electrons. With this definition, it is now possible to calculate the number of excited electrons, N_{exc} , and the number of non-excited electrons, N_{ne} , at time t :

$$N_{\text{exc}}(t) = \int_{\epsilon_{\text{F}}(t)}^{\infty} d\omega \rho_{\text{occ}}(\omega, t), \quad N_{\text{ne}}(t) = \int_{-\infty}^{\epsilon_{\text{F}}(t)} d\omega \rho_{\text{occ}}(\omega, t) = N - N_{\text{exc}}(t). \quad (3.65)$$

In the same way as before, the spin-resolved, and also the region- and spin-resolved number of excited, and non-excited electrons can be calculated (see (3.62)). For example, the number of excited and non-excited electrons in the spin-up and spin-down channel in the MT is given by

$$N_{\text{exc}}^{\alpha,\text{MT}}(t) = \int_{\epsilon_{\text{F}}(t)}^{\infty} d\omega \rho_{\text{occ}}^{\alpha,\text{MT}}(\omega, t), \quad N_{\text{ne}}^{\alpha,\text{MT}}(t) = \int_{-\infty}^{\epsilon_{\text{F}}(t)} d\omega \rho_{\text{occ}}^{\alpha,\text{MT}}(\omega, t), \quad (3.66)$$

with $\alpha = \{\uparrow, \downarrow\}$. With these definitions, the contribution of the the excited and non-excited electrons to M_3 can be calculated (see (3.63)). For example, the contribution to the moment from the excited electrons in the MT is given by

$$M_{\text{exc},3}^{\text{MT}}(t) = N_{\text{exc}}^{\uparrow,\text{MT}}(t) - N_{\text{exc}}^{\downarrow,\text{MT}}(t). \quad (3.67)$$

The calculation of the contribution from the non-excited electrons is analog, and the moment in the MT would simply follow from

$$M_3^{\text{MT}}(t) = M_{\text{exc},3}^{\text{MT}}(t) + M_{\text{ne},3}^{\text{MT}}(t). \quad (3.68)$$

The equivalent quantities for the IR can be calculated in a similar way. We will, however, not give any further examples at this point, since the calculations are straightforward.

Finally, we wish to discuss one last point concerning the reliability of the previously defined TDDOS. The TDDOS and all related quantities have been derived

from the non-equilibrium Green functions of non-interacting systems. By looking at the result (3.57) one could argue that an appropriate TDDOS might also be defined by referring to the set of eigenstates at $t = 0$:

$$\rho'(\omega, t) = \sum_u \delta(\omega - \epsilon_{0,u}) \sum_i f_i |d_{ui}(t)|^2, \quad \text{with} \quad d_{ui}(t) = \langle \varphi_u(0) | \varphi_i(t) \rangle. \quad (3.69)$$

This definition, however, turns out to be deficient regarding some of its properties. For example, a very slowly changing external potential would, at some time t for certain i , lead to: $0 < |d_{ii}(t)| < 1$. Hence, the definition (3.69) would lead to $N_{\text{exc}}(t) > 0$, which contradicts the expectation that, for slowly changing potentials, the number of excited electrons should remain zero (considering e.g. the adiabatic theorem, which also holds for KS systems). The definition (3.57), on the other hand, would always give $N_{\text{exc}}(t) = 0$ as long as the external potential changes slowly enough. Therefore, the TDDOS defined by (3.69) cannot serve as a proper TDDOS.

4. Ultrafast change of the moment in extended systems

To study the behavior of excited spin-magnetic extended systems, we will in the following apply the previously derived simulation framework to different situations. In the first two sections, we will investigate the response of bulk nickel to different external pulses and find that excitation leads always to a loss in the moment. Moreover, we will find that this loss in the moment must be caused by spin-orbit coupling. The spin-orbit coupling mediated process that leads to the demagnetization will be investigated in detail in the third section. In the last two sections, we will study the response of the moment of bulk iron and of a five-atom thick nickel slab. Finally, we will discuss the experimental results in this field and compare to our calculations.

4.1. A first investigation in bulk nickel

In the previous chapter, the framework used to study ultrafast spin-dynamics was introduced. In this section, we will apply this framework to investigate the spin-magnetic response of bulk Ni subjected to an ultrashort intense pulse.

As stated before, in each simulation the KS equations (3.16) have been solved by a forward propagation. To be more precise: the time evolution of each system was simulated for a certain time, while in the first part of each run the system was excited by an external pulse, and in the second part, no external field was present and the response of the system was studied. The simulations of bulk Ni that will be discussed in all following sections used the lattice structure of Ni at room temperature, i.e. a fcc structure with a lattice constant of $a = 6.66 \text{ a.u.}$ ($= 0.352 \text{ nm}$) was used. The system was represented by one primitive unit cell with the basis vectors $\mathbf{a}_1 = a/2 (1, 1, 0)$, $\mathbf{a}_2 = a/2 (1, 0, 1)$, $\mathbf{a}_3 = a/2 (0, 1, 1)$, and 8^3 \mathbf{k} -points were used in each calculation.

The external field that has been applied corresponds to a pulse that propagates along the \mathbf{e}_3 -direction, and that is polarized along the \mathbf{e}_1 -direction, meaning that, according to the DA, a purely time-dependent \mathbf{A} -field parallel to \mathbf{e}_1 , and a purely time-dependent \mathbf{B} -field parallel to \mathbf{e}_2 was used. The corresponding fields are shown in figure 4.1. The peak intensity of the \mathbf{A} -field was 10^{15} W/cm^2 and the pulse duration was approximately 290 a.u. ($\approx 7 \text{ fs}$), while the total propagation time was 800 a.u. ($\approx 19.3 \text{ fs}$).

The left panel of figure 4.2 shows the time development of the moment. For $t = 0$, the system is in its ferromagnetic ground state with a magnetization along the \mathbf{e}_3 -direction, and with a moment of $M_3(0) = -0.69 \text{ a.u.}$. We see that the magnitude of M_3 starts to drop off slightly during the pulse interaction, and the drop-off becomes stronger at the end of the pulse. This drop-off continues until

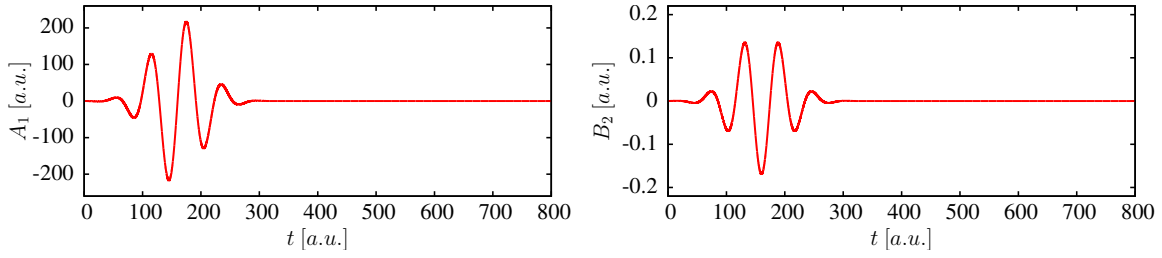


Fig. 4.1.: Left: Applied \mathbf{A} -field along \mathbf{e}_1 . The intensity FWHM is approx. 100 a.u. ($\approx 2.5 \text{ fs}$), and the corresponding center wavelength is $\lambda \approx 8.6 \cdot 10^3 \text{ a.u.}$ ($\approx 455 \text{ nm}$). Right: Applied \mathbf{B} -field along \mathbf{e}_2 .

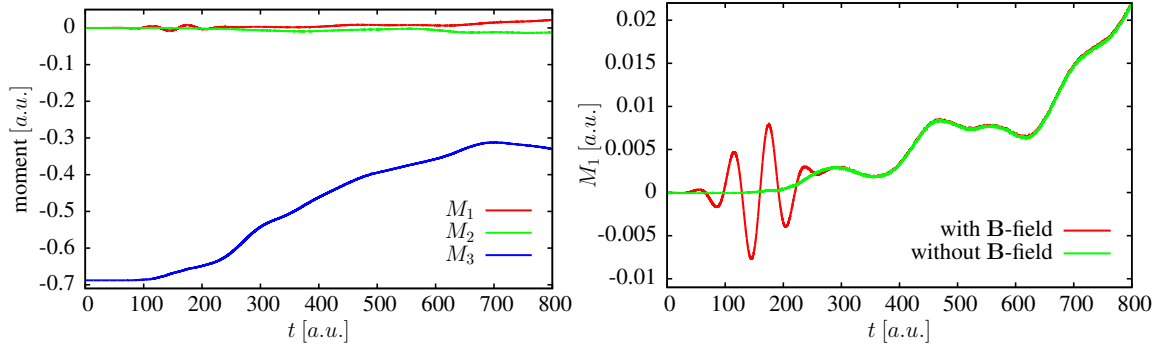


Fig. 4.2.: Left: Time development of the moment in bulk Ni, excited by the pulse from figure 4.1. Right: Time development of M_1 with, and without the external \mathbf{B} -field.

a plateau is reached at $t \approx 700 \text{ a.u.}$ with $M_3 \approx -0.35 \text{ a.u.}$. For $t > 700 \text{ a.u.}$ M_3 starts to oscillates around -0.35 a.u. for all later times (this oscillation can be seen in the right panel of figure 4.5 where the development of the moment is shown on a longer time scale). Furthermore, we see that M_1 and M_2 do not significantly change and they remain approximately zero. In conclusion, this first analysis shows that an ultrashort pulse, with a total duration of $\approx 7 \text{ fs}$ and a peak intensity of 10^{15} W/cm^2 , leads to a demagnetization of about 50 % in bulk Ni. This demagnetization takes place on a time scale of $\approx 15 \text{ fs}$, and it is most probably caused by a spin-flip-like process because the magnitude of M_3 decreases, while M_1 and M_2 do not significantly change.

To get some insight into the process that leads to the demagnetization, we will in the following employ the dynamical equation of the moment. We see from equation (3.24) that the torque on the moment has two contributions: one comes from the \mathbf{B} -field, and one comes from SOC. First, we will investigate the contribution from the \mathbf{B} -field torque term $\partial_t \mathbf{M}_{\mathbf{B}}$. Remember that this term has, in general, also two contributions: one comes from the xc \mathbf{B} -field, and one comes from the \mathbf{B} -field component of the external pulse. Since the ALSDA is used, the contribution from the xc \mathbf{B} -field is zero (see (3.20)). Hence, the \mathbf{B} -field torque term is given by

$$\partial_t \mathbf{M}_{\mathbf{B}} = \frac{1}{c} \int d\mathbf{r} \left[\mathbf{B}_{\text{ext}}(t) \times \mathbf{m}(\mathbf{r}, t) \right] = \frac{1}{c} \mathbf{B}_{\text{ext}}(t) \times \mathbf{M}(t). \quad (4.1)$$

We see that this torque term reduces to a simple Larmor precession term that contains the moment, which follows from the fact that the external \mathbf{B} -field is

purely time-dependent. Note that we have for $t = 0$: $M_1(0) = M_2(0) = 0$. Hence, any initial change of the moment that would come directly from the contribution (4.1) could only change the components M_1 and M_2 , but not M_3 . Moreover, this change would only happen if the external \mathbf{B} -field would have a non-zero \mathbf{e}_1 - or \mathbf{e}_2 -component.

For the discussed run, the external \mathbf{B} -field was parallel to \mathbf{e}_2 . Thus, any direct change that comes from (4.1) should only change M_1 . This change can, in fact, be seen in the left panel of figure 4.2, which manifests itself by a small oscillation that is nearly proportional to the \mathbf{A} -field (this proportionality results from the fact that the integral of \mathbf{B}_{ext} is proportional to \mathbf{A}_{ext}). However, the change that is caused by $\partial_t \mathbf{M}_{\mathbf{B}}$ appears to be very small and it also does not seem to have any persistent effect.

The plot in the right panel of figure 4.2 shows a closeup of M_1 and compares it to the M_1 that has been obtained by a run that was similar to the discussed run, with the difference that no external \mathbf{B} -field was used. It is clear to see that the change of M_1 that is caused by the external \mathbf{B} -field is only present as long as the external \mathbf{B} -field changes. Once the \mathbf{B} -field remains zero, the M_1 obtained with the \mathbf{B} -field becomes identical to the M_1 obtained without the \mathbf{B} -field. This behavior can be explained by the fact that M_3 does not change very much as long as the external field is present (which is in fact the case as can be seen in figure 4.2): With (4.1) we get, for the change of M_1 , the following \mathbf{B} -field contribution:

$$\Delta M_{\mathbf{B},1}(T) = \int_0^T dt \partial_t M_{\mathbf{B},1}(t) = \int_0^T dt B_{\text{ext},2}(t) M_3(t) \approx M_3(0) \underbrace{\int_0^T dt B_{\text{ext},2}(t)}_{=0} = 0, \quad (4.2)$$

where T is the duration of the external pulse. Here we have used that the \mathbf{E} -field, and thus also the \mathbf{B} -field, of a pulse must integrate to zero, which has been discussed at the end of section 2.4.1.

We can conclude that the direct change of the moment that is caused by the external \mathbf{B} -field is negligible, resulting from the nature of the external field. However, even for external fields that do not integrate to zero, this direct effect would most probably always be very small (as seen in figure 4.2). Moreover, the external \mathbf{B} -field does also not lead to any significant indirect effects. Indirect meaning that the external \mathbf{B} -field could change the magnetization, which would then change the xc \mathbf{B} -field, and which could then contribute to the change of the moment via SOC. The direct and also the indirect effect of the external \mathbf{B} -field on the dynamics of the moment has been tested in several runs, and it was found that the contribution from the external \mathbf{B} -field was always negligible. We emphasize, however, that only one linear polarized external pulse was applied in all runs. If more than one pulse is applied, or if a circularly polarized pulse is used, the \mathbf{B} -field contribution might become more important.

We conclude that the contribution of the external \mathbf{B} -field to the dynamics of the moment is negligible (at least for the situations considered in this work). Hence, all runs that will be presented in the following neglect the external \mathbf{B} -field. Similarly, all following theoretical discussions will neglect the external \mathbf{B} -field as well. Since the external \mathbf{B} -field has no significant effect, we can conclude that the dynamics

of the moment follows solely from the term $\partial_t \mathbf{M}_{\text{SOC}}$ (see (3.22)), meaning that the ultrafast demagnetization observed in our simulation has to be caused by SOC. The underlying process that leads to the change of the moment via SOC was already roughly outlined in the last part of section 3.1.4: spin-currents that flow around the nuclear potential feel an effective \mathbf{B} -field, which leads to a torque on the moving spins, and hence to a change of the moment. The whole process that leads to the demagnetization via SOC will be investigated in section 4.3 in more detail.

4.2. Response of the moment for different fields in bulk nickel

In this section we will investigate how the moment of bulk Ni changes when different parameters for the external field are applied. In all runs, the Ni system was at $t = 0$ in its ferromagnetic ground state with a magnetization along the \mathbf{e}_3 -direction, i.e. $M_1(0) = M_2(0) = 0$ and $M_3(0) = -0.69 a.u.$.

First, we will investigate how the response of the moment changes if pulses with different center frequencies are applied. The pulses applied are shown in the left

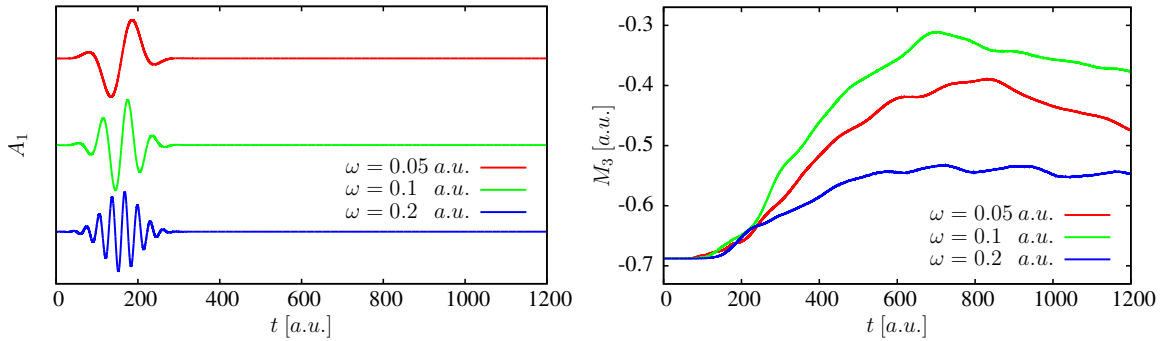


Fig. 4.3.: Left: Applied \mathbf{A} -fields along \mathbf{e}_1 . The intensity FWHM of each pulse is $\approx 100 a.u.$ ($\approx 2.5 fs$), and the center frequencies (and corresponding wavelengths) are $\omega = 0.05 a.u.$ ($\lambda \approx 910 nm$), $\omega = 0.1 a.u.$ ($\lambda \approx 455 nm$), and $\omega = 0.2 a.u.$ ($\lambda \approx 228 nm$). Right: \mathbf{e}_3 -component of the moment for the different pulses.

panel of figure 4.3. All pulses had the same peak intensity of $I_0 = 10^{15} W/cm^2$ and a total duration of about $290 a.u.$ ($\approx 7 fs$), while the total propagation time was $1200 a.u.$ ($\approx 29 fs$). The response of M_3 is shown in the right panel of figure 4.3. It is clear to see that all pulses lead to a demagnetization, and the demagnetization process happens on a time scale of about $700 a.u.$ ($\approx 15 fs$). Moreover, we see that the demagnetization starts approximately at the peak of the pulse, while most of the demagnetization happens after the end of the pulse. We also see that the magnitude of the demagnetization is different. The strongest demagnetization (about 50%) happens for the pulse with $\omega = 0.1 a.u.$, while the demagnetization for the pulse with the lower frequency of $\omega = 0.05 a.u.$ leads to a somewhat weaker demagnetization (about 43%). The pulse with the highest frequency of $\omega = 0.2 a.u.$ leads to an even weaker demagnetization (about 22%). The change of M_1 and M_2 was, for all runs, very small compared to the change of M_3 .

Next, we will investigate the dependence of the moment on the peak intensity of the external pulse. The shape and duration of the applied pulses were equal to the shape and duration of the pulse with the center frequency $\omega = 0.1 \text{ a.u.}$ from the previous paragraph (see figure 4.3), but this time three different peak intensities have been used: $I_0 = 10^{14} \text{ W/cm}^2$, $I_0 = 5 \cdot 10^{14} \text{ W/cm}^2$, and $I_0 = 10^{15} \text{ W/cm}^2$. The polarization direction was along \mathbf{e}_1 . For reference, the pulse shape is again shown in the left panel of figure 4.4. The time development of M_3 is provided in

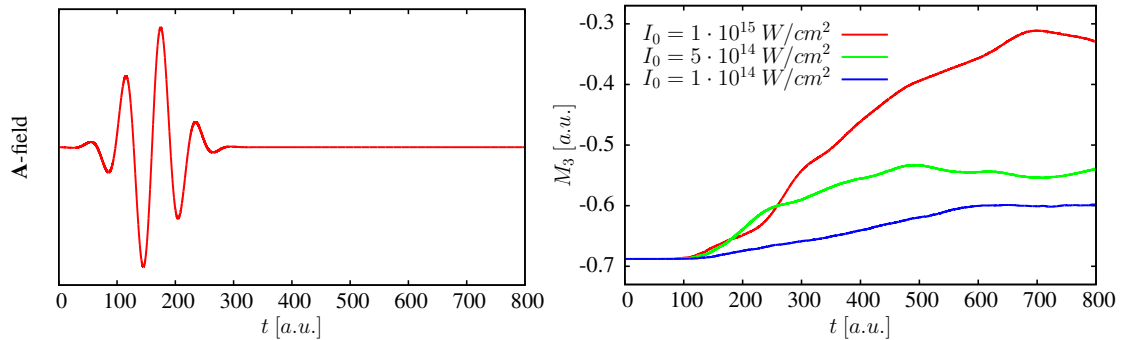


Fig. 4.4.: Left: Shape of the \mathbf{A} -field applied for different peak intensities and polarizations. Right: \mathbf{e}_3 -component of the moment for the different peak intensities.

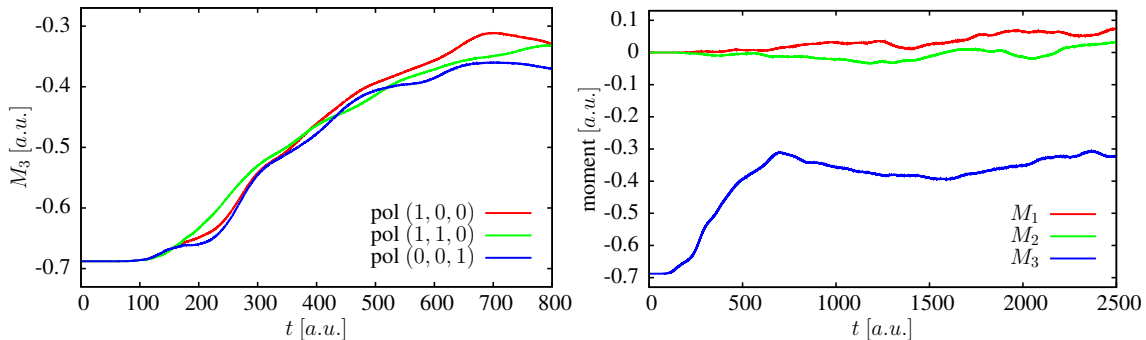


Fig. 4.5.: Left: \mathbf{e}_3 -component of the moment for different polarization directions of the external field. Right: Evolution of the moment on a longer time scale for the pulse from the figure 4.4, with $I_0 = 10^{15} \text{ W/cm}^2$ and the polarization along \mathbf{e}_1 .

the right panel of figure 4.4. It is clear to see that a demagnetization occurs for all intensities, and that the demagnetization is stronger for higher intensities. While the loss in the moment is about 50 % for $I_0 = 10^{15} \text{ W/cm}^2$, it goes down to 13 % for $I_0 = 10^{14} \text{ W/cm}^2$ (note that the loss is not linear in I_0). Again, the change of M_1 and M_2 was, for all runs, very small compared to the change of M_3 .

Next, we will investigate the dependence of the moment on the polarization direction of the external field. For this purpose, three different pulses similar to that shown in the left panel of figure 4.4 and with a peak intensity of 10^{15} W/cm^2 , but with different polarizations, have been applied. One polarization was again along $(1, 0, 0)$, while the two other polarization directions were $(1, 1, 0)$ and $(0, 0, 1)$. The corresponding change of M_3 is shown in the left panel of figure 4.5. We see that the difference in the change of the moment between the various polarizations is small.

The right panel of figure 4.5 shows again the response of the moment for the pulse from the left panel of figure 4.4 (with $I_0 = 10^{15} \text{ W/cm}^2$ and polarization

along \mathbf{e}_1), but this time on a longer time scale of $2500 a.u.$ ($\approx 60 fs$). We see that M_3 is reduced to about 50 % in the first $700 a.u.$. After this initial loss, the value of M_3 is almost kept, aside from some small oscillations. Beside M_3 , also M_1 and M_2 are shown. As already stated, the change of M_1 and M_2 during the initial demagnetization is small compared to the change of M_3 . Nevertheless, we see that the change of M_1 and M_2 increases on longer time scales, but it still remains much less than the initial change of M_3 .

Previously, the response of the moment on very short pulses has been investigated. Now, we will investigate how the moment behaves if longer pulses are used. The shape of the applied pulses is shown in the left panel of figure 4.6. (Note that this pulse has many wave cycles and not only a few, like the pulses shown before. Experimentally, such many cycle pulses are typically much easier to construct than few cycle pulses [48].) The center frequency was for all pulses

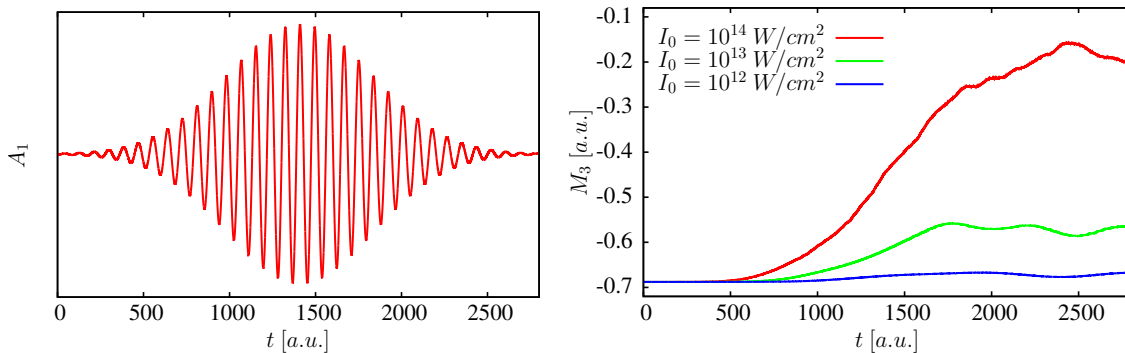


Fig. 4.6.: Left: Shape of the \mathbf{A} -field applied for different peak intensities. The intensity FWHM is $\approx 700 a.u.$ ($\approx 17 fs$), and the center frequency (and corresponding wavelength) is $\omega = 0.073 a.u.$ ($\lambda \approx 620 nm$). Right: \mathbf{e}_3 -component of the moment for different peak intensities.

$\omega = 0.073 a.u.$, while three different peak intensities have been tested. The total propagation time was $2800 a.u.$ ($\approx 68 fs$). The time evolution of M_3 is shown in the right panel of figure 4.6. As expected, the demagnetization increases for higher peak intensities. For a peak intensity of $I_0 = 10^{14} W/cm^2$ we have a loss in the moment of about 75 %, for $I_0 = 10^{13} W/cm^2$ we have a loss of about 19 %, and for $I_0 = 10^{12} W/cm^2$ we have a loss of about 4 %. By comparing these results to the results obtained with the short pulses (see figure 4.4), it follows that the demagnetization depends also on the fluence of the pulse, i.e. a larger fluence leads to a stronger demagnetization (the fluence is proportional to $\int dt E^2(t)$; $E(t)$ is the electric field). As before, the change of M_1 and M_2 was, for all runs, very small compared to the change of M_3 .

From the previously shown results, we come to the following conclusions: First, the loss in the moment of ferromagnetic bulk Ni increases for higher pulse intensities, and for larger pulse fluences. Moreover, the loss in the moment depends strongly on the center frequency of the pulse, while there seem to exist optimal frequencies which lead to stronger demagnetizations. The polarization direction of the external pulse, on the other hand, has no strong influence on the demagnetization behavior. Furthermore, we see the following general behavior: there is always a demagnetization, i.e. the magnitude of the moment is never increased,

w.r.t. $t = 0$, and the loss in the moment always lags behind the external pulse (this is particularly noticeable for the short pulses).

From the previous section we know that the change of the moment has to be caused by the SOC term from (3.24), but why we get the previously discussed behavior is still unclear. Therefore, the SOC torque term and the corresponding demagnetization process will be investigated in more detail in the following section.

As a last point in this section, we wish to say a few words about the convergence. In section 3.2 it was pointed out that the number of states for the expansion N_{\max} , the time step size Δt , and the number of \mathbf{k} -points $N^{\mathbf{k}}$ have to be converged to give accurate results. For all runs that are presented in this work, N_{\max} and Δt were sufficiently converged. $N^{\mathbf{k}}$, on the other hand, was not completely converged. However, it was found that the choice of $N^{\mathbf{k}}$ is more crucial for the ground state calculation (and the corresponding value of the moment, see left panel of figure 4.7 for $t = 0$) than for the calculation of the time-dependent change of the moment. This fact is shown in the right panel of figure 4.7, where we see that the relative

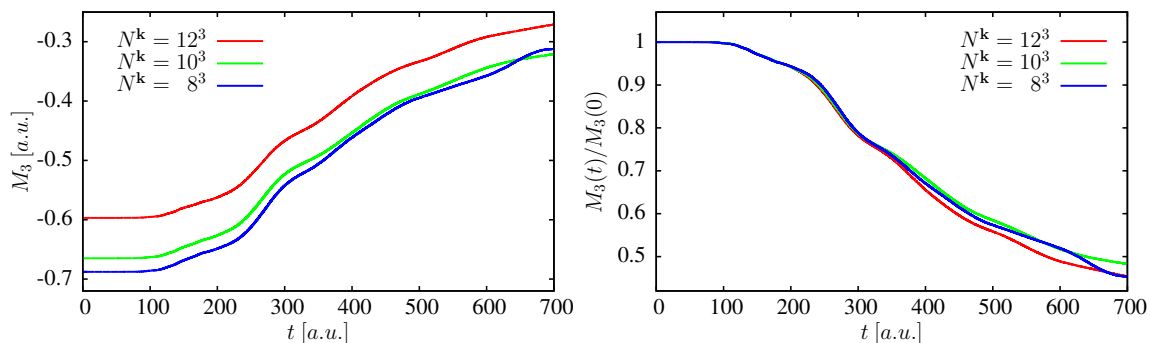


Fig. 4.7.: Left: e_3 -component of the moment for a different number of \mathbf{k} -points. The applied pulse was similar to that from the left panel of figure 4.4, the center frequency was $\omega = 0.1$ a.u., and the peak intensity was $I_0 = 10^{15}$ W/cm². Right: Relative change of M_3 for a different number of \mathbf{k} -points.

change of the moment is very similar for the three different choices of $N^{\mathbf{k}}$. Since the main concern of this work is the investigation of the demagnetization and the understanding of the underlying process, emphasis was not put on an entirely converged \mathbf{k} -point grid. Hence, all simulations of bulk systems that are presented in this work used a \mathbf{k} -point grid with $N^{\mathbf{k}} = 8^3$.

4.3. The demagnetization process

In section 4.1 we have shown that an ultrashort external pulse induces a fast demagnetization in bulk Ni. Additionally, we have found that this demagnetization has to be caused by SOC. In the previous section we have shown that a demagnetization always happens, as long as the pulse is intense enough, independent of the pulse parameters. Moreover, we have seen that the loss in the moment increases for higher pulse fluences and intensities, while the polarization direction has almost no influence on the demagnetization behavior.

In this section, we will investigate the demagnetization process in more detail. We will see that several steps are involved, and that different processes have to be taken into account. In the following subsections, the different steps and processes will be discussed individually, and we will find that the previously discussed behavior of the moment can be understood. All following investigations refer to the short pulse run with the peak intensity $I_0 = 10^{15} \text{ W/cm}^2$, the center frequency $\omega = 0.1 \text{ a.u.}$, and the polarization along \mathbf{e}_1 , shown in figure 4.4.

4.3.1. Initial change of the local moment and charge

As stated in section 4.1, the bulk Ni system was represented by a primitive unit cell with the lattice constant $a = 6.66 \text{ a.u.}$. The corresponding volume of the unit cell was 73.8 a.u. . Moreover, we recall that the unit cell is divided in two different regions: in the MT and the IR (remember that the MT corresponds to a sphere around the atom; see section 3.2). In the bulk Ni calculations the radius of the MT was 2.0 a.u. , corresponding to a MT volume of 33.5 a.u. . Hence, the volume of the IR (which is the region outside the MT) was 40.3 a.u. .

In this section we will investigate the initial response of the local charge and moment in the MT and in the IR. In the left panel of figure 4.8, the intensity

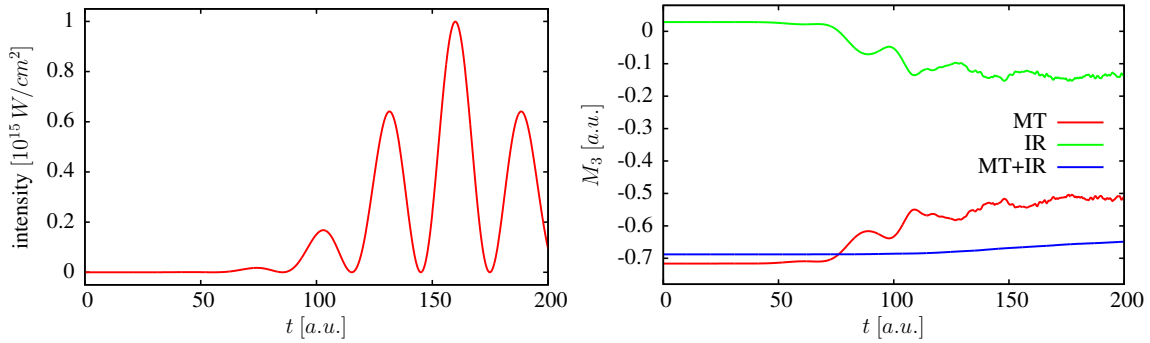


Fig. 4.8.: Left: Intensity of the applied pulse. Right: \mathbf{e}_3 -component of the moment in the MT and IR, and \mathbf{e}_3 -component of the total moment (i.e. MT+IR).

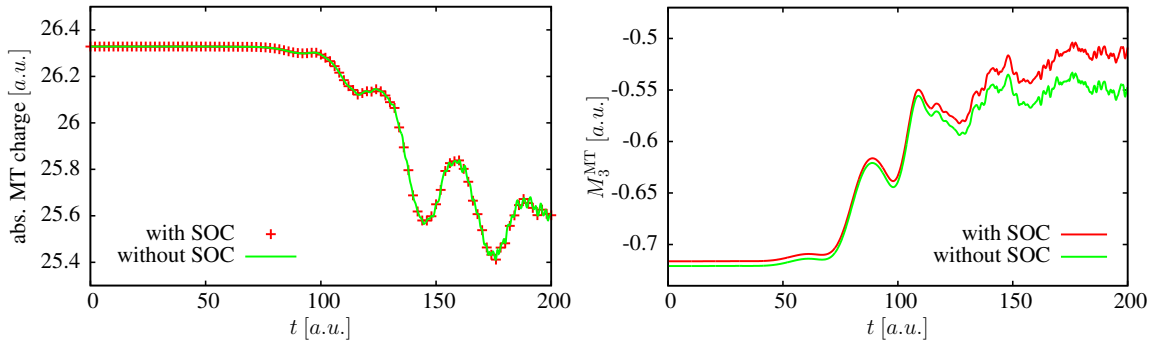


Fig. 4.9.: Left: Absolute value of the electronic charge in the MT with, and without SOC (the total charge in the unit cell is 28). Right: \mathbf{e}_3 -component of the moment in the MT with, and without SOC.

of the external pulse is shown for the first 200 a.u. ($\approx 3.8 \text{ fs}$). The right panel of figure 4.8 shows the moment in the MT, the moment in the IR, and the total moment. First of all, we notice a fast loss in the moment of the MT, and at the

same time, we see an increase in the moment of the IR. Furthermore, we see that the total moment remains almost constant during this initial time, meaning that the amount of moment that is lost in the MT is roughly equal to the amount of moment that is gained in the IR. Moreover, we notice that this process takes place on a very fast time scale, and it starts immediately when the intensity of the external field changes significantly. The \mathbf{e}_1 - and \mathbf{e}_2 -component of the moment in the two regions was approximately zero during the investigated time scale.

As stated before, the change of the total moment during the initial time is almost negligible. Thus, one could argue that the change of the moment in the MT and IR is accomplished by spin-currents that transport parts of the moment from one region to the other. To investigate this statement, and to exclude any SOC contributions, an identical run has been performed, but this time SOC was switched off. The left panel of figure 4.9 shows the change of the charge in the MT for the run with, and for the run without SOC. It is clear to see that the change of the charge is identical in both runs. Moreover, we see that the amount of charge in the MT decreases, meaning that the charge in the IR increases, since the total charge in the unit cell is constant. This is also what one would expect, because an excitation leads typically to a delocalization of the charge. We conclude that SOC has no influence on the change of the local charge during the initial excitation process.

The right panel of figure 4.9 shows the change of the moment in the MT for both runs. We see that the moment is almost identical for $t = 0 \dots 130 \text{ a.u.}$, and it starts to become slightly different for later times (note that this difference has to be caused by SOC). The important result is that the initial change of the local moment is nearly identical in both runs, meaning that this initial change is not related to SOC. Furthermore, we recall that the total moment has to be conserved if no SOC is present. Hence, the initial change of the moment in the MT has to be accomplished by spin-currents that flow through the MT surface, and that transport parts of the moment to the IR. This can be seen by integrating the dynamical equation of m_3 over the MT volume for a system without SOC (the corresponding equation is similar to equation (3.19), with the difference that the last two terms are not present, since these terms are SOC contributions):

$$\begin{aligned} M_3^{\text{MT}}(t) - M_3^{\text{MT}}(0) &= \int_0^t dt' \int_{\text{MT}} d\mathbf{r} \partial_{t'} m_3(\mathbf{r}, t') = - \int_0^t dt' \int_{\text{MT}} d\mathbf{r} \nabla \cdot \mathbf{j}^3(\mathbf{r}, t') \\ &= - \int_0^t dt' \oint_{\text{MT}} d\mathbf{s} \cdot \mathbf{j}^3(\mathbf{r}, t'). \end{aligned} \quad (4.3)$$

We have used (3.20) and (2.27), and we have applied Gauss's theorem.

Another way to investigate the initial change of the local moment is to employ the TDDOS, introduced in section 3.3. The two upper panels of figure 4.10 show the spin-resolved TDDOS in the MT and IR at $t = 0$ (note that this TDDOS corresponds to the ground state DOS). We see that all available states up to the Fermi energy (which is shifted to $\omega = 0$) are occupied. Remember that M_3 follows from the corresponding occupation of the spin-up and spin-down states. We wish to mention that the total moment comes, for the ground state, almost entirely from the MT (which can be seen in figure 4.12).

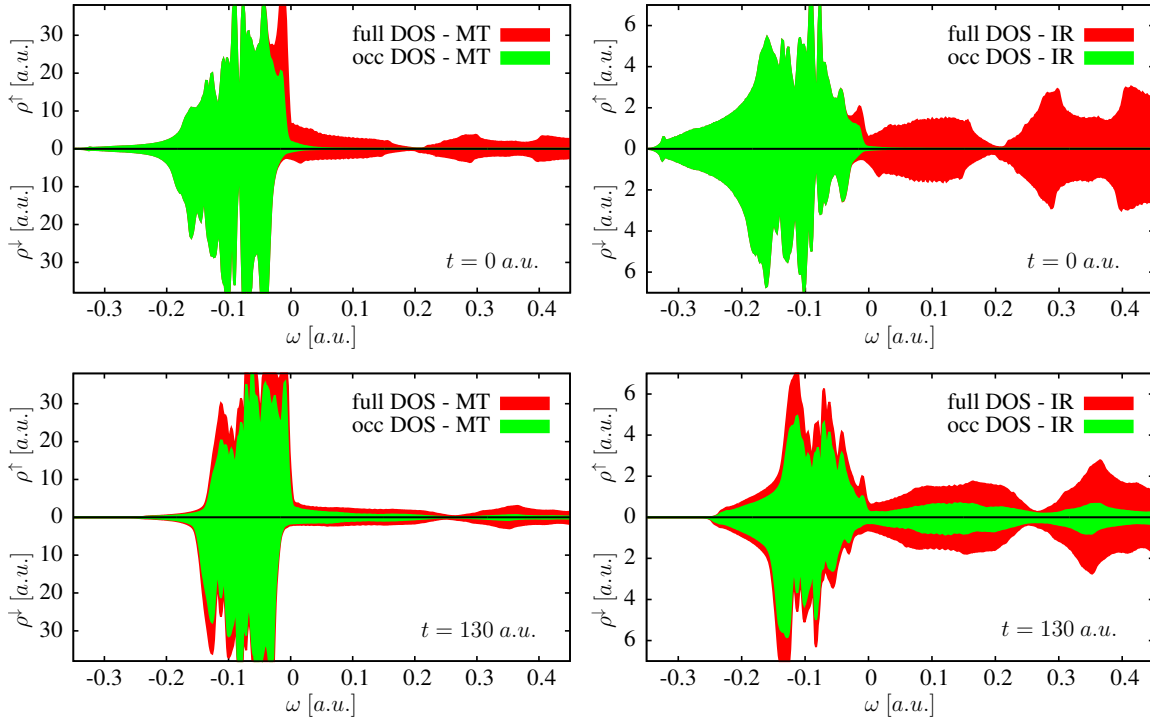


Fig. 4.10.: Spin- and region-resolved density of states in the MT and IR at the initial time $t = 0$, and at $t = 130 a.u.$. The Fermi energy is shifted to $\omega = 0$.

When the system is excited, the available states above the Fermi energy become occupied. Fermi's golden rule tells us that the probability of occupying a certain state is proportional to its DOS value. Hence, the region- and spin-resolved full DOS can give information about how each spin channel in each region will be occupied by an excitation, and, correspondingly, how each local moment changes. However, we have to keep in mind that the situation is a bit more involved in our case, because the full TDDOS itself changes with time. Thus, it is not entirely possible to predict how the spin channels will be occupied solely from the ground state DOS. The two lower panels of figure 4.10 show the spin-resolved TDDOS in the MT and IR at $t = 130 a.u.$. It is clear to see that the states above the Fermi energy became occupied (note that this occupation is approximately proportional to the full DOS values), while at the same time some states below the Fermi energy became unoccupied, which led to the change of the local moment. Moreover, we see that the full TDDOS has clearly changed between $t = 0$ and $t = 130 a.u.$. Finally, we wish to mention that the TDDOS was almost identical for the run with SOC and without SOC for $t = 0 \dots 130 a.u.$ (the TDDOS from figure 4.10 corresponds to the run with SOC).

Instead of directly investigating the TDDOS, we can also investigate how the corresponding number of excited and non-excited electrons in the different spin channels and regions changes (see (3.66)). In the left panel of figure 4.11 we see that the number of excited electrons in the MT behaves almost equal for both spin channels during the initial excitation. Furthermore, we see that the number of non-excited spin-down electrons decreases more than the number of non-excited spin-up electrons, meaning that we have a loss in the moment of the MT that is

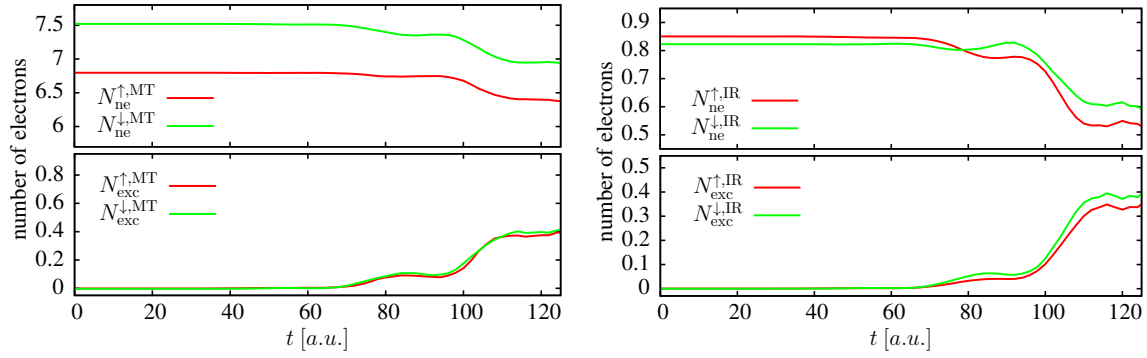


Fig. 4.11.: Number of excited and non-excited valence electrons in each spin channel in the MT (left), and in the IR (right). The spin-up channel is plotted with red lines, and the spin-down channel is plotted with green lines (see also (3.66)).

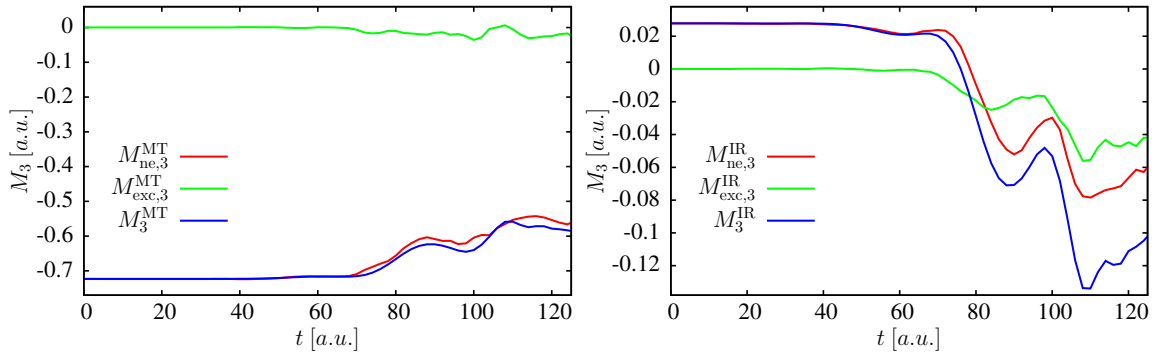


Fig. 4.12.: Contribution to the \mathbf{e}_3 -component of the moment from the excited and non-excited electrons, and total moment, in the MT (left), and in the IR (right) (see also (3.67) and (3.68)).

caused by the non-excited electrons. This can also be seen in the left panel of figure 4.12, where the corresponding contributions of M_3 are shown. The right panel of figure 4.11 shows how the different spin channels in the IR behave. The number of non-excited spin-up electrons decreases more than the number of non-excited spin-down electrons. Moreover, the number of excited spin-down electrons increases stronger than the number of excited spin-up electrons. Both processes lead to an increase in the magnitude of the moment, meaning that the change of the moment in the IR is caused by both, excited and non-excited electrons. The change of the corresponding M_3 contributions is shown in the right panel of figure 4.12. Finally, we wish to mention that the total number of electrons in each spin channel is approximately constant, because the total moment $M_3 = N^\uparrow - N^\downarrow$ is almost constant for $t = 0 \dots 130$ a.u., and since the total number of electrons $N = N^\uparrow + N^\downarrow$ is constant.

We conclude that a short and intense \mathbf{A} -field pulse leads to a very fast delocalization of the charge in ferromagnetic bulk Ni (as a direct result of the excitation process). This initial change of the charge is accompanied with a very fast change of the local moment, i.e. the magnitude of the moment in the MT decreases, and the magnitude of the moment in the IR increases. The total moment, on the other hand, is approximately constant, meaning that the change of the local moment is caused by spin-currents which transfer parts of the moment. The change of the local moment can also be explained by the time-dependent change of the

occupation of the spin-resolved local TDDOS. Since the TDDOS depends on the band structure of the system, the initial change of the local moment has to be a characteristic property of the system. Note that this change of the local moment is not caused by SOC.

4.3.2. Approximation of the spin-orbit coupling term

In this section we will show how the SOC term can be approximated, and we will explain why this approximation is reasonable. The approximation of SOC will be very useful for the investigation and understanding of the demagnetization process, as will be seen in the following sections. Furthermore, we will investigate in which region the demagnetization process takes place, which will also be useful for subsequent sections.

In section 4.1 we found that the demagnetization is caused by SOC. The corresponding term in the KS equations is (see the scheme (3.16))

$$\frac{1}{4c^2} \underline{\underline{\boldsymbol{\sigma}}} \cdot \left(\nabla v_s(\mathbf{r}, t) \times \left[\hat{\mathbf{p}} + \frac{1}{c} \mathbf{A}_{\text{ext}}(t) \right] \right), \quad (4.4)$$

where the effective potential is given by

$$v_s(\mathbf{r}, t) = v_n(\mathbf{r}) + v_H(\mathbf{r}, t) + v_{\text{xc}}(\mathbf{r}, t). \quad (4.5)$$

First, it is assumed that the change of the potential along the radial direction is much larger than the change along any other direction (we assume that the nucleus is at the origin of the spherical coordinate system). Thus, the gradient can be approximated by

$$\nabla v_s(\mathbf{r}, t) \longrightarrow \nabla v_s(r, t) = \partial_r v_s(r, t) \mathbf{e}_r, \quad (4.6)$$

where r is the radial coordinate, \mathbf{e}_r is the radial unit vector, and the nucleus sits at $r = 0$. Next, it is assumed that the time-dependent change of (4.6) is negligible, meaning that (4.6) can be approximated by its ground state value:

$$\partial_r v_s(r, t) \mathbf{e}_r \longrightarrow \partial_r v_s(r, 0) \mathbf{e}_r. \quad (4.7)$$

Note that this approximation concerns only the Hartree and the xc potential, because the nuclear potential is time-independent. Before we continue we wish to emphasize that the approximations concern only the SOC term, and no other term in the Hamiltonian.

With the definition of the gauge invariant orbital angular momentum operator

$$\hat{\mathbf{L}} = r \mathbf{e}_r \times \left(\hat{\mathbf{p}} + \frac{1}{c} \mathbf{A}_{\text{ext}}(t) \right), \quad (4.8)$$

and with the definition of the SOC radial function

$$\xi(r) = \frac{1}{2c^2 r} \partial_r v_s(r, 0), \quad (4.9)$$

the SOC term (4.4) reduces with the assumed approximations to

$$\frac{1}{4c^2} \underline{\underline{\boldsymbol{\sigma}}} \cdot \left(\nabla v_s(\mathbf{r}, t) \times \left[\hat{\mathbf{p}} + \frac{1}{c} \mathbf{A}_{\text{ext}}(t) \right] \right) \xrightarrow{(4.6), (4.7)} \frac{1}{2} \xi(r) \underline{\underline{\boldsymbol{\sigma}}} \cdot \hat{\mathbf{L}}. \quad (4.10)$$

To be physically correct, the gauge invariant orbital angular momentum (4.8) should be used in approximation (4.10). As stated before, however, the diamagnetic part of the SOC term, $\xi(\hat{r}) \hat{\boldsymbol{\sigma}} \cdot (\hat{\mathbf{r}} \times \mathbf{A})/2c$, also turned out to be negligible (at the end of appendix A.6.4 we give a theoretical explanation for this behavior). Hence, for simplicity, we will neglect this term in all following investigations and consider only the bare orbital angular momentum operator in the SOC term.

Since the approximation (4.10) seems, at first glance, to be rather crude, the consequence of this approximation has been investigated for such situations that are discussed in this work. To be more precise: calculations that have been performed with the approximate SOC term have been compared to calculations that have been performed with the full SOC term. These showed that the difference in the observables between the various runs (and in particular the difference in the time-dependent moment) was very small and always negligible. Hence, all calculations that are presented in this work applied the approximate SOC.

In the following, we will explain why the approximation (4.10) is sufficient to describe the dynamics of the moment. Moreover, we will consider the approximate SOC term in all following theoretical investigations, because this will simplify the analytical discussions. Note, however, that the treatment of the full SOC might become important for situations that are different to those discussed in this work (i.e. for different systems or different external pulses).

In section 3.1.4 the dynamical equation of the moment has been derived. Following this procedure and considering the approximate SOC term (4.10) gives

$$\partial_t \mathbf{M}(t) = \sum_i \left\langle \frac{1}{i} [\hat{\boldsymbol{\sigma}}_i, \frac{1}{2} \xi(\hat{r}_i) \hat{\boldsymbol{\sigma}}_i \cdot \hat{\mathbf{L}}_i] \right\rangle (t) = \sum_i \langle \xi(\hat{r}_i) \hat{\mathbf{L}}_i \times \hat{\boldsymbol{\sigma}}_i \rangle (t), \quad (4.11)$$

where we have used that the change of the total moment comes solely from SOC. In section 4.1, we found that the loss in the moment has to be caused by a spin-flip-like process, because only M_3 changes, while M_1 and M_2 remain approximately zero (i.e. this spin-flip process has to be SOC mediated). We will now use the equation (4.11), and modify it slightly, to find the region in which the spin-flip process takes place:

$$\mathbf{M}(t; R) = \mathbf{M}(0) + \int_0^t dt' \sum_i \langle \Theta(R - \hat{r}_i) \xi(\hat{r}_i) \hat{\mathbf{L}}_i \times \hat{\boldsymbol{\sigma}}_i \rangle (t'). \quad (4.12)$$

Here, we calculate with the help of the Heaviside step function Θ the partial torque on the moment that occurs in a sphere with radius R around the nucleus. This partial torque is then integrated over time, and summed together with the initial total moment, to calculate the time-dependent moment, $\mathbf{M}(t; R)$, that would be obtained solely from the partial torque (i.e. solely from the torque that occurs in the sphere with radius R).

The left panel of figure 4.13 shows $M_3(t; R)$ for different radii R , and compares it to the total moment (remember that all plots refer to the run with

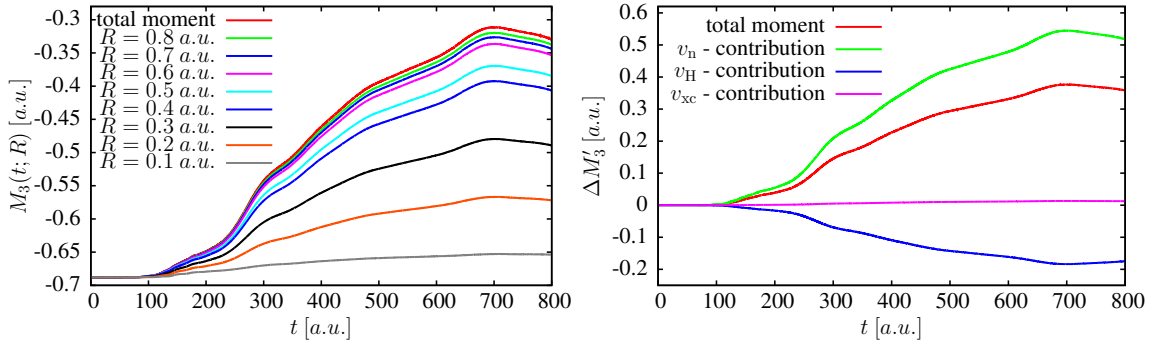


Fig. 4.13.: Left: e_3 -component of the partial moment $\mathbf{M}(t; R)$, defined by (4.12), for different radii R . For comparison, also the total moment is shown. Right: Contribution to the change of M_3 from the nuclear, from the Hartree, and from the xc potential (see definition (4.13); ξ' is calculated from v_n , from v_H , or from v_{xc}). For comparison, also the change of the total moment is shown.

$I_0 = 10^{15} \text{ W/cm}^2$ from figure 4.4). From the graph we learn the following: First, we see that nearly the entire spin-flip process occurs in a sphere around the nucleus with a radius of about $R = 0.7 \text{ a.u.}$. Furthermore, we notice that the major contribution of the loss in the moment comes from the region between the radii $R = 0.1 \text{ a.u.}$ and $R = 0.4 \text{ a.u.}$. In this region, basically only the radial potential from the nucleus in the center of the sphere plays a role, while the potential from all other nuclei of the lattice should be negligible. Hence, also the electronic charge should be nearly radial in this region, meaning that the Hartree potential should be nearly radial as well. When we additionally assume that the xc potential gives only a minor contribution to the dynamics of the moment, it becomes clear why the radial approximation (4.6) is reasonable.

Next, we will investigate how strong each potential from (4.5) contributes to the loss in the moment. In order to do this, we will use equation (4.11) and integrate it in time, which allows us to calculate the change of the moment:

$$\Delta \mathbf{M}'(t) = \int_0^t dt' \sum_i \langle \xi'(\hat{r}_i) \hat{\mathbf{L}}_i \times \hat{\boldsymbol{\sigma}}_i \rangle(t'). \quad (4.13)$$

The primed expression ξ' means that ξ' is calculated as in (4.9), with the difference that v_s is replaced by either the nuclear, the Hartree, or the xc potential (we point out that there was no difference in using the time-dependent potentials or the potentials from $t = 0$). This allows us to calculate the contribution to the change of the moment from each potential (note that the sum of the nuclear, Hartree, and xc contribution gives the change of the total moment). The corresponding contributions are shown in the right panel of figure 4.13.

First, we notice that the nuclear potential gives the strongest contribution to the change of the moment. Furthermore, we see that the Hartree potential has a smaller, but still a quite strong contribution (the magnitude is approximately 30% of the magnitude of the nuclear contribution). We also see that the Hartree contribution is negative, while the nuclear contribution is positive (note that the change of the total moment is positive). This results from the fact that the Hartree potential has its origin in the electronic density which has the opposite charge as

the nucleus. Hence, we could argue that the Hartree potential leads to a slow down, and to a decrease in the demagnetization (recall that the Hartree SOC term corresponds to a many-electron SOC contribution, as discussed in section 2.2.4). As a last point, we note that the contribution of the xc potential is very small and, in principle, negligible. We can conclude that the change of the moment comes from the time-independent nuclear potential and from the Hartree potential, while the contribution from the xc potential is negligible. Since the Hartree contribution comes mainly from the region close to the nucleus where the electrons are strongly bound, and where the change of the Hartree potential should be small, it becomes clear why the approximation (4.7) is reasonable.

In summary, we found that the full SOC term can be adequately approximated by the radial and time-independent form (4.10). From this it follows that the dynamical equation of the moment can be represented in the simplified form (4.11), which contains the orbital angular momentum operator (note that this definition refers to the orbital angular momentum around the nucleus). Moreover, we found that only the nuclear and the Hartree potential contribute to the demagnetization, while the contribution of the xc potential is negligible. Additionally, we found that the spin-flip-like demagnetization process takes place in a sphere around the nucleus with a radius of about $R = 0.7 a.u.$.

4.3.3. A closer look at the demagnetization process

In this section we will investigate in more detail how the moment changes during the demagnetization. Specifically, we will investigate how the local moment behaves in different regions. Additionally, we will have a closer look at the spin-flip process, and we will find that the change of the moment can be described via the dynamics of certain angular momentum quantities.

For the following investigations, we will divide the unit cell into three regions, as illustrated schematically in the left panel of figure 4.14. Region I corresponds to

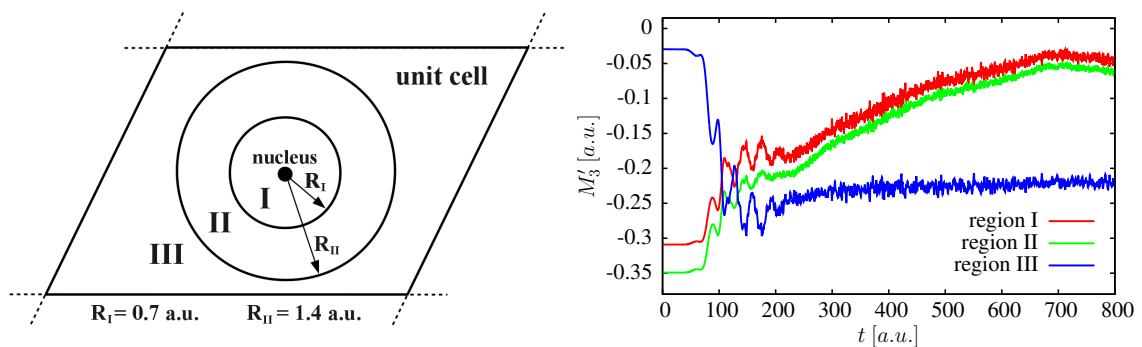


Fig. 4.14.: Left: Schematic of the Ni unit cell, which is divided into three different regions. Right: e_3 -component of the local moment of each region corresponding to the schematic from the left panel.

a sphere around the nucleus with the radius $R_I = 0.7 a.u.$. Region II corresponds to the region between the spheres with the radii $R_I = 0.7 a.u.$ and $R_{II} = 1.4 a.u.$. Finally, region III corresponds to the region outside the sphere with the radius $R_{II} = 1.4 a.u.$. In the following, we will investigate how the moment in each of

these regions behaves (it will then also become clear why we chose these regions). To do so we will, with the help of the Heaviside step function Θ , define the following functions:

$$\Omega_{\text{I}}(r) = \Theta(R_{\text{I}} - r), \quad \Omega_{\text{II}}(r) = \Theta(R_{\text{II}} - r) - \Omega_{\text{I}}(r), \quad \Omega_{\text{III}}(r) = 1 - \Theta(R_{\text{II}} - r),$$

with $R_{\text{I}} = 0.7 \text{ a.u.}$, and $R_{\text{II}} = 1.4 \text{ a.u.}$. (4.14)

These functions are zero outside, and one inside the respective region. We will use these functions to calculate local expectation values in the different regions.

Recall that we found in the previous section that the spin-flip process takes place in region I (we used the equation (4.12) to determine the local spin-torque contributions). However, this finding does not necessarily mean that the corresponding local moment changes only in this region. In order to investigate this issue, the local moments

$$\mathbf{M}'(t) = \sum_i \langle \Omega'(\hat{r}_i) \hat{\boldsymbol{\sigma}}_i \rangle(t) \quad (4.15)$$

have been calculated, where Ω' corresponds to the functions from (4.14), respectively. The corresponding M_3 quantities are shown in the right panel of figure 4.14. First, we notice that the moment changes very quickly during the first 150 *a.u.* in all three regions. This quick change of the local moment, which is a result of the excitation process, has been explained in section 4.3.1 (the magnitude of the moment decreases in the regions around the nucleus, i.e. in region I and II, while the magnitude of the moment increases in region III, which coincides with what we found in section 4.3.1). Recall that the total moment is, however, nearly constant during this initial period.

Next, we notice that, for $t > 200 \text{ a.u.}$, the moment changes in region I and II, while it remains nearly constant in region III (i.e. the change of the total moment follows from the change of the local moments of region I and II; compare e.g. to the total moment from figure 4.13). As stated before, the spin-flip process takes place in region I, meaning that the change of the moment in region II has to be caused by spin-currents. In fact, the only mechanism that can explain the behavior of the local moments from figure 4.14 is the following: The spin-flip process in region I leads to a loss in the local moment of region I. During this spin-flip process, positive-valued spin-currents flow from region I into region II and lead to an increase in the local moment of region II (which means a loss in the magnitude, because the local moment is negative). I.e., we have a spin-current mediated transport of the local moment from region I to region II that happens simultaneously to the spin-flip process. (We wish to mention that it is also valid to argue that negative-valued spin-currents flow from region II into region I, because there is no difference by the quantum mechanical point of view.) Note that the major part of the total moment comes from region III after the demagnetization. The local charge in the different regions changes only during the excitation process. Once the external field is zero, the charge in the various regions remains constant (apart from tiny oscillations).

We will now come back to the spin-flip process. We know from the previous section that the change of the moment is adequately described by equation (4.11).

Moreover, we know that the spin-flip process takes place in region I. Hence, the change of M_3 (and the spin-flip process, respectively) is described by

$$\partial_t M_3(t) = \sum_i \langle \Omega_I(\hat{r}_i) \xi(\hat{r}_i) (\hat{\sigma}_{2,i} \hat{L}_{1,i} - \hat{\sigma}_{1,i} \hat{L}_{2,i}) \rangle(t). \quad (4.16)$$

Before we continue, we wish to mention that the mechanism of the change of the moment according to equation (4.16) can be imagined in a similar way as discussed at the end of section 3.1.4. For example, the contribution of the $\sigma_2 L_1$ -component to the change of the moment can, in a simplified manner, be interpreted as follows: The σ_2 -component corresponds to a magnetic dipole that moves according to the angular momentum L_1 in the radial electric field. The movement in the electric field leads to an effective magnetic field, which leads then to a torque on the dipole (or spin, respectively), and hence to a change of the spin. However, as also stated before, we have to be careful with this interpretation due to the following reason: One might think that $\langle \hat{\sigma}_2 \hat{L}_1 \rangle$ is, in region I, approximately given by the mean field expression $\langle \hat{\sigma}_2 \rangle \langle \hat{L}_1 \rangle$. On the contrary one finds that this is not true, and that the mean field expression is approximately zero, because $\langle \hat{\sigma}_2 \rangle \approx 0$ during the entire time evolution. A similar behavior is found for $\langle \hat{\sigma}_1 \hat{L}_2 \rangle$. Hence, the full combined $\sigma_p L_q$ -operator has to be considered in the investigations. (Note that $\langle \hat{\sigma}_p \hat{L}_q \rangle$ corresponds to an integrated spin-current density; see also appendix A.2.)

The spin-flip process is described by equation (4.16). In order to investigate the spin-flip process in more detail, it would be advantageous if the problem could be described by an even simpler expression. Such an expression could, for example, be obtained by simply replacing the radial function $\xi(r)$ by an effective scaling factor β (which might be a justified simplification, due to the radial character of the problem):

$$\partial_t M_3(t) = \sum_i \beta \langle \Omega_I(\hat{r}_i) (\hat{\sigma}_{2,i} \hat{L}_{1,i} - \hat{\sigma}_{1,i} \hat{L}_{2,i}) \rangle(t). \quad (4.17)$$

This simplification has been tested, and it was, in fact, found that equation (4.17) describes the spin-flip process quite well (with $\beta = 10.5 \cdot 10^{-3}$). This can be seen in the left panel of figure 4.15, where the $\sigma_2 L_1$ and $\sigma_1 L_2$ contributions of $\partial_t M_3$ from equation (4.16) are compared to their simplified, scaled terms from (4.17). It is clear to see that the simplified, scaled terms show nearly the same time evolution as their corresponding full terms. However, it is also clear to see that the full terms show slightly stronger oscillations than the simplified terms, and one might ask whether the simplified terms would actually lead to the correct time evolution of the moment. The right panel of figure 4.15 compares the total moment to the corresponding value that has been obtained from the integration of equation (4.17). We see that the moment that has been calculated from the simplified $\partial_t M_3$ -expression describes the time evolution of the moment very well.

We can conclude that the time evolution of $\partial_t M_3$, and hence the spin-flip process, is in principle completely described by the time evolution of the following two quantities:

$$\sum_i \langle \Omega_I(\hat{r}_i) \hat{\sigma}_{2,i} \hat{L}_{1,i} \rangle, \quad \text{and} \quad \sum_i \langle \Omega_I(\hat{r}_i) \hat{\sigma}_{1,i} \hat{L}_{2,i} \rangle. \quad (4.18)$$

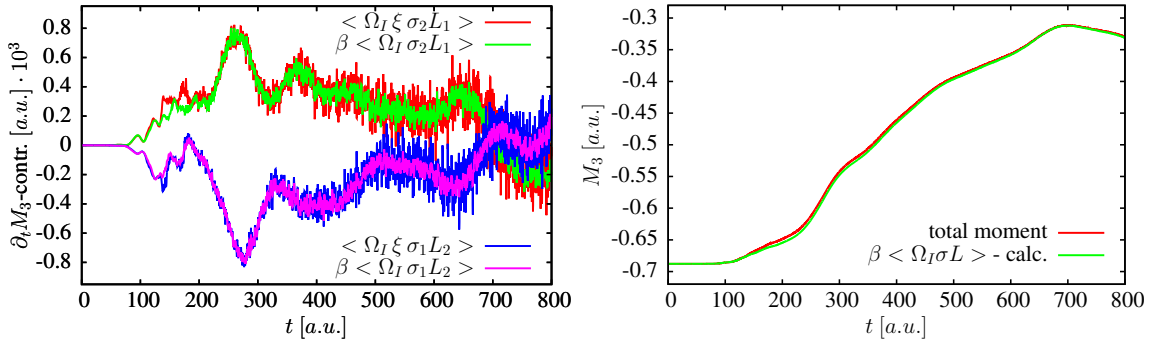


Fig. 4.15.: Left: The $\sigma_2 L_1$ and $\sigma_1 L_2$ contribution of $\partial_t M_3$ for the full calculation (according to (4.16)), and for the simplified calculation (according to (4.17)). The two terms from the simplified calculation are scaled with the factor: $\beta = 10.5 \cdot 10^{-3}$. Right: e_3 -component of the total moment, and the corresponding value that has been obtained from the integration of (4.17) with $\beta = 10.5 \cdot 10^{-3}$.

In the following, we will refer to the quantities from (4.18) as “spin-orbit angular momenta”. (The quantities from (4.18) should, to be more precise, be named “local spin-orbit angular momenta”, since the σL -expectation values are calculated only in region I. However, for simplicity we will in the following omit the word “local”.)

In summary, we have found that the change of the total moment in bulk Ni takes place in two regions: in region I and in region II (see figure 4.14). The actual spin-flip process takes place in region I, which causes a loss in the local moment of region I. Moreover, it was found that, during the spin-flip process, spin-currents flow from region I into region II, causing a loss in the local moment of region II as well. Furthermore, it was found that the region outside of region II (i.e. region III) does not directly contribute to the loss in the moment. Finally, we found that the spin-flip process is completely described by the time evolution of the spin-orbit angular momenta in region I, i.e. by the two quantities from (4.18).

4.3.4. Spin-orbit angular momentum torques and the ground state

In section 4.2 we found that the amplitude of the total moment in ferromagnetic bulk Ni always decreases when the system is excited by an intense external pulse. We did not, however, find a reason why a loss in the moment is always observed. In the previous section, we found that the dynamics of the total moment is completely determined by the dynamics of the spin-orbit angular momenta. To be more precise, it was found that the dynamics of M_3 is related to the two quantities from (4.18) via

$$\partial_t M_3(t) \sim \sum_i \langle \Omega_I(\hat{r}_i) \hat{\sigma}_{2,i} \hat{L}_{1,i} \rangle(t) - \sum_i \langle \Omega_I(\hat{r}_i) \hat{\sigma}_{1,i} \hat{L}_{2,i} \rangle(t). \quad (4.19)$$

Hence, one could try to explain the behavior of the moment by means of the spin-orbit angular momenta. In the next section, we will follow this idea, and we will investigate the time evolution of the spin-orbit angular momenta in detail. It is reasonable to investigate the spin-orbit angular momenta from (4.19) individually,

because each of these two quantities gives a more or less similar contribution to the dynamics of the moment (this can be seen from the left panel of figure 4.15).

In this section, we will investigate the spin-orbit angular momenta and the related torque quantities for the ground state, because it is important first to understand the corresponding behavior of the ground state before the time-dependence can be discussed (this will become more clear in the next section). First of all, we point out that each of the two spin-orbit angular momenta from (4.19) is zero for the ground state, which can be seen in figure 4.15 (this results from the symmetry). Therefore, we have

$$\sum_i \langle \Omega_I(\hat{\mathbf{r}}_i) \hat{\sigma}_{2,i} \hat{L}_{1,i} \rangle(t) = \int_0^t dt' \sum_i \partial_{t'} \langle \Omega_I(\hat{\mathbf{r}}_i) \hat{\sigma}_{2,i} \hat{L}_{1,i} \rangle(t'), \quad (4.20)$$

and an equivalent equation for the other spin-orbit angular momentum, meaning that the change of the moment follows solely from the time derivative of the spin-orbit angular momenta (via the integration of (4.17)). In the following, we will refer to the time derivative of the spin-orbit angular momenta as spin-orbit angular momentum torques.

Each spin-orbit angular momentum torque has several torque contributions. The different torque contributions follow from the application of Ehrenfest's theorem. In the following, we will use Γ_{pq} to refer to the spin-orbit angular momentum torque of spin-component p and orbital angular momentum component q . Calculating the torque contributions of the $\sigma_p L_q$ -spin-orbit angular momentum gives

$$\begin{aligned} \Gamma_{pq}(t) &= \sum_i \partial_t \langle \Omega_I(\hat{\mathbf{r}}_i) \hat{\sigma}_{p,i} \hat{L}_{q,i} \rangle(t) \quad (4.21) \\ &= - \underbrace{\sum_i \oint_{\Omega_I} ds \cdot \text{Re}[\langle \delta(\mathbf{r} - \hat{\mathbf{r}}_i)(\hat{\mathbf{p}}_i + \frac{1}{c} \mathbf{A}_{\text{ext}}(t)) \hat{\sigma}_{p,i} \hat{L}_{q,i} \rangle(t)]}_{=\Gamma_{pq}^{\text{S}}(t)} \\ &\quad + \underbrace{\sum_i \frac{1}{c} \mathbf{A}_{\text{ext}}(t) \times \text{Re}[\langle \Omega_I(\hat{\mathbf{r}}_i) \hat{\sigma}_{p,i} \hat{\mathbf{p}}_i \rangle(t)]_q}_{=\Gamma_{pq}^{\text{A}}(t)} + \sum_i \langle \Omega_I(\hat{\mathbf{r}}_i) \hat{\sigma}_{p,i} \nabla v_s(\hat{\mathbf{r}}_i) \times \hat{\mathbf{r}}_i \rangle(t) \Big|_q \\ &\quad + \sum_i \frac{1}{2c} \langle \Omega_I(\hat{\mathbf{r}}_i) \nabla B_{\text{xc},p}(\hat{\mathbf{r}}_i) \times \hat{\mathbf{r}}_i \rangle(t) \Big|_q + \underbrace{\sum_i \text{Re}[\langle \Omega_I(\hat{\mathbf{r}}_i) \frac{1}{c} \mathbf{B}_{\text{xc}}(\hat{\mathbf{r}}_i) \times \hat{\sigma}_i \hat{L}_{q,i} \rangle(t)]_p}_{=\Gamma_{pq}^{\text{B}}(t)} \\ &\quad + \sum_i \sum_{m=1}^3 \varepsilon_{qpm} \frac{1}{2} \langle \Omega_I(\hat{\mathbf{r}}_i) \xi(\hat{\mathbf{r}}_i) \hat{L}_{m,i} \rangle(t) + \underbrace{\sum_i \text{Re}[\langle \Omega_I(\hat{\mathbf{r}}_i) \xi(\hat{\mathbf{r}}_i) \hat{\mathbf{L}}_i \times \hat{\sigma}_i \hat{L}_{q,i} \rangle(t)]_p}_{=\Gamma_{pq}^{\text{SOC}}(t)}, \end{aligned}$$

with $p, q = \{1, 2, 3\}$. We have assumed that we have a KS Hamiltonian of the form (3.16), with the difference that the SOC term is replaced by the radial SOC term (4.10), and we have neglected the external \mathbf{B} -field. The derivation of (4.21) is shown in detail in appendix A.6.4. Note that the \mathbf{r} -operator refers to a coordinate

system with the origin at the nucleus (according to the definition of the angular momentum operator).

Equation (4.21) shows all spin-orbit angular momentum torque contributions, while some terms are specifically labeled. In the calculations, it was found that the unlabeled terms were approximately zero in the ground state. Furthermore, it was found that these terms did also not give any significant contributions in the time-dependent situation (this behavior results most probably from the spherical nature of the problem in region I). Hence, we will in the following discussions only consider the labeled terms, and we will neglect all other terms.

The first term, $\Gamma_{pq}^{\mathbf{s}}$, corresponds to a spin-orbit angular momentum current contribution, i.e. the spin-orbit angular momentum in region I is changed via currents that flow through the surface of Ω_I and that transport parts of the spin-orbit angular momentum. The second torque contribution, $\Gamma_{pq}^{\mathbf{A}}$, results from the direct coupling of the external \mathbf{A} -field to the spin-orbit angular momentum. Note that this contribution comes, in a sense, from the torque on the orbital angular momentum (since $[\hat{\mathbf{L}}, \mathbf{A} \cdot \hat{\mathbf{p}}]/i = \mathbf{A} \times \hat{\mathbf{p}}$). The last two terms, $\Gamma_{pq}^{\mathbf{B}}$ and Γ_{pq}^{SOC} , correspond to the interaction of the moving spin with the xc \mathbf{B} -field, and with the potential v_s via SOC, respectively. Note that these two torque contributions result in principle from the torque on the spin component (this can be seen from the $\hat{\mathbf{B}}_{\text{xc}} \times \hat{\boldsymbol{\sigma}}$ and $\hat{\xi} \hat{\mathbf{L}} \times \hat{\boldsymbol{\sigma}}$ expressions, which correspond to spin-torque contributions; see (3.22) and (4.11)).

For our concerns, only the spin-orbit angular momentum torques Γ_{21} and Γ_{12} and their contributions are of interest, because the change of M_3 follows solely from these two quantities. The \mathbf{B} -field torque contributions, $\Gamma_{21}^{\mathbf{B}}$ and $\Gamma_{12}^{\mathbf{B}}$, consist of two parts, respectively (as a result of the cross product). In the calculations, however, it was found that one part was always negligible, i.e.:

$$\begin{aligned}\Gamma_{21}^{\mathbf{B}}(t) &\approx \sum_i \text{Re} \left[\langle \Omega_I(\hat{r}_i) \frac{1}{c} B_{\text{xc},3}(\hat{\mathbf{r}}_i) \hat{\sigma}_{1,i} \hat{L}_{1,i} \rangle(t) \right], \\ \Gamma_{12}^{\mathbf{B}}(t) &\approx - \sum_i \text{Re} \left[\langle \Omega_I(\hat{r}_i) \frac{1}{c} B_{\text{xc},3}(\hat{\mathbf{r}}_i) \hat{\sigma}_{2,i} \hat{L}_{2,i} \rangle(t) \right],\end{aligned}\quad (4.22)$$

which results from the fact that the \mathbf{e}_1 - and \mathbf{e}_2 -component of \mathbf{B}_{xc} was, in average, always approximately zero in region I. Additionally, it was found that one part of the SOC torque contributions (which consist also of two parts, due to the cross product) was always negligible as well:

$$\begin{aligned}\Gamma_{21}^{\text{SOC}}(t) &\approx - \sum_i \langle \Omega_I(\hat{r}_i) \xi(\hat{r}_i) \hat{L}_{1,i}^2 \hat{\sigma}_{3,i} \rangle(t), \\ \Gamma_{12}^{\text{SOC}}(t) &\approx \sum_i \langle \Omega_I(\hat{r}_i) \xi(\hat{r}_i) \hat{L}_{2,i}^2 \hat{\sigma}_{3,i} \rangle(t),\end{aligned}\quad (4.23)$$

which most probably results from the fact that the \mathbf{e}_1 - and \mathbf{e}_2 -component of the local moment of region I was, in average, always approximately zero. In the following, we will discuss how the various torque terms behave for the ground state of bulk Ni. But before we can do that, we first need to have a closer look at the spin-current densities.

First, we note that the KS ground state energy contribution, coming from the radial SOC term, can be represented via the spin-current densities (see appendix A.6.5):

$$\sum_i \langle \frac{1}{2} \xi(\hat{r}_i) \hat{\sigma}_i \cdot \hat{\mathbf{L}}_i \rangle = \sum_{k=1}^3 \frac{1}{2} \int d\mathbf{r} \xi(r) (\mathbf{r} \times \mathbf{j}^k(\mathbf{r})) \cdot \mathbf{e}_k, \quad (4.24)$$

where the origin of \mathbf{r} is at the nucleus. The radial function $\xi(r)$ is, in region I, always positive. This becomes immediately clear when we assume, for simplicity, that the potential v_s can approximately be described by an effective Coulomb-like potential in region I: $v_s(r) \approx -Z_{\text{eff}}/r$. From the definition of the radial function (4.9) follows then immediately: $\xi(r) \approx Z_{\text{eff}}/(2c^2 r^3) > 0$. Hence, the SOC energy contribution (4.24) becomes negative (meaning that the system can minimize its total energy) when we have in region I:

$$(\mathbf{r} \times \mathbf{j}^k(\mathbf{r})) \cdot \mathbf{e}_k < 0, \quad \text{with} \quad k = \{1, 2, 3\}. \quad (4.25)$$

In fact, one finds that (4.25) is true for the ground state of bulk Ni, which manifests itself by non-vanishing spin-currents that flow around the nucleus. This can be seen in figure 4.16 where we show, as an example, \mathbf{j}^1 and $(\mathbf{r} \times \mathbf{j}^1) \cdot \mathbf{e}_1$. Note that \mathbf{j}^1 flows clockwise around \mathbf{e}_1 in order to fulfill the relation (4.25). The

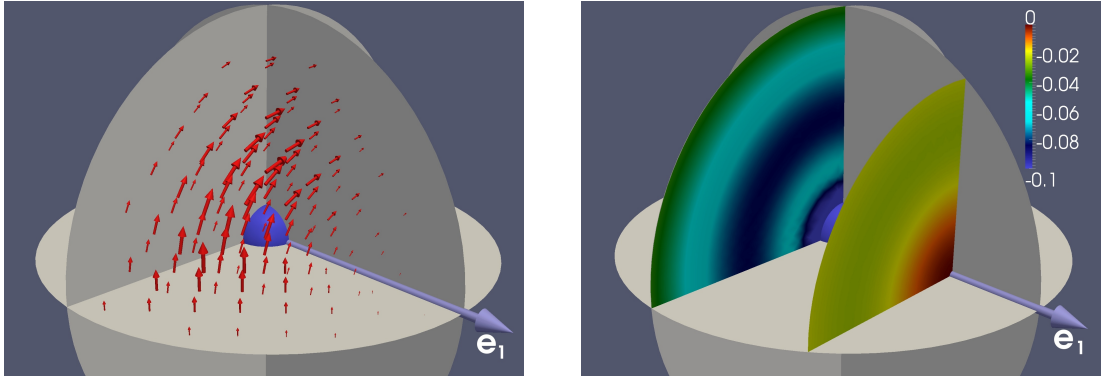


Fig. 4.16.: Shown is region I and three planes which are perpendicular to the unit vectors. The small blue sphere represents the nucleus. Left: Spin-current density \mathbf{j}^1 for the ground state of bulk Ni flowing clockwise around \mathbf{e}_1 (the size of the arrows is proportional to $|\mathbf{j}^1|$). Right: Two slices through the field $(\mathbf{r} \times \mathbf{j}^1) \cdot \mathbf{e}_1$ (the color scale is in *a.u.*).

other spin-current densities behave in an analogous manner, i.e. \mathbf{j}^2 flows clockwise around \mathbf{e}_2 , and \mathbf{j}^3 flows clockwise around \mathbf{e}_3 . We wish to mention that the kinetic energy contribution increases with increasing spin-current densities, which prevents infinitely large spin-current densities in the ground state. (Remark: The magnetization components m_1 and m_2 are zero in the ground state in region I, however, the corresponding spin-currents \mathbf{j}^1 and \mathbf{j}^2 are not zero. This seems to be a specific feature of the energetically lowest state of a ferromagnet polarized along \mathbf{e}_3 if SOC is present; see also appendix A.2.)

The \mathbf{B}_{xc} spin-orbit angular momentum torque contributions (4.22) can also be written in terms of the spin-current densities (see appendix A.6.5):

$$\sum_i \text{Re} \left[\langle \Omega_I(\hat{r}_i) \frac{1}{c} B_{\text{xc},3}(\hat{\mathbf{r}}_i) \hat{\sigma}_{k,i} \hat{L}_{k,i} \rangle(t) \right] = \frac{1}{c} \int_{\Omega_I} d\mathbf{r} B_{\text{xc},3}(\mathbf{r}) (\mathbf{r} \times \mathbf{j}^k(\mathbf{r})) \cdot \mathbf{e}_k. \quad (4.26)$$

In our case, the local moment in region I points in the $-\mathbf{e}_3$ -direction in the ground state, i.e. $M_3 < 0$. Hence, the \mathbf{B}_{xc} in region I points in the \mathbf{e}_3 -direction, i.e. $B_{\text{xc},3} > 0$ (which follows from the Hamiltonian element $\hat{\boldsymbol{\sigma}} \cdot \hat{\mathbf{B}}_{\text{xc}}/2c$ and from the LSDA (2.60)). Therefore, it follows immediately from (4.26), together with (4.25), that the torque contribution $\Gamma_{21}^{\mathbf{B}}$ has to be negative, and that $\Gamma_{12}^{\mathbf{B}}$ has to be positive:

$$\Omega_{\text{I}} : \quad M_3 < 0, \quad B_{\text{xc},3}(\mathbf{r}) > 0 \quad \longrightarrow \quad \Gamma_{21}^{\mathbf{B}} < 0, \quad \Gamma_{12}^{\mathbf{B}} > 0. \quad (4.27)$$

Note that the same investigation can also be done if the system is spin-polarized along the \mathbf{e}_3 -direction, i.e. $M_3 > 0$, which gives: $\Gamma_{21}^{\mathbf{B}} > 0$ and $\Gamma_{12}^{\mathbf{B}} < 0$.

In the ground state, the total torque on each spin-orbit angular momentum has to be zero. Hence, the sum of the torque contributions has to be zero as well, meaning that system is in a spin-orbit angular momentum torque equilibrium:

$$\Gamma_{pq}(0) = \Gamma_{pq}^{\text{s}}(0) + \Gamma_{pq}^{\mathbf{B}}(0) + \Gamma_{pq}^{\text{SOC}}(0) = 0. \quad (4.28)$$

Note that the $\Gamma_{pq}^{\mathbf{A}}$ term is zero, because we have $\mathbf{A}_{\text{ext}}(0) = 0$. Additionally, one finds from the ground state calculation that the torque contributions of Γ_{21} and Γ_{12} are related in the following way:

$$\Gamma_{21}^{\text{s}}(0) = -\Gamma_{12}^{\text{s}}(0), \quad \Gamma_{21}^{\mathbf{B}}(0) = -\Gamma_{12}^{\mathbf{B}}(0), \quad \Gamma_{21}^{\text{SOC}}(0) = -\Gamma_{12}^{\text{SOC}}(0), \quad (4.29)$$

which most probably results from the symmetry (the values of the ground state torque contributions can be seen in the left panel of figure 4.17 at $t = 0$; note that the relations (4.29) approximately hold, at least initially, in the time-dependent situation as well). With the previous relations we can also make a statement about the sign of the SOC torque terms:

$$\begin{aligned} \Gamma_{21}^{\text{SOC}} &\stackrel{(4.29)}{=} \frac{1}{2}(\Gamma_{21}^{\text{SOC}} - \Gamma_{12}^{\text{SOC}}) \stackrel{(4.23)}{\approx} -\frac{1}{2} \sum_i \langle \Omega_{\text{I}}(\hat{r}_i) \xi(\hat{r}_i) (\hat{L}_{1,i}^2 + \hat{L}_{2,i}^2) \hat{\sigma}_{3,i} \rangle \\ &= \frac{1}{2} \sum_i \langle \Omega_{\text{I}}(\hat{r}_i) \xi(\hat{r}_i) (\hat{L}_{3,i}^2 - \hat{L}_i^2) \hat{\sigma}_{3,i} \rangle \\ &\approx \underbrace{\sim \langle \sum_i \Omega_{\text{I}}(\hat{r}_i) (\hat{L}_{3,i}^2 - \hat{L}_i^2) \rangle}_{< 0} \underbrace{\langle \sum_i \Omega_{\text{I}}(\hat{r}_i) \hat{\sigma}_{3,i} \rangle}_{< 0}. \end{aligned} \quad (4.30)$$

In the calculations it was found that the expression from the second line is approximately proportional to the mean field expression from the last line (this holds for the whole time evolution). The relation from last line reveals immediately that $\Gamma_{21}^{\text{SOC}} > 0$ and that $\Gamma_{12}^{\text{SOC}} < 0$. If the system would be spin-polarized along the \mathbf{e}_3 -direction, we would have $\Gamma_{21}^{\text{SOC}} < 0$ and $\Gamma_{12}^{\text{SOC}} > 0$, because the right term in the last line of (4.30), which is the local moment, would be > 0 . The left term of (4.30) has to be always ≤ 0 . This follows immediately from the representation of the KS states via spherical harmonics: $\hat{L}_3^2 - \hat{L}^2 \rightarrow m^2 - l(l+1) \leq 0$, since $l \geq 0$ and $|m| \leq l$.

The spin-orbit angular momenta and the corresponding torque contributions discussed previously have been defined for the region I. Similar quantities can, in

an analogous manner, also be defined for region II. Calculating the corresponding torque contributions for region II leads to similar expressions as in (4.21), however, there are some differences: First, one finds that the surface term Γ_{pq}^s has, for region II, two contributions. One contribution corresponds to the spin-orbit angular momentum current that flows from region III into region II, and the other corresponds to the current flowing from region I into region II. Note that the latter torque contribution has to be equal to the negative Γ_{pq}^s contribution of region I. Next, one finds that the Γ_{pq}^{SOC} contribution of region II is very small and negligible, because the SOC effects are only present in region I (as discussed in section 4.3.2). In fact, one finds that Γ_{pq}^{B} is, beside the surface contributions, the only important term in region II. Hence, we have different torque contributions in the various regions, meaning that the surface terms can be understood as contributions that transfer parts of the spin-orbit angular momentum between the regions, in order to obtain a spin-orbit angular momentum torque equilibrium (note that such an equilibrium has to be satisfied in each region in the ground state).

In conclusion, we have discussed the possibility of analyzing the change of the total moment by means of the spin-orbit angular momentum torques (i.e. the time derivative of the spin-orbit angular momenta in region I). Each spin-orbit angular momentum torque consists of several torque contributions, while only four contributions are important (see (4.21)): the surface term Γ_{pq}^s , the direct \mathbf{A} -coupling term $\Gamma_{pq}^{\mathbf{A}}$, and the $\Gamma_{pq}^{\mathbf{B}}$ and Γ_{pq}^{SOC} terms, which result from the torque on the spin by the \mathbf{B}_{xc} -field and by SOC, respectively. The behavior of the different torque quantities has been specifically discussed for the ground state. It was found that the sum of the torque contributions has to vanish, meaning that system is in a spin-orbit angular momentum torque equilibrium (see (4.28)). Moreover, it was shown that the SOC leads to non-vanishing spin-currents in the ground state. These spin-currents lead, depending on the orientation of the local moment, to a specific sign of the \mathbf{B}_{xc} -torque contributions.

4.3.5. The Spin-flip process

In section 4.3.2 and 4.3.3 we found that the demagnetization in bulk Ni is caused by a spin-flip process that takes place in region I (see figure 4.14). Moreover, it was found that the spin-flip process is caused by induced spin-orbit angular momenta that lead, via the local potential (and the corresponding electric field, respectively), to a torque on the spin. However, so far it was not possible to understand why the spin-orbit angular momenta are induced, and furthermore why the magnitude of the moment always decreases. In this section we will tackle these problems by means of the spin-orbit angular momentum torques introduced in the previous section.

The change of the total moment is governed by the dynamics of certain spin-orbit angular momenta (see (4.19)), while the time evolution of each spin-orbit angular momentum follows from the integral of its torque (see (4.20)), i.e.:

$$\partial_t M_3(t) \sim \int_0^t dt' \Gamma_{21}(t') - \int_0^t dt' \Gamma_{12}(t'). \quad (4.31)$$

Each torque is substantially determined by four torque contributions (as discussed in the previous section; see (4.21)):

$$\Gamma_{pq}(t) = \Gamma_{pq}^{\text{S}}(t) + \Gamma_{pq}^{\text{A}}(t) + \Gamma_{pq}^{\text{B}}(t) + \Gamma_{pq}^{\text{SOC}}(t). \quad (4.32)$$

When the system is in its ground state, the torque contributions cancel each other, meaning that the system is in a spin-orbit angular momentum torque equilibrium. If the system is excited, the torque contributions change (usually differently from each other, as we will see), meaning that the equilibrium is disturbed. This results in non-vanishing net spin-orbit angular momentum torques, leading to induced spin-orbit angular momenta. These induced spin-orbit angular momenta lead then to a torque on the spin, and thus to a change of the moment. This is, in principle, how the spin-flip process can be described. In the following, we will investigate how the different torque contributions change, allowing us to explain why we always observe a loss in the moment of bulk Ni.

Before we investigate the torque contributions, we wish to say a few words about the \mathbf{B}_{xc} -field, because we will find that the time behavior of this field is essential for the demagnetization process. The \mathbf{B}_{xc} -field represents an effective field that incorporates xc contributions, and that couples in the KS system to the magnetization, in order to achieve the same spin-polarization as the reference interacting system. For the ground state, the \mathbf{B}_{xc} -field is defined via the xc energy functional (see e.g. (2.36)), while the definition for time-dependent situations is more involved (see the discussion at the end of section 2.3.1). In our calculations, the \mathbf{B}_{xc} was approximated by the ALSDA. Since the ALSDA is based on a ground state functional and on the homogenous electron gas, one might wonder if the application of this approximation leads to any spurious effects (regarding particularly the spin properties) that would not be present in the true interacting system.

First of all, we emphasize that the spin-flip process occurs in region I (i.e. the behavior of \mathbf{B}_{xc} in this region is of particular interest). The magnetization (i.e. the spin-density) in this region is, compared to the other regions, quite large. Next, we point out that the major contribution of the xc interaction comes, for high densities, from the exchange. Since the exchange interaction is, for high densities, quite well described by the LSDA, the previously mentioned points might suggest that most of the important spin related exchange effects that occur during the dynamics in the true interacting system are covered by our approximation. (Note that a true Coulomb interacting many-electron system does not have a \mathbf{B}_{xc} -field that couples directly to the spin. Hence, one might wonder if there are actually any time-dependent spin related exchange effects in a many-electron system that behave similar to a \mathbf{B}_{xc} -field. In appendix A.7 we discuss this subject by means of a Coulomb interacting two-electron systems, and we show that an interacting system in fact contains exchange contributions that act similar to a time-dependent \mathbf{B}_{xc} -field.)

The change of the moment follows from the two spin-orbit angular momentum torques Γ_{21} and Γ_{12} . As stated in the previous section, the two torques give a more or less similar contribution to the dynamics of the moment. Moreover, the various contributions of the two torques behave similar as well (except for Γ_{pq}^{A}). Hence,

we will in the following only discuss the contributions of Γ_{21} in detail. Recall that all investigations in this main section (i.e. all investigations of section 4.3) refer to the run with $I_0 = 10^{15} \text{ W/cm}^2$ from figure 4.4, meaning that $\Gamma_{21}^{\mathbf{A}}(t) = 0$ since the polarization of the \mathbf{A} -field was along \mathbf{e}_1 (see (4.21)).

The left panel of figure 4.17 shows the surface-, the \mathbf{B}_{xc} -, and the SOC-torque contributions of Γ_{21} for the initial time $t = 0 \dots 200 \text{ a.u.}$ (The Γ_{21}^{s} shown has been smoothed via a convolution with a rectangular function, since the original Γ_{21}^{s} shows very fast oscillations that are not relevant for us. The integral of the smoothed and the original quantity is equal.) It is clear to see that the three

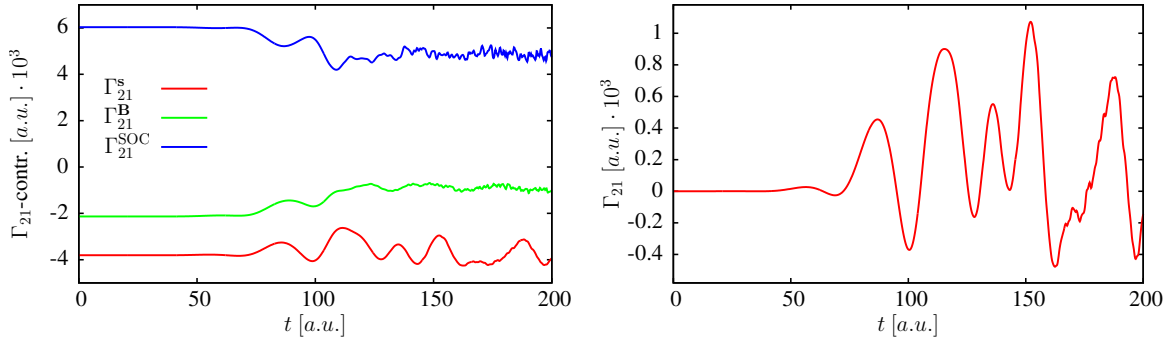


Fig. 4.17.: Left: Surface-, \mathbf{B}_{xc} -, and SOC-torque contributions of Γ_{21} . Right: Time evolution of the spin-orbit angular momentum torque Γ_{21} .

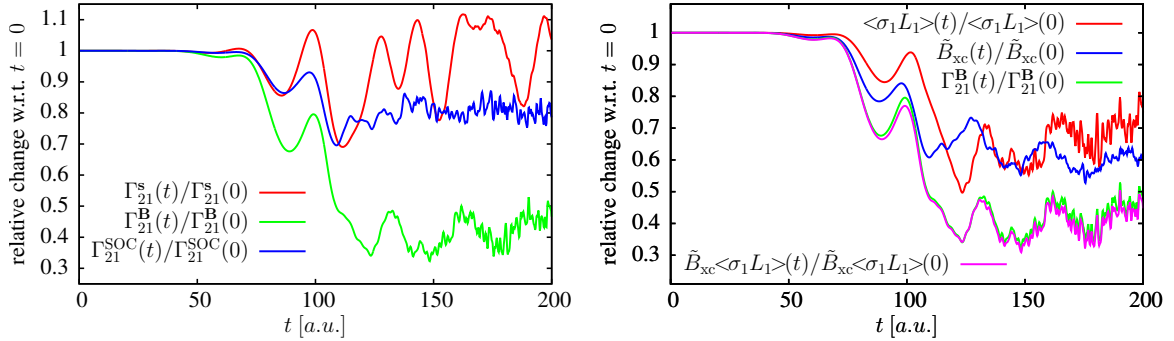


Fig. 4.18.: Left: Relative value of each torque contribution with respect to $t = 0$. Right: Relative value (w.r.t. $t = 0$) of the $\sigma_2 L_1$ -spin-orbit angular momentum, of the average \mathbf{B}_{xc} , and of Γ_{21} . Additionally, the combined relative value of the $\sigma_2 L_1$ -spin-orbit angular momentum and the average \mathbf{B}_{xc} (i.e. their product) is shown.

torque contributions cancel each other at $t = 0$. Moreover, we see that Γ_{21}^{SOC} is positive, while Γ_{21}^{s} and Γ_{21}^{B} are negative. Remember that Γ_{21}^{B} has to be < 0 and that Γ_{21}^{SOC} has to be > 0 in the ground state if $M_3 < 0$, as shown in the previous section.

At around $t = 75 \text{ a.u.}$, the intensity of the external pulse increases significantly and the system is excited (see figure 4.8 and 4.9). As a consequence, also the torque contributions start to change at that time, which is clear to see in the left panel of figure 4.17. However, it is not obvious how the sum of the different contributions, i.e. the total spin-orbit angular momentum torque Γ_{21} , behaves. The time evolution of Γ_{21} is shown in the right panel of figure 4.17. We see that Γ_{21} starts also to change significantly at around $t = 75 \text{ a.u.}$, and it shows some oscillations at later times. However, it is also clear to see that Γ_{21} is, during the

initial time $t = 0 \dots 200 \text{ a.u.}$, more in the positive region than in the negative region. Therefore, its integral value is positive (i.e. the $\sigma_2 L_1$ -spin-orbit angular momentum is positive; see figure 4.15), which leads to a positive $\partial_t M_3$ contribution (according to 4.31), and hence to a decrease in the magnitude of the moment, since $M_3(0) < 0$.

We have seen before that all relevant torque contributions change during the initial excitation process, and we have seen that the resulting torque Γ_{21} is on average positive, which leads to the loss in the moment. However, so far it is not clear why Γ_{21} is on average positive. In order to understand this behavior, the relative change of the torque contributions with respect to $t = 0$ (i.e. $\Gamma'_{21}(t)/\Gamma'_{21}(0)$, where Γ'_{21} corresponds to the different contributions) can be investigated. Before we discuss the relative change of the torque contributions, recall that the initial excitation process leads to a loss in the electronic charge in region I. Hence, the magnitude of each torque contribution in this region would likely also decrease (which is in fact what we see). If the relative change of all torque contributions would be equal, the system would stay in a torque equilibrium, and Γ_{21} would remain zero. That this is not the case can be seen in the left panel of figure 4.18, where the relative change of all torque contributions is shown.

We see from figure 4.18 that the relative values of $\Gamma_{21}^{\mathbf{B}}$ and Γ_{21}^{SOC} decrease during the initial excitation (up to $t \approx 120 \text{ a.u.}$). Note that this initial change follows the loss in the local charge, as stated before (compare to figure 4.9). We also see that the initial loss in the relative value of $\Gamma_{21}^{\mathbf{B}}$ is much stronger than the loss in the relative value of the other contributions. As a consequence, the value of Γ_{21} (i.e. the sum of all contributions) has to become larger than zero, because $\Gamma_{21}^{\mathbf{B}} < 0$. Therefore, we can reason that the initial loss in the moment (which results from the initial change of Γ_{21} to positive values) results from the strong initial loss in the \mathbf{B}_{xc} -spin-orbit angular momentum torque contribution. In the following, we will investigate why the loss in the relative value of $\Gamma_{21}^{\mathbf{B}}$ is so strong, but before we do that, we will say a few words about the behavior of Γ_{21}^{s} .

We see from the left panel of figure 4.18 that the initial change of the relative value of Γ_{21}^{s} (at around $t = 75 \text{ a.u.}$) follows the change of the relative value of Γ_{21}^{SOC} . We also see that the relative value of Γ_{21}^{s} increases right after this initial loss, and it shows some oscillations for later times. This behavior might be explained in the following way: The system has, in each region, a spin-orbit angular momentum torque equilibrium in the ground state. During the excitation, the equilibrium in each region vanishes. We discussed previously how the torque contributions $\Gamma_{21}^{\mathbf{B}}$ and Γ_{21}^{SOC} , and hence how the total torque, changes in region I. However, the change of the torque in region II is in general different to the change in region I. This results from the fact that only the $\Gamma_{21}^{\mathbf{B}}$ torque contribution is, beside the surface terms, present in region II (the SOC contribution is negligible in this region). The Γ_{21}^{s} might be imagined as contribution that tries to minimize the torque in region I and II (in order to restore the torque equilibrium) via the transport of spin-orbit angular momentum between these two regions. Since the excitation process leads to fast changing differences in the spin-orbit angular momentum torque between the regions, the surface contribution starts to oscillate. (Remember that there exists also a flow of spin-currents between region I and

region II (see section 4.3.3), which indirectly leads to a change of the \mathbf{B}_{xc} -torque contribution in each region. This additional coupling channel probably contributes to the oscillational behavior observed.) Note that the oscillations of Γ_{21} come mainly from the oscillations of Γ_{21}^{s} .

As stated before, the initial loss in the relative value of Γ_{21}^{B} is stronger than the loss in the relative value of the two other torque contributions. This behavior can be explained by the fact that the time evolution of Γ_{21}^{B} is, in principle, determined by two quantities: by the $\sigma_1 L_1$ -spin-orbit angular momentum, and by the \mathbf{e}_3 -component of the \mathbf{B}_{xc} -field (this can be seen from relation (4.22)). The right panel of figure 4.18 shows the relative change of the $\sigma_1 L_1$ -spin-orbit angular momentum, and the relative change of the average \mathbf{B}_{xc} -field in region I (i.e. $\tilde{B}_{\text{xc}} = \int_{\Omega_{\text{I}}} d\mathbf{r} B_{\text{xc},3}(\mathbf{r})/\Omega_{\text{I}}$). The change of the $\sigma_1 L_1$ -spin-orbit angular momentum is a direct result of the initial excitation (i.e. parts of the spin-orbit angular momentum are lost due to the loss of electronic charge in region I). However, we also see that we have a loss in the relative value of the average \mathbf{B}_{xc} -field, which is an indirect effect of the initial excitation: The excitation leads to a change of the local moment and charge in region I (this change has been explained in detail in section 4.3.1). This change of the moment and charge leads then, via the functional, to a loss in the \mathbf{B}_{xc} of region I. (Note that the change of the \mathbf{B}_{xc} -field occurs instantaneously, as a result of the ALSDA. In the true many-electron system, this process corresponds, in some sense, to a fast change in the local exchange interaction, which is instantaneous as well.) Hence, we could argue that the strong loss in the relative value of Γ_{21}^{B} comes from the combined loss in the $\sigma_1 L_1$ -spin-orbit angular momentum and in the \mathbf{B}_{xc} -field. That this is, in fact, true can be seen in the right panel of figure 4.18, where we see that the combined loss in the relative value of the $\sigma_1 L_1$ -spin-orbit angular momentum and in the relative value of \tilde{B}_{xc} (i.e. their product) behaves very similar to the change of the relative value of Γ_{21}^{B} .

The loss in the magnitude of the $\sigma_1 L_1$ -spin-orbit angular momentum in region I corresponds to an increase in the SOC energy, because the SOC energy (see (4.24)) as well as the $\sigma_1 L_1$ -spin-orbit angular momentum are negative in the ground state (note that the $\sigma_2 L_2$ - and $\sigma_3 L_3$ -spin-orbit angular momenta behave similar to the $\sigma_1 L_1$ -spin-orbit angular momentum during the excitation). Hence, we can conclude that the strong initial loss in the relative value of Γ_{21}^{B} results from the fact that the SOC energy increases, and the average \mathbf{B}_{xc} in region I decreases during the initial excitation. Since $\Gamma_{21}^{\text{B}} < 0$, the strong loss in its magnitude leads to $\Gamma_{21} > 0$, which leads then, via the relation (4.31), to a loss in the total moment, because $M_3(0) < 0$. Note that the loss in the moment occurs in an analogous manner if the system has an opposite spin-polarization, because the Γ_{21}^{B} torque contribution has always the same sign as the local M_3 in region I in the ground state, as shown in the previous section.

Next, we point out that the initial excitation process and the corresponding change of the local moment and charge, and hence the change of the \mathbf{B}_{xc} , can be described by the local (TD)DOS, as discussed in section 4.3.1. Since the (TD)DOS is a characteristic property of each material, the dynamical behavior of the moment after an excitation has to be a characteristic property as well, which follows from the previous discussion. We have seen that the initial characteristic

excitation in bulk Ni leads to a strong loss in the \mathbf{B}_{xc} around the nucleus, and hence to a loss in the moment. If, however, a material would respond to an excitation in such a way that the change of the local moment and charge would lead to an increase in the \mathbf{B}_{xc} around the nucleus, the magnitude of the total moment might not change, or even increase. Nevertheless, in all calculations that have been performed for bulk Ni and Fe, such a behavior has never been observed, because the initial excitation always led to a loss in the \mathbf{B}_{xc} around the nucleus.

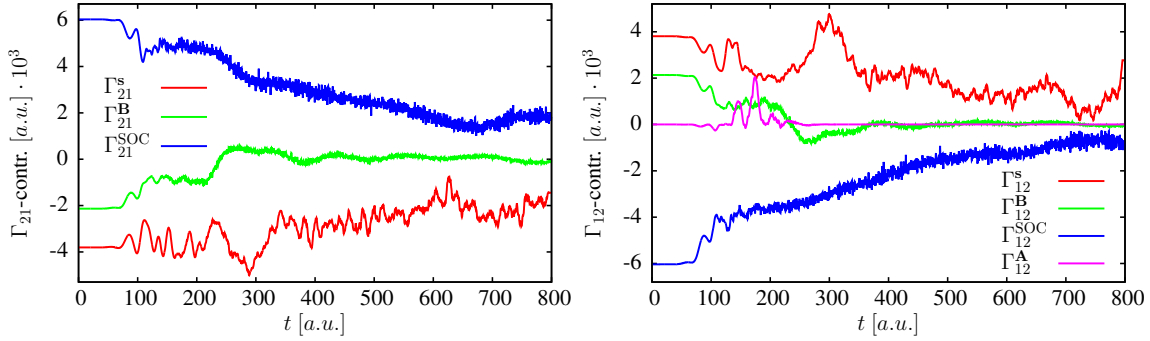


Fig. 4.19.: All important spin-orbit angular momentum torque contributions of Γ_{21} (left), and of Γ_{12} (right).

So far, we only discussed the initial behavior of Γ_{21} . As stated, the torque contributions of Γ_{12} behave, in principle, similar to the torque contributions of Γ_{21} , with the difference that all torque contributions have the opposite sign, as can be seen in figure 4.19. Since Γ_{12} contributes with its negative value to $\partial_t M_3$ (see (4.31)), the torque terms of Γ_{12} and Γ_{21} give at the end similar contributions to the change of the moment. In particular we point out that the process leading to the initial loss in the moment is for Γ_{12} similar to the process described before: The initial increase in the SOC energy and the loss in the \mathbf{B}_{xc} around the nucleus leads to a strong decrease of Γ_{12}^{B} , meaning that $\Gamma_{12} < 0$. Hence, the $\partial_t M_3$ contribution is positive, leading to a loss in the moment because $M_3(0) < 0$. We see from figure 4.19 that Γ_{12} has an \mathbf{A} -field contribution that is not present for Γ_{21} (this results from the polarization of the external \mathbf{A} -field along \mathbf{e}_1). This additional contribution, which is present between $t \approx 100 \dots 250 a.u.$, leads to small differences between Γ_{21} and Γ_{12} , which can be seen in the evolution of the corresponding spin-orbit angular momenta (see left panel of figure 4.15). Note that this direct \mathbf{A} -field contribution seems, however, not to be very important.

In the previous discussion, we investigated the initial behavior of the spin-orbit angular momentum torques in detail. Moreover, we explained why an initial loss in the moment is always observed. In the same way as before, the time evolution of the torque contributions could be investigated beyond the initial change (i.e. for $t > 200 a.u.$), and the corresponding change of the moment could be discussed. Since the investigation of the dynamics of the torque contributions is, for longer time scales, quite involved, we will only mention some main characteristics, and not discuss any further details.

The time evolution of the torque contributions of Γ_{21} and Γ_{12} for the whole demagnetization process (i.e. $t = 0 \dots 800 a.u.$) is shown in figure 4.19. The general behavior of the torque contributions can be described in the following way:

In the ground state, the torque contributions cancel each other, meaning that the system is in a spin-orbit angular momentum torque equilibrium. This equilibrium is disturbed by the excitation, which leads to a change of each torque contribution, and hence to non-vanishing net spin-orbit angular momentum torques. After the excitation, the torque contributions evolve in time until they cancel each other again, i.e. until a spin-orbit angular momentum torque equilibrium is, at least approximately, reached again. The equilibrium is reached at $t \approx 700 a.u.$, and from that point on the torque contributions essentially oscillate around their new equilibrium values. This behavior manifests itself by the dynamics of the total moment, which changes up to $t \approx 700 a.u.$, and oscillates around its new equilibrium value for all later times (see right panel of figure 4.5).

We wish to mention two important processes that occur after the excitation and before the equilibrium is reached. First, we notice that the demagnetization involves a feedback mechanism: The change of the local moment leads to a change of the \mathbf{B}_{xc} , and the change of the \mathbf{B}_{xc} leads to a change of the \mathbf{B}_{xc} -torque contributions, which, on the other hand, leads to changing non-zero total torques, and hence to a change of the moment again. This process, in fact, continues until the loss in the local moment leads to more or less vanishing \mathbf{B}_{xc} -torque contributions (see figure 4.14 and 4.19). Additionally, the SOC-torque contribution depends on the moment as well (see (4.30)). Next, we recall that each \mathbf{B}_{xc} -torque contribution depends also on a spin-orbit angular momentum (we have shown before that $\Gamma_{21}^{\mathbf{B}}$ and $\Gamma_{12}^{\mathbf{B}}$ depend on the $\sigma_1 L_1$ - and $\sigma_2 L_2$ -spin-orbit angular momentum, respectively). Hence, a change of certain spin-orbit angular momenta influences the \mathbf{B}_{xc} -torque contributions (while the \mathbf{B}_{xc} -torque contributions influence certain spin-orbit angular momenta again). This effect can be seen in figure 4.19 at $t \approx 230 a.u.$, where we see that $\Gamma_{21}^{\mathbf{B}}$ and $\Gamma_{12}^{\mathbf{B}}$ change their sign, which results from the fact that the $\sigma_1 L_1$ - and $\sigma_2 L_2$ -spin-orbit angular momenta changed their sign as well. This change leads to a strong increase in Γ_{21} and to a strong decrease in Γ_{12} , which leads then to an increase in $\partial_t M_3$, and hence to a stronger loss in the total moment (see the kink at $t \approx 230 a.u.$ in the evolution of the total moment, e.g. in figure 4.15).

In conclusion, we found that the initial excitation process disturbs the spin-orbit angular momentum torque equilibrium existing in the ground state. This leads to induced spin-orbit angular momenta, and hence to a change of the total moment. Moreover, we found that the initial excitation leads to an increase in the SOC energy and to a loss in the \mathbf{B}_{xc} around the nucleus, resulting in a strong decrease in the magnitude of the \mathbf{B}_{xc} -torque contributions. This strong decrease, on the other hand, changes the total spin-orbit angular momentum torques such that the magnitude of the total moment decreases right after the excitation. This loss in the moment continues until the system has reached a spin-orbit angular momentum torque equilibrium again. Note that the initial change of the SOC energy and the \mathbf{B}_{xc} around the nucleus follows solely from the excitation (i.e. the de-occupation) of the $3d$ -states in the MT.

4.3.6. Summary

In the previous sections, we investigated all processes that are involved in the demagnetization of bulk Ni in detail. In this section, we will briefly summarize all important results, and we will list all major steps that are involved in the demagnetization process. Furthermore, we will talk about some issues that are related to the demagnetization and that have not been mentioned before, and we will discuss the differences in the moment observed in section 4.2.

The main aspects concerning the dynamics of the moment in bulk Ni can be summarized as follows:

- The change of the moment results from a spin-flip mechanism that takes place in a region close to the nucleus (i.e. in region I; see left panel of figure 4.14).
- The spin-flip process is caused by induced spin-orbit angular momenta that lead, via the strong electric field around the nucleus, to a torque on the spin. (At the end of section 3.1.4 we have explained how this process can be imagined: spins that move in an electric field feel a magnetic field, and hence a torque.)
- The spin-orbit angular momenta involved in the change of the moment are completely described by their torques, while both the momenta and their torques are zero in the ground state (see section 4.3.3 for the definition of the spin-orbit angular momenta).
- Each spin-orbit angular momentum torque has several torque contributions. The contributions cancel each other in the ground state, meaning that the system is in a spin-orbit angular momentum torque equilibrium (see section 4.3.4 for the definition of the spin-orbit angular momentum torques and the torque contributions).

The previous points concern the behavior of the spin-orbit angular momentum quantities in the ground state, and the change of the moment in general. We have seen that an excitation of bulk Ni shows always a loss in the moment. The specific steps that lead to this loss can be summarized as follows:

- The initial excitation leads to a fast delocalization of the local moment and charge (i.e. parts of the charge and moment are transferred from the region close to the nucleus to a more distant region), resulting in a strong loss in the \mathbf{B}_{xc} around the nucleus. This loss is characteristic for bulk Ni, because the initial change of the moment and charge is directly related to the local (TD)DOS (see section 4.3.1 for details).
- Additionally, the SOC energy (which is negative in the ground state) increases during the excitation.
- The strong loss in the \mathbf{B}_{xc} and the increase in the SOC energy disturbs the spin-orbit angular momentum torque equilibrium in such a way, that the resulting total torques and induced spin-orbit angular momenta lead necessarily to an initial loss in the total moment (see section 4.3.5 for details).

- The loss in the total moment continues until a spin-orbit angular momentum torque equilibrium is reached again.
- During the spin-flip process, spin-currents flow from region I (where the spin-flip process takes place) into region II, leading to a loss in the local moment of this region. After the demagnetization, the major part of the total moment comes from region III (see figure 4.14 for a schematic of the various regions, and section 4.3.3 for details).

The previous points reveal that the change of the total moment is crucially determined by the initial excitation process and the accompanied change of the \mathbf{B}_{xc} . The initial excitation process, on the other hand, is strongly dependent on the fluence and peak intensity of the external pulse, which determine the occupation of the empty states and the de-occupation of the occupied states, respectively (according to Fermi's golden rule). The de-occupation of the local states around the nucleus leads, in bulk Ni (according to the local TDDOS), to a loss in the local moment (see figure 4.11 and 4.12). This loss, and therefore also the loss in the \mathbf{B}_{xc} , increases if the fluence or peak intensity of the external pulse increases, explaining why we see a stronger demagnetization for higher pulse fluences or peak intensities. Moreover, the initial excitation process is, in bulk Ni, only weakly dependent on the polarization direction of the external \mathbf{A} -field, explaining why the demagnetization behavior is weakly dependent on the polarization as well.

Before we discuss the next point, we recall how a system absorbs light of a certain frequency ω : the absorption occurs typically in such a way that the empty states that have an eigenvalue that is by ω larger than the occupied states become occupied (this follows e.g. from first order perturbation theory for a harmonic perturbation [57]). Hence, an efficient de-occupation of a state with the eigenvalue ε occurs only if empty states at $\varepsilon + \omega$ are available in the DOS. Since the de-occupation of the local states around the nucleus determines the demagnetization significantly (as explained before), it becomes clear why the change of the moment depends considerably on the center frequency of the external field. This fact explains also why the demagnetization in bulk Ni by the pulse with the center frequency $\omega = 0.2 a.u.$ is much smaller than the demagnetization from the other pulses (see figure 4.3): We see from the local MT-DOS (upper left panel of figure 4.10) that almost no states are available at around $\omega = 0.2 a.u.$. Hence, all states around the Fermi energy (i.e. around $\omega = 0$) will not be considerably de-occupied, which results in a smaller initial loss in the local moment, and hence in a smaller demagnetization.

Next, we come to an issue that has not been mentioned before. As shown in section 3.2, the underlying basis used to represent the KS states uses a spherical harmonics expansion in the MT, i.e. a sum over the azimuthal number l is employed. This expansion allows it to calculate the l -dependent contribution to the moment in the MT, which reveals that the moment comes, for the ground state of bulk Ni, almost entirely from the $l = 2$ states (i.e. from the so-called d -states). In section 3.3, we derived the TDDOS, and we have explicitly shown how a spin- and region-resolved TDDOS can be defined. In a similar way, also a l -resolved TDDOS can be defined. Such a l -resolved TDDOS was, in fact, used to

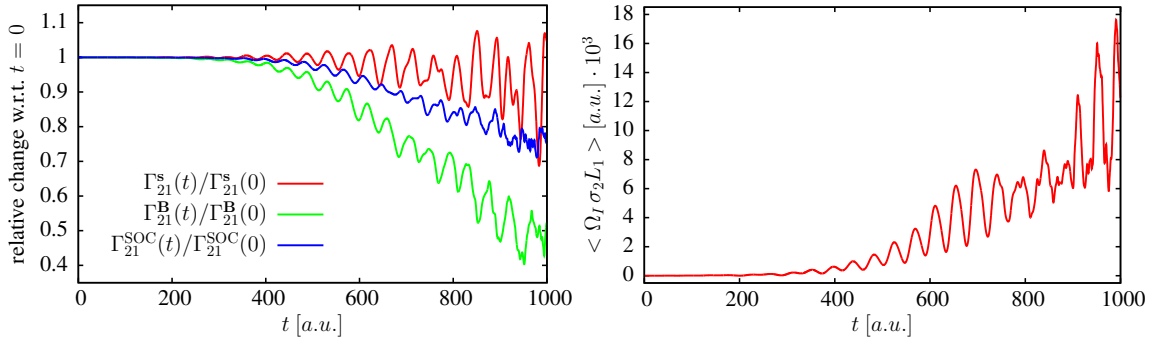


Fig. 4.20.: Left: Relative value of each torque contribution of Γ_{21} with respect to $t = 0$. Right: The corresponding $\sigma_2 L_1$ -spin-orbit angular momentum.

investigate the time-dependent behavior of the d -states (we refer in the following again to the run that has been referred to in the previous sections). It was found that the excitation leads to a strong initial decrease in the moment coming from the non-excited d -states (while the major part of the moment is transferred to the IR). Additionally, it was found that the subsequent loss in the total moment comes solely from the non-excited d -states, and the moment coming from the non-excited d -states is almost entirely lost during the demagnetization.

The previously mentioned result that only the non-excited d -states contribute to the the loss in the moment can be explained by the fact that only the residual moment, left in the d -states, is close enough to the nucleus such that SOC can effectively flip the spin. The moment coming from the excited states, on the other hand, is usually further away, meaning that a SOC mediated spin-flip does not occur. These points suggest that there should exist a certain peak intensity of the external field above which the loss in the moment should become less again. The reason being that the loss in the moment occurs only on the non-excited d -states, telling us that if the excitation of the system is strong enough, such that almost no electronic charge (and hence nearly no residual moment) is left in the non-excited d -states, no considerable spin-flip can occur. However, this statement holds only if the excitation and the spin-flip process is well separated, which is only true for very short pulses. For longer pulses, the spin-flip process and the interaction with the external field occur in parallel (as will be shown in the following). Hence, spin-dependent excitations and de-excitations (i.e. stimulated emission) take place simultaneously during the spin-flip, which can influence the behavior of the demagnetization. The aspects previously discussed have so far not been investigated in detail, hence, they will be the subject of future work.

Now we come back to the investigation of the demagnetization process from the previous sections. The run that was analyzed applied a quite short external pulse. In fact, the excitation process and the spin-flip process were, for this short pulse, more or less separated. In the same manner as presented before, the response of bulk Ni has been investigated for the longer pulse. It turned out that the demagnetization process works in a similar way as described for the short pulse, with the difference that the excitation and the spin-flip occur in parallel (we refer in the following to the run with $I_0 = 10^{14} \text{ W/cm}^2$ from figure 4.6). This can be seen in the left panel of figure 4.20, where the initial change of the relative value

of the torque contributions of Γ_{21} is shown (note that we refer again to the local quantities in region I). It is clear to see how each wave cycle of the increasing external field (see left panel of figure 4.6) excites the system and, in consequence, how each torque contribution changes. Moreover, we see that the loss in the relative value of the \mathbf{B}_{xc} -torque contribution is, like for the short pulse, stronger than the change of the other quantities. Hence, a positive valued $\sigma_2 L_1$ -spin-orbit angular momentum is necessarily induced (see right panel of figure 4.20), leading to a loss in the total moment (see right panel of figure 4.6). As the case for the short pulse, Γ_{12} , its torque contributions, and the corresponding spin-orbit angular momentum behaved similar to the Γ_{21} quantities.

We wish to mention that Fe shows a similar demagnetization behavior to that discussed before. In the following section, we will show some results obtained for bulk Fe. Next, we wish to say some words about the fact that M_1 and M_2 do not change significantly. The change of M_3 has been explained via the change of the spin-orbit angular momentum torque contributions. In a similar manner, the change of M_1 and M_2 could be explained. Following this procedure, one finds that all involved torque contributions are more or less zero, which results from the fact that the \mathbf{e}_1 - and \mathbf{e}_2 -components of the \mathbf{B}_{xc} and the local moment are nearly zero. Hence, a strong change of M_1 and M_2 can not occur. Finally, we point out that the spin-flip process depends crucially on the fast change of the \mathbf{B}_{xc} around the nucleus. Thus, the observed demagnetization depends strongly on the applied \mathbf{B}_{xc} -functional. In our calculations, the ALSDA-functional was used. At the moment, it is not clear if this functional is sufficient to describe all important effects that occur during the change of the moment in the true interacting system. Therefore, in future work the dependence of the demagnetization on the functional has to be carefully investigated. (Note that a change of the total moment in a true Coulomb interacting system is discussed in appendix A.7. It is shown that a change of the moment can be interpreted as the result of a change in the exchange interaction, while the whole spin-flip mechanism is similar to the one discussed previously.)

4.4. Response of the moment in bulk iron

In this section, the response of the moment in bulk Fe, subjected to an external pulse, will be investigated. The simulation discussed in the following used the lattice structure of Fe at room temperature, i.e. a bcc structure with a lattice constant of $a = 5.416 a.u.$ ($= 286.6 pm$) was applied. The system was represented by one primitive unit cell with the basis vectors $\mathbf{a}_1 = a/2(1, 1, -1)$, $\mathbf{a}_2 = a/2(1, -1, 1)$ and $\mathbf{a}_3 = a/2(-1, 1, 1)$. Furthermore, 8^3 \mathbf{k} -points have been used. The external pulse applied was identical to the pulse used in the investigation of bulk Ni from section 4.3, i.e. the pulse shown in figure 4.4 with the peak intensity $I_0 = 10^{15} W/cm^2$ and the polarization along \mathbf{e}_1 was used.

The left panel of figure 4.21 shows the response of M_3 . We see that the behavior of the moment is similar to that from Ni, i.e. the system starts to demagnetize at the peak of the pulse (at $\approx 150 a.u.$), while the major part of the loss in the moment occurs after the pulse. The demagnetization stops at around $900 a.u.$

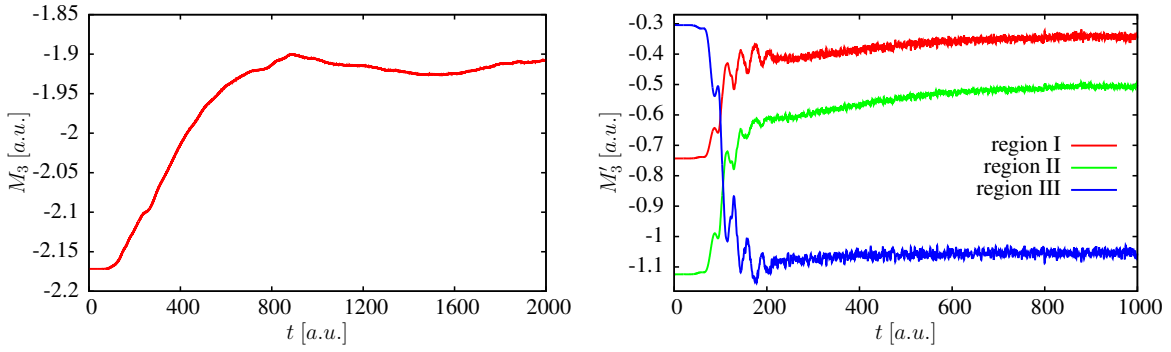


Fig. 4.21.: Left: e_3 -component of the moment in bulk Fe excited by the pulse from figure 4.4 with the peak intensity $I_0 = 10^{15} \text{W}/\text{cm}^2$, and with the polarization along e_1 . Right: Local moment in the three regions according to figure 4.14.

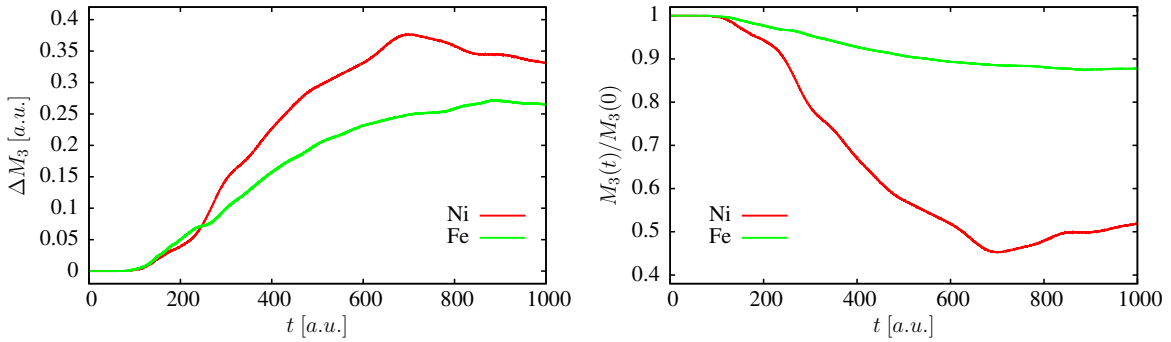


Fig. 4.22.: Absolute change (left) and relative change (right) of M_3 with respect to $t = 0$ in bulk Fe and Ni.

($\approx 21.8 \text{ fs}$), and from that point on, the moment merely oscillates around its new equilibrium position. Similarly to Ni, the change of M_1 and M_2 was very small compared to the change M_3 .

The demagnetization process in bulk Fe has been analyzed in the same manner as presented in section 4.3. It was found that the change of the moment in bulk Fe occurs in a similar way as in bulk Ni: First, the system is excited by the external pulse, resulting in a very quick change of the local moment and charge. The fast initial change of the local moment can be seen in the right panel of figure 4.21, where the evolution of the local moment in three regions is shown. Note that the three regions correspond to the same regions as defined before (i.e. different spheres around the nucleus; see left panel of figure 4.14). As for Ni, the initial excitation leads to an increase in the SOC energy. Additionally, the fast change of the local moment and charge leads to a fast loss in the \mathbf{B}_{xc} in region I, leading then, via the previously explained mechanism, to induced spin-orbit angular momenta and hence to a loss in the moment. Similarly to Ni, the spin-flip process takes place in region I, and, during this process, spin-currents flow from region I into region II, leading to a loss in the local moment of this region (see right panel of figure 4.21). The local moment in region III remains after the initial change nearly constant.

The left panel of figure 4.22 shows the absolute change of the moment with respect to $t = 0$ in bulk Fe (i.e. $\Delta M_3(t) = M_3(t) - M_3(0)$), and compares it to the corresponding value obtained in bulk Ni with an identical pulse. We see that

the initial change of the moment (up to $t \approx 250 a.u.$) is similar in both materials. This results from the fact that the SOC radial function $\xi(r)$ (which determines the strength of the SOC mediated spin-flip; see (4.9)), and also the initially induced spin-orbit angular momenta are similar in both materials. Furthermore, we see that ΔM_3 shows a kink at $t \approx 230 a.u.$ for bulk Ni, leading to a larger ΔM_3 in Ni than in Fe for all later times. In section 4.3.5, it has been explained that the increase in ΔM_3 in Ni at $t \approx 230 a.u.$ results from the change of the sign of the $\sigma_1 L_1$ - and $\sigma_2 L_2$ -spin-orbit angular momentum. This change, however, does not occur in Fe, explaining why ΔM_3 does not show any significant subsequent increase in Fe.

We have seen before that the change of the moment in Ni is stronger than in Fe, however, the difference is not significantly large (the change of the moment in Ni is $\approx 35\%$ larger as in Fe). On the other hand, this difference becomes more significant when we look at the relative change of the moment (i.e. $M_3(t)/M_3(0)$), shown in the right panel of figure 4.22. We see that approximately 50% of the moment is lost in Ni, while only 12% of the moment is lost in Fe. This much smaller loss in the relative moment of Fe can, to some extent, be explained by the fact that the moment in Fe is, in the ground state, much larger than in Ni. To be more precise: the initial excitation leads to a transfer of the local moment such that approximately 50% of the total moment are localized in region III after the excitation (see right panel of figure 4.21), which is more than in Ni. Hence, the relative change of the moment is smaller in Fe, because the moment in region III remains constant during the demagnetization. On the other hand, the absolute change of the moment in Fe is also less than in Ni, which contributes to the smaller change of the relative moment.

In conclusion, it was found that the excitation of bulk Fe leads also to a fast loss in the total moment. The mechanism leading to this demagnetization is very similar to the mechanism in bulk Ni that has been investigated and described in section 4.3. Moreover, it was found that the relative loss in the moment of bulk Fe is much smaller than in bulk Ni, which results to some extent from the large initial transfer of the moment from region I and II into region III, where the local moment remains nearly constant during the spin-flip process.

4.5. Response of the moment in a five-atom nickel slab

4.5.1. Simulation, results and discussion

In the previous sections, the behavior of the moment of excited bulk materials (i.e. materials that are periodic in three dimensions) has been investigated. In this section, we will investigate how the moment of a Ni slab, subjected to an external pulse, behaves. The slab was modeled by the unit cell that is shown in the left panel of figure 4.23. The unit cell corresponds to five primitive Ni unit cells stacked on top of each other, and to an empty space (i.e. vacuum) below and above the cells, while the empty space is as large as the stacked cells (the geometry

of the primitive cells corresponds to the bulk Ni structure at room temperature; see section 4.1). The corresponding slab has a periodic structure along the two

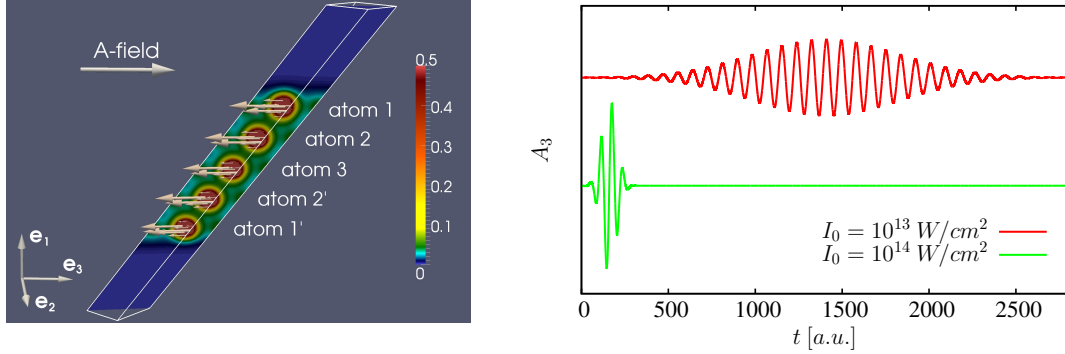


Fig. 4.23.: Left: Unit cell of the slab calculation, and a slice through the cell showing the density (the density color scale is in *a.u.*, and the slice is parallel to the \mathbf{e}_3 - \mathbf{e}_1 -plane). The arrows in the unit cell indicate the direction and the strength of the magnetization. Right: The applied \mathbf{A} -field pulses.

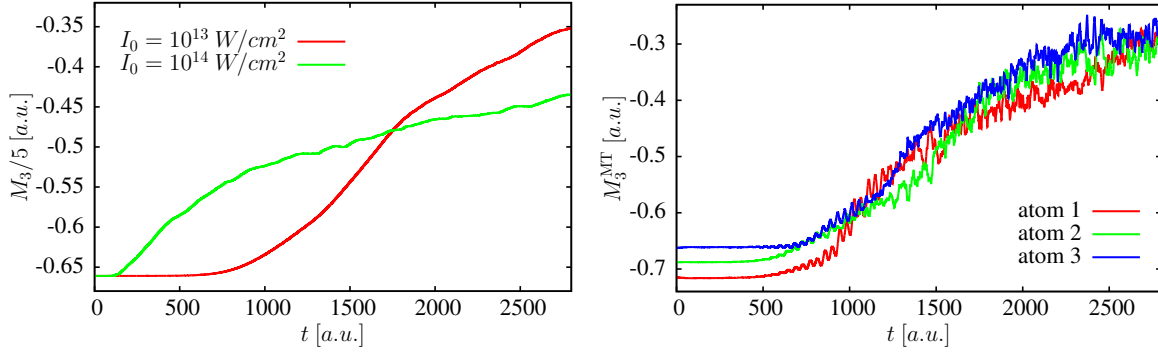


Fig. 4.24.: Left: \mathbf{e}_3 -component of the moment for the short and the long pulse. Right: Moment in the different MTs for the long pulse.

short unit cell vectors ($1 \times 8 \times 8$ \mathbf{k} -points have been applied). The surface of the slab corresponds to a $\{1, 1, 1\}$ -plane (by referring to the fcc-structure), and the coordinate system is chosen such that the surface of the slab is parallel to the \mathbf{e}_2 - \mathbf{e}_3 -plane (i.e. the surface is perpendicular to the \mathbf{e}_1 -vector).

The direction of the total moment in the ground state points along the $-\mathbf{e}_3$ -direction, meaning that the moment is in plane. The polarization of the external \mathbf{A} -field pulse is along the \mathbf{e}_3 -direction as well. Note that this setup corresponds to a clear physical situation: a free standing Ni slab that is magnetized in plane, and a pulse that travels perpendicular to the surface and that propagates through the slab. Similarly to bulk Ni, two different pulses have been applied: a short pulse with a peak intensity of $I_0 = 10^{14} \text{ W/cm}^2$, and a long pulse with $I_0 = 10^{13} \text{ W/cm}^2$. The pulses are shown in the right panel of figure 4.23 (the pulses are the same as in figure 4.3 (for $\omega = 0.1 \text{ a.u.}$) and figure 4.6).

The left panel of figure 4.24 shows M_3 per atom for the two pulses. First of all, we notice that magnitude of the moment is, for the ground state, in the slab slightly smaller than in the bulk system. This results from the fact that the slab has, compared to the bulk system, lost the translational symmetry for those lattice vectors that are not parallel to the \mathbf{e}_2 - \mathbf{e}_3 -plane. Hence, the moment of the unit

cells closer to the surface is different to the moment of the unit cells located in the center of the slab, resulting in a different moment per atom compared to the bulk system (note that this difference in the moment between the unit cells could also be interpreted as an effect of the surface; see also the right panel of figure 4.24 which shows the moment in the different MTs).

Next, we see from figure 4.24 that we have, at $t = 2800 a.u.$ ($\approx 68 fs$), a loss in the moment of about 35 % for the short pulse, and an even higher loss of about 47 % for the long pulse. Note that these losses in the moment are stronger than the losses obtained in the bulk system with identical pulses (we got a loss of 13 % for the short, and 19 % for the long pulse in bulk Ni). The stronger loss in the moment results most probably from the previously mentioned fewer symmetries of the slab. Furthermore, we point out that the demagnetization in the slab almost certainly continues for $t > 2800 a.u.$, which would lead to even higher losses in the moment (as can be seen in figure 4.24). Note that such a behavior was not observed in bulk Ni, where we saw that the moment reaches its new equilibrium position at earlier times (see figure 4.4 and 4.6). Similarly as observed in the bulk systems, the change of M_1 and M_2 was, compared to M_3 , very small.

The demagnetization mechanism in the slab has to be similar to the mechanism explained in section 4.3, with the difference that the contribution coming from each atom (or more precisely: from the region close to each nucleus) is most probably slightly different, as will be discussed in the following. The right panel of figure 4.24 shows the moment in the MT of atom 1, 2 and 3 for the long pulse (note that the moment of atom 1' and 2' behaves similar to the moment of atom 1 and 2, respectively, due to symmetry; the corresponding atoms are shown in figure 4.23). We see that the moment in the various MTs is different in the ground state. Additionally, we see that the change of the moment behaves differently as well. Hence, also the spin-orbit angular momenta and the corresponding torques must behave differently. This difference in the torques might lead to an exchange of spin-orbit angular momentum between the regions around each atom (where the spin-flip process occurs), which could be the reason for the stronger loss in the moment compared to the bulk system (note that such an exchange of spin-orbit angular momentum via the surface term Γ_{pq}^s has, to some extent, already been discussed in section 4.3.5).

In conclusion, we found that a short laser pulse, propagating through a five-atom slab of Ni that is magnetized in plane, leads to a demagnetization of the slab. Moreover, it was found that this demagnetization is stronger than the demagnetization obtained in bulk systems with identical pulses. The stronger loss in the moment observed for the slab results most probably from the fewer symmetries.

4.5.2. Relation to experiments

So far we have not referred to any experimental results, as emphasis was primarily put on the understanding of the SOC mediated demagnetization mechanism in extended periodic systems. Moreover, the comparison of the calculations from the previous sections with experiments is not straightforward (and one should be careful with any direct comparison), because the effective \mathbf{A} -field felt by the

electrons is, in a true system, generally different to the applied external laser pulse (since the field changes during the propagation through the material; see the discussion at the end of section 3.1.3). This situation is, however, different in the previously discussed study, since the change of a propagating \mathbf{A} -field pulse during the propagation through a very thin slab would most likely be small and hence probably negligible. Furthermore, the slab calculation considers, to a certain extent, surface effects (and the associated fewer symmetries, respectively), which are also present in true systems. These facts suggest that the comparison of the slab calculation with experiments is more reasonable.

Unfortunately, to the best of our knowledge there exists so far no experiment that investigated the behavior of an isolated ferromagnetic Ni slab subjected to an intense laser pulse, and that could directly test the predicted ultrafast SOC mediated loss in the moment. Most of the experiments that investigated the change of the moment in ferromagnetic materials, irradiated by intense laser pulses, used samples where a thin layer of the ferromagnetic material (usually a few nm thick) was on top of a larger carrier substrate (which was typically made from a metal, e.g. Al). If such a sample is irradiated by an intense pulse, spin-polarized currents occur leading, due to the difference in the scattering between the spin-up and spin-down electrons in the various materials, to a loss in the moment of the ferromagnetic layer. This process could, in a more general manner, also be described as follows: the excitation and subsequent time evolution of the whole system leads to spin-currents that transport parts of the moment from the ferromagnetic layer into the carrier substrate. This mechanism was first modeled by the so-called superdiffuse spin transport approach [8]. In fact, recent comparisons to experiments confirmed that the superdiffuse spin transport mechanism describes the observed change in the moment of the ferromagnetic layer quite well [58]. (Note that the total moment of the whole substrate is conserved within this mechanism, because the moment is transferred from one region to another.)

Most of the experiments that investigated the ultrafast laser induced demagnetization had one thing in common: laser pulses with an intensity FWHM of about $30 \dots 70 fs$, and with fluences up to $10 mJ/cm^2$ were typically used. The pulses used in our calculations, on the other hand, used shorter pulses with higher fluences (which result from the much higher intensities of the pulses, compared to experiment). The experiment described in [3], for example, applied laser pulses with a FWHM of $\approx 50 fs$ and a fluence of $8 mJ/cm^2$ on a $15 nm$ Ni layer deposited on a Al substrate. With this setup, a loss in the moment of the Ni layer of about 65% within $\approx 300 fs$ was measured. In the Ni slab calculation, on the other hand, the demagnetization is less (at least within the computed time range; loss in the moment: 35% for the short pulse, 47% for the long pulse), and the fluences are more than one order of magnitude larger ($93.5 mJ/cm^2$ for the short pulse, $91.3 mJ/cm^2$ for the long pulse). Even if longer pulses seem to lead to a stronger demagnetization for constant fluences, the demagnetization observed in experiments can certainly not be achieved by our calculations (the two pulses used in the slab calculation have approximately the same fluence, but the longer pulse, which has a FWHM of $\approx 17 fs$, leads to a stronger demagnetization). Additionally, we found in our calculations that the loss in the moment in bulk Ni,

which should, at least approximately, describe a major part of the Ni film from experiments, is even less. Hence, the SOC mediated spin-flip mechanism is almost certainly not the dominating process that leads to the loss in the moment observed in [3]. However, from our results it can also not be excluded that the SOC mediated spin-flip mechanism gives a certain contribution to the loss in the moment observed. Thus, in future experiments the response of the moment for higher pulse fluences, where the SOC mediated spin-flip mechanism might become more relevant, should be investigated.

In conclusion, at the moment it is difficult to say if the SOC mediated spin-flip mechanism described in this work gives any significant contributions to the loss in the moment observed in various experiments. This results from the fact that the substrates that have been used allowed a transport of the moment from the ferromagnetic layer into the carrier material. Hence, isolated ferromagnetic structures, which exclude the transport of moment into adjacent materials, should be investigated in future experiments in order to test the predicted SOC mediated loss in the moment. We point out that the SOC mediated demagnetization could be of particular interest for ultrafast spin-manipulation, because this process seems to be even faster than diffusive mechanisms.

5. Conclusions

In this work the spin-magnetic response properties of excited extended systems have been studied within the framework of TDDFT. For this purpose, a real-time propagation algorithm has been developed and implemented in the ELK code. The study was focused on the investigation of laser induced ultrafast demagnetization in nickel and iron, observed in various experiments.

Chapter 2 and 3 were devoted to theoretical aspects. After an introduction to TDDFT and a general discussion concerning the interaction with laser pulses in chapter 2, all possible mechanisms that could, in a periodic system, significantly change the moment have been discussed in chapter 3. It is clear that SOC and the **B**-field component of the external laser pulse are the only sources that directly lead to a change of the moment. Moreover, the SOC mediated change of the moment can be pictured as follows: induced spin-currents flow around the nuclear potential and feel an effective **B**-field, which leads to a torque on the moving spins, and hence to a change of the moment. The various approximations used in the calculations (e.g. the xc functionals), and some particularities that arise when calculating extended systems have been critically assessed.

Chapter 4 was devoted to the application of the TDDFT framework in order to investigate the spin-magnetic behavior of excited nickel and iron systems. First, the time evolution of bulk nickel subjected to a short intense pulse has been studied. Furthermore, the contribution to the change of the moment coming from the **B**-field component of the pulse and from SOC has been investigated. It was found that a fraction of the moment is lost within a few femtoseconds after the excitation, and that this loss is caused solely by SOC, i.e. the **B**-field component of the pulse is, even for very intense pulses, negligible. Next, different external pulses have been applied on bulk nickel and the corresponding response of the moment has been studied. It was found that a loss in the moment always occurs (within the range of the tested laser pulse parameters). Furthermore, it was found that the loss in the moment becomes stronger for higher pulse intensities and fluences, while the laser polarization has almost no relevance. It was also observed that the frequency of the applied pulse influences the behavior of the moment significantly.

The SOC mediated process leading to the loss in the moment has been studied in detail in section 4.3. It was found that the change of the moment is caused by what we call “spin-orbit angular momenta” (e.g. $\langle \hat{\sigma}_1 \hat{L}_2 \rangle$) that are induced in the region close to the screened nucleus during the excitation of the system. Moreover, it was found that the evolution of these spin-orbit angular momenta, and hence also the change of the moment, is significantly determined by the behavior of the xc **B**-field. It was shown that the moment has to be necessarily lost if the magnitude of the xc **B**-field decreases abruptly in the region close to the nucleus. This also explains why an increase in the moment was never observed in the calculations:

The excitation always led to a transfer of moment from the region close to the nucleus to the region further away, no matter what pulse parameters were used. Consequently, the xc \mathbf{B} -field always decreased in magnitude close to the nucleus. Additionally, it was shown that the initial excitation process, leading to the change of the xc \mathbf{B} -field, is described by the time-dependent occupation of the individual density of states. This explains the different demagnetization behavior observed for the different materials and also for the various pulse parameters, since the pulse determines how the time-dependent occupation changes. We point out that, due to the strong dependence on the xc \mathbf{B} -field functional, the demagnetization behavior has to be investigated for different functionals in future work (recall that the LSDA was applied in all calculations).

The spin-magnetic response of excited bulk iron has been investigated in section 4.4. It was found that the relative loss in the moment is much less than the loss in nickel. This smaller loss in iron results, to some extent, from the fact that a larger part of the moment is transferred away from the nucleus during the excitation, compared to nickel. Since only the moment left close to the nucleus takes part in the SOC mediated spin-flip process, a larger part of the moment is necessarily conserved in iron.

In section 4.5, the behavior of the moment in a five-atom nickel slab has been studied. It was found that the loss in the moment is stronger than in the bulk nickel system. Most likely this behavior results from the fewer symmetries of the slab. Moreover, it was found that longer pulses lead to a stronger loss in the moment if the pulse fluence is kept constant. Finally, the results from the calculations have been compared to the results obtained in experiments. It was concluded that the SOC mediated loss in the moment is most probably not the dominating process leading to the moment loss observed in various experiments. The reason being that the pulse fluences needed to achieve a certain loss in the moment are too high in our calculations, compared to the fluences used in the experiments. Hence, the dominating electronic process leading to the loss in the moment observed in experiments results most probably from a transfer of moment from the probed layer into the adjacent carrier material, as described within the superdiffuse spin transport mechanism.

We point out, however, that the SOC mediated spin-flip process described in this work should become more dominant when higher pulse intensities are used. In fact, this mechanism may be of particular interest when very fast spin manipulations are pursued, as the demagnetization observed in the calculations is even faster than what has been observed in experiments so far. Hence, the predicted SOC mediated ultrafast loss in the moment should be tested by specifically designed experiments, i.e. by experiments that allow shorter pulses with higher intensities, and that exclude a flow of the moment into adjacent materials.

A. Appendix

A.1. The general concept of densities and current densities

In the following we will show that each observable quantity can be described by its corresponding density. In time-dependent phenomena, these densities usually change. This change is typically accompanied by associated current densities. The current densities, their operator representation and the coupling to fields will be discussed in this section as well.

The following derivations will, for simplicity, assume single-particle systems. The generalization to many-particle systems is straightforward. Note that the states are in general time-dependent. For a clear view the t -variable will be omitted.

A.1.1. Observable densities

We assume to have an arbitrary hermitian operator \hat{O} . Its expectation value can be calculated by using the density operator $\hat{n}(\mathbf{r})$:

$$\begin{aligned}\langle \hat{O} \rangle &= \sum_{\alpha=\uparrow,\downarrow} \int d\mathbf{r} \langle \Psi | \alpha, \mathbf{r} \rangle \langle \alpha, \mathbf{r} | \hat{O} | \Psi \rangle \\ &= \sum_{\alpha=\uparrow,\downarrow} \int d\mathbf{r} \int d\mathbf{r}' \delta(\mathbf{r} - \mathbf{r}') \langle \Psi | \alpha, \mathbf{r}' \rangle \langle \alpha, \mathbf{r}' | \hat{O} | \Psi \rangle \\ &= \int d\mathbf{r} \langle \Psi | \delta(\mathbf{r} - \hat{\mathbf{r}}) \hat{O} | \Psi \rangle = \int d\mathbf{r} \langle \Psi | \hat{n}(\mathbf{r}) \hat{O} | \Psi \rangle \\ &= \int d\mathbf{r} \operatorname{Re} \left[\langle \hat{n}(\mathbf{r}) \hat{O} \rangle \right] = \int d\mathbf{r} \frac{1}{2} \left[\langle \hat{n}(\mathbf{r}) \hat{O} \rangle + \langle \hat{n}(\mathbf{r}) \hat{O} \rangle^* \right] \\ &= \int d\mathbf{r} \left\langle \frac{1}{2} \{ \hat{n}(\mathbf{r}), \hat{O} \} \right\rangle.\end{aligned}\tag{A.1}$$

We used that the expectation value has to be real, and we used the δ -representation of the density operator:

$$\hat{n}(\mathbf{r}) = \delta(\mathbf{r} - \hat{\mathbf{r}}) = \sum_{\alpha=\uparrow,\downarrow} \int d\mathbf{r}' \delta(\mathbf{r} - \mathbf{r}') |\alpha, \mathbf{r}' \rangle \langle \alpha, \mathbf{r}'|.\tag{A.2}$$

From (A.1) we see that the expectation value can be expressed over the integral of a local expectation value, which will be defined as the observable density:

$$n_{\hat{O}}(\mathbf{r}) = \left\langle \frac{1}{2} \{ \hat{n}(\mathbf{r}), \hat{O} \} \right\rangle.\tag{A.3}$$

From (A.3) it follows immediately two well known densities, the probability (or charge) density ($\hat{O} = \mathbf{1}$), to which we will refer simply as the density, and the spin-density ($\hat{O} = \hat{\sigma}_i$), to which we will refer as the magnetization:

$$n_1(\mathbf{r}) = \langle \hat{n}(\mathbf{r}) \rangle = n(\mathbf{r}), \quad n_{\hat{\sigma}_i}(\mathbf{r}) = \langle \hat{n}(\mathbf{r}) \hat{\sigma}_i \rangle = m_i(\mathbf{r}). \quad (\text{A.4})$$

$\hat{\sigma}_i$ is the Pauli operator of spin-component $i = \{1, 2, 3\}$.

A.1.2. Observable current densities

As previously stated, in time-dependent situations, the densities usually change. These changes can be calculated by making use of Ehrenfest's theorem:

$$\partial_t \langle \frac{1}{2} \{ \hat{n}(\mathbf{r}), \hat{O} \} \rangle = \langle \frac{1}{2i} [\{ \hat{n}(\mathbf{r}), \hat{O} \}, \hat{H}] \rangle = \frac{1}{2i} \langle [\{ \hat{n}(\mathbf{r}), \hat{O} \}, (\hat{T} + \hat{V} + \dots)] \rangle. \quad (\text{A.5})$$

In the following we will see that the current densities arise naturally from the dynamical equation of the corresponding densities, that is, they emerge from the kinetic part of (A.5) (i.e. the commutator with \hat{T}):

$$\begin{aligned} \partial_t \langle \frac{1}{2} \{ \hat{n}(\mathbf{r}), \hat{O} \} \rangle_{\hat{T}} &= \langle \frac{1}{2i} [\{ \hat{n}(\mathbf{r}), \hat{O} \}, \frac{\hat{p}^2}{2}] \rangle \\ &= \underbrace{\text{Re} \left[\langle \frac{1}{2i} [\hat{n}(\mathbf{r}), \hat{p}^2] \hat{O} \rangle \right]}_{\text{current density term}} + \underbrace{\text{Re} \left[\langle \frac{1}{2i} \hat{n}(\mathbf{r}) [\hat{O}, \hat{p}^2] \rangle \right]}_{\text{local source term}}, \end{aligned} \quad (\text{A.6})$$

where we used the relation $\{ \hat{A}, \hat{B} \}, \hat{C} \} = \{ \hat{A}, \hat{C} \}, \hat{B} \} + \{ \hat{A}, [\hat{B}, \hat{C}] \}$ together with (A.64) and (A.67). We see that calculating the commutator with \hat{T} gives two contributions: a current term and a source term. Note that the source term is zero if $[\hat{O}, \hat{p}^2] = 0$. Next, we will show that the left term can be written as the divergence of a vector field, meaning that this term, in fact, corresponds to a current density term for which the integral always vanishes (assuming finite or periodic systems).

The following relation holds for any differentiable function $g(\mathbf{r})$ [57]:

$$[g(\hat{\mathbf{r}}), \hat{p}_i] = i \partial_{\hat{r}_i} g(\hat{\mathbf{r}}). \quad (\text{A.7})$$

Together with (A.2) (and with the assumption that the δ -distribution is described by a differentiable trial function which gives in some limit the δ -distribution) we get for the current density term from (A.6):

$$\text{Re} \left[\langle \frac{1}{2i} [\hat{n}(\mathbf{r}), \hat{p}^2] \hat{O} \rangle \right] = \sum_{i=1}^3 \frac{1}{2} \text{Re} \left[\underbrace{\langle (\partial_{\hat{r}_i} \delta(\mathbf{r} - \hat{\mathbf{r}})) \hat{p}_i \hat{O} \rangle}_{=: (a)} + \underbrace{\langle \hat{p}_i (\partial_{\hat{r}_i} \delta(\mathbf{r} - \hat{\mathbf{r}})) \hat{O} \rangle}_{=: (b)} \right]. \quad (\text{A.8})$$

Using the completeness relation gives for (a):

$$\begin{aligned}
(a) &= \sum_{\alpha=\uparrow,\downarrow} \int d\mathbf{r}' \langle \Psi | (\partial_{\hat{r}_i} \delta(\mathbf{r} - \hat{\mathbf{r}})) | \alpha \mathbf{r}' \rangle \langle \alpha \mathbf{r}' | \hat{p}_i \hat{O} | \Psi \rangle \\
&= \sum_{\alpha=\uparrow,\downarrow} \int d\mathbf{r}' (\partial_{r'_i} \delta(\mathbf{r} - \mathbf{r}')) \langle \Psi | \alpha \mathbf{r}' \rangle \langle \alpha \mathbf{r}' | \hat{p}_i \hat{O} | \Psi \rangle \\
&= - \sum_{\alpha=\uparrow,\downarrow} \int d\mathbf{r}' \delta(\mathbf{r} - \mathbf{r}') \partial_{r'_i} \langle \Psi | \alpha \mathbf{r}' \rangle \langle \alpha \mathbf{r}' | \hat{p}_i \hat{O} | \Psi \rangle \\
&= -\partial_{r_i} \left[\underline{\Psi}^\dagger(\mathbf{r}) \hat{p}_i \underline{\hat{O}} \underline{\Psi}(\mathbf{r}) \right]. \tag{A.9}
\end{aligned}$$

We used integration by parts and we assumed that the system is either finite or periodic. In the last step we switched to the spinor representation. In an analogous manner we get for term (b):

$$(b) = -\partial_{r_i} \left[(\hat{p}_i \underline{\Psi})^\dagger(\mathbf{r}) \underline{\hat{O}} \underline{\Psi}(\mathbf{r}) \right]. \tag{A.10}$$

With the help of the completeness relation, the local source term from (A.6) can be transformed to a spinor representation as well, leading, together with (A.8), (A.9) and (A.10), to the following expression for the kinetic part of the dynamical density equation:

$$\partial_t \left\langle \frac{1}{2} \{ \hat{n}(\mathbf{r}), \hat{O} \} \right\rangle_{\hat{T}} = -\nabla \cdot \mathbf{j}_{\hat{O}}(\mathbf{r}) + \frac{1}{2} \text{Im} \left[\underline{\Psi}^\dagger(\mathbf{r}) [\underline{\hat{O}}, \hat{p}^2] \underline{\Psi}(\mathbf{r}) \right], \tag{A.11}$$

where we have defined the general observable current density:

$$\mathbf{j}_{\hat{O}}(\mathbf{r}) = \frac{1}{2} \text{Re} \left[\underline{\Psi}^\dagger(\mathbf{r}) \hat{\mathbf{p}} \underline{\hat{O}} \underline{\Psi}(\mathbf{r}) + (\hat{\mathbf{p}} \underline{\Psi})^\dagger(\mathbf{r}) \underline{\hat{O}} \underline{\Psi}(\mathbf{r}) \right]. \tag{A.12}$$

In conclusion, we have shown that the observable current densities arise naturally when calculating the local change of observables. In time-dependent situations, these currents will flow into or out of a region, and increase or decrease the corresponding local expectation value.

Similarly to the previous section, from (A.12) follow two well known current densities, the probability (or charge) current density ($\underline{\hat{O}} = \mathbf{1}$):

$$\mathbf{j}_{\mathbf{1}}(\mathbf{r}) = \mathbf{j}(\mathbf{r}) = \text{Re} \left[\underline{\Psi}^\dagger(\mathbf{r}) \hat{\mathbf{p}} \underline{\Psi}(\mathbf{r}) \right] = \text{Im} \left[\underline{\Psi}^\dagger(\mathbf{r}) \nabla \underline{\Psi}(\mathbf{r}) \right], \tag{A.13}$$

to which we will refer simply as the current density, and the spin-current density ($\underline{\hat{O}} = \underline{\sigma}_i$):

$$\mathbf{j}_{\hat{\sigma}_i}(\mathbf{r}) \Big|_j = \overset{\leftrightarrow}{J}_{ij}(\mathbf{r}) = \text{Re} \left[\underline{\Psi}^\dagger(\mathbf{r}) \underline{\sigma}_i \hat{p}_j \underline{\Psi}(\mathbf{r}) \right] = \text{Im} \left[\underline{\Psi}^\dagger(\mathbf{r}) \underline{\sigma}_i \nabla_j \underline{\Psi}(\mathbf{r}) \right], \tag{A.14}$$

with $i, j = \{1, 2, 3\}$. $\overset{\leftrightarrow}{J}_{ij}(\mathbf{r})$ is the spin-current tensor. This object, which is a 3×3 matrix, is often used in literature when spin-dynamics is discussed. Note that the spin-current tensor can also be represented via the outer product:

$$\overset{\leftrightarrow}{J}(\mathbf{r}) = \text{Re} \left[\underline{\Psi}^\dagger(\mathbf{r}) \underline{\sigma} \otimes \hat{\mathbf{p}} \underline{\Psi}(\mathbf{r}) \right] = \text{Re} \left[\underline{\Psi}^\dagger(\mathbf{r}) \underline{\sigma} \cdot \hat{\mathbf{p}}^T \underline{\Psi}(\mathbf{r}) \right]. \tag{A.15}$$

In some situations, however, it is important to look at the current vector of each spin-component individually. Therefore it is convenient to define the spin-current density of spin-component i by the i th row of \vec{J} :

$$\mathbf{j}^i(\mathbf{r}) \Big|_j = \vec{J}_{ij}(\mathbf{r}). \quad (\text{A.16})$$

A.1.3. Gauge invariance - paramagnetic and diamagnetic current densities

In the previous derivation we assumed that the kinetic term has the form $\hat{T} = \frac{\hat{p}^2}{2}$. When an external vector potential, $\mathbf{A}(\mathbf{r})$, is present, the momentum operator in the kinetic term has to be replaced by

$$\hat{\mathbf{p}} \longrightarrow \hat{\mathbf{p}} + \frac{1}{c}\mathbf{A}(\hat{\mathbf{r}}), \quad (\text{A.17})$$

which is called minimal coupling. As a result, the contribution in the dynamics coming from the kinetic term (see (A.6)) changes to

$$\begin{aligned} \partial_t \langle \frac{1}{2} \{ \hat{n}(\mathbf{r}), \hat{O} \} \rangle_{\hat{T}} &= \underbrace{\text{Re} \left[\langle \frac{1}{2i} [\hat{n}(\mathbf{r}), (\hat{\mathbf{p}} + \frac{1}{c}\mathbf{A}(\hat{\mathbf{r}}))^2] \hat{O} \rangle \right]}_{\text{current density term}} \\ &+ \underbrace{\text{Re} \left[\langle \frac{1}{2i} \hat{n}(\mathbf{r}) [\hat{O}, (\hat{\mathbf{p}} + \frac{1}{c}\mathbf{A}(\hat{\mathbf{r}}))^2] \rangle \right]}_{\text{local source term}}. \end{aligned} \quad (\text{A.18})$$

Following the same derivations as before leads, in the spinor representation, to

$$\partial_t \langle \frac{1}{2} \{ \hat{n}(\mathbf{r}), \hat{O} \} \rangle_{\hat{T}} = -\nabla \cdot \mathbf{j}_{\hat{O}}(\mathbf{r}) + \frac{1}{2} \text{Im} \left[\underline{\Psi}^\dagger(\mathbf{r}) [\underline{\hat{O}}, (\hat{\mathbf{p}} + \frac{1}{c}\mathbf{A}(\mathbf{r}))^2] \underline{\Psi}(\mathbf{r}) \right], \quad (\text{A.19})$$

where we have defined the general gauge invariant observable current density:

$$\mathbf{j}_{\hat{O}}(\mathbf{r}) = \frac{1}{2} \text{Re} \left[\underline{\Psi}^\dagger(\mathbf{r}) (\hat{\mathbf{p}} + \frac{1}{c}\mathbf{A}(\mathbf{r})) \underline{\hat{O}} \underline{\Psi}(\mathbf{r}) + \left((\hat{\mathbf{p}} + \frac{1}{c}\mathbf{A}(\mathbf{r})) \underline{\Psi} \right)^\dagger(\mathbf{r}) \underline{\hat{O}} \underline{\Psi}(\mathbf{r}) \right]. \quad (\text{A.20})$$

This current density can be separated into two parts: into the so-called paramagnetic (subscript ‘‘p’’), and into the diamagnetic (subscript ‘‘d’’) current density. The sum of these two current densities gives the gauge invariant, i.e. the physical current density (which is invariant under a gauge transformation; see section A.3), leading for the (probability) current density to

$$\mathbf{j}(\mathbf{r}) = \underbrace{\text{Re} \left[\underline{\Psi}^\dagger(\mathbf{r}) \hat{\mathbf{p}} \underline{\Psi}(\mathbf{r}) \right]}_{=\mathbf{j}_p(\mathbf{r})} + \underbrace{\frac{1}{c}\mathbf{A}(\mathbf{r})n(\mathbf{r})}_{=\mathbf{j}_d(\mathbf{r})}. \quad (\text{A.21})$$

In a similar way we get for the spin-current density

$$\mathbf{j}^i(\mathbf{r}) = \underbrace{\text{Re} \left[\underline{\Psi}^\dagger(\mathbf{r}) \underline{\sigma}_i \hat{\mathbf{p}} \underline{\Psi}(\mathbf{r}) \right]}_{=\mathbf{j}_p^i(\mathbf{r})} + \underbrace{\frac{1}{c}\mathbf{A}(\mathbf{r})m_i(\mathbf{r})}_{=\mathbf{j}_d^i(\mathbf{r})}, \quad (\text{A.22})$$

or alternatively for the spin-current tensor

$$\mathbf{j}_p^i(\mathbf{r}) \Big|_j = \overleftrightarrow{J}_{p,ij}(\mathbf{r}), \quad \mathbf{j}_d^i(\mathbf{r}) \Big|_j = \overleftrightarrow{J}_{d,ij}(\mathbf{r}). \quad (\text{A.23})$$

Note that the vector potential couples directly to the densities in order to obtain the corresponding gauge invariant current densities.

A.1.4. Operator representation of the current densities

Previously, we have shown that the current densities arise when calculating the dynamics of local quantities. Hence, the current densities can be imagined as some kind of local momentum densities of observables. In the following we will show that this picture in fact leads to an operator representation of the current densities. First, we define the local momentum density operator by combining the local density operator and the momentum operator:

$$\frac{1}{2}\{n(\hat{r}), \hat{\mathbf{p}}\}. \quad (\text{A.24})$$

We applied the anti-commutator in order to “hermitianize” the operator (i.e. to get an operator that represents an observable). Next, we define the general current density operator by combining the observable \hat{O} with (A.24):

$$\hat{\mathbf{j}}_O(\mathbf{r}) = \frac{1}{4}\{\{\hat{n}(\mathbf{r}), \hat{\mathbf{p}}\}, \hat{O}\}. \quad (\text{A.25})$$

Again, we applied the anti-commutator in order to obtain a hermitian operator. It is now straightforward to show that the expectation value of (A.25) gives the current density as defined in (A.12):

$$\begin{aligned} \langle \hat{\mathbf{j}}_O(\mathbf{r}) \rangle &\stackrel{(\text{A.67})}{=} \frac{1}{2}\text{Re}(\langle \{\hat{n}(\mathbf{r}), \hat{\mathbf{p}}\} \hat{O} \rangle) \\ &= \frac{1}{2}\text{Re}(\langle \Psi | \hat{n}(\mathbf{r}) | \hat{\mathbf{p}} \hat{O} \Psi \rangle + \langle \hat{\mathbf{p}} \Psi | \hat{n}(\mathbf{r}) | \hat{O} \Psi \rangle) \stackrel{(\text{A.12})}{=} \mathbf{j}_O(\mathbf{r}). \end{aligned} \quad (\text{A.26})$$

The gauge invariant current density operators can be obtained in the same way as discussed before, i.e. simply by replacing the momentum operator according to (A.17).

From (A.25) it follows the gauge invariant current density operator

$$\hat{\mathbf{j}}(\mathbf{r}) = \underbrace{\frac{1}{2}\{\hat{n}(\mathbf{r}), \hat{\mathbf{p}}\}}_{=\hat{\mathbf{j}}_p(\mathbf{r})} + \underbrace{\frac{1}{c}\mathbf{A}(\mathbf{r})\hat{n}(\mathbf{r})}_{=\hat{\mathbf{j}}_d(\mathbf{r})}, \quad (\text{A.27})$$

and the gauge invariant spin-current density operator of spin-component i

$$\hat{\mathbf{j}}^i(\mathbf{r}) = \underbrace{\frac{1}{2}\hat{\sigma}_i\{\hat{n}(\mathbf{r}), \hat{\mathbf{p}}\}}_{=\hat{\mathbf{j}}_p^i(\mathbf{r})} + \underbrace{\frac{1}{c}\mathbf{A}(\mathbf{r})\hat{n}_i(\mathbf{r})}_{=\hat{\mathbf{j}}_d^i(\mathbf{r})}. \quad (\text{A.28})$$

As before, each of these operators is given as the sum of a paramagnetic and diamagnetic term. The definition of the spin-current tensor operator $\overleftrightarrow{J}(\mathbf{r})$ is straightforward (see (A.23)).

A.1.5. Coupling to local fields

Hamiltonian elements containing local fields that couple to the momentum operator can be seen as elements containing a coupling to a current density. To illustrate this concept, we will look at the kinetic operator with minimal coupling (A.17):

$$\frac{1}{2} \left[\hat{\mathbf{p}} + \frac{1}{c} \mathbf{A}(\hat{\mathbf{r}}) \right]^2 = \frac{\hat{p}^2}{2} + \underbrace{\frac{1}{2c} \hat{\mathbf{p}} \cdot \mathbf{A}(\hat{\mathbf{r}}) + \frac{1}{2c} \mathbf{A}(\hat{\mathbf{r}}) \cdot \hat{\mathbf{p}}}_{=: (a)} + \frac{1}{2c^2} A^2(\hat{\mathbf{r}}). \quad (\text{A.29})$$

With the density operator representation of the local field (see e.g. (A.1))

$$\mathbf{A}(\hat{\mathbf{r}}) = \int d\mathbf{r} \mathbf{A}(\mathbf{r}) \hat{n}(\mathbf{r}) \quad (\text{A.30})$$

follows for term (a):

$$(a) = \sum_{i=1}^3 \frac{1}{2c} \{A_i(\hat{\mathbf{r}}), \hat{p}_i\} = \int d\mathbf{r} \sum_{i=1}^3 \frac{1}{c} A_i(\mathbf{r}) \frac{1}{2} \{ \hat{n}(\mathbf{r}), \hat{p}_i \} = \int d\mathbf{r} \frac{1}{c} \mathbf{A}(\mathbf{r}) \cdot \hat{\mathbf{j}}_p(\mathbf{r}). \quad (\text{A.31})$$

We see that the term (a) from (A.29) can be represented as a local field that couples to the paramagnetic spin-current density operator. In the same way you can show that elements having the form $(f(\hat{\mathbf{r}}) \hat{\sigma}_i \hat{\mathbf{p}})$, with arbitrary local fields $f(\mathbf{r})$, can be represented as local fields that couple to the paramagnetic spin-current density operator $\hat{\mathbf{j}}_p^i(\mathbf{r})$. This is, for example, the case for the spin-orbit coupling term.

A.2. Magnetization, current and spin-currents for many-electron systems

In this section we will briefly discuss how the magnetization, the current density, and the spin-current densities might behave when many electrons are considered. As a simple example, we will assume a collinear (non-interacting) two electron system, described, in a certain region, by the following two spinors:

$$\underline{\varphi}_1(\mathbf{r}) = \begin{pmatrix} A e^{i\alpha(\mathbf{r})} \\ 0 \end{pmatrix}, \quad \underline{\varphi}_2(\mathbf{r}) = \begin{pmatrix} 0 \\ B e^{-i\alpha(\mathbf{r})} \end{pmatrix}, \quad (\text{A.32})$$

where A and B are real numbers, and where $\alpha(\mathbf{r})$ is a real function. (In a more general case, A and B should be functions of \mathbf{r} as well. However, we assume only a small region, and we assume that the \mathbf{r} -dependence of A and B is negligible). Note that the following conclusions also carry over to the general (non-collinear) two-component spinor case (which follows e.g. from a spin-rotation of (A.32)).

First, we consider only one electron, $\underline{\varphi}_1$, and we calculate the magnetization m_3 , the corresponding spin-current density, and the current density (see (A.13) and (A.16)):

$$m_3(\mathbf{r}) = A^2, \quad \mathbf{j}(\mathbf{r}) = \mathbf{j}^3(\mathbf{r}) = A^2 \nabla \alpha(\mathbf{r}). \quad (\text{A.33})$$

This simple calculation demonstrates that φ_1 can be interpreted as a part of the electronic density that has a spin-up polarization, and that moves with the velocity $\nabla\alpha(\mathbf{r})$. The previous picture is very intuitive, and it also agrees with the fact that the current density is equal to the spin-current density. When we, however, consider more than one electron, the picture changes.

As before, we will calculate the magnetization, the current density, and the spin-current density, but now for the two electron system (A.32) (we assume non-interacting electrons, i.e. each total expectation values follow from the sum of the individual expectation values):

$$m_3(\mathbf{r}) = A^2 - B^2, \quad \mathbf{j}(\mathbf{r}) = (A^2 - B^2)\nabla\alpha(\mathbf{r}), \quad \mathbf{j}^3(\mathbf{r}) = (A^2 + B^2)\nabla\alpha(\mathbf{r}). \quad (\text{A.34})$$

When $A^2 \neq B^2$, we have a non-zero magnetization, and a non-zero current and spin-current density, which are, however, different. Such a situation is found for the ground state of Ni and Fe if SOC is present (i.e. when we have a spin-polarization along \mathbf{e}_3 , we have, around the nucleus, a $\mathbf{j}(\mathbf{r})$ and a $\mathbf{j}^3(\mathbf{r})$ that behave very similar; see also section 4.3.4).

If $A^2 = B^2$, then the magnetization and the current density are zero. The spin-current density, however, is not zero which seems, at first sight, to be a very counterintuitive result (when thinking of the electron density as a whole). To overcome this apparent issue, we can imagine the following picture: We have two parts of the electronic density. The first part has a spin-up polarization and it moves with the velocity $\nabla\alpha(\mathbf{r})$. The second part has a spin-down polarization and it also moves with the velocity $\nabla\alpha(\mathbf{r})$, but in the opposite direction, meaning that the two current densities cancel. Next, we realize that (when in motion) a spin-down polarization acts like a negative spin-up polarization, leading to the fact that the two spin-current densities add together.

The previous situation (i.e. zero magnetization component and current density, but a non-zero corresponding spin-current density) is found for $\mathbf{j}^1(\mathbf{r})$ and $\mathbf{j}^2(\mathbf{r})$ for the ground state of Ni and Fe if SOC is present and if the spin-polarization is along \mathbf{e}_3 . Furthermore, the previous situation holds for all three spin-current densities (which behave identical) if the material is non-ferromagnetic and if SOC is present, as found for Al. Note that the spin-currents are non-zero in order to minimize the SOC energy, as discussed in section 4.3.4.

A.3. The gauge transformation

The concept of the gauge transformation appeared first in classical electrodynamics, where the physical fields, i.e. the \mathbf{E} -field and the \mathbf{B} -field, are described by two auxiliary fields, namely by the scalar potential $\phi(\mathbf{r}, t)$ and by the vector potential $\mathbf{A}(\mathbf{r}, t)$ [47]:

$$\mathbf{E}(\mathbf{r}, t) = -\nabla\phi(\mathbf{r}, t) - \frac{1}{c}\partial_t\mathbf{A}(\mathbf{r}, t), \quad \mathbf{B}(\mathbf{r}, t) = \nabla \times \mathbf{A}(\mathbf{r}, t). \quad (\text{A.35})$$

With these relations it is straightforward to show that a transformation of the kind

$$\phi(\mathbf{r}, t) \longrightarrow \phi(\mathbf{r}, t) - \partial_t\Lambda(\mathbf{r}, t), \quad \frac{1}{c}\mathbf{A}(\mathbf{r}, t) \longrightarrow \frac{1}{c}\mathbf{A}(\mathbf{r}, t) + \nabla\Lambda(\mathbf{r}, t), \quad (\text{A.36})$$

leaves the physical \mathbf{E} - and \mathbf{B} -field, for arbitrary $\Lambda(\mathbf{r}, t)$, unchanged. The transformation (A.36) is called gauge transformation, and $\Lambda(\mathbf{r}, t)$ is called gauge field. The gauge transformation does not change the \mathbf{E} - and \mathbf{B} field, i.e. it does not change the physics, but at the same time it changes the actual numerical values of the scalar and vector potential. This freedom allows one to choose certain properties for the potentials, to which is referred as “choose a gauge”. A specific gauge is usually formulated via an additional constraint on the potentials, e.g. the Coulomb gauge: $\nabla \cdot \mathbf{A} = 0$, or the Weyl gauge: $\phi = 0$.

In quantum mechanics, a gauge transformation (or more specific: an U(1) local gauge transformation) is formulated by the following 3 transformations:

$$v(\mathbf{r}, t) \longrightarrow v'(\mathbf{r}, t) = v(\mathbf{r}, t) + \partial_t \Lambda(\mathbf{r}, t), \quad (\text{A.37})$$

$$\frac{1}{c} \mathbf{A}(\mathbf{r}, t) \longrightarrow \frac{1}{c} \mathbf{A}'(\mathbf{r}, t) = \frac{1}{c} \mathbf{A}(\mathbf{r}, t) + \nabla \Lambda(\mathbf{r}, t), \quad (\text{A.38})$$

$$\varphi(\mathbf{r}, t) \longrightarrow \varphi'(\mathbf{r}, t) = e^{-i\Lambda(\mathbf{r}, t)} \varphi(\mathbf{r}, t), \quad (\text{A.39})$$

where we have used that the local potential is related to the scalar potential by $v = -\phi$ (in atomic units). The meaning of this transformations is the following: If φ solves the Schrödinger equation

$$\partial_t \varphi(\mathbf{r}, t) = \hat{h}(t) \varphi(\mathbf{r}, t), \quad (\text{A.40})$$

then φ' , defined via (A.39), solves the Schrödinger equation

$$\partial_t \varphi'(\mathbf{r}, t) = \hat{h}'(t) \varphi'(\mathbf{r}, t), \quad (\text{A.41})$$

where \mathbf{A} and v in \hat{h} have been transformed via (A.37) and (A.38). This property is called gauge invariance. If this relation is not fulfilled, the Hamiltonian is not constructed in a gauge invariant way, meaning that an unphysical situation is described. With

$$\left[\hat{p}_l + \frac{1}{c} A_l(\mathbf{r}, t) \right] e^{i\Lambda(\mathbf{r}, t)} \varphi(\mathbf{r}, t) = e^{i\Lambda(\mathbf{r}, t)} \left[\hat{p}_l + \frac{1}{c} A_l(\mathbf{r}, t) + \partial_{\mathbf{r}_l} \Lambda(\mathbf{r}, t) \right] \varphi(\mathbf{r}, t) \quad (\text{A.42})$$

and

$$i \partial_t e^{i\Lambda(\mathbf{r}, t)} \varphi(\mathbf{r}, t) = e^{i\Lambda(\mathbf{r}, t)} [i \partial_t - (\partial_t \Lambda(\mathbf{r}, t))] \varphi(\mathbf{r}, t) \quad (\text{A.43})$$

it follows immediately that the coupling to an electromagnetic field via minimal coupling:

$$\hat{\mathbf{p}} \longrightarrow \hat{\mathbf{p}} + \frac{1}{c} \mathbf{A}(\mathbf{r}, t), \quad (\text{A.44})$$

leads, for example for free particles, to gauge invariance. To test if an arbitrary time-dependent Hamiltonian leads to gauge invariance, the following property can be checked:

$$\left[\hat{h}(t) - v(\mathbf{r}, t) \right]' e^{-i\Lambda(\mathbf{r}, t)} \psi(\mathbf{r}) \longrightarrow e^{-i\Lambda(\mathbf{r}, t)} \left[\hat{h}(t) - v(\mathbf{r}, t) \right] \psi(\mathbf{r}), \quad (\text{A.45})$$

where $\psi(\mathbf{r})$ is some arbitrary trial wave function, and $v(\mathbf{r}, t)$ is the local potential present in $\hat{h}(t)$. The meaning of (A.45) is the following: the expression on the left hand side, which is primed (i.e. all transformations according to (A.37) and

(A.38) have to be performed), should reduce to the expression on the right hand side in order to show gauge invariance for the time-dependent system. Note that gauge invariance can immediately be seen if $[\hat{h}(t) - v(\mathbf{r}, t)]$ is represented in terms of $\mathbf{E} = (\nabla v - \partial_t \mathbf{A}/c)$, $\mathbf{B} = (\nabla \times \mathbf{A})$ and $(\hat{\mathbf{p}} + \mathbf{A}/c)$, i.e. only constructed from gauge invariant terms.

We point out that the general concept behind the gauge invariance is the same as discussed for classical electrodynamics: the change of the potentials by a gauge field $\Lambda(\mathbf{r}, t)$ should not change the physics. Since the physical framework in quantum mechanics is described by the dynamical equation and the observables, also the observables have to be formulated in a gauge invariant manner. The gauge invariance of observables containing the momentum operator is guaranteed when they are defined in terms of $(\hat{\mathbf{p}} + \mathbf{A}/c)$ instead of $\hat{\mathbf{p}}$, which follows from (A.42).

We wish to mention one more important point concerning the calculation of commutators. Each operator can, in principle, be represented in terms of position and momentum operators (and in terms of Pauli operators if spin is considered). Hence, the calculation of each commutator can, in principle, be reduced to the application of the fundamental commutator relations of the position and momentum operators. The position-position commutator does not change under a gauge transformation: $[\hat{r}_i, \hat{r}_j] = 0$. Also the canonical commutation relation does not change:

$$[\hat{r}_i, \hat{p}_j + \frac{1}{c}A_j(\hat{\mathbf{r}})] = [\hat{r}_i, \hat{p}_j] + \frac{1}{c} \underbrace{[\hat{r}_i, A_j(\hat{\mathbf{r}})]}_{=0} = i\delta_{ij}. \quad (\text{A.46})$$

The gauge invariant momentum-momentum commutator relation, however, can change:

$$\begin{aligned} [(\hat{p}_i + \frac{1}{c}A_i(\hat{\mathbf{r}})), (\hat{p}_j + \frac{1}{c}A_j(\hat{\mathbf{r}}))] &= [\hat{p}_i, \frac{1}{c}A_j(\hat{\mathbf{r}})] + [\frac{1}{c}A_i(\hat{\mathbf{r}}), \hat{p}_j] \\ &= -\frac{i}{c}(\partial_{\hat{r}_i}A_j(\hat{\mathbf{r}}) - \partial_{\hat{r}_j}A_i(\hat{\mathbf{r}})) \\ &= -\frac{i}{c} \sum_k^3 \varepsilon_{ijk} (\nabla_{\hat{\mathbf{r}}} \times \mathbf{A}(\hat{\mathbf{r}})) \cdot \mathbf{e}_k. \end{aligned} \quad (\text{A.47})$$

If the \mathbf{A} -field is a purely longitudinal vector field (i.e. such that it can be gauged away), which is the case in our calculations, the last line of (A.47) becomes zero (see next subsection). Hence, if the \mathbf{A} -field is longitudinal, the momentum-momentum commutator behaves as usual: $[\hat{p}_i, \hat{p}_j] = 0$, meaning in practice that each commutator, containing only operators that are formulated in a gauge invariant way, is calculated in the same way as if there would be no external \mathbf{A} -field present. The result will always be gauge invariant as well, as it should be.

So far, all considerations assumed one-particle systems. The generalization to many-electron systems is straightforward and leads to similar statements: the transformations (A.37) and (A.38) apply for many-electron systems as well, only the form of (A.39) changes to

$$\Psi(\mathbf{r}_1, \dots, \mathbf{r}_N, t) \longrightarrow \Psi'(\mathbf{r}_1, \dots, \mathbf{r}_N, t) = e^{-i[\Lambda(\mathbf{r}_1, t) + \dots + \Lambda(\mathbf{r}_N, t)]} \Psi(\mathbf{r}_1, \dots, \mathbf{r}_N, t). \quad (\text{A.48})$$

A.4. The Helmholtz decomposition

The Helmholtz decomposition (also known as the fundamental theorem of vector calculus) states that an arbitrary differentiable vector field $\mathbf{v}(\mathbf{r})$ can be decomposed into a curl-free component and a divergence-free component [47]. Hence, $\mathbf{v}(\mathbf{r})$ can be described by a vector field $\mathbf{a}(\mathbf{r})$ and by a scalar field $b(\mathbf{r})$ in the following way:

$$\mathbf{v}(\mathbf{r}) = \underbrace{\nabla \times \mathbf{a}(\mathbf{r})}_{=:\mathbf{v}_T(\mathbf{r})} + \underbrace{\nabla b(\mathbf{r})}_{=:\mathbf{v}_L(\mathbf{r})}. \quad (\text{A.49})$$

The first term on the right hand side is called transversal component, and the second term is called longitudinal component of $\mathbf{v}(\mathbf{r})$. With $\nabla \cdot (\nabla \times \mathbf{a}) = 0$ and $\nabla \times \nabla b = 0$ it follows immediately that the divergence of any vector field is determined solely from the longitudinal component, while the curl is determined solely from the transversal component:

$$\nabla \cdot \mathbf{v}(\mathbf{r}) = \nabla \cdot \mathbf{v}_L(\mathbf{r}), \quad \nabla \times \mathbf{v}(\mathbf{r}) = \nabla \times \mathbf{v}_T(\mathbf{r}). \quad (\text{A.50})$$

If $\mathbf{v}(\mathbf{r})$ vanishes at infinity faster than $1/|\mathbf{r}|$, the vector and the scalar field from (A.49) can be calculated from

$$\mathbf{a}(\mathbf{r}) = \frac{1}{4\pi} \int d\mathbf{r}' \frac{\nabla_{\mathbf{r}'} \times \mathbf{v}(\mathbf{r}')}{|\mathbf{r} - \mathbf{r}'|}, \quad b(\mathbf{r}) = -\frac{1}{4\pi} \int d\mathbf{r}' \frac{\nabla_{\mathbf{r}'} \cdot \mathbf{v}(\mathbf{r}')}{|\mathbf{r} - \mathbf{r}'|}. \quad (\text{A.51})$$

A.5. Time-dependent Bloch states and the \mathbf{k} -point method

The basis of the \mathbf{k} -point method forms the assumption that the system under study can be described by an infinite periodic crystal. Such a crystal is usually defined by three lattice vectors: $\mathbf{a}_1, \mathbf{a}_2, \mathbf{a}_3$. These lattice vectors define the smallest periodic volume in the crystal, called unit cell. Periodic means that the lattice potential, or more general: the Hamiltonian of the system, does not change under any lattice translation $\mathbf{R} = m_1\mathbf{a}_1 + m_2\mathbf{a}_2 + m_3\mathbf{a}_3$, with m_i as integers. In the following we will assume to have a non-interacting system (also in view of the KS scheme). We define now the translation operator $\hat{t}_{\mathbf{R}}$ that acts on each local operator with a lattice translation via: $\hat{t}_{\mathbf{R}}f(\hat{\mathbf{r}}) = f(\hat{\mathbf{r}} + \mathbf{R})\hat{t}_{\mathbf{R}}$ ($\hat{t}_{\mathbf{R}}$ can, for example, be represented by $\hat{t}_{\mathbf{R}} = \int d\mathbf{r} |\mathbf{r} + \mathbf{R}\rangle \langle \mathbf{r}|$; note that $[\hat{t}_{\mathbf{R}}, \hat{p}_l] = 0$). From the periodicity of the system it follows immediately that this operator commutes with the Hamiltonian, meaning that a set of common eigenstates exist:

$$[\hat{t}_{\mathbf{R}}, \hat{h}] = 0 \quad \longrightarrow \quad \hat{h}|\varphi_i^{\mathbf{k}}\rangle = \epsilon_i|\varphi_i^{\mathbf{k}}\rangle, \quad \hat{t}_{\mathbf{R}}|\varphi_i^{\mathbf{k}}\rangle = e^{i\mathbf{k}\cdot\mathbf{R}}|\varphi_i^{\mathbf{k}}\rangle. \quad (\text{A.52})$$

The $|\varphi_i^{\mathbf{k}}\rangle$ are called Bloch states, and the relation (A.52) is called Bloch theorem, which states that the eigenvalues of the translation operator $\hat{t}_{\mathbf{R}}$ have the form $e^{i\mathbf{k}\cdot\mathbf{R}}$. The \mathbf{k} -vectors from $e^{i\mathbf{k}\cdot\mathbf{R}}$ and from the corresponding eigenstates $|\varphi_i^{\mathbf{k}}\rangle$ can take on all values within the so-called Brillouin zone.

The Bloch theorem can also be extended to the time-dependent domain. Considering a time-dependent Hamiltonian that is periodic for all times gives together with Ehrenfest's theorem:

$$[\hat{t}_{\mathbf{R}}, \hat{h}(t)] = 0 \quad \longrightarrow \quad \partial_t \langle \hat{t}_{\mathbf{R}} \rangle = -i \langle [\hat{t}_{\mathbf{R}}, \hat{h}(t)] \rangle = 0. \quad (\text{A.53})$$

When we now assume that the system evolves from the ground state at $t = 0$, and that the Hamiltonian was periodic at that time, it follows with (A.53) that the time-dependent states remain Bloch states:

$$\langle \varphi_i^{\mathbf{k}}(t) | \hat{t}_{\mathbf{R}} | \varphi_i^{\mathbf{k}}(t) \rangle = \langle \varphi_i^{\mathbf{k}}(0) | \hat{t}_{\mathbf{R}} | \varphi_i^{\mathbf{k}}(0) \rangle = e^{i\mathbf{k} \cdot \mathbf{R}} \rightarrow \hat{t}_{\mathbf{R}} | \varphi_i^{\mathbf{k}}(t) \rangle = e^{i\mathbf{k} \cdot \mathbf{R}} | \varphi_i^{\mathbf{k}}(t) \rangle. \quad (\text{A.54})$$

A common way to represent the Bloch states is the representation as so-called Bloch waves:

$$\langle \mathbf{r} | \varphi_i^{\mathbf{k}}(t) \rangle = e^{i\mathbf{k} \cdot \mathbf{r}} u_i^{\mathbf{k}}(\mathbf{r}, t), \quad \text{with} \quad u_i^{\mathbf{k}}(\mathbf{r} + \mathbf{R}, t) = u_i^{\mathbf{k}}(\mathbf{r}, t). \quad (\text{A.55})$$

The usual way to calculate properties of infinite periodic systems is to consider a macroscopic cell which is constructed from multiple unit cells. Additionally, it is demanded that the states satisfy periodic boundary conditions in this macroscopic cell, i.e.: $\varphi(\mathbf{r} + M_j \mathbf{a}_j) = \varphi(\mathbf{r})$, with $j = \{1, 2, 3\}$ (note that the integers M_j are used to define the size of the macroscopic cell). Moreover, it is assumed that the states are Bloch states, leading to the condition: $e^{i\mathbf{k} \cdot M_j \mathbf{a}_j} = 1$. This condition, together with the assumption that all \mathbf{k} -vectors have to be in the Brillouin zone, defines all valid \mathbf{k} -vectors, which are called \mathbf{k} -points. The number of unit cells in the macroscopic cell is $M = M_1 \cdot M_2 \cdot M_3$, which is equal to the number of \mathbf{k} -points.

The properties (i.e. the expectation values) of an infinite system can then be calculated by taking the infinite limit of the macroscopic cell:

$$\lim_{M \rightarrow \infty} \frac{1}{M} \sum_{\mathbf{k}, i} f_i^{\mathbf{k}} \langle \varphi_i^{\mathbf{k}} | \hat{O} | \varphi_i^{\mathbf{k}} \rangle = \frac{\Omega}{(2\pi)^3} \int_{\text{BZ}} d\mathbf{k} \sum_i f_i(\mathbf{k}) \langle \varphi_i^{\mathbf{k}} | \hat{O} | \varphi_i^{\mathbf{k}} \rangle, \quad (\text{A.56})$$

where $f_i^{\mathbf{k}}$ is the occupation number and Ω is the volume of the unit cell. As can be seen from the right hand side, the sum over the \mathbf{k} -points becomes an integral over the Brillouin zone in the infinite limit. However, it shows that a limited number of \mathbf{k} -points is sufficient to calculate the properties of infinite systems, meaning, in practice, that the system is successively calculated by increasing the number of \mathbf{k} -points until convergence is reached (with respect to the desired quantity). Note that the observables are usually calculated per unit cell, (according to (A.56)), and that all local observables have the same periodicity as the Hamiltonian (which follows directly from the Bloch theorem (A.52)).

The important advantage of the \mathbf{k} -point method is that only one unit cell is necessary for the calculation. This follows, for example, from the Bloch wave representation (A.55):

$$\hat{h} e^{i\mathbf{k} \cdot \mathbf{r}} u^{\mathbf{k}}(\mathbf{r}, t) = e^{i\mathbf{k} \cdot \mathbf{r}} \hat{h}^{\mathbf{k}} u^{\mathbf{k}}(\mathbf{r}, t) \quad \longrightarrow \quad i \partial_t u^{\mathbf{k}}(\mathbf{r}, t) = \hat{h}^{\mathbf{k}} u^{\mathbf{k}}(\mathbf{r}, t), \quad (\text{A.57})$$

where $\hat{h}^{\mathbf{k}}$ corresponds to \hat{h} with the difference that the momentum operator $\hat{\mathbf{p}}$ is replaced by $(\hat{\mathbf{p}} + \mathbf{k})$. As result the Schrödinger equation on the right hand side of (A.57) needs to be calculated only in one unit cell for each \mathbf{k} -point, since $u^{\mathbf{k}}(\mathbf{r}, t)$ and $\hat{h}^{\mathbf{k}}$ are lattice periodic.

A.6. Auxiliary calculations

In this section, we will show some derivations in detail. In the derivations we will, from time to time, make use of the density operator. The density operator will be represented by the δ -distribution, while the δ -distribution has to be understood as a differentiable trial function that becomes the δ -distribution in some limit.

A.6.1. Rules

Below, some short derivations and rules are listed that will be used in this section.

$$[\hat{n}(\mathbf{r}), \hat{p}_j] = [\delta(\mathbf{r} - \hat{\mathbf{r}}), \hat{p}_j] \stackrel{(A.7)}{=} i\partial_{\hat{r}_j}\delta(\mathbf{r} - \hat{\mathbf{r}}) = -i\partial_{r_j}\delta(\mathbf{r} - \hat{\mathbf{r}}) = -i\partial_{r_j}\hat{n}(\mathbf{r}) \quad (\text{A.58})$$

$$\sum_i^3 \varepsilon_{ijk}\varepsilon_{imn} = \delta_{jm}\delta_{kn} - \delta_{jn}\delta_{km} \quad (\text{A.59})$$

$$[\hat{\sigma}_i, \hat{\sigma}_j] = 2i \sum_k^3 \varepsilon_{ijk}\hat{\sigma}_k \quad (\text{A.60})$$

$$\{\hat{\sigma}_i, \hat{\sigma}_j\} = 2\delta_{ij} \quad (\text{A.61})$$

$$[\hat{p}_i, \hat{L}_j] = i \sum_k^3 \varepsilon_{ijk}\hat{p}_k \quad (\text{A.62})$$

$$[\hat{A}\hat{B}, \hat{C}] = \hat{A}[\hat{B}, \hat{C}] + [\hat{A}, \hat{C}]\hat{B} \quad (\text{A.63})$$

$$\hat{A} = \hat{A}^\dagger, \hat{B} = \hat{B}^\dagger \quad \longrightarrow \quad \left(\frac{1}{i}[\hat{A}, \hat{B}]\right) = \left(\frac{1}{i}[\hat{A}, \hat{B}]\right)^\dagger \quad (\text{A.64})$$

$$\text{Re}(\langle \hat{A} \rangle) = \frac{1}{2}\langle \hat{A} + \hat{A}^\dagger \rangle \quad (\text{A.65})$$

$$\hat{A} = \hat{A}^\dagger \quad \longrightarrow \quad \hat{A} = \frac{1}{2}(\hat{A} + \hat{A}^\dagger) \quad (\text{A.66})$$

$$\hat{A} = \hat{A}^\dagger, \hat{B} = \hat{B}^\dagger \quad \longrightarrow \quad \frac{1}{2}\langle \{\hat{A}, \hat{B}\} \rangle = \text{Re}(\langle \hat{A}\hat{B} \rangle) = \text{Re}(\langle \hat{B}\hat{A} \rangle) \quad (\text{A.67})$$

A.6.2. Spin-orbit coupling

In the following, we will consider the SOC operator of a single-particle system, and we will rewrite this operator to a form where we have a local coupling to the

potential. For simplicity, we will neglect the factor $1/4c^2$.

$$\begin{aligned}
\hat{\boldsymbol{\sigma}} \cdot (\nabla v(\hat{\mathbf{r}}) \times \hat{\mathbf{p}}) &= \sum_{i,j,k}^3 \varepsilon_{ijk} \hat{\sigma}_i \partial_{\hat{r}_j} v(\hat{\mathbf{r}}) \hat{p}_k \\
&\stackrel{\text{A.30}}{=} \sum_{i,j,k}^3 \varepsilon_{ijk} \hat{\sigma}_i \left(\int d\mathbf{r} (\partial_{r_j} v(\mathbf{r})) \hat{n}(\mathbf{r}) \right) \hat{p}_k \\
&= \sum_j^3 \int d\mathbf{r} \partial_{r_j} v(\mathbf{r}) \sum_{i,k}^3 \varepsilon_{ijk} \hat{\sigma}_i \hat{n}(\mathbf{r}) \hat{p}_k \\
&\stackrel{\text{(A.66)}}{=} \sum_j^3 \int d\mathbf{r} \partial_{r_j} v(\mathbf{r}) \sum_{i,k}^3 \varepsilon_{ijk} \frac{1}{2} (\hat{\sigma}_i \hat{n}(\mathbf{r}) \hat{p}_k + \hat{p}_k \hat{n}(\mathbf{r}) \hat{\sigma}_i) \\
&= \sum_j^3 \int d\mathbf{r} \partial_{r_j} v(\mathbf{r}) \sum_{i,k}^3 \varepsilon_{ijk} \hat{\sigma}_i \frac{1}{2} \{\hat{n}(\mathbf{r}), \hat{p}_k\} \\
&= - \int d\mathbf{r} v(\mathbf{r}) \sum_{i,j,k}^3 \varepsilon_{ijk} \partial_{r_j} \hat{\sigma}_i \frac{1}{2} \{\hat{n}(\mathbf{r}), \hat{p}_k\} \\
&= - \int d\mathbf{r} v(\mathbf{r}) \sum_i^3 (\nabla_{\mathbf{r}} \times \hat{\sigma}_i \frac{1}{2} \{\hat{n}(\mathbf{r}), \hat{\mathbf{p}}\}) \cdot \mathbf{e}_i, \quad (\text{A.68})
\end{aligned}$$

where ε_{ijk} is the Levi-Civita symbol and \mathbf{e}_i is the Cartesian unit vector of component i . We used that the SOC operator is hermitian, we applied integration by parts, and we assumed that the system is either finite or periodic. An analogous derivation can be carried out for a many-electron system:

$$\begin{aligned}
\sum_l^N \hat{\boldsymbol{\sigma}}_l \cdot (\nabla v(\hat{\mathbf{r}}_l) \times \hat{\mathbf{p}}_l) &\stackrel{\text{(A.68)}}{=} - \sum_l^N \int d\mathbf{r} v(\mathbf{r}) \sum_i^3 (\nabla_{\mathbf{r}} \times \hat{\sigma}_{i,l} \frac{1}{2} \{\delta(\mathbf{r} - \hat{\mathbf{r}}_l), \hat{\mathbf{p}}_l\}) \cdot \mathbf{e}_i \\
&= - \int d\mathbf{r} v(\mathbf{r}) \sum_i^3 (\nabla_{\mathbf{r}} \times \sum_l^N \frac{1}{2} \hat{\sigma}_{i,l} \{\delta(\mathbf{r} - \hat{\mathbf{r}}_l), \hat{\mathbf{p}}_l\}) \cdot \mathbf{e}_i \\
&\stackrel{\text{2.26}}{=} - \int d\mathbf{r} v(\mathbf{r}) \sum_i^3 (\nabla_{\mathbf{r}} \times \hat{\mathbf{j}}_p^i(\mathbf{r})) \cdot \mathbf{e}_i. \quad (\text{A.69})
\end{aligned}$$

Note that (A.69) could also be represented via the spin-current tensor operator:

$$\sum_l^N \hat{\boldsymbol{\sigma}}_l \cdot (\nabla v(\hat{\mathbf{r}}_l) \times \hat{\mathbf{p}}_l) = - \int d\mathbf{r} v(\mathbf{r}) \text{Tr} \{ \nabla_{\mathbf{r}} \times \hat{\hat{J}}_p(\mathbf{r}) \}, \quad (\text{A.70})$$

where the curl acts on each row vector of the tensor.

A.6.3. Time-dependent density, magnetization, and moment

In the following, we will derive the dynamical equations of the density, the magnetization, and the moment. For simplicity, only single-electron systems will be

considered. The generalization to many-electron systems is straightforward. We will consider a Hamiltonian of the type (3.16), and we will, for a clearer view, omit the t -variable and all labels, i.e. fields of equal types will not be distinguished (e.g. $(\mathbf{B}_{\text{ext}} + \mathbf{B}_{\text{xc}}) \rightarrow \mathbf{B}$):

$$\hat{h} = \frac{1}{2} \left(\hat{\mathbf{p}} + \frac{1}{c} \mathbf{A} \right)^2 + v(\hat{\mathbf{r}}) + \frac{1}{2c} \hat{\boldsymbol{\sigma}} \cdot \mathbf{B}(\hat{\mathbf{r}}) + \frac{1}{4c^2} \hat{\boldsymbol{\sigma}} \cdot (\nabla v(\hat{\mathbf{r}}) \times [\hat{\mathbf{p}} + \frac{1}{c} \mathbf{A}]). \quad (\text{A.71})$$

Time-dependent density

The dynamical equation of the density for the Hamiltonian (A.71) follows from the application of Ehrenfest's theorem:

$$\begin{aligned} \partial_t \langle \hat{n}(\mathbf{r}) \rangle &= \frac{1}{i} \langle [\hat{n}(\mathbf{r}), \hat{h}] \rangle = \frac{1}{i} \underbrace{\langle [\hat{n}(\mathbf{r}), \frac{1}{2} (\hat{\mathbf{p}} + \frac{1}{c} \mathbf{A})^2] \rangle}_{=(a)} + \frac{1}{i} \underbrace{\langle [\hat{n}(\mathbf{r}), v(\hat{\mathbf{r}})] \rangle}_{=0} \\ &+ \frac{1}{i} \underbrace{\langle [\hat{n}(\mathbf{r}), \frac{1}{2c} \hat{\boldsymbol{\sigma}} \cdot \mathbf{B}(\hat{\mathbf{r}})] \rangle}_{=0} + \frac{1}{i} \underbrace{\langle [\hat{n}(\mathbf{r}), \frac{1}{4c^2} \hat{\boldsymbol{\sigma}} \cdot (\nabla v(\hat{\mathbf{r}}) \times [\hat{\mathbf{p}} + \frac{1}{c} \mathbf{A}])] \rangle}_{=(b)}. \end{aligned} \quad (\text{A.72})$$

The calculation of the term (a) has been discussed in detail in section (A.1), giving

$$(a) = -\nabla \cdot (\mathbf{j}_p(\mathbf{r}) + \mathbf{j}_d(\mathbf{r})) = -\nabla \cdot \mathbf{j}(\mathbf{r}), \quad (\text{A.73})$$

where \mathbf{j} is the gauge invariant current density (A.21). For term (b) follows

$$\begin{aligned} (b) &= \frac{1}{4c^2 i} \langle [\hat{n}(\mathbf{r}), \sum_{i,j,k} \varepsilon_{ijk} \hat{\sigma}_i (\partial_{\hat{r}_j} v(\hat{\mathbf{r}})) (\hat{p}_k + \frac{1}{c} A_k)] \rangle \\ &= \frac{1}{4c^2 i} \sum_{i,j,k} \varepsilon_{ijk} \langle \hat{\sigma}_i (\partial_{\hat{r}_j} v(\hat{\mathbf{r}})) [\hat{n}(\mathbf{r}), \hat{p}_k] \rangle \\ &\stackrel{(\text{A.58})}{=} -\frac{1}{4c^2} \sum_k \partial_{r_k} \sum_{i,j} \varepsilon_{kij} \langle (\hat{\sigma}_i \hat{n}(\mathbf{r})) (\partial_{\hat{r}_j} v(\hat{\mathbf{r}})) \rangle \\ &= -\frac{1}{4c^2} \sum_k \partial_{r_k} \mathbf{m}(\mathbf{r}) \times \nabla v(\mathbf{r}) \Big|_k \end{aligned} \quad (\text{A.74})$$

$$= -\nabla \cdot \frac{1}{4c^2} [\mathbf{m}(\mathbf{r}) \times \nabla v(\mathbf{r})], \quad (\text{A.75})$$

where we decomposed the triple product with the help of the Levi-Civita symbol. In summary, we get

$$\partial_t n(\mathbf{r}) = -\nabla \cdot \mathbf{j}(\mathbf{r}) - \nabla \cdot \frac{1}{4c^2} [\mathbf{m}(\mathbf{r}) \times \nabla v(\mathbf{r})]. \quad (\text{A.76})$$

Time-dependent magnetization

The dynamical equation of the magnetization for the Hamiltonian (A.71) follows from

$$\begin{aligned} \partial_t \langle \hat{\sigma}_i \hat{n}(\mathbf{r}) \rangle &= \frac{1}{i} \langle [\hat{\sigma}_i \hat{n}(\mathbf{r}), \hat{h}] \rangle = \frac{1}{i} \langle [\hat{\sigma}_i \hat{n}(\mathbf{r}), \underbrace{\frac{1}{2} \left(\hat{\mathbf{p}} + \frac{1}{c} \mathbf{A} \right)^2}_{=(a)}] \rangle + \underbrace{\frac{1}{i} \langle [\hat{\sigma}_i \hat{n}(\mathbf{r}), v(\hat{\mathbf{r}})] \rangle}_{=0} \\ &+ \underbrace{\frac{1}{i} \langle [\hat{\sigma}_i \hat{n}(\mathbf{r}), \frac{1}{2c} \hat{\boldsymbol{\sigma}} \cdot \mathbf{B}(\hat{\mathbf{r}})] \rangle}_{=(b)} + \underbrace{\frac{1}{i} \langle [\hat{\sigma}_i \hat{n}(\mathbf{r}), \frac{1}{4c^2} \hat{\boldsymbol{\sigma}} \cdot (\nabla v(\hat{\mathbf{r}}) \times [\hat{\mathbf{p}} + \frac{1}{c} \mathbf{A}])] \rangle}_{=(c)}. \end{aligned} \quad (\text{A.77})$$

The calculation of the term (a) has been discussed in detail in section (A.1), leading to

$$\begin{aligned} (a) &= -\nabla \cdot \left(\mathbf{j}_p^i(\mathbf{r}) + \mathbf{j}_d^i(\mathbf{r}) \right) = -\nabla \cdot \mathbf{j}^i(\mathbf{r}) \\ &= -\nabla \cdot \left(\overset{\leftrightarrow}{J}_p(\mathbf{r}) + \overset{\leftrightarrow}{J}_d(\mathbf{r}) \right) \Big|_i = -\nabla \cdot \overset{\leftrightarrow}{J}(\mathbf{r}) \Big|_i, \end{aligned} \quad (\text{A.78})$$

where we used the gauge invariant spin-current density representation (A.22) in the first line, and the gauge invariant spin-current tensor representation (A.23) in the second line. The notation in the second line has to be understood as follows: the spin-current tensor is a 3×3 matrix, and the ∇ -operation contracts each row of this matrix by taking the divergence of each row vector, such that a vector is left (and we are interested in the i th component of this vector). For term (b) follows

$$\begin{aligned} (b) &= \frac{1}{2ci} \langle [\hat{\sigma}_i \hat{n}(\mathbf{r}), \sum_j \hat{\sigma}_j B_j(\hat{\mathbf{r}})] \rangle = \frac{1}{2ci} \sum_j \langle \hat{n}(\mathbf{r}) B_j(\hat{\mathbf{r}}) [\hat{\sigma}_i, \hat{\sigma}_j] \rangle \\ &\stackrel{(\text{A.60})}{=} \frac{1}{c} \sum_{j,k} \varepsilon_{ijk} \langle B_j(\hat{\mathbf{r}}) (\hat{\sigma}_k \hat{n}(\mathbf{r})) \rangle = \frac{1}{c} \mathbf{B}(\mathbf{r}) \times \mathbf{m}(\mathbf{r}) \Big|_i, \end{aligned} \quad (\text{A.79})$$

where we used the Levi-Civita symbol to represent the cross product.

Next, we will calculate the contribution of the SOC term (c). First, we separate the gauge invariant momentum operator term, leading to the following two terms:

$$(c) = \underbrace{\frac{1}{4c^2 i} \langle [\hat{\sigma}_i \hat{n}(\mathbf{r}), \hat{\boldsymbol{\sigma}} \cdot (\nabla v(\hat{\mathbf{r}}) \times \hat{\mathbf{p}})] \rangle}_{=(d)} + \underbrace{\frac{1}{4c^3 i} \langle [\hat{\sigma}_i \hat{n}(\mathbf{r}), \hat{\boldsymbol{\sigma}} \cdot (\nabla v(\hat{\mathbf{r}}) \times \mathbf{A})] \rangle}_{=(e)}. \quad (\text{A.80})$$

Each expectation value of a hermitian operator is a real number. Therefore, it follows from the relation (A.64) together with the hermiticity of the paramagnetic SOC operator that (d) has to be a real number. Thus, we get for term (d) with the relation (A.63):

$$\begin{aligned} (d) &= \frac{1}{4c^2} \text{Re} \left(\underbrace{\frac{1}{i} \langle [\hat{\sigma}_i, \hat{\boldsymbol{\sigma}} \cdot (\nabla v(\hat{\mathbf{r}}) \times \hat{\mathbf{p}})] \hat{n}(\mathbf{r}) \rangle}_{=(f)} \right) \\ &+ \frac{1}{4c^2} \text{Re} \left(\underbrace{\frac{1}{i} \langle \hat{\sigma}_i [\hat{n}(\mathbf{r}), \hat{\boldsymbol{\sigma}} \cdot (\nabla v(\hat{\mathbf{r}}) \times \hat{\mathbf{p}})] \rangle}_{=(g)} \right). \end{aligned} \quad (\text{A.81})$$

We will now calculate the term (f):

$$\begin{aligned}
(f) &= \frac{1}{4c^2} \text{Re} \left(\frac{1}{i} \left\langle [\hat{\sigma}_i, \sum_{j,k,l}^3 \varepsilon_{jkl} \hat{\sigma}_j (\partial_{\hat{r}_k} v(\hat{\mathbf{r}})) \hat{p}_l] \hat{n}(\mathbf{r}) \right\rangle \right) \\
&= \frac{1}{4c^2} \sum_{j,k,l}^3 \varepsilon_{jkl} \text{Re} \left(\frac{1}{i} \left\langle [\hat{\sigma}_i, \hat{\sigma}_j] (\partial_{\hat{r}_k} v(\hat{\mathbf{r}})) \hat{p}_l \hat{n}(\mathbf{r}) \right\rangle \right) \\
&\stackrel{(A.60)}{=} \frac{1}{2c^2} \sum_{j,k,l,m}^3 \varepsilon_{jkl} \varepsilon_{ijm} \text{Re} \left(\left\langle \hat{\sigma}_m (\partial_{\hat{r}_k} v(\hat{\mathbf{r}})) \hat{p}_l \hat{n}(\mathbf{r}) \right\rangle \right) \\
&\stackrel{(A.65)}{=} \frac{1}{4c^2} \sum_{j,k,l,m}^3 \varepsilon_{jkl} \varepsilon_{ijm} \left(\left\langle \hat{\sigma}_m (\partial_{\hat{r}_k} v(\hat{\mathbf{r}})) \hat{p}_l \hat{n}(\mathbf{r}) + [\hat{\sigma}_m (\partial_{\hat{r}_k} v(\hat{\mathbf{r}})) \hat{p}_l \hat{n}(\mathbf{r})]^\dagger \right\rangle \right) \\
&\stackrel{(A.7)}{=} \frac{1}{4c^2} \sum_{j,k,l,m}^3 \varepsilon_{jkl} \varepsilon_{ijm} \left\langle \hat{\sigma}_m (\partial_{\hat{r}_k} v(\hat{\mathbf{r}})) [\hat{p}_l \hat{n}(\mathbf{r}) + \hat{n}(\mathbf{r}) \hat{p}_l] \right\rangle \\
&+ \frac{1}{4c^2 i} \sum_{j,m}^3 \varepsilon_{ijm} \underbrace{\sum_{k,l}^3 \varepsilon_{jkl} \left\langle \hat{\sigma}_m \partial_{\hat{r}_i} \partial_{\hat{r}_k} v(\hat{\mathbf{r}}) \right\rangle}_{=0} \\
&= \frac{1}{2c^2} \sum_{j,k,l,m}^3 \varepsilon_{jkl} \varepsilon_{ijm} \left\langle (\partial_{\hat{r}_k} v(\hat{\mathbf{r}})) \underbrace{\frac{1}{2} \hat{\sigma}_m \{ \hat{n}(\mathbf{r}), \hat{p}_l \}}_{\stackrel{(A.28)}{=} \hat{\mathbf{j}}_p^m(\mathbf{r})|_l} \right\rangle \\
&\stackrel{(A.23)}{=} \frac{1}{2c^2} \sum_{j,k,l,m}^3 \varepsilon_{jkl} \varepsilon_{ijm} \overset{\leftrightarrow}{J}_{p,ml}(\mathbf{r}) \partial_{r_k} v(\mathbf{r}) \\
&\stackrel{(A.59)}{=} \frac{1}{2c^2} \sum_{k,l,m}^3 \delta_{km} \delta_{li} \overset{\leftrightarrow}{J}_{p,ml}(\mathbf{r}) \partial_{r_k} v(\mathbf{r}) - \frac{1}{2c^2} \sum_{k,l,m}^3 \delta_{ki} \delta_{lm} \overset{\leftrightarrow}{J}_{p,ml}(\mathbf{r}) \partial_{r_k} v(\mathbf{r}) \\
&= \frac{1}{2c^2} \sum_k^3 \overset{\leftrightarrow}{J}_{p,ki}(\mathbf{r}) \partial_{r_k} v(\mathbf{r}) - \frac{1}{2c^2} \sum_l^3 \overset{\leftrightarrow}{J}_{p,ll}(\mathbf{r}) \partial_{r_i} v(\mathbf{r}) \\
&= \frac{1}{2c^2} \left[\overset{\leftrightarrow}{J}_p^T(\mathbf{r}) - \text{Tr} \{ \overset{\leftrightarrow}{J}_p(\mathbf{r}) \} \right] \cdot \nabla v(\mathbf{r}) \Big|_i. \tag{A.82}
\end{aligned}$$

The expression in the last line has to be understood as follows: The trace of the paramagnetic spin-current tensor is subtracted from diagonal elements of the transpose of the paramagnetic spin-current tensor, which gives a 3×3 matrix. This matrix is then multiplied by the vector $\nabla v(\mathbf{r})$ which gives a vector, and we are interested in the i th component of this vector.

Next, we will calculate the term (g) from (A.81):

$$\begin{aligned}
(g) &= \frac{1}{4c^2} \text{Re} \left(\frac{1}{i} \langle \hat{\sigma}_i [\hat{n}(\mathbf{r}), \sum_{j,k,l}^3 \varepsilon_{jkl} \hat{\sigma}_j (\partial_{\hat{r}_k} v(\hat{\mathbf{r}})) \hat{p}_l] \rangle \right) \\
&= \frac{1}{4c^2} \sum_{j,k,l}^3 \varepsilon_{jkl} \text{Re} \left(\frac{1}{i} \langle \hat{\sigma}_i \hat{\sigma}_j (\partial_{\hat{r}_k} v(\hat{\mathbf{r}})) [\hat{n}(\mathbf{r}), \hat{p}_l] \rangle \right) \\
&\stackrel{(A.58)}{=} \frac{1}{4c^2} \sum_{j,k,l}^3 \varepsilon_{jlk} \partial_{r_l} \text{Re} \left(\langle \hat{\sigma}_i \hat{\sigma}_j \hat{n}(\mathbf{r}) \partial_{\hat{r}_k} v(\hat{\mathbf{r}}) \rangle \right) \\
&\stackrel{(A.65)}{=} \frac{1}{4c^2} \sum_{j,k,l}^3 \varepsilon_{jlk} \partial_{r_l} \langle \hat{n}(\mathbf{r}) \partial_{\hat{r}_k} v(\hat{\mathbf{r}}) \frac{1}{2} \{ \hat{\sigma}_i, \hat{\sigma}_j \} \rangle \\
&\stackrel{(A.61)}{=} \frac{1}{4c^2} \sum_{k,l}^3 \varepsilon_{ilk} \partial_{r_l} \langle \hat{n}(\mathbf{r}) \partial_{\hat{r}_k} v(\hat{\mathbf{r}}) \rangle \\
&= \frac{1}{4c^2} \sum_{k,l}^3 \varepsilon_{ilk} (\partial_{r_l} n(\mathbf{r})) (\partial_{r_k} v(\mathbf{r})) + \frac{1}{4c^2} n(\mathbf{r}) \underbrace{\sum_{k,l}^3 \varepsilon_{ilk} \partial_{r_l} \partial_{r_k} v(\mathbf{r})}_{=0} \\
&= \frac{1}{4c^2} \nabla n(\mathbf{r}) \times \nabla v(\mathbf{r}) \Big|_i. \tag{A.83}
\end{aligned}$$

Finally, we will calculate the term (e) from (A.80):

$$\begin{aligned}
(e) &= \frac{1}{4c^3 i} \langle [\hat{\sigma}_i \hat{n}(\mathbf{r}), \sum_{j,k,l}^3 \varepsilon_{jkl} \hat{\sigma}_j \partial_{\hat{r}_k} v(\hat{\mathbf{r}}) A_l] \rangle \\
&= \frac{1}{4c^3 i} \sum_{j,k,l}^3 \varepsilon_{jkl} \langle [\hat{\sigma}_i, \hat{\sigma}_j] \hat{n}(\mathbf{r}) \partial_{\hat{r}_k} v(\hat{\mathbf{r}}) \rangle A_l \\
&\stackrel{(A.60)}{=} \frac{1}{2c^3} \sum_{j,k,l,m}^3 \varepsilon_{jkl} \varepsilon_{ijm} \langle \hat{\sigma}_m \hat{n}(\mathbf{r}) \partial_{\hat{r}_k} v(\hat{\mathbf{r}}) \rangle A_l \\
&\stackrel{(A.23)}{=} \frac{1}{2c^2} \sum_{j,k,l,m}^3 \varepsilon_{jkl} \varepsilon_{ijm} \overset{\leftrightarrow}{J}_{d,ml}(\mathbf{r}) \partial_{r_k} v(\mathbf{r}) \\
&= \frac{1}{2c^2} \left[\overset{\leftrightarrow}{J}_d^T(\mathbf{r}) - \text{Tr} \{ \overset{\leftrightarrow}{J}_d(\mathbf{r}) \} \right] \cdot \nabla v(\mathbf{r}) \Big|_i. \tag{A.84}
\end{aligned}$$

In the last step, we followed the same route as shown in derivation (A.82) in the last three steps. We see that we get a similar result as in (A.82), but now with the diamagnetic spin-current tensor. Thus, both results can be combined and written with the gauge invariant spin-current tensor.

By collecting the results from (A.78), (A.79), (A.82), (A.83), and (A.84), we can write down the dynamical equation of the magnetization:

$$\begin{aligned} \partial_t \mathbf{m}(\mathbf{r}) = & - \nabla \cdot \overleftrightarrow{J}(\mathbf{r}) + \frac{1}{c} [\mathbf{B}(\mathbf{r}) \times \mathbf{m}(\mathbf{r})] + \frac{1}{4c^2} [\nabla n(\mathbf{r}) \times \nabla v(\mathbf{r})] \\ & + \frac{1}{2c^2} [\overleftrightarrow{J}^T(\mathbf{r}) - \text{Tr}\{\overleftrightarrow{J}(\mathbf{r})\}] \cdot \nabla v(\mathbf{r}), \end{aligned} \quad (\text{A.85})$$

where we considered the vector of the magnetization, and not only one component as in the derivation. Note that the notation of the kinetic term (the first term on the right hand side) is mathematically not entirely correct. What we mean is that each row vector of the spin-current tensor is contracted by taking the divergence, i.e. the correct notation would be

$$\nabla \cdot \overleftrightarrow{J}(\mathbf{r}) \longrightarrow (\nabla^T \cdot \overleftrightarrow{J}^T(\mathbf{r}))^T = \sum_{j,k}^3 \partial_{r_k} \overleftrightarrow{J}_{jk}(\mathbf{r}) \mathbf{e}_j. \quad (\text{A.86})$$

For a clear view, we will use the simplified notation from (A.85) in this work.

Time-dependent moment

The dynamical equation of the moment for the Hamiltonian (A.71) follows from

$$\begin{aligned} \partial_t \langle \hat{\sigma}_i \rangle = & \frac{1}{i} \langle [\hat{\sigma}_i, \hat{h}] \rangle = \frac{1}{i} \underbrace{\langle [\hat{\sigma}_i, \frac{1}{2} (\hat{\mathbf{p}} + \frac{1}{c} \mathbf{A})^2] \rangle}_{=0} + \frac{1}{i} \underbrace{\langle [\hat{\sigma}_i, v(\hat{\mathbf{r}})] \rangle}_{=0} \\ & + \underbrace{\frac{1}{i} \langle [\hat{\sigma}_i, \frac{1}{2c} \hat{\boldsymbol{\sigma}} \cdot \mathbf{B}(\hat{\mathbf{r}})] \rangle}_{=(a)} + \underbrace{\frac{1}{i} \langle [\hat{\sigma}_i, \frac{1}{4c^2} \hat{\boldsymbol{\sigma}} \cdot (\nabla v(\hat{\mathbf{r}}) \times [\hat{\mathbf{p}} + \frac{1}{c} \mathbf{A}])] \rangle}_{=(b)}. \end{aligned} \quad (\text{A.87})$$

We get for term (a)

$$\begin{aligned} (a) & = \frac{1}{2ci} \langle [\hat{\sigma}_i, \sum_j^3 \hat{\sigma}_j B_j(\hat{\mathbf{r}})] \rangle = \frac{1}{2ci} \sum_j^3 \langle B_j(\hat{\mathbf{r}}) [\hat{\sigma}_i, \hat{\sigma}_j] \rangle \\ & \stackrel{(A.60)}{=} \frac{1}{c} \sum_{j,k}^3 \varepsilon_{ijk} \langle B_j(\hat{\mathbf{r}}) (\hat{\sigma}_k) \rangle = \frac{1}{c} \langle \mathbf{B}(\hat{\mathbf{r}}) \times \hat{\boldsymbol{\sigma}} \rangle \Big|_i. \end{aligned} \quad (\text{A.88})$$

For term (b) follows

$$\begin{aligned} (b) & = \frac{1}{4c^2 i} \langle [\hat{\sigma}_i, \sum_{j,k,l}^3 \varepsilon_{jkl} \hat{\sigma}_j (\partial_{\hat{r}_k} v(\hat{\mathbf{r}})) (\hat{p}_l + \frac{1}{c} A_l)] \rangle \\ & = \frac{1}{4c^2 i} \sum_{j,k,l}^3 \varepsilon_{jkl} \langle [\hat{\sigma}_i, \hat{\sigma}_j] (\partial_{\hat{r}_k} v(\hat{\mathbf{r}})) (\hat{p}_l + \frac{1}{c} A_l) \rangle \\ & \stackrel{(A.60)}{=} \frac{1}{2c^2} \sum_{j,k,l,m}^3 \varepsilon_{jkl} \varepsilon_{ijm} \langle \hat{\sigma}_m (\partial_{\hat{r}_k} v(\hat{\mathbf{r}})) (\hat{p}_l + \frac{1}{c} A_l) \rangle \\ & = \frac{1}{2c^2} \langle (\nabla v(\hat{\mathbf{r}}) \times [\hat{\mathbf{p}} + \frac{1}{c} \mathbf{A}]) \times \hat{\boldsymbol{\sigma}} \rangle \Big|_i. \end{aligned} \quad (\text{A.89})$$

Thus, the dynamical equation of the moment is given by

$$\partial_t \mathbf{M} = \underbrace{\frac{1}{c} \langle \mathbf{B}(\hat{\mathbf{r}}) \times \hat{\boldsymbol{\sigma}} \rangle}_{=\partial_t \mathbf{M}_{\mathbf{B}}} + \underbrace{\frac{1}{2c^2} \langle (\nabla v(\hat{\mathbf{r}}) \times [\hat{\mathbf{p}} + \frac{1}{c} \mathbf{A}]) \times \hat{\boldsymbol{\sigma}} \rangle}_{=\partial_t \mathbf{M}_{\text{SOC}}}. \quad (\text{A.90})$$

The moment and its time derivative is also given by the integral of the magnetization and its time derivative (which follows from (A.1)):

$$\mathbf{M} = \langle \hat{\boldsymbol{\sigma}} \rangle = \int d\mathbf{r} \langle \hat{n}(\mathbf{r}) \hat{\boldsymbol{\sigma}} \rangle = \int d\mathbf{r} \mathbf{m}(\mathbf{r}) \quad \longrightarrow \quad \partial_t \mathbf{M} = \int d\mathbf{r} \partial_t \mathbf{m}(\mathbf{r}). \quad (\text{A.91})$$

Hence, the two terms from (A.90) should also be representable as integrals over the corresponding terms from (A.85). In order to investigate this statement we will first, with the help of relation (A.1), rewrite the \mathbf{B} -term from (A.90):

$$\begin{aligned} \partial_t \mathbf{M}_{\mathbf{B}} &= \int d\mathbf{r} \frac{1}{c} \langle \hat{n}(\mathbf{r}) (\mathbf{B}(\hat{\mathbf{r}}) \times \hat{\boldsymbol{\sigma}}) \rangle = \int d\mathbf{r} \frac{1}{c} \langle \mathbf{B}(\hat{\mathbf{r}}) \times (\hat{n}(\mathbf{r}) \hat{\boldsymbol{\sigma}}) \rangle \\ &= \frac{1}{c} \int d\mathbf{r} \left[\mathbf{B}(\mathbf{r}) \times \mathbf{m}(\mathbf{r}) \right] \end{aligned} \quad (\text{A.92})$$

which, in fact, gives the integral over the corresponding \mathbf{B} -term from (A.85). Next, we will rewrite the SOC term from (A.90), and we will start from the line next to the last line of (A.89):

$$\begin{aligned} \partial_t \mathbf{M}_{\text{SOC}} \Big|_i &= \frac{1}{2c^2} \sum_{j,k,l,m}^3 \varepsilon_{jkl} \varepsilon_{ijm} \langle \hat{\sigma}_m (\partial_{\hat{r}_k} v(\hat{\mathbf{r}})) (\hat{p}_l + \frac{1}{c} A_l) \rangle \\ &\stackrel{(\text{A.1})}{=} \frac{1}{2c^2} \int d\mathbf{r} \sum_{j,k,l,m}^3 \varepsilon_{jkl} \varepsilon_{ijm} \langle (\partial_{\hat{r}_k} v(\hat{\mathbf{r}})) \underbrace{\frac{1}{2} \hat{\sigma}_m \{ \hat{n}(\mathbf{r}), (\hat{p}_l + \frac{1}{c} A_l) \}}_{\stackrel{(2.27)}{=} \overleftrightarrow{J}_{ml}(\mathbf{r})} \rangle \\ &= \frac{1}{2c^2} \int d\mathbf{r} \sum_{j,k,l,m}^3 \varepsilon_{jkl} \varepsilon_{ijm} \overleftrightarrow{J}_{ml}(\mathbf{r}) \partial_{r_k} v(\mathbf{r}) \\ &= \frac{1}{2c^2} \int d\mathbf{r} \left[\overleftrightarrow{J}^{\text{T}}(\mathbf{r}) - \text{Tr}\{\overleftrightarrow{J}(\mathbf{r})\} \right] \cdot \nabla v(\mathbf{r}) \Big|_i. \end{aligned} \quad (\text{A.93})$$

In the last step, we followed the last three steps from (A.82). With (A.92) and (A.93) we can now rewrite the expression (A.90):

$$\partial_t \mathbf{M}(t) = \frac{1}{c} \int d\mathbf{r} \left[\mathbf{B}(\mathbf{r}) \times \mathbf{m}(\mathbf{r}) \right] + \frac{1}{2c^2} \int d\mathbf{r} \left[\overleftrightarrow{J}^{\text{T}}(\mathbf{r}) - \text{Tr}\{\overleftrightarrow{J}(\mathbf{r})\} \right] \cdot \nabla v(\mathbf{r}). \quad (\text{A.94})$$

As a result, we see that the first and the third term from (A.85) are not present, meaning that these terms do not contribute to the dynamics of the moment. The first term vanishes by means of Gauss's theorem, and the third term can be shown

to vanish via integration by parts:

$$\begin{aligned}
\int d\mathbf{r} \nabla n(\mathbf{r}) \times \nabla v(\mathbf{r}) \Big|_i &= \sum_{j,k} \varepsilon_{ijk} \int d\mathbf{r} (\partial_{r_j} n(\mathbf{r})) \partial_{r_k} v(\mathbf{r}) \\
&= - \sum_{j,k} \varepsilon_{ijk} \int d\mathbf{r} n(\mathbf{r}) \partial_{r_j} \partial_{r_k} v(\mathbf{r}) \\
&= - \int d\mathbf{r} n(\mathbf{r}) \underbrace{\nabla \times \nabla v(\mathbf{r}) \Big|_i}_{=0} \\
&= 0.
\end{aligned} \tag{A.95}$$

As a last point, we wish to demonstrate that the SOC term (A.93) can be represented in a different form, i.e. by using the spin-current densities instead of the spin-current tensor. With (A.23) we get from the line next to the last line of (A.93)

$$\begin{aligned}
\partial_t \mathbf{M}_{\text{SOC}} \Big|_i &= \frac{1}{2c^2} \int d\mathbf{r} \sum_{j,k,l,m}^3 \varepsilon_{jkl} \varepsilon_{ijm} \mathbf{j}^m(\mathbf{r}) \Big|_l \partial_{r_k} v(\mathbf{r}) \\
&= \frac{1}{2c^2} \int d\mathbf{r} \sum_{j,m}^3 \varepsilon_{ijm} \nabla v(\mathbf{r}) \times \mathbf{j}^m(\mathbf{r}) \Big|_j \\
&= \frac{1}{2c^2} \int d\mathbf{r} \sum_{j,m}^3 \varepsilon_{ijm} \mathbf{e}_j \cdot [\nabla v(\mathbf{r}) \times \mathbf{j}^m(\mathbf{r})] \\
&= \frac{1}{2c^2} \int d\mathbf{r} \begin{pmatrix} \mathbf{e}_1 \\ \mathbf{e}_2 \\ \mathbf{e}_3 \end{pmatrix} \times \begin{pmatrix} [\nabla v(\mathbf{r}) \times \mathbf{j}^1(\mathbf{r})] \\ [\nabla v(\mathbf{r}) \times \mathbf{j}^2(\mathbf{r})] \\ [\nabla v(\mathbf{r}) \times \mathbf{j}^3(\mathbf{r})] \end{pmatrix} \Big|_i,
\end{aligned} \tag{A.96}$$

where $\{\mathbf{e}_l\}$ are the unit vectors. Here, we have defined a cross product of vectors that are constructed from vectors, which is calculated in the usual sense, while the regular multiplication corresponds here to the dot product.

A.6.4. Spin-orbit angular momentum torque terms

In this section we will derive the dynamical equation for the spin-orbit angular momenta

$$\langle \Omega(\hat{r}) \hat{\sigma}_p \hat{L}_q \rangle, \quad \text{with} \quad p, q = \{1, 2, 3\}, \tag{A.97}$$

where $\Omega(r)$ is a radial function that is one inside, and zero outside an arbitrary sphere (see e.g. (4.14)). Note that the angular momentum is defined around the origin of $\Omega(r)$, and that $\Omega(\hat{r}) \hat{\sigma}_p \hat{L}_q$ is hermitian (since $[\Omega(\hat{r}), \hat{L}_q] = 0$). We will neglect the diamagnetic part of the angular momentum operator (in (A.97) and in the SOC term), because it was found that there is no difference in using the gauge invariant angular momentum operator or the bare \hat{L}_q . We will explain this fact at the end of this subsection. For simplicity, only single-electron systems will be considered below. The generalization to many-electron systems is straightforward.

We will consider a Hamiltonian of the type (3.16), with the difference that the radial SOC term (4.10) will be used. As in the previous section we will, for a clearer view, omit the t -variable and all labels, i.e. we will consider the Hamiltonian

$$\hat{h} = \frac{1}{2}(\hat{\mathbf{p}} + \frac{1}{c}\mathbf{A})^2 + v(\hat{\mathbf{r}}) + \frac{1}{2c}\hat{\boldsymbol{\sigma}} \cdot \mathbf{B}(\hat{\mathbf{r}}) + \frac{1}{2}\xi(\hat{r})\hat{\boldsymbol{\sigma}} \cdot \hat{\mathbf{L}}. \quad (\text{A.98})$$

The dynamical equation of the spin-orbit angular momenta (A.97) for the Hamiltonian (A.98) follows from Ehrenfest's theorem:

$$\begin{aligned} \partial_t \langle \Omega(\hat{r})\hat{\sigma}_p \hat{L}_q \rangle &= \frac{1}{i} \langle [\Omega(\hat{r})\hat{\sigma}_p \hat{L}_q, \hat{h}] \rangle \\ &= \underbrace{\frac{1}{i} \langle [\Omega(\hat{r})\hat{\sigma}_p \hat{L}_q, \frac{1}{2}(\hat{\mathbf{p}} + \frac{1}{c}\mathbf{A})^2] \rangle}_{=(a)} + \underbrace{\frac{1}{i} \langle [\Omega(\hat{r})\hat{\sigma}_p \hat{L}_q, v(\hat{\mathbf{r}})] \rangle}_{=(b)} \\ &+ \underbrace{\frac{1}{i} \langle [\Omega(\hat{r})\hat{\sigma}_p \hat{L}_q, \frac{1}{2c}\hat{\boldsymbol{\sigma}} \cdot \mathbf{B}(\hat{\mathbf{r}})] \rangle}_{=(c)} + \underbrace{\frac{1}{i} \langle [\Omega(\hat{r})\hat{\sigma}_p \hat{L}_q, \frac{1}{2}\xi(\hat{r})\hat{\boldsymbol{\sigma}} \cdot \hat{\mathbf{L}}] \rangle}_{=(d)}. \end{aligned} \quad (\text{A.99})$$

We start with the calculation of term (a), and we will split this term into its kinetic and \mathbf{A} -coupling part:

$$(a) = \underbrace{\frac{1}{2i} \langle [\Omega(\hat{r})\hat{\sigma}_p \hat{L}_q, \hat{p}^2] \rangle}_{=(f)} + \underbrace{\frac{1}{ci} \langle [\Omega(\hat{r})\hat{\sigma}_p \hat{L}_q, \mathbf{A} \cdot \hat{\mathbf{p}}] \rangle}_{=(g)}. \quad (\text{A.100})$$

First, we calculate the term (f). Simplifying the commutator gives

$$(f) \stackrel{(A.63)}{=} \frac{1}{2} \langle \frac{1}{i} [\Omega(\hat{r}), \hat{p}^2] \hat{\sigma}_p \hat{L}_q \rangle = \text{Re} \left(\frac{1}{2i} \langle [\Omega(\hat{r}), \hat{p}^2] \hat{\sigma}_p \hat{L}_q \rangle \right). \quad (\text{A.101})$$

As a next step, we will show that this term corresponds to a surface contribution:

$$\begin{aligned} (f) &\stackrel{(A.30)}{=} \int d\mathbf{r} \Omega(r) \text{Re} \left(\frac{1}{2i} \langle [\hat{n}(\mathbf{r}), \hat{p}^2] \hat{\sigma}_p \hat{L}_q \rangle \right) \\ &= \int d\mathbf{r} \Omega(r) \sum_l^3 \text{Re} \left(\frac{1}{2i} \langle [\hat{n}(\mathbf{r}), \hat{p}_l] \hat{p}_l \hat{\sigma}_p \hat{L}_q + \hat{p}_l [\hat{n}(\mathbf{r}), \hat{p}_l] \hat{\sigma}_p \hat{L}_q \rangle \right) \\ &\stackrel{(A.58)}{=} - \int d\mathbf{r} \Omega(r) \sum_l^3 \partial_{r_l} \text{Re} \left(\frac{1}{2} \langle \hat{n}(\mathbf{r}) \hat{p}_l \hat{\sigma}_p \hat{L}_q + \hat{p}_l \hat{n}(\mathbf{r}) \hat{\sigma}_p \hat{L}_q \rangle \right) \\ &= - \int d\mathbf{r} \Omega(r) \underbrace{\nabla \cdot \frac{1}{2} \text{Re} \left(\langle \{\hat{n}(\mathbf{r}), \hat{\mathbf{p}}\} \hat{\sigma}_p \hat{L}_q \rangle \right)}_{\text{spin-orbit angular momentum current density}}. \end{aligned} \quad (\text{A.102})$$

We see that the term (f) can be represented via a spin-current density expression (as it should be; see sections A.1.2 and A.1.4). This expression can be written as a surface term by applying Gauss's theorem. Note that the spin-current density from (A.102) corresponds to a paramagnetic spin-orbit angular momentum current

density. We will now show that the surface term (A.102) can be further simplified (to be more precise: we will show that the anti-commutator expression from (A.102) is not needed in the surface integral representation). Applying the relation

$$[\Omega(\hat{r}), \hat{p}^2] = \nabla_{\hat{r}}^2 \Omega(\hat{r}) - \frac{2}{i} \nabla_{\hat{r}} \Omega(\hat{r}) \cdot \hat{\mathbf{p}} \quad (\text{A.103})$$

on (A.101) gives

$$\begin{aligned} (f) &= \underbrace{\text{Re}\left(\frac{1}{2i} \langle \nabla_{\hat{r}}^2 \Omega(\hat{r}) \hat{\sigma}_p \hat{L}_q \rangle\right)}_{=0} + \text{Re}\left(\langle \nabla_{\hat{r}} \Omega(\hat{r}) \cdot \hat{\mathbf{p}} \hat{\sigma}_p \hat{L}_q \rangle\right) \\ &\stackrel{(\text{A.30})}{=} \int d\mathbf{r} (\nabla_{\mathbf{r}} \Omega(r)) \cdot \text{Re}\left(\langle \hat{n}(\mathbf{r}) \hat{\mathbf{p}} \hat{\sigma}_p \hat{L}_q \rangle\right) \\ &= - \int d\mathbf{r} \delta(R-r) \mathbf{e}_r(\mathbf{r}) \cdot \text{Re}\left(\langle \hat{n}(\mathbf{r}) \hat{\mathbf{p}} \hat{\sigma}_p \hat{L}_q \rangle\right) \\ &= - \oint_{\Omega} ds \cdot \text{Re}\left(\langle \hat{n}(\mathbf{r}) \hat{\mathbf{p}} \hat{\sigma}_p \hat{L}_q \rangle\right), \end{aligned} \quad (\text{A.104})$$

where \mathbf{e}_r is the radial unit vector. The first term on the right hand side of the first line vanishes because the expectation value is real (since the operators commute). Moreover, we assumed that the radial function $\Omega(r)$ is given by $\Omega(r) = \Theta(R-r)$ (i.e. by a function that is one inside a sphere with radius R and zero outside, as stated at the beginning of this section). We point out that (A.104) corresponds to a spin-orbit angular momentum torque term that changes the spin-orbit angular momentum inside Ω via (paramagnetic) spin-orbit angular momentum currents that flow through the surface.

Next, we will calculate the term (g) from (A.100):

$$\begin{aligned} (g) &\stackrel{(\text{A.63})}{=} \sum_l^3 \frac{1}{c_i} A_l \langle \hat{\sigma}_p [\Omega(\hat{r}), \hat{p}_l] \hat{L}_q \rangle + \sum_l^3 \frac{1}{c_i} A_l \langle \Omega(\hat{r}) \hat{\sigma}_p [\hat{L}_q, \hat{p}_l] \rangle \\ &\stackrel{(\text{A.30})}{=} \sum_l^3 \frac{1}{c_i} A_l \langle \hat{\sigma}_p \left[\left(\int d\mathbf{r} \Omega(r) \hat{n}(\mathbf{r}) \right), \hat{p}_l \right] \hat{L}_q \rangle + \sum_l^3 \frac{1}{c_i} A_l \langle \Omega(\hat{r}) \hat{\sigma}_p [\hat{L}_q, \hat{p}_l] \rangle \\ &\stackrel{(\text{A.62})}{=} \int d\mathbf{r} \Omega(r) \sum_l^3 \frac{1}{c_i} A_l \langle \hat{\sigma}_p [\hat{n}(\mathbf{r}), \hat{p}_l] \hat{L}_q \rangle + \sum_{l,m}^3 \varepsilon_{qlm} \frac{1}{c} A_l \langle \Omega(\hat{r}) \hat{\sigma}_p \hat{p}_m \rangle \\ &\stackrel{(\text{A.58})}{=} - \int d\mathbf{r} \Omega(r) \sum_l^3 \frac{1}{c} A_l \partial_{r_l} \text{Re}\left(\langle \hat{n}(\mathbf{r}) \hat{\sigma}_p \hat{L}_q \rangle\right) + \sum_{l,m}^3 \varepsilon_{qlm} \frac{1}{c} A_l \text{Re}\left(\langle \Omega(\hat{r}) \hat{\sigma}_p \hat{p}_m \rangle\right) \\ &= - \oint_{\Omega} ds \cdot \text{Re}\left(\langle \hat{n}(\mathbf{r}) \frac{1}{c} \mathbf{A} \hat{\sigma}_p \hat{L}_q \rangle\right) + \frac{1}{c} \mathbf{A} \times \text{Re}\left(\langle \Omega(\hat{r}) \hat{\sigma}_p \hat{\mathbf{p}} \rangle\right) \Big|_q. \end{aligned} \quad (\text{A.105})$$

We have used that the term (g) is real, and we applied Gauss's theorem. With (A.104) and (A.105) we can write the spin-orbit angular momentum torque term (a) from (A.100) as

$$(a) = - \oint_{\Omega} ds \cdot \text{Re}\left(\langle \hat{n}(\mathbf{r}) (\hat{\mathbf{p}} + \frac{1}{c} \mathbf{A}) \hat{\sigma}_p \hat{L}_q \rangle\right) + \frac{1}{c} \mathbf{A} \times \text{Re}\left(\langle \Omega(\hat{r}) \hat{\sigma}_p \hat{\mathbf{p}} \rangle\right) \Big|_q. \quad (\text{A.106})$$

We see that the torque term (a) has two contributions. The first term corresponds to a gauge invariant spin-orbit angular momentum current contribution that changes the spin-orbit angular momentum via currents that flow into Ω . The second term corresponds to a direct coupling of the external \mathbf{A} -field to the spin-current in region Ω .

We will now calculate the torque term (b) from (A.99):

$$\begin{aligned}
(b) &= \frac{1}{i} \langle \Omega(\hat{r}) \hat{\sigma}_p [\hat{L}_q, v(\hat{r})] \rangle = \sum_{l,m}^3 \varepsilon_{qlm} \frac{1}{i} \langle \Omega(\hat{r}) \hat{\sigma}_p \hat{r}_l [\hat{p}_m, v(\hat{r})] \rangle \\
&\stackrel{(A.7)}{=} - \sum_{l,m}^3 \varepsilon_{qlm} \langle \Omega(\hat{r}) \hat{\sigma}_p \hat{r}_l \partial_{\hat{r}_m} v(\hat{r}) \rangle = \langle \Omega(\hat{r}) \hat{\sigma}_p \nabla v(\hat{r}) \times \hat{r} \rangle \Big|_q. \quad (A.107)
\end{aligned}$$

Note that this torque term corresponds to the usual angular momentum torque caused by the electric field of the local potential.

Next, we calculate the term (c):

$$\begin{aligned}
(c) &\stackrel{(A.63)}{=} \sum_l^3 \frac{1}{2ci} \langle \Omega(\hat{r}) \hat{\sigma}_p \hat{\sigma}_l \underbrace{[\hat{L}_q, B_l(\hat{r})]}_{=i \nabla B_l(\hat{r}) \times \hat{r}|_q} \rangle + \sum_l^3 \frac{1}{2ci} \langle \Omega(\hat{r}) [\hat{\sigma}_p, \hat{\sigma}_l] B_l(\hat{r}) \hat{L}_q \rangle \\
&\stackrel{(A.60)}{=} \sum_l^3 \frac{1}{2c} \text{Re}(\langle \Omega(\hat{r}) \hat{\sigma}_p \hat{\sigma}_l \nabla B_l(\hat{r}) \times \hat{r} \rangle \Big|_q) + \sum_{l,m}^3 \varepsilon_{plm} \frac{1}{c} \text{Re}(\langle \Omega(\hat{r}) B_l(\hat{r}) \hat{\sigma}_m \hat{L}_q \rangle) \\
&\stackrel{(A.65)}{=} \sum_l^3 \frac{1}{2c} \langle \Omega(\hat{r}) \frac{1}{2} \{ \hat{\sigma}_p, \hat{\sigma}_l \} \nabla B_l(\hat{r}) \times \hat{r} \rangle \Big|_q + \sum_{l,m}^3 \varepsilon_{plm} \frac{1}{c} \text{Re}(\langle \Omega(\hat{r}) B_l(\hat{r}) \hat{\sigma}_m \hat{L}_q \rangle) \\
&\stackrel{(A.61)}{=} \frac{1}{2c} \langle \Omega(\hat{r}) \nabla B_p(\hat{r}) \times \hat{r} \rangle \Big|_q + \text{Re}(\langle \Omega(\hat{r}) \frac{1}{c} \mathbf{B}(\hat{r}) \times \hat{\sigma} \hat{L}_q \rangle) \Big|_p, \quad (A.108)
\end{aligned}$$

which gives two torque contributions. Note that the two contributions can, in a sense, be understood as a result of the product rule: the first torque contribution results from the change of the angular momentum contribution (i.e. from the angular momentum torque), while the second term results from the change of the spin contribution (i.e. from the spin-torque). This is particularly obvious for the second term, which contains the usual $\mathbf{B} \times \boldsymbol{\sigma}/c$ -spin-torque term (see e.g. (A.90)).

We continue with the calculation of term (d) from (A.99):

$$\begin{aligned}
(d) &\stackrel{(A.63)}{=} \sum_l^3 \frac{1}{2i} \langle \Omega(\hat{r}) \xi(\hat{r}) \hat{\sigma}_p \hat{\sigma}_l \underbrace{[\hat{L}_q, \hat{L}_l]}_{=i \sum_m \varepsilon_{qlm} \hat{L}_m} \rangle + \sum_l^3 \frac{1}{2i} \langle \Omega(\hat{r}) \xi(\hat{r}) [\hat{\sigma}_p, \hat{\sigma}_l] \hat{L}_l \hat{L}_q \rangle \\
&\stackrel{(A.60)}{=} \sum_{l,m}^3 \varepsilon_{qlm} \frac{1}{2} \text{Re}(\langle \Omega(\hat{r}) \xi(\hat{r}) \hat{\sigma}_p \hat{\sigma}_l \hat{L}_m \rangle) + \sum_{l,m}^3 \varepsilon_{qlm} \text{Re}(\langle \Omega(\hat{r}) \xi(\hat{r}) \hat{L}_l \hat{\sigma}_m \hat{L}_q \rangle) \\
&\stackrel{(A.65)}{=} \sum_{l,m}^3 \varepsilon_{qlm} \frac{1}{2} \text{Re}(\langle \Omega(\hat{r}) \xi(\hat{r}) \frac{1}{2} \{ \hat{\sigma}_p, \hat{\sigma}_l \} \hat{L}_m \rangle) + \sum_{l,m}^3 \varepsilon_{qlm} \text{Re}(\langle \Omega(\hat{r}) \xi(\hat{r}) \hat{L}_l \hat{\sigma}_m \hat{L}_q \rangle) \\
&\stackrel{(A.61)}{=} \sum_m^3 \varepsilon_{qpm} \frac{1}{2} \langle \Omega(\hat{r}) \xi(\hat{r}) \hat{L}_m \rangle + \text{Re}(\langle \Omega(\hat{r}) \xi(\hat{r}) \hat{\mathbf{L}} \times \hat{\sigma} \hat{L}_q \rangle) \Big|_p. \quad (A.109)
\end{aligned}$$

The calculation is very similar to the calculation of term (c) and also leads to two torque contributions. As before, the first torque contribution results from the angular momentum torque contribution and the second contribution results from the spin-torque contribution (compare the second term to the spin-torque term from (4.11)).

We can now collect the terms (a) to (d), i.e. all spin-orbit angular momentum torque contributions corresponding to (A.99), and write down the dynamical equation of the spin-orbit angular momentum $\langle \Omega(\hat{r})\hat{\sigma}_p\hat{L}_q \rangle$ that evolves according to the Hamiltonian (A.98):

$$\begin{aligned}
& \partial_t \langle \Omega(\hat{r})\hat{\sigma}_p\hat{L}_q \rangle \tag{A.110} \\
&= - \oint_{\Omega} d\mathbf{s} \cdot \text{Re}(\langle \hat{n}(\mathbf{r})(\hat{\mathbf{p}} + \frac{1}{c}\mathbf{A})\hat{\sigma}_p\hat{L}_q \rangle) + \frac{1}{c}\mathbf{A} \times \text{Re}(\langle \Omega(\hat{r})\hat{\sigma}_p\hat{\mathbf{p}} \rangle) \Big|_q \\
&+ \langle \Omega(\hat{r})\hat{\sigma}_p \nabla v(\hat{\mathbf{r}}) \times \hat{\mathbf{r}} \rangle \Big|_q + \frac{1}{2c} \langle \Omega(\hat{r}) \nabla B_p(\hat{\mathbf{r}}) \times \hat{\mathbf{r}} \rangle \Big|_q + \text{Re}(\langle \Omega(\hat{r}) \frac{1}{c}\mathbf{B}(\hat{\mathbf{r}}) \times \hat{\boldsymbol{\sigma}} \hat{L}_q \rangle) \Big|_p \\
&+ \sum_m^3 \varepsilon_{qpm} \frac{1}{2} \langle \Omega(\hat{r})\xi(\hat{r})\hat{L}_m \rangle + \text{Re}(\langle \Omega(\hat{r})\xi(\hat{r})\hat{\mathbf{L}} \times \hat{\boldsymbol{\sigma}} \hat{L}_q \rangle) \Big|_p.
\end{aligned}$$

Gauge invariant spin-orbit angular momentum

To be physically more accurate, the gauge invariant angular momentum operators should be used in the radial SOC term (4.10):

$$\hat{L}_q \longrightarrow \hat{L}_q + \hat{\mathbf{r}} \times \frac{1}{c}\mathbf{A}(t) \Big|_q. \tag{A.111}$$

As a result, the gauge invariant spin-orbit angular momenta (i.e. (A.97) with the replacement (A.111)) would be the quantities describing the demagnetization. In fact, the same analysis as before can be done with the gauge invariant spin-orbit angular momenta, leading to a similar equation as (A.110) (with the replacement (A.111) for all \hat{L}_q operators). However, there would be two major differences:

First, the direct \mathbf{A} -coupling term (the right term of the second line from (A.110)) would vanish, since this term corresponds to the kinetic source term (see (A.18)), which is zero if the gauge invariant \hat{L}_q is used (since $[\hat{L}_q, \hat{p}^2] = 0$). Second, an additional torque term would, according to Ehrenfest's theorem, emerge, because the \mathbf{A} -field in (A.111) has an explicit time-dependence:

$$\langle \Omega(\hat{r})\hat{\sigma}_p(\partial_t \hat{L}_q(t)) \rangle \stackrel{(A.111)}{=} \langle \Omega(\hat{r})\hat{\sigma}_p \hat{\mathbf{r}} \times \frac{1}{c}\partial_t \mathbf{A}(t) \rangle \Big|_q \stackrel{(2.80)}{=} \mathbf{E}(t) \times \langle \Omega(\hat{r})\hat{\sigma}_p \hat{\mathbf{r}} \rangle \Big|_q. \tag{A.112}$$

We have used that the external electric field \mathbf{E} follows directly from the time derivative of the external \mathbf{A} -field in the DA. As a conclusion, we find that the direct \mathbf{A} -coupling term (present in the non gauge invariant formulation) would vanish, but a new direct \mathbf{A} -coupling (or \mathbf{E} -coupling) term would appear.

We will now show that these two terms give very similar contributions to the dynamics of the spin-orbit angular momenta. To show this, we integrate the torque term (A.112) in time:

$$\int_0^T dt \langle \Omega(\hat{r}) \hat{\sigma}_p \hat{r} \times \frac{1}{c} \partial_t \mathbf{A}(t) \rangle \Big|_q = \int_0^T dt \frac{1}{c} \mathbf{A}(t) \times \partial_t \langle \Omega(\hat{r}) \hat{\sigma}_p \hat{r} \rangle \Big|_q. \quad (\text{A.113})$$

We used integration by parts, and we assumed that T is any point in time where the \mathbf{A} -field is zero during its interaction, or any time after the pulse interaction. Next, we use Ehrenfest's theorem to calculate the time derivative of the quantity under the integral from the right hand side:

$$\partial_t \langle \Omega(\hat{r}) \hat{\sigma}_p \hat{r} \rangle = \frac{1}{i} \langle [\Omega(\hat{r}) \hat{\sigma}_p \hat{r}, \hat{h}] \rangle = \text{Re} \left(\langle \Omega(\hat{r}) \hat{\sigma}_p \left(\hat{\mathbf{p}} + \frac{1}{c} \mathbf{A}(t) \right) \rangle \right) + \dots, \quad (\text{A.114})$$

where \hat{h} is the gauge invariant Hamiltonian. The term on the right hand side is the kinetic source term (note that this term corresponds, in principle, to the original Ehrenfest position momentum relation: $\partial_t \langle \hat{r} \rangle = \langle \hat{\mathbf{p}} \rangle$). “...” stands for the kinetic surface term, and for a SOC torque term, which should be small due to the prefactor $1/c^2$ (there would also be a \mathbf{B}_{xc} -term, but this term vanishes due to (3.20)). When we assume that these two terms are negligible, which seems to be the case, we get with (A.114) for (A.113):

$$\int_0^T dt \langle \Omega(\hat{r}) \hat{\sigma}_p \hat{r} \times \frac{1}{c} \partial_t \mathbf{A}(t) \rangle \Big|_q \approx \int_0^T dt \frac{1}{c} \mathbf{A}(t) \times \text{Re} \left(\langle \Omega(\hat{r}) \hat{\sigma}_p \hat{\mathbf{p}} \rangle \right) \Big|_q. \quad (\text{A.115})$$

We see that the term in the integral on the right hand side is the direct \mathbf{A} -coupling term from (A.110).

In summary, we find that direct \mathbf{A} -coupling term that vanishes when going from the non gauge invariant to the gauge invariant formulation is replaced by a very similar term, explaining why we found no significant differences in the magnetization dynamics between applying the gauge and non gauge invariant \hat{L}_q in SOC. Hence, the direct \mathbf{A} -coupling torque term from the non gauge invariant formulation (which should actually not be there) corresponds, in fact, to a very similar true \mathbf{A} -coupling torque term that would appear in the gauge invariant formulation.

A.6.5. Spin-current representation for the radial SOC and for the spin-orbit angular momentum torque

In the following we will, for simplicity, only consider single-electron systems. The generalization to many-electron systems is straightforward. Additionally, we will omit the t -variable and all labels. First, we will show that the radial SOC term

(4.10) can be rewritten into a spin-current density operator form:

$$\begin{aligned}
\frac{1}{2}\xi(\hat{r})\hat{\sigma}\cdot\hat{\mathbf{L}} &= \sum_{k,l,m}^3 \varepsilon_{klm} \frac{1}{2}\xi(\hat{r})\hat{\sigma}_k \hat{r}_l (\hat{p}_m + \frac{1}{c}A_m) \\
&\stackrel{(A.30)}{=} \sum_{k,l,m}^3 \varepsilon_{klm} \frac{1}{2} \left(\int d\mathbf{r} \xi(r) r_l \hat{n}(\mathbf{r}) \right) \hat{\sigma}_k (\hat{p}_m + \frac{1}{c}A_m) \\
&\stackrel{(A.66)}{=} \sum_{k,l,m}^3 \varepsilon_{klm} \frac{1}{2} \int d\mathbf{r} \xi(r) r_l \hat{\sigma}_k \frac{1}{2} \{ \hat{n}(\mathbf{r}), (\hat{p}_m + \frac{1}{c}A_m) \} \\
&\stackrel{(A.28)}{=} \sum_{k,l,m}^3 \varepsilon_{klm} \frac{1}{2} \int d\mathbf{r} \xi(r) r_l \hat{\mathbf{j}}^k(\mathbf{r})|_m \\
&= \sum_k^3 \frac{1}{2} \int d\mathbf{r} \xi(r) (\mathbf{r} \times \hat{\mathbf{j}}^k(\mathbf{r})) \cdot \mathbf{e}_k. \tag{A.116}
\end{aligned}$$

In a similar manner, we can show that the \mathbf{B}_{xc} spin-orbit angular momentum torque contributions from (4.22) can also be represented in terms of the spin-current density:

$$\begin{aligned}
&\text{Re} \left[\langle \Omega(\hat{r}) \frac{1}{c} B_{xc,3}(\hat{\mathbf{r}}) \hat{\sigma}_k \hat{L}_k \rangle \right] \\
&\stackrel{(A.30)}{=} \sum_{l,m}^3 \varepsilon_{klm} \frac{1}{c} \int d\mathbf{r} \Omega(r) B_{xc,3}(\mathbf{r}) r_l \text{Re} \left[\langle \hat{n}(\mathbf{r}) \hat{\sigma}_k (\hat{p}_m + \frac{1}{c}A_m) \rangle \right] \\
&\stackrel{(A.66)}{=} \sum_{l,m}^3 \varepsilon_{klm} \frac{1}{c} \int d\mathbf{r} \Omega(r) B_{xc,3}(\mathbf{r}) r_l \langle \hat{\sigma}_k \frac{1}{2} \{ \hat{n}(\mathbf{r}), (\hat{p}_m + \frac{1}{c}A_m) \} \rangle \\
&\stackrel{(A.28)}{=} \frac{1}{c} \int_{\Omega} d\mathbf{r} B_{xc,3}(\mathbf{r}) (\mathbf{r} \times \hat{\mathbf{j}}^k(\mathbf{r})) \cdot \mathbf{e}_k. \tag{A.117}
\end{aligned}$$

A.7. Many-electron systems and change of the moment

In section 4.3 we found that a loss in the moment of bulk Ni occurs due to spin-orbit angular momenta that are induced around the nuclei during the excitation. Furthermore, we found that the change of the spin-orbit angular momenta can be described by their torques. It was shown that the loss in the moment results essentially from the behavior of the spin-orbit angular momentum torque stemming from the xc \mathbf{B} -field (i.e. from the $\Gamma_{pq}^{\mathbf{B}}$ terms; see (4.21)). In a true many-electron system only a bare Coulomb interaction exists (i.e. there is no xc \mathbf{B} -field that couples directly to the spin). Hence, one might wonder if the demagnetization process explained in section 4.3 applies, at least to some extent, also to Coulomb interacting many-electron systems, or if the observed behavior might be an artifact arising from the application of the DFT framework.

To investigate this concern, the spin-orbit angular momentum torque related to the Coulomb interaction, and the associated change in the moment will be investigated for an interacting system in this section. For simplicity, we will consider a two-electron system (the two electrons could for example be seen as the electrons in an outer shell of an atom or molecule). A common way to discuss the spin properties of a two-electron system is to employ the so-called exchange Hamiltonian approach, where the Coulomb interaction is rewritten to an effective spin-spin interaction (see e.g. [59]). In our discussion, we will loosely follow some ideas of this approach. Furthermore, we will employ a mean field approximation at some places (which allows us to draw some parallels between the many-electron problem and the KS approach, as we will see). It is clear that such an approximation is only reasonable if systems with many electrons are considered. However, we should keep in mind that the purpose of the following investigation is the discussion of general aspects that arise when interacting many-electron spin-systems with spin-orbit coupling are considered. Hence, for reasons of simplicity but without loss of generality, only a two-electron system is considered in the following investigations. Note that similar investigations could be carried out in an analog manner for many-electrons systems by, for example, considering only the exchange part of the Coulomb interaction, or by employing multi-band Hubbard-like models (e.g. Heisenberg model Hamiltonians can be derived from Hubbard models [60]).

We consider a two-electron system described by the following Hamiltonian:

$$\hat{H} = \sum_i^2 \left(\underbrace{\frac{\hat{p}_i^2}{2} + v_{\text{ext}}(\hat{\mathbf{r}}_i, t)}_{=\hat{h}_i^0(t)} + \underbrace{\frac{1}{2}\xi(\hat{r}_i)\hat{\boldsymbol{\sigma}}_i \cdot \hat{\mathbf{L}}_i}_{=\hat{h}_i^{\text{SOC}}} \right) + \underbrace{\frac{1}{|\hat{\mathbf{r}}_1 - \hat{\mathbf{r}}_2|}}_{=\hat{W}}. \quad (\text{A.118})$$

We assume that v_{ext} contains a static potential (e.g. the nuclear potential) and a time-dependent potential, which is zero at $t = 0$. Next, we assume that the system is in the ground state at $t = 0$, and that the time-dependent state that solves the Schrödinger equation is expanded in a two-electron basis:

$$|\Psi(t)\rangle = \sum_{\mathbf{u}} c_{\mathbf{u}}(t)|\mathbf{u}\rangle, \quad (\text{A.119})$$

while each basis state is characterized by a tuple of elements, represented by \mathbf{u} . As next step, we will specify this basis (which will also explain what \mathbf{u} means).

A possible two-electron basis can be constructed from the following singlet and triplet states:

$$\begin{aligned} \text{singlet:} \quad |a, b, s\rangle &= 1/\sqrt{2} (|a \uparrow, b \downarrow\rangle - |a \downarrow, b \uparrow\rangle), \\ \text{triplet:} \quad |a, b, t_{\downarrow}\rangle &= |a \downarrow, b \downarrow\rangle, \\ &|a, b, t_{\uparrow}\rangle = |a \uparrow, b \uparrow\rangle, \\ &|a, b, t_0\rangle = 1/\sqrt{2} (|a \uparrow, b \downarrow\rangle + |a \downarrow, b \uparrow\rangle), \end{aligned} \quad (\text{A.120})$$

while the states on the right hand side are two-particle Slater determinants, i.e.:

$$|a\gamma, b\eta\rangle = 1/\sqrt{2} (|a\rangle_1|\gamma\rangle_1|b\rangle_2|\eta\rangle_2 - |b\rangle_1|\eta\rangle_1|a\rangle_2|\gamma\rangle_2), \quad \gamma, \eta \in \{\uparrow, \downarrow\}. \quad (\text{A.121})$$

Here, γ and η represent the spinor states (i.e. the two eigenstates of $\hat{\sigma}_3$), while a and b correspond to a complete set of spin-less one-particle states, e.g. to the eigenstates of $\hat{h}^0(t=0)$:

$$\hat{h}^0|n\rangle = \epsilon_n|n\rangle \quad \longrightarrow \quad a, b \in \{n\}. \quad (\text{A.122})$$

Next, we demand for (A.120) that $a < b$ (note that the interchange $a \leftrightarrow b$, with $a \neq b$, leads to equivalent states). The states (A.120) are orthogonal, however, the condition $a < b$ leads to a non-complete basis. In order to obtain a complete basis, the set of intra-orbital singlet states $\{|a \uparrow, a \downarrow\rangle\}$ would have to be included. In the following discussion we will, for simplicity, omit these singlet states. It is clear that this is in general a strong simplification, however, we point out that the following investigation could also be performed with the complete basis (e.g. simply by considering only the subset (A.120); we will say later a few words about this subject). In summary, the basis $\{|\mathbf{u}\rangle\}$ from (A.119) is given by all basis states from (A.120), meaning that

$$|\mathbf{u}\rangle = |a, b, c\rangle, \quad \text{with } a < b, \quad a, b \stackrel{(\text{A.122})}{\in} \{n\}, \quad \text{and } c \in \{\underbrace{s, t_\downarrow, t_\uparrow, t_0}_t\}. \quad (\text{A.123})$$

The last element, c , simply determines whether the basis state is a singlet state or one of the triplet states (note that we will use the label ‘‘t’’ when we refer to any of the three types of triplet states).

The first main step in our investigation consists in the rewriting of the interaction term \hat{W} . First, we use our basis to define the Coulomb operator

$$\hat{C} = \sum_c \sum_{a,b,a',b'} C_{ab}^{a'b'} |a, b, c\rangle \langle a', b', c|, \quad (\text{A.124})$$

and the exchange operator

$$\hat{J} = \sum_c \sum_{a,b,a',b'} J_{ab}^{a'b'} |a, b, c\rangle \langle a', b', c|. \quad (\text{A.125})$$

Note that these operators are diagonal in the singlet-triplet subspace (hence, the first sum runs only over the single element c). The matrix elements (leading to the hermiticity of the operators) are defined by

$$C_{ab}^{a'b'} = \int d\mathbf{r} \int d\mathbf{r}' \frac{\varphi_a^*(\mathbf{r})\varphi_{a'}(\mathbf{r})\varphi_b^*(\mathbf{r}')\varphi_{b'}(\mathbf{r}')}{|\mathbf{r} - \mathbf{r}'|}, \quad (\text{A.126})$$

and by

$$J_{ab}^{a'b'} = \int d\mathbf{r} \int d\mathbf{r}' \frac{\varphi_a^*(\mathbf{r})\varphi_{b'}(\mathbf{r})\varphi_b^*(\mathbf{r}')\varphi_{a'}(\mathbf{r}')}{|\mathbf{r} - \mathbf{r}'|}, \quad (\text{A.127})$$

where the orbitals are given by the single-particle wave functions according to (A.122), i.e. $\varphi_n(\mathbf{r}) = \langle \mathbf{r}|n\rangle$. The diagonal elements of (A.126) and (A.127) in the individual subspace (i.e. $a = a'$ and $b = b'$) are the usual Coulomb and exchange integral expressions. With the definition of the Coulomb and exchange operator,

it follows that the action of the interaction operator \hat{W} on the singlet and triplet states is, within our basis, given by

$$\hat{W}|a, b, s\rangle = (\hat{C} + \hat{J})|a, b, s\rangle, \quad \text{and} \quad \hat{W}|a, b, t\rangle = (\hat{C} - \hat{J})|a, b, t\rangle, \quad (\text{A.128})$$

which holds for all a and b . When we additionally use the following relation of the spin-spin coupling operator $\hat{\sigma}_1 \cdot \hat{\sigma}_2$:

$$\hat{\sigma}_1 \cdot \hat{\sigma}_2|a, b, s\rangle = -3|a, b, s\rangle, \quad \text{and} \quad \hat{\sigma}_1 \cdot \hat{\sigma}_2|a, b, t\rangle = |a, b, t\rangle, \quad (\text{A.129})$$

which holds for all a and b as well (see e.g. [59]), it follows immediately that the interaction operator \hat{W} can be rewritten to the following spin-spin coupling form:

$$\hat{W} = \hat{C} - \frac{1}{2}\hat{J} - \frac{1}{2}\hat{\sigma}_1 \cdot \hat{\sigma}_2\hat{J}, \quad (\text{A.130})$$

where we used that $[\hat{\sigma}_1 \cdot \hat{\sigma}_2, \hat{J}] = 0$. The interaction term on the right hand side of (A.130), which corresponds to an exchange dependent spin-spin interaction, will be of particular interest for the following discussion. (As stated before, we have excluded the intra-orbital singlet states $\{|a \uparrow, a \downarrow\rangle\}$). In order to describe a complete system, (A.130) would have to be extended by a term that describes all additional interactions with the intra-orbital singlet states, i.e. this term would include the interaction matrix elements $\langle a' \uparrow, a' \downarrow | \hat{W} | a \uparrow, a \downarrow \rangle = C_{a'a'}^{aa}$ and $\langle a', b', s | \hat{W} | a \uparrow, a \downarrow \rangle = \sqrt{2} C_{a'b'}^{aa}$. Note, however, that this additional interaction operator would only act in the singlet-singlet subspace because $\langle a', b', t | \hat{W} | a \uparrow, a \downarrow \rangle = 0$. For simplicity, we will omit this additional interaction term in the following discussion.)

The ground state energy of our system is given by

$$\langle \hat{H} \rangle = \dots + \langle \hat{W} \rangle = \dots + \langle \hat{C} - \frac{1}{2}\hat{J} \rangle - \frac{1}{2}\langle \hat{\sigma}_1 \cdot \hat{\sigma}_2\hat{J} \rangle. \quad (\text{A.131})$$

Rewriting and approximating the energy contribution from the right hand side gives

$$-\frac{1}{2}\langle \hat{\sigma}_1 \cdot \hat{\sigma}_2\hat{J} \rangle = -\frac{1}{4}\langle \sum_i^2 \hat{\sigma}_i \cdot \left(\sum_{j \neq i}^2 \hat{\sigma}_j\hat{J} \right) \rangle \approx -\frac{1}{4}\underbrace{\langle \sum_i^2 \hat{\sigma}_i \rangle}_{\mathbf{M}} \cdot \langle \sum_j^2 \hat{\sigma}_j\hat{J} \rangle. \quad (\text{A.132})$$

In the last step we have assumed that the corresponding energy contribution is approximately given by a mean field expression (which should be reasonable if the system shows a ferromagnetic character in the ground state, i.e. if the system has parallel aligned spins). From (A.132) it follows immediately that the system can minimize its energy if the moment \mathbf{M} is parallel to the effective ‘‘spin-exchange field’’ $\langle \sum_j \hat{\sigma}_j\hat{J} \rangle$. This finding also allows us to draw a parallel to SDFT: the spin-exchange field $\langle \sum_j \hat{\sigma}_j\hat{J} \rangle$ acts, in principle, as a (time-dependent) exchange field that couples to the spin, i.e. it is similar to the \mathbf{B}_{xc} -field from SDFT (to be more precise: it is similar to $-2\langle \hat{\mathbf{B}}_{\text{xc}} \rangle / c$). In the following discussion, we will assume that our system shows a ferromagnetic behavior in the ground state. Similarly to the situations discussed in this work, we will assume that the moment, and

hence also the spin-exchange field, points in the $-\mathbf{e}_3$ -direction in the ground state, meaning that

$$M_3 < 0 \quad \xrightarrow{(A.132)} \quad \left\langle \sum_j^2 \hat{\sigma}_{3,j} \hat{J} \right\rangle < 0, \quad (A.133)$$

and that

$$M_1 = M_2 = 0, \quad \left\langle \sum_j^2 \hat{\sigma}_{1,j} \hat{J} \right\rangle = \left\langle \sum_j^2 \hat{\sigma}_{2,j} \hat{J} \right\rangle = 0. \quad (A.134)$$

Next, we will say a few words about the ground state energy contribution coming from SOC, which is given by

$$\left\langle \sum_i^2 \hat{h}_i^{\text{SOC}} \right\rangle = \frac{1}{2} \sum_i^2 \langle \xi(\hat{r}_i) \hat{\boldsymbol{\sigma}}_i \cdot \hat{\mathbf{L}}_i \rangle = \frac{1}{2} \sum_i^2 \sum_k^3 \langle \xi(\hat{r}_i) \hat{\sigma}_{k,i} \hat{L}_{k,i} \rangle. \quad (A.135)$$

This energy contribution becomes minimal (i.e. negative) if

$$\langle \xi(\hat{r}_i) \hat{\sigma}_{k,i} \hat{L}_{k,i} \rangle < 0 \quad (A.136)$$

(we considered some general symmetries, such as symmetry by particle exchange). The radial function $\xi(r)$ is typically positive valued and has only a contribution close to the nucleus. Hence, relation (A.136) demands that the system has, in the ground state, non-vanishing spin-currents that flow around the nucleus (see the discussion from section 4.3.4). The SOC is typically only ‘‘active’’ in a certain region around the nucleus (see e.g. section 4.3.2). In the following, we will represent this region by $\Omega(r)$, which is a radial function that is 1 inside the active region, and 0 outside. From the ground state property (A.136) it follows immediately for this region that

$$\langle \Omega(\hat{r}_i) \hat{\sigma}_{k,i} \hat{L}_{k,i} \rangle < 0. \quad (A.137)$$

(Previously, we assumed that we have only one atom or ion, explaining the specific form of SOC. Note that the angular momentum is defined around the nucleus for this form of SOC (see section 4.3.2). However, the generalization to more atoms or ions is straightforward, and the previous conclusions would hold as well. The only difference is that the SOC term would contain a sum of $\boldsymbol{\sigma} \cdot \mathbf{L}$ -terms running over all atoms, and each \mathbf{L} would be defined around the corresponding atom. Hence, the system would have non-vanishing spin-currents around each atom in the ground state.)

So far we have discussed only ground state properties. Now, we will come to the time-dependent behavior of our system. According to Ehrenfest’s theorem and (A.118), the change of the moment is given by

$$\partial_t \mathbf{M}(t) = \langle \Psi(t) | \frac{1}{i} \left[\sum_i^2 \hat{\boldsymbol{\sigma}}_i, \hat{H} \right] | \Psi(t) \rangle = \left\langle \sum_i^2 \xi(\hat{r}_i) \hat{\mathbf{L}}_i \times \hat{\boldsymbol{\sigma}}_i \right\rangle(t). \quad (A.138)$$

$\xi(r)$ is a function that is radial and gives a contribution only in the region close to the nucleus. Hence, we assume, due to the same reasons as discussed in section

4.3.3, that the change of M_3 is determined by

$$\partial_t M_3 \sim \left\langle \sum_i^2 \Omega(\hat{r}_i) \hat{\mathbf{L}}_i \times \hat{\boldsymbol{\sigma}}_i \right\rangle_3. \quad (\text{A.139})$$

Remember that we refer to the two quantities from the right hand side (due to the cross product) as spin-orbit angular momenta, and that $\partial_t M_3(0) = 0$ since the system is in the ground state at $t = 0$.

Next, we will investigate the change of $\partial_t M_3$ by applying Ehrenfest's theorem to the right hand side of (A.139):

$$\begin{aligned} \partial_t \left\langle \sum_i^2 \Omega(\hat{r}_i) \hat{\mathbf{L}}_i \times \hat{\boldsymbol{\sigma}}_i \right\rangle_3 &= \left\langle \frac{1}{i} \left[\sum_i^2 \Omega(\hat{r}_i) \hat{\mathbf{L}}_i \times \hat{\boldsymbol{\sigma}}_i, \sum_j^2 (\hat{h}_j^0 + \hat{h}_j^{\text{SOC}}) \right] \right\rangle_3 \\ &+ \left\langle \frac{1}{i} \left[\sum_i^2 \Omega(\hat{r}_i) \hat{\mathbf{L}}_i \times \hat{\boldsymbol{\sigma}}_i, \hat{W} \right] \right\rangle_3. \end{aligned} \quad (\text{A.140})$$

The terms on the right hand side represent the different spin-orbit angular momentum torque contributions. Calculating the commutator expression of the first line leads to several torque contributions (the torque contributions are similar to the terms derived in A.6.4). Among these contributions are surface- and SOC-torque terms. According to the discussion from section 4.3.4 it is reasonable to assume that only these two types of contributions are important. Of particular interest for the discussion of spin-dynamics in a Coulomb interacting system is the commutator expression of the second line, which will be investigated now.

The expression from the second line of (A.140) contains the commutator with \hat{W} , which can be decomposed:

$$\begin{aligned} [\hat{O}, \hat{W}] &\stackrel{(\text{A.130})}{=} \left[\hat{O}, \hat{C} - \frac{1}{2} \hat{J} - \frac{1}{2} \hat{\boldsymbol{\sigma}}_1 \cdot \hat{\boldsymbol{\sigma}}_2 \hat{J} \right] \\ &= \underbrace{\left[\hat{O}, \hat{C} - \frac{1}{2} \hat{J} \right]}_{(a)} \underbrace{- \frac{1}{2} \hat{\boldsymbol{\sigma}}_1 \cdot \hat{\boldsymbol{\sigma}}_2 [\hat{O}, \hat{J}]}_{(b)} \underbrace{- \frac{1}{2} [\hat{O}, \hat{\boldsymbol{\sigma}}_1 \cdot \hat{\boldsymbol{\sigma}}_2] \hat{J}}_{(c)}. \end{aligned} \quad (\text{A.141})$$

Applying the relation (A.141) to the second line of (A.140) leads to three types of spin-orbit angular momentum torque contributions. By comparing these contributions to the terms of the KS system, one finds again that each contribution has a corresponding SDFT term. The torque contribution stemming from term (a) is similar to the $\nabla v_{\text{H,xc}} \times \mathbf{r}$ -term (see e.g. first term in the third line of (A.110)), while the contribution stemming from term (b) is similar to the $\nabla B_{\text{xc},3} \times \mathbf{r}$ -term (see e.g. second term in the third line of (A.110)). Due to similar reasons as discussed in section 4.3.4 (i.e. due to the nearly spherical symmetry close to the nucleus) it is reasonable to assume that these two contributions are negligible. Hence, the torque contribution coming from the Coulomb interaction between the electrons

should approximately be given by the contribution coming from the term (c):

$$\begin{aligned}
& \left\langle \frac{1}{i} \left[\sum_i^2 \Omega(\hat{r}_i) \hat{\mathbf{L}}_i \times \hat{\boldsymbol{\sigma}}_i, \hat{W} \right] \right\rangle_3 \\
& \approx -\frac{1}{2} \left\langle \frac{1}{i} \left[\sum_i^2 \Omega(\hat{r}_i) \hat{\mathbf{L}}_i \times \hat{\boldsymbol{\sigma}}_i, \hat{\boldsymbol{\sigma}}_1 \cdot \hat{\boldsymbol{\sigma}}_2 \right] \hat{J} \right\rangle_3 \\
& \quad \vdots \quad \text{(A.60); Grassmann identity} \\
& = \sum_i^2 \sum_{j \neq i}^2 \langle \Omega(\hat{r}_i) (\hat{\mathbf{L}}_i \cdot \hat{\boldsymbol{\sigma}}_j \hat{\sigma}_{3,i} - \hat{\mathbf{L}}_i \cdot \hat{\boldsymbol{\sigma}}_i \hat{\sigma}_{3,j}) \hat{J} \rangle \\
& = \sum_k^2 \langle \sum_i^2 \Omega(\hat{r}_i) \hat{L}_{k,i} \hat{\sigma}_{3,i} \sum_{j \neq i}^2 \hat{\sigma}_{k,j} \hat{J} \rangle - \sum_k^2 \langle \sum_i^2 \Omega(\hat{r}_i) \hat{L}_{k,i} \hat{\sigma}_{k,i} \sum_{j \neq i}^2 \hat{\sigma}_{3,j} \hat{J} \rangle \\
& \approx \sum_k^2 \langle \sum_i^2 \Omega(\hat{r}_i) \hat{L}_{k,i} \hat{\sigma}_{3,i} \underbrace{\langle \sum_j^2 \hat{\sigma}_{k,j} \hat{J} \rangle}_{\substack{\text{(A.134)}_0 \\ = 0}} \rangle - \sum_k^2 \langle \sum_i^2 \Omega(\hat{r}_i) \hat{L}_{k,i} \hat{\sigma}_{k,i} \underbrace{\langle \sum_j^2 \hat{\sigma}_{3,j} \hat{J} \rangle}_{\substack{\text{(A.133)}_0 \\ < 0}} \rangle \\
& = - \underbrace{\langle \sum_{i,k}^2 \Omega(\hat{r}_i) \hat{L}_{k,i} \hat{\sigma}_{k,i} \rangle}_{\substack{\text{(A.137)}_0 \\ < 0}} \underbrace{\langle \sum_j^2 \hat{\sigma}_{3,j} \hat{J} \rangle}_{\substack{\text{(A.133)}_0 \\ < 0}} < 0. \tag{A.142}
\end{aligned}$$

In the line next to the last line we applied again a mean field approximation, and we used that the spin-exchange field points along $-\mathbf{e}_3$ (note that we also assumed that the spin-exchange field keeps, at least approximately, this orientation during the time evolution, as is the case for the \mathbf{B}_{xc} -field in the KS system).

The central result of (A.142) is that we have in the Coulomb interacting system a non-vanishing spin-orbit angular momentum torque contribution, coming from the Coulomb interaction, that is (at least approximately) determined by the effective spin-exchange field and by the spin-orbit angular momenta around the nucleus (and hence by the SOC energy; see (A.135)). This contribution is similar to the \mathbf{B}_{xc} -torque contribution of the KS system (see (4.22) and (4.31)). Furthermore, we have shown in (A.142) that the corresponding torque contribution is negative (at least at $t = 0$). Hence, we have a similar situations as for the KS system and it is to expect that the total moment is lost if we get

$$\begin{aligned}
& \left| \langle \sum_j^2 \hat{\sigma}_{3,j} \hat{J} \rangle(t) \right| < \left| \langle \sum_j^2 \hat{\sigma}_{3,j} \hat{J} \rangle(0) \right|, \quad \text{and} \\
& \left| \langle \sum_{i,k}^2 \Omega(\hat{r}_i) \hat{L}_{k,i} \hat{\sigma}_{k,i} \rangle(t) \right| < \left| \langle \sum_{i,k}^2 \Omega(\hat{r}_i) \hat{L}_{k,i} \hat{\sigma}_{k,i} \rangle(0) \right| \tag{A.143}
\end{aligned}$$

during the excitation of the system, since we demanded $M_3(0) < 0$ (note that the second line of (A.143) corresponds to an increase in the SOC energy). This is in analogy to the mechanism explained for the KS system (see section 4.3.5).

Note that the excitation of the systems investigated this work led to $|\langle \hat{B}_{\text{xc},3} \rangle|(t) < |\langle \hat{B}_{\text{xc},3} \rangle|(0)$.

We can conclude that the change of the moment in a Coulomb interacting system can be explained in a similar way as discussed for the KS system (given that the applied mean field approximations are justified). In the interacting system, the effective spin-exchange field $\langle \sum_j \hat{\sigma}_j \hat{J} \rangle(t)$ (defined via the exchange operator \hat{J} , see (A.125) and (A.127)) plays a similar role as the $\mathbf{B}_{\text{xc}}(t)$ -field. If $|\langle \sum_j \hat{\sigma}_j \hat{J} \rangle|$ decreases abruptly, and if the SOC energy increases during the excitation, the moment will most probably reduce. Whether the spin-exchange field would reduce in a true interacting ferromagnetic system, or not, cannot easily be stated a priori. Hence, the previously discussed points have to be investigated in more detail in future work.

Finally, we wish to mention that the initially derived spin-spin interaction could also be approximated via an exchange mean field expression (whether such an approximation is justified, or not, would have to be investigated in the individual case):

$$-\frac{1}{2} \hat{\sigma}_1 \cdot \hat{\sigma}_2 \hat{J} \quad \longrightarrow \quad -\frac{1}{2} \hat{\sigma}_1 \cdot \hat{\sigma}_2 \langle \hat{J} \rangle \hat{=} -\frac{1}{2} \hat{\sigma}_1 \cdot \hat{\sigma}_2 J(t). \quad (\text{A.144})$$

With this simplified interaction as the starting point, the change of the moment could, in a similar way as shown before, also be discussed. The change of the moment could then be interpreted as a result of the change in the exchange interaction (due to the excitation). The effective interaction (A.144) could also be used to investigate the spin-dynamics within a time-dependent Hubbard- or Heisenberg-like model. Note that such a model should, beside the time-dependent exchange “constant” $J(t)$ (which depends on the excitation), also consider higher laying states (which are unoccupied in the ground state) and SOC in order to see the previously described change in the moment.

Bibliography

- [1] E. Beaurepaire, J.-C. Merle, A. Daunois, and J.-Y. Bigot. Ultrafast spin dynamics in ferromagnetic nickel. *Phys. Rev. Lett.*, 76:4250–4253, May 1996.
- [2] A. Scholl, L. Baumgarten, R. Jacquemin, and W. Eberhardt. Ultrafast spin dynamics of ferromagnetic thin films observed by fs spin-resolved two-photon photoemission. *Phys. Rev. Lett.*, 79:5146–5149, Dec 1997.
- [3] C. Stamm, T. Kachel, N. Pontius, R. Mitzner, T. Quast, K. Holldack, S. Khan, C. Lupulescu, E. F. Aziz, M. Wietstruk, H. A. Dürr, and W. Eberhardt. Femtosecond modification of electron localization and transfer of angular momentum in nickel. *Nature Materials*, 6:740, 2007.
- [4] E. Carpene, E. Mancini, C. Dallera, M. Brenna, E. Puppini, and S. De Silvestri. Dynamics of electron-magnon interaction and ultrafast demagnetization in thin iron films. *Phys. Rev. B*, 78:174422, 2008.
- [5] J.-Y. Bigot, M. Vomir, and E. Beaurepaire. Coherent ultrafast magnetism induced by femtosecond laser pulses. *Nature Phys.*, 5:515, 2009.
- [6] B. Koopmans, G. Malinowski, F. Dalla Longa, D. Steiauf, M. Fhnlé, T. Roth, M. Cinchetti, and M. Aeschlimann. Explaining the paradoxical diversity of ultrafast laser-induced demagnetization. *Nature Mat.*, 9:259, 2009.
- [7] D. Steiauf and M. Fhnlé. Elliott-yafet mechanism and the discussion of femtosecond magnetization dynamics. *Phys. Rev. B*, 79:140401(R), 2009.
- [8] M. Battiato, K. Carva, and P. M. Oppeneer. Superdiffusive spin transport as a mechanism of ultrafast demagnetization. *Phys. Rev. Lett.*, 105:027203, Jul 2010.
- [9] G. P. Zhang and W. Hübner. Laser-induced ultrafast demagnetization in ferromagnetic metals. *Phys. Rev. Lett.*, 85:3025–3028, Oct 2000.
- [10] M. Krau, T. Roth, S. Alebrand, D. Steil, M. Cinchetti, M. Aeschlimann, and H. C. Schneider. Ultrafast demagnetization of ferromagnetic transition metals: The role of the coulomb interaction. *Phys. Rev. B*, 80:180407(R), 2009.
- [11] Erich Runge and E. K. U. Gross. Density-functional theory for time-dependent systems. *Phys. Rev. Lett.*, 52(12):997, Mar 1984.
- [12] P. Hohenberg and W. Kohn. Inhomogeneous electron gas. *Phys. Rev.*, 136(3B):B864–B871, Nov 1964.

-
- [13] W. Kohn. *Highlights of Condensed Matter Theory*. North-Holland, Amsterdam, 1985.
- [14] W. Kohn and L. J. Sham. Self-consistent equations including exchange and correlation effects. *Phys. Rev.*, 140(4A):A1133–A1138, Nov 1965.
- [15] U. von Barth and L. Hedin. A local exchange-correlation potential for the spin polarized case. *Journal of Physics C: Solid State Physics*, 5(13):1629, 1972.
- [16] G. Vignale and M. Rasolt. Density-functional theory in strong magnetic fields. *Phys. Rev. Lett.*, 59:2360, 1987.
- [17] G. Vignale and M. Rasolt. Current- and spin-density-functional theory for inhomogeneous electronic systems in strong magnetic fields. *Phys. Rev. B*, 37:10685, 1988.
- [18] Bencheikh K. Spin-orbit coupling in the spin-current-density-functional theory. *J. Phys. A:Math. Gen.*, 36:11929, 2003.
- [19] Rohra S. and Görling A. Exact-exchange spin-current density-functional theory. *Phys. Rev. Lett.*, 97:013005, 2006.
- [20] Rohra S. *Exact-Exchange Kohn-Sham Spin-Current Density-Functional Theory*. PhD thesis. 2006.
- [21] Reineker P., Schulz M., and Schulz B. *Theoretische Physik IV - Quantenmechanik 2*. Lehrbuch Physik. WILEY-VCH, 2008.
- [22] R. M. Dreizler and E. K. U. Gross. *Density Functional Theory: An Approach to the Quantum Many-Body Problem*. Springer-Verlag, 1990.
- [23] Takashi Itoh. Derivation of nonrelativistic hamiltonian for electrons from quantum electrodynamics. *Rev. Mod. Phys.*, 37:159, 1965.
- [24] D. D. Koelling and B. N. Harmon. A technique for relativistic spin-polarised calculations. *J. Phys. C*, 10:3107, 1977.
- [25] A. K. Rajagopal and J. Callaway. *Phys. Rev. B*, 7:1912, 1973.
- [26] A. H. MacDonald and S. H. Vosko. *J. Phys. C: Solid State Phys.*, 12:2977, 1979.
- [27] E. van Lenthe, E. J. Baerends, and J. G. Snijders. Relativistic regular two-component hamiltonians. *J. Chem. Phys.*, 99:4597, 1993.
- [28] E. Engel and R. M. Dreizler. *Density Functional Theory - An Advanced Course*. Springer, 2011.
- [29] D. M. Ceperley and B. J. Alder. Ground state of the electron gas by a stochastic method. *Phys. Rev. Lett.*, 45:566, 1980.

- [30] J. P. Perdew and Alex Zunger. Self-interaction correction to density-functional approximations for many-electron systems. *Phys. Rev. B*, 23(10):5048–5079, May 1981.
- [31] M. Ernzerhof, J. P. Perdew, and K. Burke. *Density functionals: Where do they come from, why do they work?*, volume 180 of *Topics in Current Chemistry*. Springer, 1996.
- [32] G. Ortiz and P. Ballone. Correlation energy, structure factor, radial distribution function, and momentum distribution of the spin-polarized uniform electron gas. *Phys. Rev. B*, 50:1391, 1994.
- [33] John P. Perdew and Yue Wang. Accurate and simple analytic representation of the electron-gas correlation energy. *Phys. Rev. B*, 45(23):13244–13249, Jun 1992.
- [34] J. Kübler, K.-H. Höck, J. Sticht, and A. R. Williams. *J. Appl. Phys.*, 63:3482, 1988.
- [35] R. van Leeuwen. Mapping from densities to potentials in time-dependent density-functional theory. *Phys. Rev. Lett.*, 82:3863, 1999.
- [36] R. van Leeuwen. Causality and symmetry in time-dependent density functional theory. *Phys. Rev. Lett.*, 80:1280, 1998.
- [37] K. Capelle, G. Vignale, and B. L. Györfy. Spin currents and spin dynamics in time-dependent density-functional theory. *Phys. Rev. Lett.*, 87:206403, 2001.
- [38] S.K. Ghosh and A.K. Dhara. *Phys. Rev. A*, 38:1149, 1988.
- [39] A. K. Rajagopal. Time-dependent functional theory of coupled electron and electromagnetic fields in condensed-matter systems. *Phys. Rev. A*, 50:3759, 1994.
- [40] M. Ruggenthaler, F. Mackenroth, and D. Bauer. Time-dependent kohn-sham approach to quantum electrodynamics. *Phys. Rev. A*, 84:042107, 2011.
- [41] G. Xianlong, M. Polini, Diego Rainis, M. P. Tosi, and G. Vignale. Time-dependent current-density-functional theory of spin-charge separation and spin drag in one-dimensional ultracold fermi gases. *Phys. Rev. Lett.*, 101:206402, 2008.
- [42] Z. Qian, A. Constantinescu, and G. Vignale. Solving the ultranonlocality problem in time-dependent spin-density-functional theory. *Phys. Rev. Lett.*, 90:066402, 2003.
- [43] G. Vignale. Mapping from current densities to vector potentials in time-dependent current-density functional theory. *Phys. Rev. B*, 70:201102, 2004.
- [44] M. Marques, C. A. Ullrich, F. Noguiera, A. Rubio, K. Burke, and E. K. U. Gross, editors. *Time-dependent density functional theory*. Springer, Heidelberg, 2006.

- [45] J. J. Sakurai. *Advanced Quantum Mechanics*. Addison-Wesley, 1967.
- [46] A. M. Weiner. *Rev. Sci. Instrum.*, 71(1929), 2000.
- [47] J. D. Jackson. *Classical Electrodynamics*. third edition. Wiley, New York, 1998.
- [48] J.-C. Diels and W. Rudolph. *Ultrashort Laser Pulse Phenomena*. second edition. Academic Press, 2006.
- [49] M. Fähnle and C. Illg. Electron theory of fast and ultrafast dissipative magnetization dynamics. *J. phys. condens. matter*, 23:493201, 2011.
- [50] J. M. Ziman. *Principles of the theory of solids*. second edition. Cambridge Univ. Press, 1998.
- [51] Neepa T. Maitra, Ivo Souza, and Kieron Burke. Current-density functional theory of the response of solids. *Phys. Rev. B*, 68(4):045109, Jul 2003.
- [52] K. Yabana, T. Sugiyama, Y. Shinohara, T. Otobe, and G. F. Bertsch. Time-dependent density functional theory for strong electromagnetic fields in crystalline solids. *Phys. Rev. B*, 85:045134, 2012.
- [53] T. Otobe, M. Yamagiwa, J.-I. Iwata, K. Yabana, T. Nakatsukasa, and G. F. Bertsch. First-principles electron dynamics simulation for optical breakdown of dielectrics under an intense laser field. *Phys. Rev. B*, 85:165104, 2008.
- [54] <http://elk.sourceforge.net>.
- [55] D. J. Singh and L. Nordstrom. *Planewaves, Pseudopotentials, and the LAPW Method*. second edition. Springer, 2006.
- [56] H. Haug and A.-P. Jauho. *Quantum Kinetics in Transport and Optics of Semiconductors*. Springer, 1998.
- [57] Reineker P., Schulz M., and Schulz B. *Theoretische Physik III - Quantenmechanik 1*. Lehrbuch Physik. WILEY-VCH, 2007.
- [58] A. Eschenlohr, M. Battiato, P. Maldonado, N. Pontius, T. Kachel, K. Holl-dack, R. Mitzner, A. Föhlisch, P. M. Oppeneer, and C. Stamm. Ultrafast spin transport as key to femtosecond demagnetization. *Nature Materials*, 3546:332, 2013.
- [59] P. Fazekas. *Lecture Notes on Electron Correlation and Magnetism*. World Scientific, 1999.
- [60] H. Tasaki. Ferromagnetism in hubbard models. *Phys. Rev. Lett.*, 75:4678, 1995.

Angaben zur Person und Werdegang

Vor-, Familienname: Kevin Krieger
Geburtsdatum: 07.01.1979
Geburtsort: Zeulenroda
Staatsangehörigkeit: deutsch
Geschlecht: männlich

Ausbildung

04/2010 - 08/2015 Doktorand am Max-Planck Institut für Mikrostrukturphysik in der Gruppe Prof. E.K.U. Gross
10/2006 - 04/2010 Diplomstudium Physik and der Freien Universität Berlin, Diplomarbeit in der Gruppe Prof. E.K.U. Gross
10/2001 - 09/2006 Studium Dipl. Ing. für Physikalische Technik and der Westsächsischen Hochschule Zwickau, Diplom am DESY Zeuthen in der Gruppe Dr. R. Nahnauer
08/2000 - 07/2001 Fachoberschule EO Plauen
09/1995 - 08/1998 Berufsausbildung zum Steinmetz

Eidesstattliche Erklärung

Hiermit erkläre ich, gemäß §5 Abs. 4 der Promotionsordnung der Naturwissenschaftlichen Fakultät II Chemie, Physik und Mathematik der Martin-Luther Universität Halle-Wittenberg vom August 2012, dass ich die vorliegende Arbeit selbständig und ohne fremde Hilfe verfasst habe. Es wurden keine, außer die angegebenen Quellen und Hilfsmittel benutzt und die den benutzten Werken wörtlich oder inhaltlich entnommenen Stellen wurden als solche kenntlich gemacht. Desweiteren erkläre ich gemäß §5 Abs. 5 der Promotionsordnung, dass ich bisher keine vergeblichen Promotionsversuche an dieser oder einer anderen Fakultät unternommen habe.

Halle (Saale), 09. Juli 2015

Kevin Krieger